

Applications for Nanobodies in Therapy and Cell Research



Jack Anthony Bates

Dissertation der Fakultät für Biologie

Ludwig-Maximilians-Universität

München 2020

Erstgutachter:	Prof. Dr. Heinrich Leonhardt
Zweitgutachter:	Prof. Dr. Christof Osman
Tag der Abgabe:	23.01.2020
Tag der mündliche Prüfung:	21.02.2020

Applications for Nanobodies in Therapy and Cell Research

Dissertation

Ludwig-Maximilians-Universität München, Department Biologie II

Written by Jack Anthony Bates from Shrewsbury, England

München 2020



Table of Contents

List of Figures and Tables.....	v
Abstract.....	vii
Introduction	1
Antibodies.....	1
Antibody structure	1
Antibody Applications.....	3
Limitations of Full Length Antibodies	3
Antibody derivatives and mimetics.....	4
Nanobody Structure and Attributes	6
Generating Nanobody Libraries.....	9
Camelid origin nanobody libraries.....	9
Immune Libraries	9
Naïve Libraries.....	11
Synthetic Libraries.....	11
Considerations for Constructing Synthetic Libraries	12
De novo antibody design	15
Screening nanobodies.....	15
Cell dependent systems	15
Cell Free/ <i>in vitro</i> display systems.....	21
Nanobody expression and purification.....	23
Microbial production	23
Nanobody purification	24
Cell Free binder synthesis	24
Nanobodies Applications in Research.....	25
Microscopy.....	25
Nanobody Tools for Investigating and Manipulating Protein function	27
Diagnostic and Therapeutic Nanobody Applications.....	36
Mechanisms of Nanobody Therapeutics and Diagnostics	37
Nanobody Serum Half-life.....	39

Therapeutic Applications of Nanobodies.....	39
Protein delivery.....	41
<i>In vivo</i> protein delivery technologies.....	42
Results.....	47
Nanoparticle mediated delivery and small molecule triggered activation of proteins in the nucleus ..	47
Supplemental: Nanoparticle mediated delivery and small molecule triggered activation of proteins in the nucleus.....	63
Tunable light and drug induced depletion of target proteins	69
Supplemental: Tunable light and drug induced depletion of target proteins	85
Engineering binder-guided apoptotic proteins responsive to intracellular antigens.....	113
Supplemental: Engineering binder-guided apoptotic proteins responsive to intracellular antigens...	135
Discussion.....	151
Protein Delivery	151
Optimizing <i>in vitro</i> protein delivery	151
Optimizing <i>in vivo</i> protein delivery	152
MSNs for protein delivery.....	153
Targeted Apoptosis.....	155
Considerations for TRAPs.....	155
Delivering TRAPs	157
System improvements	159
Potential targets.....	163
Targeted Protein Degradation	164
LiPD and DiPD Mediated Protein Degradation	165
Failed or Incomplete Degradation	167
Orientation Requirements and Improving Generality.....	168
Off-target Considerations and Controls.....	169
Potential therapeutic Applications of Nb-E3 ligases.....	171
Extended Outlook	173
Function Specific Intrabody Screening.....	173
Cell lines for intrabody assays.....	174
A Fluorescent Intrabody Selection Assay (FISA).....	175
Dual Fluorescent Intrabody Selection Assay (D-FISA).....	177

Fluorescent Intrabody Degradation Assay (FIDA).....	178
Annex	181
References	181
Abbreviations	219
List of Publications	223
Contributions	225
Declaration.....	227
Acknowledgements.....	229
Curriculum Vitae	231

List of Figures and Tables

Figure 1: Antibody Structure.....	2
Figure 2: Fabs and scFvs.....	5
Figure 3: Antibody Mimetics.....	6
Figure 4: Single Domain Antibodies.....	7
Figure 5: Multimeric Nanobodies.....	9
Figure 6: Generating Camelid Immune Libraries.....	10
Figure 7: Biopanning with Phage Display.....	16
Figure 8: Microbial Display.....	18
Figure 9: Nanobody Research Applications.....	25
Figure 10: Protein Ubiquitination.....	31
Figure 11: A Timeline of Binder-E3 Ligase Methods.....	32
Figure 12: Proximity Mediated Protein Activation.....	36
Figure 13: Therapeutic and Diagnostic Nanobody Applications.....	37
Figure 14: A Potential <i>in vivo</i> Protein Delivery Sensor.....	153
Figure 15: Modifying Caspase-9 Dimer Interface Residues.....	158
Figure 16: Generating a Caspase-9 with Improved Resistance to Inhibition.....	160
Figure 17: HEK293T Intrabody Selection Cell Lines.....	169
Figure 18: A Fluorescent Intrabody Selection Assay (FISA)	171
Figure 19: A Dual Fluorescent Intrabody Selection Assay (D-FISA)	172
Figure 20: A Fluorescent Intrabody Degradation Assay (FIDA)	173
Table 1: sdAb Clinical Trials and Approvals.....	40

Abstract

The incidental discovery of special heavy chain only antibodies (HCAbs) in the early 90s has gone on to become an important landmark in numerous fields of antibody application. HCAbs are lightweight camelid derived antibodies that lack both the light chains and CH1 domains of standard structure antibodies. Unlike classic antibodies, HCAbs therefore bind to antigens using only monomeric heavy chain variable domains (VHHs). When these VHHs, also called nanobodies, are expressed in isolation, they form single domain antibodies (sdAbs) with some extraordinary properties. Their minute size enables them to bind to otherwise inaccessible epitopes and to diffuse excellently through tissues, they are often exceptionally stable and minimally immunogenic and since nanobodies remain soluble when expressed in the cytoplasm, they can also be used to target intracellular antigens and guide fused effectors modules. By exploiting such attributes nanobody technology has now evolved to fill a massive range of scientific, pharmaceutical and diagnostic functions.

In this work we have made use of these exciting molecules to generate new methods with applications in therapy and cell research. To assist in the study of the protein function, we have constructed highly tunable nanobody targeted tools, which enable the rapid modulation of target protein levels upon the application of light or small molecules. These DiPD (drug induced protein degradation) and LiPD (light induced protein degradation) systems can be programmed to target unmodified cellular proteins within diverse organisms and furthermore, can be combined to degrade multiple proteins simultaneously. We anticipate that these systems will be extremely useful to those studying long half-life, essential and redundant proteins. To therapeutically target disease machinery present inside of cells, we have designed and developed highly optimized nanobody chimeras capable of potently and selectively killing cells that harbor these antigens. We have demonstrated the function of these target responsive apoptotic proteins (TRAPs) using the capsid proteins of HIV-1 and Hepatitis B virus and a pipeline for the production of these molecules has been described. We suggest that almost any cytosolic or nuclear protein of permissive concentration could be targeted using this system and that TRAP-like molecules could therefore be effective against a number of diseases. Lastly, since the successful delivery of nanobodies to the cytosol still represents a major obstacle to their therapeutic implementation, we have investigated and optimized cellular protein delivery using Mesoporous Silica Nanoparticles (MSNs). We developed a background free sensor to track protein delivered into *in vitro* cell populations and showed that MSNs can facilitate impressive rates of protein transfection which are comparable to those of numerous commercial products. This study demonstrates the great potential of MSN mediated protein delivery and also provides a highly tractable protein delivery sensor which would be well suited to study a range of delivery methods.

Introduction

Antibodies

Combating the diverse and evolving repertoire of molecules hazardous to an organism requires correspondingly versatile machinery. Whilst mechanisms of innate immunity can contain pathogens with immediacy through the recognition of patterns and commonalities¹, the complexity of the adaptive immune system is required to address more unique antigens and provide targeted and lasting immunity².

Central to the success of the adaptive immune system is the capacity to combine receptor DNA diversification with clonal selection^{3,4}. Using mechanisms of genetic rearrangement and mutagenesis the adaptive system generates massive receptor repertoires which are displayed across populations of cells with each clone bearing a structurally unique receptor with distinct binding attributes. These cells act in concert with other cells of the immune system in a perpetual screening process to discover receptors with affinity for foreign or disease relevant antigens. When antigen specific receptors are selected, clonal expansion begins and a means of recognizing and interacting with the antigen is propagated throughout the organism. Once this physical connection between the specific antigen and the immune apparatus is established, more generalized responses can be initiated to eradicate the threat. Whilst T cells and T cell receptors (TCRs) mediate the 'cellular' component of the adaptive immune response⁴, 'humoral' immunity is dependent upon targeting via B cell receptors (BCRs) and their related molecules, antibodies⁵.

Antibody structure

Antibodies, also known as immunoglobulins, are heterotetrameric glycoprotein molecules consisting of pairs of heavy (H) and light (L) chains (Figure 1)⁶. Each of these chains is composed of multiple Ig (immunoglobulin) domains beginning N terminally with a single 'variable' (V) domain and followed C-terminally by between one and four 'constant' (C) domains. Antibody Ig domains are two layer beta sandwiches consisting of 7-9 beta folds interspaced by loop regions and bound by intradomain cysteine-cysteine disulfide bonds. Interactions, both covalent and non-covalent in nature, between interchain domains drive the formation of the Y-shaped antibody molecule⁷.

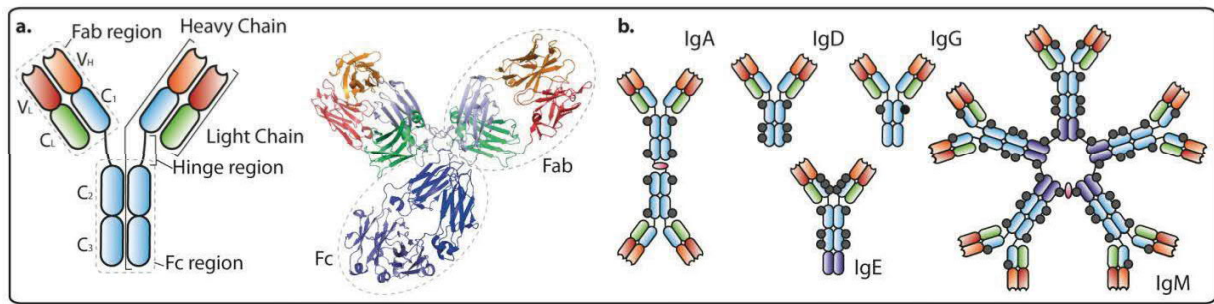


Figure 1. Antibody Structure. (a) The structure of a typical IgG antibody is shown diagrammatically and in crystal structure form (PDB 5DK3). (b) The typical structure of the five human antibody isotypes are displayed including N-glycan groups (grey).

Antibodies are functionally divisible into two Fab (fragment antigen binding) regions and one Fc (fragment crystallizable) region. Fab moieties consist of heavy and light chain variable domains (V_H and V_L) and their corresponding C₁ domains. Unlike antibody constant domains, which do not vary from the germline sequence, variable domains contain three surface loops, after which they are named, which exhibit extraordinary hypervariability between clones. These sequences, termed complementarity determining regions (CDRs) are the site of antigen interaction and the basis of the unique antigen binding properties of each antibody. Through a hydrophobic lateral interface, V_H and V_L domains form a heterodimer with a single apical binder surface featuring the six hypervariable CDRs. When antibody-antigen interactions occur it is this surface, known as the paratope, which interacts with a region of the antigen, called the epitope.

Whilst antibodies may also neutralize a target through simple binding, much of the efficacy of the humoral response depends upon the function of antibodies as adaptor molecules. As adaptors, antibodies bridge specific antigens, via the Fabs, to generalized effector apparatus, through the Fc. The antibody Fc region is the homodimeric C-terminal portion of the heavy chain which is comprised of either two (CH₂, CH₃) or three (CH₂-CH₄) heavy chain constant domains. The number and sequence of these heavy chain constant domains, as well as the composition of CH₁, defines and is consistent within the isotype and subclass of the antibody. Humans have five antibody isotypes (IgA, IgD, IgG, IgE, and IgM) and four subclasses of IgG (IgG1-4), which are non-randomly generated following B-cell activation to facilitate specific immune outcomes⁸. Whilst these antibody subdivisions utilize the same variable domain sequences, differences in the heavy chain constant domains affect their structure, valency, half-life and adaptor functions. The associated effector functions are defined by properties of the Fc region, with the Fc of each isotype and subclass binding to a distinct repertoire of Fc receptors (FcR) and having a variable capacity to bind to complement machinery⁹.

In addition to the protein make-up of the antibody, glycosylation is a key determinant of antibody structure and function. Various glycan groups may be associated with an antibody with isotype and subclass influencing the location and type of glycosylation^{6,10,11}. Glycosylation has been demonstrated to be highly important for antibody stability, solubility, serum half-life and the execution of effector properties¹²⁻¹⁴.

Antibody Applications

Consistent with their natural function, antibodies generated against pathogenic targets can make remarkable therapeutics. Approved indications include; cancers¹⁵; auto-immune diseases¹⁶; bacterial infections¹⁷; and migraine headaches¹⁸, with many more antibodies presently being trialed. In addition to fully biological antibodies, chemical modifications can be implemented to deliver additional functionalities. For example, antibody drug conjugates (ADCs) can be produced to induce highly potent cell killing and radionuclide labeled theranostic antibodies can facilitate enhanced tumor imaging^{19,20}. In all, monoclonal antibody therapeutics are a major and accelerating focus of pharmaceutical research projected to generate annual sales of \$125 billion by 2020^{21,22}.

Outside the context of the organism, the remarkable affinities and specificities achievable in antibody interactions have led to their implementation in numerous techniques and technologies. Antibodies are routinely used by researchers seeking to identify or isolate targets with methods such as; cellular immunostaining; western blot; immunoprecipitation; and flow cytometry. Furthermore, many diagnostic tests and sensor devices depend upon antibody binding for highly sensitive and specific detection of antigen²³⁻²⁵.

Limitations of Full Length Antibodies

Despite a wide scope of application, several disadvantages are associated with the use of whole antibodies. Some of these limitations are the result of the structural properties of the antibody and are therefore difficult to circumvent. For example, a morphological dependence upon disulfide bonds renders expression in the reducing context of the cytoplasm untenable. Thus, antibodies are not viable for many potential intracellular applications. The physical size of the antibody can restrict tissue diffusion, with heterogeneous tumor penetration being particularly problematic for therapeutic applications²⁶⁻²⁸. The dimensions and topology of the antibody paratope can also limit application by prohibiting binding to some epitopes, such as the recessed active sites of some enzymes²⁹. Standard

antibodies are also monospecific, meaning that they bind only a single antigen which can limit therapeutic use. Lastly, the broad requirement for antibody glycosylation presents compatibility problems with microbial production systems and typically necessitates production in mammalian cell lines at a price premium³⁰. This both has a negative effect on antibody research, as it extends the length of each testing cycle, and also contributes to the prohibitive expense of antibody therapeutics and research antibodies³¹.

Aside from these structural restrictions, several problems of antibodies relate to the practices surrounding their production. Since antibodies are most frequently generated through time-consuming, expensive, and highly expertise dependent processes, independent antibody generation is non-viable for the majority of the research community. Because of this, many scientists are dependent upon antibodies obtained from manufacturers. Unfortunately, these research antibodies are frequently very poorly characterized and may not deliver the specificities and affinities required³². Furthermore, even when a purchased reagent is demonstrated to be effective, later versions of the product may deliver inconsistent results which can contribute significantly to reproducibility problems³³. This problem is exacerbated by the inability to obtain sequence information for a given antibody due either to its proprietary nature or the reliance upon polyclonal animal-based or hybridoma mediated manufacture rather than recombinant production. Until companies can be induced to invest in sequencing their back catalogue of antibodies, such problems will continue to compromise the quality of research.

Antibody derivatives and mimetics

Many alternative forms of affinity reagent are now available spanning a range of functional niches each with its individual advantages and pitfalls. Broadly, these proteins can be divided into; those that are derived from antibodies or feature antibody Ig domains; and those which are generated from alternative scaffolds, so called antibody mimetics.

An extensive selection of antibody Ig domain based formats has been generated ranging from simple derivatives to complex recombinant fusions with bi and trispecific functionalities^{34,35}. In large part, these antibody variants have been created in an effort to yield proteins with extended therapeutic properties³⁶. Perhaps the most widely used antibody derivatives in cellular research are the aforementioned Fab fragments as well as single chain variables fragments (scFvs) (Figure 2)³⁷⁻³⁹. ScFvs are comprised of light and heavy chain variable domains bound by a linker region and represent the smallest binding unit which can be reliably derived from a canonical antibody, without significant

sequence modification⁴⁰. ScFvs present several advantages including, compatibility with microbial production^{41,42}, the choice of production by either immune⁴³ or synthetic generation^{44,45}, good immune tolerance⁴⁶, high tissue penetration⁴⁷, and a good tolerance of protein fusion. However, despite the minimal structural complexity of scFvs only a small subset can be solubly expressed in the cytoplasm and the discovery of such intrabodies requires screening procedures⁴⁸⁻⁵⁰.

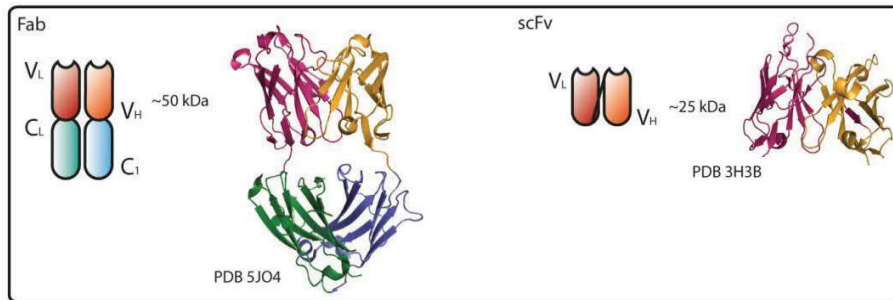


Figure 2. Fabs and scFvs. Schematic structures and crystal structures are shown for Fab and scFv fragments

Antibody mimetics are generalizable peptide or protein affinity reagents which are based upon non-antibody scaffolds⁵¹⁻⁶⁷ (Figure 3). Mimetics cannot be produced by immunization and rely instead upon binding by sections of the protein which have been artificially rendered hypervariable. Scaffolds may be chosen based on characteristics such as high solubility or stability, as well as the paratope shape and binding characteristics. Most antibody mimetics use natural human scaffolds from protein families which bind their endogenous substrates with high affinity, this strategy also serves to reduce the chance of immunogenicity if the mimetic is therapeutically applied^{52,53,55}. These proteins are generally single domain binders (SDBs) and aside from the option of immune generation, they typically deliver each of the advantages stated for scFvs with many additionally functioning reliably as intrabodies⁶⁸⁻⁷⁰. In terms of affinity and specificity, mimetic performance is frequently comparable with antibodies and the volume of these synthetic binders presently undergoing clinical trials is demonstrative of the potential of these technologies⁷¹.

Finally, whilst use of any of these alternative formats does not guarantee that the binder has been appropriately quality controlled; these products are both routinely sequenced and produced via recombinant techniques. This has two advantages; firstly, where published sequences are available for reagents, experimental reproducibility is improved; and secondly, even if for proprietary or other reasons a sequence is not disclosed, recombinant production typically ensures high batch to batch product consistency³³. Furthermore, since many of these binder types do not require work with animals,

they are amenable to more cost and expertise accessible generation methods^{72,73}. Using such methods, researchers can more readily develop and share bespoke affinity reagents, and microbial production can be used to easily and inexpensively generate binders from synthesized gene fragments.

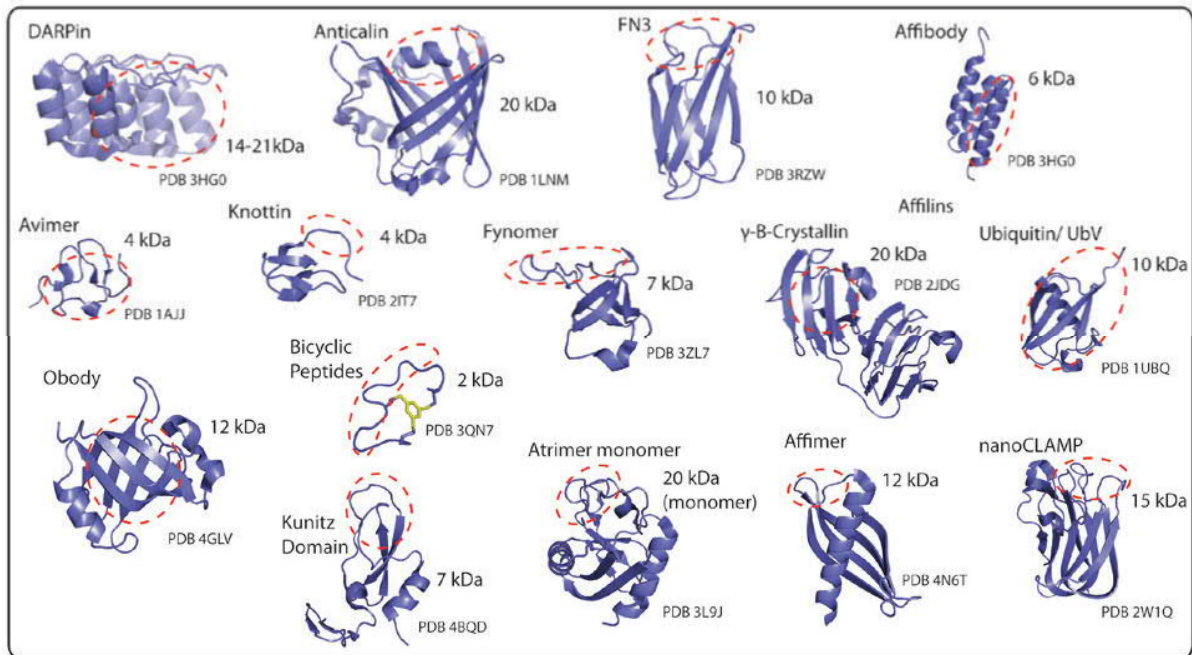


Figure 3. Antibody mimetics. Crystal structures are shown of a range of antibody mimetics or mimetic scaffold proteins. Dashed red outlines depict antigen interaction regions.

Nanobody Structure and Attributes

Nanobodies are one of two known classes of single domain antibody (sdAb) and are derived from heavy chain only antibody (hcAbs) isotypes present in camelids⁷⁴. Whilst camelids generate some conventionally structured antibodies, they additionally express unusual hcAbs formats which are distinguishable by the omission of both light chains and CH1 domains⁷⁴. These deductions leave an antibody of significantly lower molecular weight (~90 kDa) with the capacity to mediate binding through a single variable domain termed the VHH (or nanobody)⁷⁵. Together with the vNARs^{76,77}, nanobodies are the only reliable SDBs which are directly derived from natural antibodies (Figure 4).

Like canonical VH domains, VHHs consist of nine beta sheets connected by loop regions. The three CDRs are spaced and bookended by four minimally variable framework regions (FRs) which are responsible for the consistent overall structure of the nanobody. Unlike the VL and VH domains of canonical antibodies, which heterodimerize via a hydrophobic interface, VHH domains are natural monomers. The surface

corresponding to the canonical dimer interface is therefore more hydrophilic in nature⁷⁸. As a result, distinct from standard variable domains, VHs can reliably be recombinantly expressed as single domains whilst retaining high water solubility⁷⁹. VHH paratope binding also functions monomerically, using just three CDRs rather than six for interactions. As such, nanobodies can be directly subcloned from hcAbs without perturbing binding properties and can therefore be produced through animal immunization methods analogous to those used in the generation of canonical antibodies.

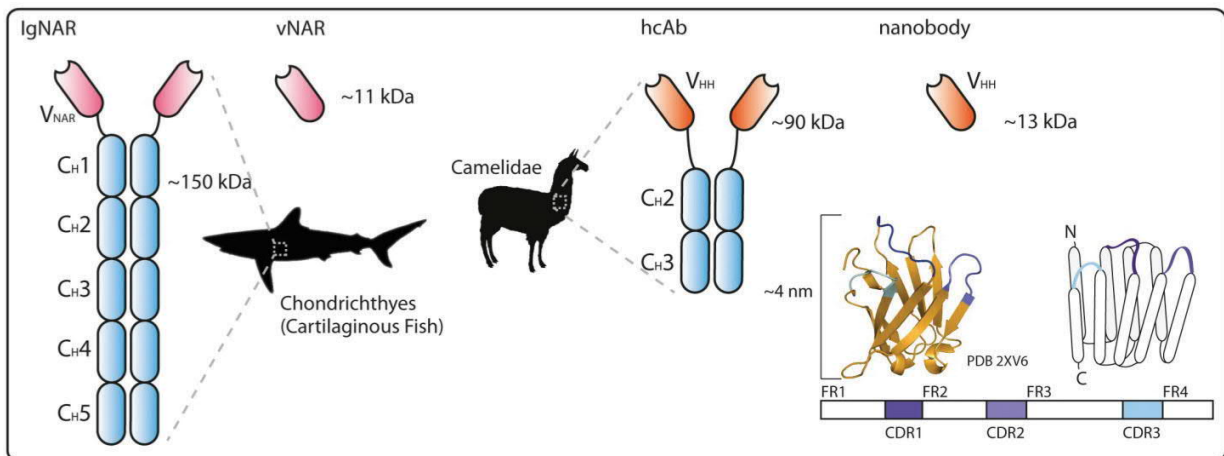


Figure 4. Single domain antibodies. Schematic structures of chondrichthyes Immunoglobulin new antigen receptors (IgNARs) and camelid heavy chain only antibody (hcAb) isotypes and their derivative single domain antibodies are depicted. The crystal structure of the CTD9 p24nb is shown adjacent to VHH sequence and structure schematics.

Natural nanobodies typically contain one or two disulfide bonds. A highly conserved cysteine pins opposing strands of the beta-sandwich and a second disulfide bond may occur between CDR loops^{80,81}. Though these disulfides may improve nanobody stability and binding affinity in some instances^{81,82}, they are frequently dispensable for correct folding⁸³. As such, most nanobodies retain good solubility and stability even when expressed in reducing environments and can therefore be exploited as cytosolic intrabodies.

Despite the small size of the nanobody binding surface, extremely high affinities, often comparable to those of standard antibodies, are frequently possible^{80,84}. This surprising quality of nanobodies, given that a maximum of three rather than six CDRs are used for binding, is thought to be due to special sequence and structural properties of the CDRs^{85,86}. CDR 3 in particular exhibits extraordinary diversity in the length of its binding loops (3-28 amino acids) relative to its counterpart in standard antibodies (8-15)^{87,88}. In contrast to the commonly flat paratopes of standard antibodies, nanobodies binding surfaces

are typically somewhat convex in nature^{53,80,89}. This convexity encourages binding to corresponding concavities on target antigens. Coupled with the small diameter of these binders (~2.5 nm), this propensity permits an unusual capacity to bind epitopes within recessed regions of targets that can be inadmissible to standard antibodies⁸⁹. This has been profitably demonstrated through binding of cryptic epitopes within proteins such as receptor channels⁹⁰ and enzyme sites^{91,92}, in addition to the generation of nanobodies against cleft parasitic proteins, which were unreachable due to the physical constraints of the binding space by surrounding structures⁹³.

VHHs are generally quite durable proteins, capable in some instances of withstanding relative physicochemical extremes without unfolding^{87,94}. Nanobody thermal denaturation typically occurs in the range of 60°C-80°C⁹⁴, though extraordinary resiliences in excess of 90°C have been frequently demonstrated⁹⁵⁻⁹⁷. Furthermore, following significant research into nanobody structure, protein engineering can now be quite reliably used to increase the stability of selected VHHs^{95,98,99}. Interestingly, some sdAbs also demonstrate an unusual capacity to refold following thermal or chemical denaturation^{82,100,101}, something which is unachievable with multidomain antibody formats⁹⁸. Refolding effectively increases nanobody durability by making denaturation bidirectional, it may also enable oral ingestion of gastrointestinal therapeutic nanobodies which refold after gastric juice exposure,¹⁰² and it is correlated with improved microbial yields¹⁰³. High VHH chemical stability has been demonstrated in the presence of low pH, multiple denaturants, and ionic and non-ionic surfactants^{94,104,105}. These properties of conformational stability are often a vital factor in many nanobody applications spanning research, pharmaceuticals and biotechnology¹⁰⁶⁻¹⁰⁸.

In some situations, it is desirable to form multimeric nanobody constructs. These include multivalent and multiparatopic formats, which may improve avidity, as well as multispecifics, which can provide additional functionalities (**Figure 5a**). Numerous methods can be applied to generate these molecules (**Figure 5b**). Perhaps most simply, nanobodies can be sequentially genetically fused using flexible interdomain linker regions¹⁰⁹⁻¹¹¹. This widely used method has been demonstrated to function with up to five nanobodies¹¹² and is utilized in many nanobody biopharmaceutical approaches^{111,113-115}. However, in some instances, N-terminal fusions to a nanobody may compromise its function, most likely due to a partial occlusion of the binding space¹⁰⁹, or sequential formats may not deliver the required orientation for application. In such cases, C-C terminal fusions can be achieved through protein-protein conjugation chemistries^{116,117} or nanobodies can be oligomerized through fusion to multimerising subunits. Simple attachment of VHHs to antibody Fc regions is a common strategy to produce bivalent or bispecific

species^{114,118} and fusion to further antibody fragments or a selection of other proteins can enable creation of up to 24mer nanobody formats¹¹⁹⁻¹²⁶.

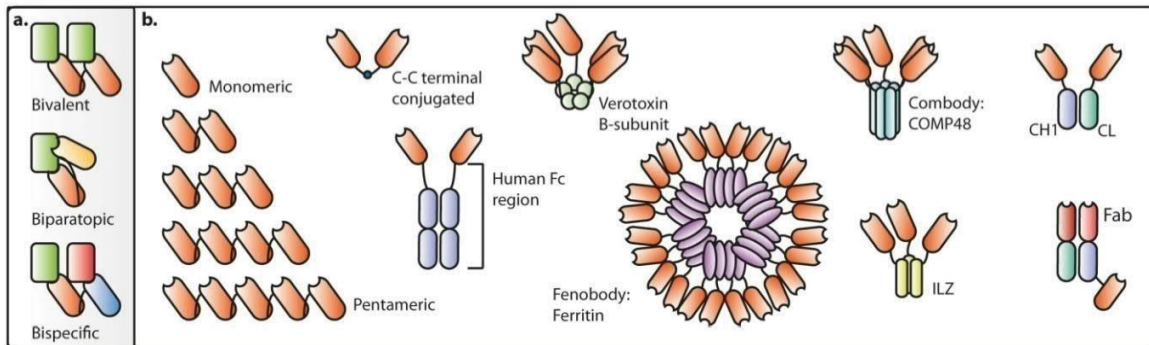


Figure 5. Multimeric nanobodies. (a) The various functions of multimeric nanobodies are illustrated. (b) Technologies for the production of multimeric vhh's are shown including; simple fusion by flexible linker; C-C terminal protein conjugation using tub tag or sortase tag methods in combination with Click Chemistry; and fusion to multimerising subunits which may or may not be antibody derived.

Generating Nanobody Libraries

Early identification of target specific nanobodies can be broadly divided into two processes; The acquisition of a repertoire of potential binders, known as library generation; and the performance of screening measures permitting the selection of high affinity candidates from the library.

Camelid origin nanobody libraries

As discussed above, VHHs can be spliced directly from the Camelid hcAb cDNA. As such, libraries can be generated from the mRNA of peripheral B-cells. Antigen immunization is more commonly used to produce a more focused nanobody pool called an immune library, though “naïve” libraries are sometimes prepared using non-immunized animals.

Immune Libraries

Animal immunization remains a popular method for the production of nanobodies. Immunization methods are analogous to those used in the generation of standard antibody types¹²⁷⁻¹²⁹ (Figure 6). Typically an animal is repeatedly inoculated with a quality controlled antigen of interest plus adjuvant over a period of weeks to months to stimulate the growth and maturation of target specific B cells. Subsequently, a small subset of the now enriched B cell population is isolated from extracted peripheral

blood¹²⁸. VHH sequences are obtained from the B cells by cDNA PCR following the reverse transcription of purified mRNAs¹³⁰⁻¹³². This focused VHH library then undergoes screening procedures which culminate in the identification of antigen binding nanobodies through sequencing.

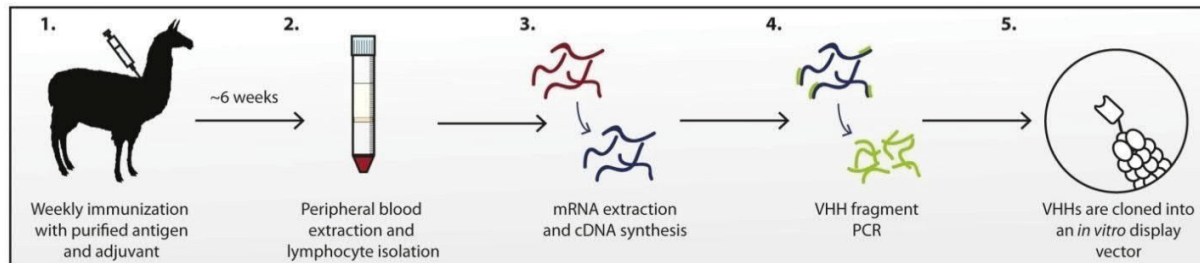


Figure 6. Generating camelid immune libraries. 1. The camelid is inoculated with purified and quality controlled antigen each week for 6 weeks 2. A small volume (~100ml) of peripheral blood is removed from the camel and lymphocytes are isolated 3. mRNA is extracted and reverse transcribed into cDNA 4. VHH sequences are lifted from the cDNA via PCR 5. VHH sequences are cloned into an *in vitro* display vector appropriate for screening.

Leveraging the complexity of the camelid immune system in this way typically delivers high affinity binders naturally selected to exhibit good solubility, high selectivity and no autoimmunity in an organism with a proteome similar to humans. A single animal can be reliably induced to generate nanobodies against five separate antigens simultaneously and so a degree of parallelization is possible¹²⁸.

Unfortunately, due largely to the delay incurred whilst waiting for the animal to mount an adaptive response, this technique is highly time consuming. Furthermore, it is considered good practice to allow a 6 month interval between sets of immunizations¹²⁸, imposing a further delay or necessitating multiple animals for those desiring continuous nanobody generation. Relative to other methods, camelid immunization is also a very costly way of producing binders. Veterinarian expertise is repeatedly required throughout the process and spacious facilities are needed to house and care for these large long-lived animals. Using an animal also imposes antigenic constraints. For obvious reasons, toxic antigens cannot be used, additionally, it may be difficult to generate binders against conserved epitopes due to self tolerance mechanisms which prevent autoimmunity. As a result of the above considerations, in particular the extensive infrastructure and expense, traditional production methods have led to poor researcher accessibility which has doubtless been rate limiting in the progression of the field.

Naïve Libraries

An alternative approach, which circumvents many of the limitations associated with immunization methods, is to construct libraries using samples of peripheral B-cells from immunologically naïve animals¹³³⁻¹³⁶. This presents several potential advantages over immunization; a library can be immediately obtained at a single time point from a blood sample; this library can be repeatedly applied in screening against a multitude of antigens; toxic antigens can be screened; VHH sequences have been naturally selected against autoimmunity; and animal welfare concerns are minimized. Such libraries are therefore significantly more financially accessible than immunization based ones and offer substantial time savings. Indeed standard antibodies continue to be produced for pharmaceutical purposes using donor sequence based naive libraries, one such library was used for example in the generation of the immensely popular Humira molecule¹³⁷. In spite of these virtues, due to the many technical challenges complicating the creation of high complexity, robust and reliable libraries, naïve libraries remain unpopular as a method for nanobody production.

Camelid naive libraries represent of a pool of VHH sequences taken from peripheral B-cells. Generally these B-cells have not been exposed to the antigens against which they will be screened, and therefore high sequence diversity is required to provide a reasonable probability of success when screening against antigen. Unfortunately, obtaining sufficient peripheral B-cells to meet this requirement is problematic. Harvesting of a maximum of 10^9 peripheral lymphocytes has been demonstrated in VHH library construction experiments^{133,136}. However, only a fraction of these cells will be b-cells (~10-20%^{138,139}), of these b-cells just a percentage will be naïve or immature (60-70% in humans¹⁴⁰) and can be considered reasonably well randomized, and a further sub division (~75%) of these will be hcAb expressing cells containing the desired VHH sequence⁷⁴. As a result of these constraints, and following further loss of diversity during processing, established VHH and vNAR naïve libraries have demonstrated only very limited complexity ($\sim 10^7$)¹³³⁻¹³⁶. Whereas standard antibody libraries can multiple this initial low complexity using variant combinations of VH and VL sequences, the single domain structure of nanobodies means that this solution is not appropriate.

Synthetic Libraries

The *de novo* creation of binder libraries using DNA synthesis technology means that natural antibody sequences can now be avoided altogether^{72,73,90,141-144}. Artificial gene synthesis permits the rational design of synthetic combinatorial libraries which combine consensus protein framework regions with

diversified antigen binding sequences. When well designed, such 'synthetic' libraries can reliably deliver highly specific binders against a range of antigens and their use nullifies many of the limitations and concerns associated with both immunized and naïve natural libraries^{72,143,145}.

Considerations for Constructing Synthetic Libraries

Complexity

For reasons of probability, the complexity of a library is a crucial determinant in its capacity to consistently deliver selective and high affinity binders. Although libraries of relatively low complexity (10^7 - 10^8) may be sufficient to find binders against antigens^{73,146,147}, a broad range of nanobody applications including; conformational locking¹⁴⁸; functional hindrance⁹¹; obstruction of interactions¹⁴⁹; tandem binding¹⁵⁰⁻¹⁵²; and distinguishing between subtly different targets¹⁵³, have stringent epitope criteria, which only a subset of nb-Ag interactions will satisfy. In these situations, the capacity to discover hundreds of active binders using larger synthetic repertoires (10^{11} - 10^{12})^{52,143} may be critical to the success of a project.

Selecting Framework Sequences

Framework sequences contribute significantly to the physicochemical and biological aspects of a binder and vary greatly between possible sequences¹⁵⁴. Sub-optimal frameworks can be problematic in a number of ways; poor expression and stability can lead to biasing problems during panning procedures and difficulties with production if manufacture is required; aggregation may result in dangerous immune responses for biotherapeutics or diagnostics¹⁵⁵, as well as inaccurate microscopy and poor intrabody function; and a failure to humanize a sequence may also negatively impact potential immunogenicity⁷⁸. Consequently, significant time may be invested after binder production to improve suitability for an application⁹⁵. Advantageously, the generation of binders from synthetic repertoires permits control over framework attributes from the outset through the creation of an optimized parent molecule. To date, synthetic frameworks have been generated which display low propensities for aggregation, enhanced physicochemical stability, improved *E. coli* expression through codon optimisation, and low likely immunogenicity. This has been achieved through processes of randomization and screening, as well as structure directed rational design^{72,73,90}.

There is some question surrounding whether the use of a single framework could have a negative effect on paratope variability which may in turn affect binding to some epitopes. In addition, whether, given that framework residues are not infrequently involved in binding, significant library quality could be lost through the absence of framework diversity¹⁵⁶. In response to this, some very advanced synthetic binder libraries include an array of different framework regions to minimize these potential impacts^{143,157,158}. Furthermore, semi-synthetic VHH libraries could be generated which combine natural framework regions derived from a naïve library with a mixture of synthetically derived and natural CDRs. Thus far, only one semi-synthetic VHH library has been demonstrated in the literature, featuring a relatively primitive approach to randomization which generated a potential diversity of 10^9 from a 10^6 naïve library¹⁵⁹. Although semi-synthetic libraries could likely be improved upon, the demonstrated success of easily producible large synthetic libraries using a single well characterized framework suggests that it may not ultimately prove worthwhile^{72,90}.

CDR Residue Composition and Loop Length

CDR amino acid composition can be similarly decisive in efforts to yield high quality binders. Studies of residue representation at Ab-Ag and endogenous protein-protein interfaces indicate strong biases in amino acid presence, suggesting that certain combinations of residues are more likely to be productive interactors than others¹⁶⁰⁻¹⁶³. In addition, it is technically impossible to perform an exhaustive equal randomization of all 20 amino acids (20^n) throughout nanobody CDRs as the maximum screenable complexity (10^{12} - 10^{13})¹⁶⁴ is breached within a decapeptide, significantly fewer amino acids than are present in hypervariable regions. Furthermore, it may also be preferable to avoid or underrepresent specific amino acids in randomized regions. For example, cysteine is typically avoided due to its capacity for non-specific disulfide bonding^{73,158} and methionine, as well as certain asparagine and aspartic acid containing dipeptide motifs, can be reduced to decrease the likelihood of post-translational modifications (PTM), which may have a negative effect on future biopharmaceutical function^{143,165}. With these considerations in mind, clearly, impartial randomization is not an optimal strategy for obtaining productive VHH sequences. To decrease the complexity of libraries, such that they can be effectively displayed without meaningful loss of effective binding diversity, the selection of amino acids is typically guided by analyses of natural CDRs or other binding surface compositions^{73,90,143,144}. Mixtures can be implemented broadly across a predicted binding surface¹⁴¹, or compositions can be tailored for individual residues on a binding loop, which permits the formation of CDRs more analogous to those found in nature^{143,72}.

Nanobodies exhibit significant variability in the lengths of their three CDR loops. Although variations in CDRs 1 and 2 are minimal, CDR 3 is unusual in its diversity and length relative to more canonical H3 CDRs^{85,166,167}. As variations in CDR 3 length very likely affect the range of epitopes that can be bound, efforts should be made to install this diversity into synthetic libraries. To date, published high quality synthetic VHH libraries have used repertoires using fixed length H1 and H2 regions with either 3 or 4 length variants for H3^{72,73,90}.

Selecting a Synthesis Strategy

Marked advancement in the pricing and production of DNA oligonucleotides has made combinatorial library synthesis viable for many researchers and presently two randomization options predominant. An older approach utilizes the stepwise addition of single nucleoside phosphoramidites to grow oligonucleotides. This method permits randomization through the creation of degenerate motifs using IUPAC codes, for example, NNK or NNS can code for any of the 20 amino acids and KMT encodes alanine, serine, tyrosine or aspartic acid. The production of such degenerate libraries is relatively inexpensive and this technology has been used to encode numerous useful antibody libraries^{168,169}. However, utilizing these codons only permits a certain degree of control over residue usage; sometimes it is impossible to encode all of the amino acids potentially desirable at a site without also encoding undesirable residues. By way of example, tyrosine and glycine are frequently desirable but cannot be simultaneously encoded without potential less desirable cysteine or aspartic acid residues becoming a possibility¹⁵⁶. Random stop codon introduction can also limit diversity in this approach and frame-shift mutations are relatively common. Alternatively, TRIM (trinucleotide mutagenesis) technology can be used, TRIM uses the incorporation of pre-formed trinucleotide phosphoramidites to enable precise percentage wise control over amino acid composition at any given site¹⁷⁰. This method of synthesis is more expensive, however, the meaningful gain in effective diversity has led to most modern high quality synthetic libraries leveraging this approach^{72,73,90,171}. Library synthesis services capable of complexities up to 10^{12} are now readily available (GeneArt) and a 10^8 complexity yeast displayed synthetic nanobody library can be obtained without cost⁷³. Thus, synthetic libraries have significantly improved researcher accessibility.

De novo antibody design

Ultimately, the computational generation of binding proteins from ‘first principles’ could provide the most cost-effective and expeditious approach to binder production. Such automated *in silico* design and screening potentially stand to permit wider exploration of the space of amino acid combinations, whilst requiring no purification of biomolecules and massively diminished laboratory time and expertise. Furthermore, it promises the capacity to select exact epitopes against which to generate binders, which would be highly beneficial when selecting for functional outcomes^{172,173}.

Long considered the holy grail of protein science¹⁷⁴, the computational prediction of tertiary protein structure has advanced significantly in recent times and unlocked the related prospect of designing proteins de novo¹⁷⁵⁻¹⁷⁷. Subsequently this progress has been implemented to a significant degree of success in attempts to define and implement rules for generating antibodies and other binders^{173,178-180}. Current binder prediction models are sufficiently unreliable to require physical screening steps when determining high quality binders^{181,182}, thus they arguably remain non-viable as true alternatives to other binder discovery technologies. However, in light of the demonstrated amenability of this task to computation, in combination with the rapid expansion and development of machine learning, it seems reasonable to expect fully computationally derived binders at some point.

Screening nanobodies

A binder sequence library can only perform optimally if paired with an appropriate screening strategy. Numerous high throughput technologies have been demonstrated for the selection of protein affinity reagents, with wide-ranging complexity accommodations and various strengths and drawbacks. Broadly, these systems can be divided into cell dependent, *in vitro*, and omics based.

Cell dependent systems

Phage display

Discovering functional nanobody sequences from a DNA library requires methods with which to pair the expressed binder to its cognate DNA or RNA sequence. The earliest large-scale technique for achieving this phenotype-genotype link utilized the M13 filamentous bacteriophage and was named phage display¹⁸³⁻¹⁸⁶. Phage display is the process of genetically fusing active peptides or proteins to the outside of the

phage in such a way that they can interact with molecules in the phage environment. This is achieved through the insertion of the protein's DNA sequence into a phage coat protein gene. This yields a *coat protein/protein of interest* fusion at the tip of the filamentous bacteriophage, with the encoding sequence encapsulated in the same virion. The protein most commonly used in phage display, G3P of the M13 phage, is highly tolerant of fusion and has been extensively demonstrated to be compatible with a variety of binder types^{127,187-190}. Where libraries of binders have been cloned into phagemids, phage display can be applied for screening through a method known as biopanning (**Figure 7**)^{128,191,192}.

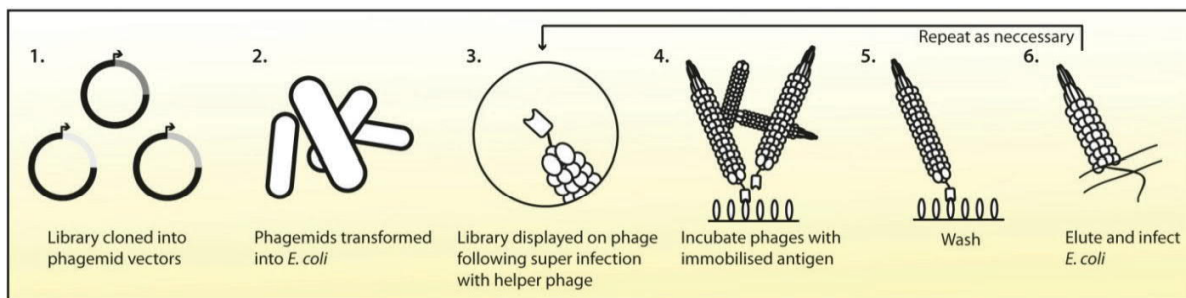


Figure 7. Biopanning with phage display. 1. A library of binder sequences is cloned into phagemid vector in fusion with the G3P protein. 2. The phagemids are transformed into *E. coli*. 3. Helper phage is superinfected into the phagemid containing bacteria and phages are produced which display binders from the library. 4. Phages are purified and incubated with antigen which has been immobilized on the surface of a bead or well 5. Washing steps are performed to remove phages which are not bound to antigen 6. An elution step releases bound phages from the antigen and phages are subsequently infected into bacteria. Another further round of biopanning may be performed and/or sequencing and quality controls of the selected binders are conducted.

Phage display remains very popular as a method for binder screening owing to its various strengths. When carefully and thoroughly applied, phage display permits the screening of potentially huge libraries ($\sim 10^{11}$)¹⁴³. Ff phage virions are remarkably stable, they tolerate extremes of pH, ionic strength, and denaturant and resist cleavage by a host of proteases¹⁹³, thus, phage handling is simple, and selection and elution conditions can be harsh without affecting the integrity of the phage¹⁹⁴. Minimal Specialist equipment and training are required for phage display, Ff phages proliferate in *E. coli*, which are widely used by molecular biologists, and panning techniques require few resources that would not already be present in a molecular biology lab. As such, phage display is relatively technically and financially accessible for researchers.

However, phage display is not without disadvantages. Achieving higher complexities (10^{10} - 10^{11}) is painstaking work involving a very large number of transformations. In addition, though many precise

protocols mean that the technique should be achievable by most molecular biologists, meticulous enactment of the procedure is nonetheless demanding. Researchers may also find that phages are somewhat sticky and there can be issues removing unbound phage during washing steps, this is particularly problematic when panning against non-soluble antigens displayed on cell surfaces¹⁹⁵. Lastly, since phage display requires protein folding in bacteria the capacity of something to be displayed is linked to how well it expresses in bacteria which can lead to significant losses in the diversity of libraries and make the display of many proteins, including some antibody fragments, impossible¹⁹⁶.

Yeast Display

Yeast display is a technology which facilitates the incorporation of recombinant proteins into the yeast cell wall in such a way that they are active on the surface of the organism¹⁹⁷⁻¹⁹⁹. This is achieved in an analogous fashion to phage display, through the fusion of recombinant proteins to one of a number of proteins pre-existing at the cell surface, termed anchor proteins²⁰⁰. Yeast display has been effectively demonstrated for a wide range of protein engineering applications including the selection and affinity maturation of binding reagents²⁰¹⁻²⁰⁴. Briefly, for the performance of affinity selections, dye is conjugated to the target antigen prior to incubation with a library of yeast cells each of which displays a single binder type. Yeast capable of complexing with the target are thereby decorated with fluorescent molecules and can be isolated by FACS (fluorescence activated cell sorting)²⁰⁵ (**Figure 8**). The predictable, monovalent binding of antigen is useful in isolating high affinity interactions and flow cytometry compatible techniques have been developed that permit selections based on equilibrium dissociation constants (K_D s) or dissociation rate constants (K_{off})^{206,207}. Such methods, when combined with normalization staining, allow reliable discrimination and enrichment of relatively minimal differences in affinity parameters²⁰⁷ and have been applied to develop antibodies of remarkable affinity ($K_D = 48\text{fM}$)²⁰⁸. Furthermore, K_D values can be estimated directly from singled clones by means of antigen titration and flow cytometry, thus eliminating the requirement for arduous binder purification steps²⁰⁹.

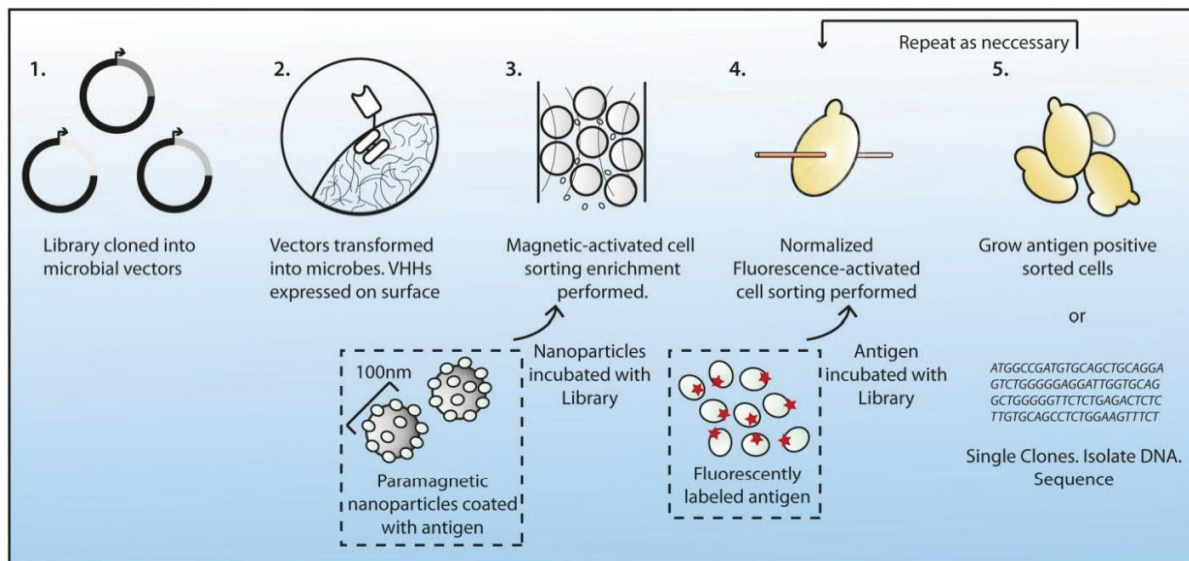


Figure 8. Microbial Display. Figure depicts a workflow applied for some yeast or bacterial display binder discovery methods. **1.** Binder sequences are cloned into a microbial display vector in frame with a surface anchoring protein. **2.** Vectors are transformed into microbes to generate a surface displayed library. Two stages of enrichment are then undertaken; initially **3.** MACs is employed to decrease the diversity of the library, thereafter **4.** FACs is used to select high affinity clones. **5.** Pooled clones are then grown out and sorted cyclically to concentrate the number of high affinity binders. Ultimately microbes are singled and sequenced to retrieve functional binder information.

Yeast display represents a highly tractable and cost effective method for displaying proteins manufactured with eukaryotic machinery. Much of this machinery is comparable to that found in mammalian cells and thus the display of similarly post-translationally modified proteins is possible and protein chaperones and foldases are present which may enhance protein folding. The absence of the correct folding apparatus in prokaryotes sometimes leads to the misfolding of recombinant proteins, a process which is difficult to predict²¹⁰. Some evidence suggests that these folding differences may be an important factor when screening antibody fragments and that due to this yeast display may provide some sensitivity improvements over phage display²¹¹. However, the extent to which this applies to VHHs, which are typically stable and soluble when expressed in the periplasm, has not been determined.

Yeast libraries tend to be relatively limited in diversity 10^7 - 10^9 due to limitations relating to yeast transformation^{73,205,211-213}. Screenable complexity may be further restricted by practical considerations relating to flow cytometry. Modern research flow cytometers can sort $\sim 10^8$ yeast cells in a two hour period²⁰¹, furthermore, It is considered desirable for a single binder sequence to be represented in at least 10 yeast cells to ensure adequate opportunity for discovery²⁰⁵. On these terms, very substantial

flow cytometry time is required to thoroughly investigate a library of variants. To circumvent this problem, some researchers have included a MACs (magnetic cell sorting) mediated enrichment phase, which serves to concentrate libraries towards effective binders^{73,205,214}.

Both VHH and vNAR libraries have been combined with yeast display to yield effective binders. Nanobodies that selectively bind a specific target conformation were isolated from a llama immune library²¹⁵, anti-idiotypic vNARs have been generated from a shark semi-synthetic repertoire²¹⁶, and a fully synthetic VHH pool has been effectively used to generate binders against multiple targets. Despite success with these synthetic libraries, given the diversity limitations of yeast display, it is likely better suited to repertoires of lower complexity, such as pools generated during some affinity maturation processes²¹⁷ as well as immunization based libraries. In such scenarios, yeast display can be a powerful and facile technique for those with expertise with the organism and access to flow cytometry.

Bacterial Display

Bacterial display utilizes anchor fusion proteins in a manner technically similar to yeast display. Unlike yeast display it does not provide eukaryotic protein processing but it does offer higher transformation efficiencies, faster growth rates, and stark reductions in the processed liquid volumes^{218,219}. Bacterial display has been demonstrated with numerous bacterial strains both gram positive^{220,221} and gram negative²²². However, the use of *E. coli* for bacterial display is widely desirable due to broad compatibility with laboratory resources, in addition to strong lab strain attributes including high transformation efficiency and plasmid stability.

Unfortunately, transporting reliably folded Ig domains to the outer membrane of gram negative bacteria has proved problematic and many approaches rely instead upon display of the recombinant protein on the inner membrane. These techniques require a permeabilisation step to strip away the outer membrane and screening is performed with the remaining binder coated spherocyte²²³⁻²²⁵. Despite success with these methods the susceptibility of spherocytes to lysis negatively impacts stringency during elution and wash steps. More recently appropriate anchors have been determined for the outer membrane display of nanobodies, which permit reliable folding and transport²²⁶. Using these anchors high affinity nanobodies have been effectively selected from immune libraries^{227,228}. Bacterial display is compatible with FACs and cell panning approaches, and MACs has been shown to be particularly efficient with *E. coli* display, leading to remarkable enrichments in just two rounds²²⁸. To date, binder library sizes applied with *E. coli* display appear to have been relatively limited (10^6 - 10^7)^{222,228,229} and no

example of use with an unfocused library format, such a synthetic or semi-synthetic library, could be found. However, the upscaling of procedures to permit screening of 10^9 libraries is considered very achievable where initial MACs enrichment is applied^{218,223}, and evidence suggests that this complexity could be sufficient to deliver binders from a synthetic library in some instances⁷³.

Other Cell dependent screening technologies

Numerous mammalian cell display platforms have been demonstrated for the isolation or maturation of antibody derivatives²³⁰⁻²³⁴. Mammalian display delivers optimal PTM and folding machinery for recombinant protein production and is also readily compatible with *in vitro* AID mediated SHM²³⁵⁻²³⁸. Introduction of AID into antibody displaying cells follows an initial affinity screening round and thereby closely replicates the two tier selection processes of the adaptive immune system. Using SHM in this way serves, in effect, to greatly increase library size whilst maintaining manageable cell population numbers²³⁹. Limitations of mammalian display include; typically low initial screenable complexity (10^6 - 10^7)^{231,235,239}, although larger commercial libraries (10^8 - 10^9) have been reported²⁴⁰; higher culture costs; and markedly longer growth durations, resulting in protracted selection times. Mammalian surface display has not been utilized with nanobodies although it is technically possible. Additionally, AID induced SHM is sequence specific *in vivo* but it may be possible to retarget AID for use with nanobodies²⁴¹.

As discussed above, nanobodies are typically a good option for cytoplasmic expression and many applications utilize their intrabody capabilities. To ensure that they feature the requisite binding, solubility and expression attributes, a handful of assays have been described which screen binders intracellularly. These screens are constructed around variant yeast^{49,242,243} and bacterial²⁴⁴ two hybrid systems and have each been shown to deliver functional binders from immune repertoires. These methods permit simple cell survival based intrabody discovery, requiring no purification of antigen during the screening phase. However, introducing stringency and assessing binder quality with such relatively binary systems is problematic and the absence of this quality control is likely to lead to the selection of sub-optimal nanobodies.

Cell Free/*in vitro* display systems

The practical limitations of transformation and transfection constitute a major bottleneck for achievable library complexity when cell dependent screening systems are used. In addition, selection speeds are constrained by the expansion and synthesis of library components in growing organisms. To address these pitfalls, Cell free systems utilize molecular techniques to generate elegantly minimal phenotype-genotype units *in vitro* which can be easily isolated and used for affinity selection. Many of these methods can be applied to rapidly generate highly complex, concentrated and well defined display libraries. Thus, these streamlined processes typically far outstrip cell dependent systems in measures of speed and critically, diversity. Use of wholly *in vitro* systems also eliminates labour intensive alternations between *in vivo* and *in vitro*, which would typically be required when applying directed evolution methods with cell dependent display²¹⁷.

RNA and DNA display technologies

Ribosome and mRNA display are popular methods for the selection of antibody mimetics and derivatives²⁴⁵. Both techniques permit screening by means of cyclical panning procedures and libraries can be generated simply via PCR in both instances. Ribosome display creates phenotype-genotype bonds through the formation of non-covalent protein-ribosome-RNA ternary complexes²⁴⁶. Complexes are achieved through the omission of stop codons within the coding mRNA sequence, this results in stalled translation at the 3' terminus of the transcript and inhibits the release of both the mRNA and nascent protein from the ribosome. A C-terminal spacer peptide is encoded on the transcript to position the protein of interest outside of the ribosomal exit tunnel where it can fold and be effectively displayed²⁴⁷. Cooling and high magnesium concentrations are employed to stabilize the complexes. Ribosome display has been extensively used for binder maturation and discovery including several uses with nanobodies^{90,134,248}.

Alternatively, a technology called mRNA display makes use of puromycin linkers at the 3' end of the coding mRNA to form covalent bonds between the RNA transcript and the nascent protein¹⁶⁴. mRNA can be converted to cDNA by means of reverse transcription, either before or after selections, which enables isolated sequences to amplified and sequenced after panning²⁴⁹. Although RNase inhibitors are typically included during mRNA display, the fusion nevertheless remains relatively labile due to the near omnipresence of RNases. As such, significant numbers of transcripts are easily lost. Later iterations of the method conjugate puromycin to a DNA primer rather than the mRNA, this is then annealed and

ligated at the 3' end of the RNA transcript. Translated proteins are thereby fused to the DNA which can be immediately reverse transcribed into cDNA, which is typically quite stable during screening procedures²⁵⁰⁻²⁵². Such cDNA display has been applied for nanobody screening and facilitated the isolation of a high affinity (kD~11.5 nM) binder from a synthetic library, without the use of affinity maturation methods²⁵³. Ribosome and mRNA display have each been shown to accommodate huge libraries greater ~10¹³ in size²⁵⁴⁻²⁵⁶ and 10¹⁵ is considered possible²⁵⁷.

Expressed proteins can also be bound to their cognate DNA for screening without the use of reverse transcription through fusion to cis-active DNA binding proteins^{258,259}. Such proteins faithfully bind adjacent to DNA CIS sequences on the same transcript from which they are transcribed during *in vitro* transcription/translational combined reactions²⁶⁰. Two such techniques, CIS display and CAD display, leverage the non-covalent binding of RepA and the covalent binding of P2A proteins respectively for this purpose. CAD display was outlined in a single proof-of-concept study²⁵⁹ and has not been used in the literature since, as such it is hard to assess its merits. CIS display is also not widely used in academic research^{261,262}, likely due to the technology being proprietary, but is applied commercially for screening by Isogenica, including for commercial Llamda nanobody screening. CIS display has several advantages; it can handle large library complexities (10¹²)²⁶¹; high magnesium concentrations and RNase free conditions are not required; transcription and translation can be carried out in a single reaction and the complex can be displayed without purification and thus processing is simple.

In vitro compartmentalization technologies

DNA display can also be achieved by means of *in vitro* compartmentalization²⁶³⁻²⁶⁹ (IVC). These methods isolate proteins and their cognate DNA molecules within microcompartments such that protein-DNA complexes can be formed in a predictably way without the need for cis acting elements. Compartments consist of low micron sized aqueous droplets in water-oil emulsions²⁶³, DNA is introduced at a concentration such that not more than one molecule is present per droplet. DNA is transcribed and translated in the droplet to yield the protein of interest in fusion with a DNA binding module. Once protein and DNA are bound in the droplet, either directly or via a microbead, droplets are dispersed and complexes are purified for screening. Relatively large libraries (10¹⁰) have been screened using emulsion methods²⁷⁰, however, complexities are significantly lower than other *in vitro* techniques and perhaps because of this, IVC is uncommonly used for binder discovery.

Screening with mass spectrometry and DNA sequencing

A relatively recent approach to nanobody discovery uses the correlation of mass spectrometry and next-gen sequencing data to determine high affinity sequences¹¹⁰. HcAbs are first purified from serum extracted from an immunized camelid, then tested for binding to immobilized antigen and eluted binders are then analysed via mass spectrometry. Simultaneously, antibodies sequences are sampled from the same animal via bone marrow aspiration, cDNA synthesis, and next-gen sequencing. Effective nanobody sequences can thereafter be determined through the comparison of mass spec and sequencing data. This method has been demonstrated to yield many high affinity nanobodies and removes the requirement for exogenous expression of the nanobodies, which may bias binder screening in other approaches. The method is not yet widely used, perhaps in part due to its very high technical and infrastructure requirements.

Nanobody expression and purification

Microbial production

Nanobodies can be expressed for purification in a wide range of organisms including bacteria, fungi, mammalian cells, insects and plants^{80,127,271-275}. Microbial production methods are generally preferred due to their high accessibility, rapid production times, low expense and good yields, with *E. coli* expression being the most widely used approach^{276,277}. Nanobody expression in bacteria can take place in either the cytoplasm or the periplasmic space. More often, researchers direct protein expression to the oxidative periplasm²⁷⁸, as this environment is permissive of disulfide bond formation which frequently improves the stability, solubility and expression of nanobodies^{279,280}. Evidence suggests that the suitability of the periplasm for nanobody expression may in some cases be further enhanced through the introduction of additional chaperone proteins to the bacteria^{281,282}. Expression in the cytoplasm can deliver very high levels of protein¹⁰⁷, however, due to reducing conditions, nanobodies often form inclusion bodies which require refolding processes before use²⁸³. It is sometimes possible to counteract this through the use of oxidative mutant *E. coli* strains. Such strains are thought to enable the formation of disulfides in the cytoplasm²⁸⁴ and have been demonstrated to permit the expression and purification of large quantities of soluble nanobody²⁸⁵, although significant contradictions regarding their function and merits are present in the literature²⁷⁴.

Various yeast and filamentous fungi have also been tested for nanobody production suitability^{271,286-288}. Strains of the yeast *S. cerevisiae* and *P. pastoris* are commonly utilized for pharmaceutical protein production²⁸⁹⁻²⁹¹ and are capable of very high volumes of protein production²⁹². These species have been used by numerous academic groups for nanobody expression^{105,271,286,293,294} and *Pichia pastoris* has been used commercially (Ablynx) for VHH production²⁹⁵. Nanobodies expressed in fungi are guided through the oxidative endoplasmic reticulum (ER), where disulfide bonds can form, before being secreted into the growth medium. Harvesting recombinant proteins from medium, rather than from bacterial lysate, results in a substantial decrease in the quantity of unwanted protein species, which is a significant advantage of fungal over *E. coli* production. N-linked glycosylation also occurs with some VHHs in the membrane system. Although glycosylation can be considered an advantage for many biopharmaceuticals, it is neither required nor desirable for VHH production and should be limited^{271,276}.

Nanobody purification

For most applications nanobodies are purified simply and effectively by metal affinity chromatography. This is achieved through his-tag fusion to the nanobody which enables high affinity binding to a Ni-NTA column and imidazole mediated elution²⁹⁶. In some instances it is desirable to purify unmodified nanobody, in such cases protein A mediated affinity chromatography can be applied to many VHHs⁸⁰. Size exclusion chromatography is often performed sequential to other methods where higher purities of nanobody are required. Although used far less commonly, the high heat tolerance of some nanobodies can be leveraged in heat treatment step prior to purification. Heating the media or extract serves to render many proteins in the mixture insoluble and allows their removal as aggregates via centrifugation²⁹⁷.

Cell Free binder synthesis

More recently, researchers have demonstrated that functional antibodies, antibody mimetics and fragments, including nanobodies, can be synthesized using cell free expression systems²⁹⁸⁻³⁰¹. Although protein quantities remain small, the investigators suggest that cell free production provides numerous intriguing prospects. For example; cell-free expression is rapid and thus stands to shorten testing cycles during protein development and can provide reagents on demand; it requires very little infrastructure and so is highly accessible; system components can be freeze-dried and stored in minimal space without refrigeration, which could improve the reach of diagnostics and pharmaceuticals into underdeveloped areas²⁹⁸; variables are highly controllable and thus cell free expression is well suited to automation³⁰¹.

Nanobodies Applications in Research

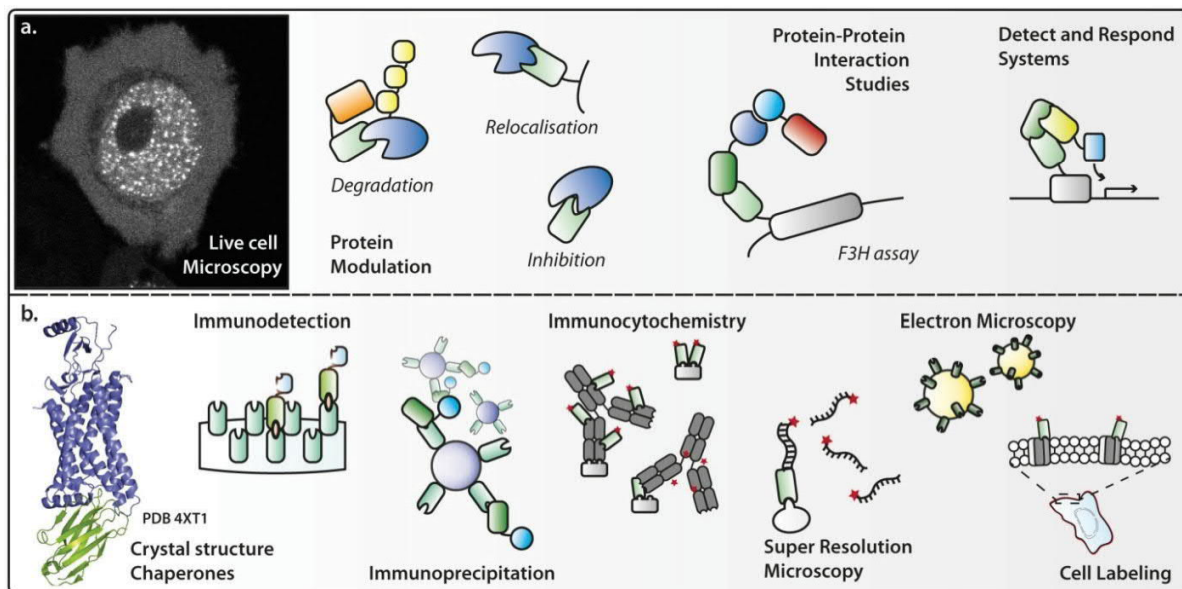


Figure 9. Nanobody Research applications. (a) Intracellular applications for nanobodies are shown. (b) Selected research applications for purified nanobodies are shown.

Microscopy

Live-cell microscopy

It is frequently informative to visualize the dynamic movements of a protein or structure within live cells. This is most commonly achieved through the genetic fusion of either fluorescent proteins or tags compatible with fluorogenic probe, to the protein of interest³⁰²⁻³⁰⁴. Despite the many successes of these approaches, numerous difficulties can be associated; fusions may prevent the correct folding or positioning of a protein; interactions or functions may be sterically hindered by the fusion; and researchers must choose between more exact, but labour intensive, modification of endogenous loci and less representative ectopic expression methods. As an alternative to direct fusion strategies, proteins can be tracked intracellularly through the use of fluorescently labeled intrabodies³⁰⁵. Use of intrabody mediated labeling may eliminate folding and interaction problems resulting from fusions and leaves protein stoichiometry unaffected. Additionally, unlike endogenously integrated fusion proteins, intrabodies can be produced to bind specifically to different isoforms³⁰⁶, conformational states⁹⁰ or PTMs³⁰⁷⁻³⁰⁹ on a protein. The exceptional applicability of nanobodies for intrabody tasks has led to their widespread use in live cell imaging^{305,310,311}. Intrabody fluorescence can be introduced through the use of

genetic fusions³¹²⁻³¹⁵, such as with the 'chromobody' approach³¹⁶, or binders may be purified and conjugated to fluorescent molecules, allowing delivery in protein form³¹⁷⁻³²¹. In addition to cell culture applications, fluorescent nanobodies can be used to highlight structures inside whole organisms either through the production of transgenic animals³²²⁻³²⁴ or via exogenous introduction of nanobody^{325,326}.

However, fluorescent intrabodies do not serve as one-to-one alternatives to either POI-FP fusions or fixed immunocytochemistry methods and thus caution must be exercised when applying them in live cell or tissue scenarios. The exact antigen epitope bound can be highly influential on the result. Binding to certain regions may affect the activity of the protein³²⁶, its position, or its capacity to interact with other structures¹⁴⁹. Alternatively, a binder may function well *in vitro* yet be outcompeted for an epitope *in vivo* and thus deliver an unhelpful or partial picture of POI localisation³²⁷. As distinct from fixed sample staining, washing steps are not performed to remove excess binder or non-specific low affinity interactions when using intrabodies. Therefore, high affinities are required to reduce background³¹⁶, and additional care must be taken to ensure that introduced binders are at a level that relates favorably to target expression. Furthermore, low abundance and highly diffusive proteins may be very difficult to distinguish from background. Unfortunately, many of these possibilities are difficult to assess but production and testing of a panel of unique antigen binders may assist in mitigating limitations.

Some researchers have attempted to improve the signal-to-noise of interacting vs unbound fluorescent intrabody by integrating various binding dependent conditions, these solutions have potential applications for both microscopy and biosensors. One such technique utilizes the conjugation of solvent sensitive dyes to the interaction surface of a binder which can be stimulated to fluoresce inside a binder interface³²⁸⁻³³⁰. This has been demonstrated with numerous binder types including scFVs, DARPins and monobodies^{329,331-333}. A second approach to this problem, is to generate a binder which is unstable unless bound to antigen^{334,335}. Such binders can be genetically fused to fluorescent modules which will be co-degraded if the binder remains unbound. Very impressive signal-to-noise ratios have been achieved with overexpression of both nanobody and antigen, although unbound fusions tended to suffer from aggregation which adversely affects imaging prospects³³⁴.

Immunocytochemistry, Super-Resolution Microscopy and Electron Microscopy

Logically, nanobodies are appropriate for use as primary antibodies in fixed cell and tissue immunostaining^{312,336-339} and have recently also been demonstrated to be ethical and cost effective alternatives to secondary antibodies³⁴⁰. Of particular recent interest, when directly labeled using site

specific conjugations³⁴¹, nanobodies have been shown to make excellent probes for super-resolution microscopy^{305,314,342,343}. Super-resolution microscopy requires fluorescent labeling of the protein of interest. An ideal probe is highly specific, predictably labeled and produces minimal 'linkage error'³⁴⁴. Linkage error describes the positional discrepancy between the structure of interest and the fluorescent molecule targeted to label it, it is a critical determinant of the achievable resolution. Labeling with classical methods such as primary and secondary antibodies can lead to significant linkage error (20 nm), using smaller probes, such as nanobodies, researchers can substantially decrease this error to <5 nm³⁴⁴. If a nanobody is unavailable for a given target, a recently developed tag-specific nanobody can be applied following CRISPR mediated tagging of the target or ectopic expression³¹⁴, which should also maintain minimal linkage error. Nanobodies can also be conjugated to DNA docking strands and subsequently usefully applied in both DNA-PAINT and DNA-exchange based imaging approaches³⁴⁵⁻³⁴⁹.

Nanobody technology has also been shown to be applicable with both electron microscopy (EM)^{350,351} and correlative light and EM techniques^{339,351,352}. VHHs have been demonstrated to assist as targeting subunits for immunogold particles³⁵⁰, to function in fusion with an enzyme which serves to increase electron density^{351,352}, and to leverage their high tissue penetration to enable correlative microscopy without harsh tissue treatment³³⁹.

Nanobody Tools for Investigating and Manipulating Protein function

Assessing Protein Interactions

Nanobodies are central to a simple and highly tractable intracellular protein-protein interaction (PPI) investigative tool called the Fluorescent-3-Hybrid (F3H) assay³⁵³. The F3H assay can be used to determine whether two proteins interact through the assessment of co-localisation of fluorescent signals at a defined site in the cell. The method uses a GFP binding nanobody³⁵⁴ fused with a DNA binding subunit which causes its accumulation at a single highly repetitive sequence integrated into the BHK genome. The concentrated nanobody then binds to and focuses GFP-fused bait proteins to form a large fluorescent dot in the nucleus. A potential interactor, the prey protein, is fused to a second fluorescent protein, typically red, which is unable to bind the nanobody. In the event of interaction, fluorescence co-localises at the dot in the nucleus. Aside from its ease of application and low infrastructure requirements, there are several qualitative benefits to applying the F3H assay for PPI study. Unlike many other methods, the F3H assay is performed in mammalian cells which may assist in

reducing type II errors where mammalian proteins are to be tested. Use of dissimilar species may result in failure to identify true interactions due to errors in protein folding or the requirement of additional factors for binding, e.g. a tertiary protein to perform a required post-translational modification. The F3H also permits the visualization of fully reversible interactions in real-time. This affords live assessment of binding kinetics upon alterations to the cell environment, such as the addition of an inhibitory drug³⁵³.

Two further VHH dependent PPI assays have recently been demonstrated, both use Förster resonance energy transfer (FRET) or FRET similar techniques³¹⁰. Vacuolar sorting was studied in plants using a nanobody assisted sensor to view protein-protein interactions in a compartment specific manner³⁵⁵. Nanobodies have been applied to the surface of upconversion nanoparticles (UCNP) to permit Lanthanide-based resonance energy transfer (LRET) when introduced into cells containing the relevant fusion bait and prey proteins³⁵⁶.

Modulating Protein Function and Positioning

Nanobody binding has been widely documented to inhibit target functions with effects varying dependent upon the nature of the epitope. Active sites may be bound to oblate enzyme functions^{29,357,358}, nanobodies can occupy interaction surfaces to prevent complex assembly^{149,359} or transient interactions³⁶⁰⁻³⁶², ion channels can be blocked³⁶³, and proteins can be conformationally locked into inactive or suboptimal conformations^{90,354,364}. These inhibitory effects have been demonstrated both extra and intracellularly and many have been posited to be of potential therapeutic benefit, as will be discussed. Such functional protein knockdowns are also of high interest to researchers and represent a highly specific alternative to drug mediated inhibition, which should also display good generality.

In some instances it is also possible to stimulate or enhance protein function through VHH binding. *Kirchhofer et al* demonstrated that direct binding to GFP with various nanobodies modulated the fluorophore's spectral properties and could diminish or intensify the fluorescence of the molecule³⁵⁴. Binding can also allosterically upregulate some target functions, for example, both increased enzymatic function^{365,366} and ion channel potentiation leading to enhanced cellular ion influx³⁶³ have been demonstrated. Additionally, nanobodies can be employed to stimulate proximity dependent events via multimeric and multispecific formats capable of co-localising targets. For example, the extrinsic apoptotic pathway can be potently stimulated through the administration of sequentially fused death receptor 5 specific VHHs¹¹² and whole cells can be tethered together using multispecific receptor binding nanobodies, which can induce cytotoxic immune processes^{114,367}.

When fused to either anchored or compartment specific proteins, or to localisation sequences, nanobodies can be used as tools to reposition proteins in the cell. Several groups have demonstrated how this can be profitably used in research including; for the concentration bait proteins, which is central to the previously discussed PPI assays^{318,353}; to research the significance of protein positioning on protein function^{315,324}; and to perform intracellular positional trapping of a protein away from substrates and interactors, which can be an effective approach to target inhibition^{69,368-371}. Curiously, although the importance of inducible mechanisms has been appreciated in earlier binder-free sequestration/inhibition techniques, such as 'Anchor-away'³⁷² and 'Knock sideways'³⁷³, they have not yet been integrated into binder based systems, significantly limiting the applications of these tools.

Targeted Protein Depletion

Attempting to infer the function of a protein from the consequences of its depletion is a routine starting point in reverse genetics, with genetic knockout, often using the CRISPR/Cas system, the most commonly employed approach³⁷⁴. Knockout techniques use direct modification of the gene sequence to block protein production. They enable complete removal of the protein from the cell in a highly specific manner, often leaving a very clear picture of protein function which is untainted by residual protein. However, in some instances knockouts cannot be applied, such as when removal of a protein is lethal to the cell or organism, or when work with primary cells or unmodified organisms is required. Additionally, biases can be introduced by genetic compensatory mechanisms which may be active during lengthy protein knockout procedures, which can confuse results³⁷⁵. As an alternative or supplement to knockout methods, knockdown techniques can be used. Knockdown techniques do not alter the genetic sequence of a protein but modulate its quantity through interference with, or degradation of, its cognate mRNA, or by direct protein depletion.

RNA knockdown is most commonly undertaken using endogenous mechanisms of RNAi (RNA interference) complemented with user selected shRNAs or siRNAs^{376,377}. In these methods dsRNA is either transcribed from a vector or introduced directly into the cell, where it is then processed and loaded onto a RNA nuclease complex called RISC (RNA-induced silencing complex) in its single stranded form. This ssRNA acts as a targeting sequence for the nuclease which is able to digest mRNAs with perfect Watson-Crick complementary base pairing, thus preventing their translation. RNA knockdown can also be performed using synthetic nucleotide analog oligos called morpholinos (MOs)^{378,379}. MOs retain RNA base pairing capability but are resistant to nucleases and thus highly stable in cells. Anti-

sense morpholinos can be generated to anneal to the translational start site of an mRNA to prevent ribosomal binding and translation³⁸⁰. RNAi and MO methods may be transiently or inducibly applied across a population which can help to mitigate genetic compensation mechanisms and can be useful for the depletion of proteins essential to cell survival. Through the variation of transfected quantities or via the chemical induction of transcription, these methods can also be dosed. Dosing permits control over the extent of protein depletion which may be useful in elucidating its function³⁸¹. RNAi also provides a simple approach to removing specific isoforms of a protein which is not easily achievable with a knockout approach³⁸².

Despite the broad prevalence and high utility of RNA knockdown techniques, major drawbacks are associated with their use. As with other methods dependent upon oligonucleotide annealing, off-target binding can be a serious problem. Although perfect base pairing is required for the siRNA RISC to degrade an mRNA via Ago2, incomplete pairings can also disrupt function using miRNA related mechanisms^{383,384}. It may be possible to dilute off-targets effects through the use of large pools of siRNAs designed against a target³⁸⁵, although this approach requires transfection and is subject to associated limitations. Antisense MOs also appear to be highly prone to off-target effects, with recent work suggesting that these effects may be sufficient to create false phenotypes and confuse results^{386,387}. Such work has spurred questions about the handling and reliability of MO derived data^{380,388}. The temporal and spatial heterogeneity of siRNA or MO delivery in a cell population or organism can be a source of complication, with hard to transfect cell types being especially problematic³⁸¹. Stable cell lines can be made using shRNAs, this reduces heterogeneity and permits the protracted knockdown of proteins which can be otherwise difficult due to the instability of RNAs. However, the inefficiency of stable cell line production makes the use of larger sets of targeting shRNAs highly challenging. Even without variations in delivery, RNA knockdown techniques deliver wide ranging potencies against mRNAs which are difficult to predict even where tools are applied and thus require significant trial and error³⁸⁹⁻³⁹¹.

A considerable repertoire of techniques has been established for the direct knockdown of protein through degradation mechanisms. Direct protein modulation can deliver many advantages; it is typically relatively fast and is appropriate for very stable proteins as it is not dependent upon the half-life of the protein; many methods are easily reversed by removal of the stimulating factor; compensation mechanisms can be avoided; populations can be easily synchronized through induction; and off-targets can be minimized, depending on the method used³⁹². Following observations that proteins can be

minimally modified or tagged to render them susceptible to proteasomal mediated degradation^{393,394} numerous inducible fusion tags were established to permit researcher control over protein abundance³⁹⁵⁻⁴⁰⁵. These methods permit the selective stabilization or degradation of a tagged POI using heat, light or chemical drugs.

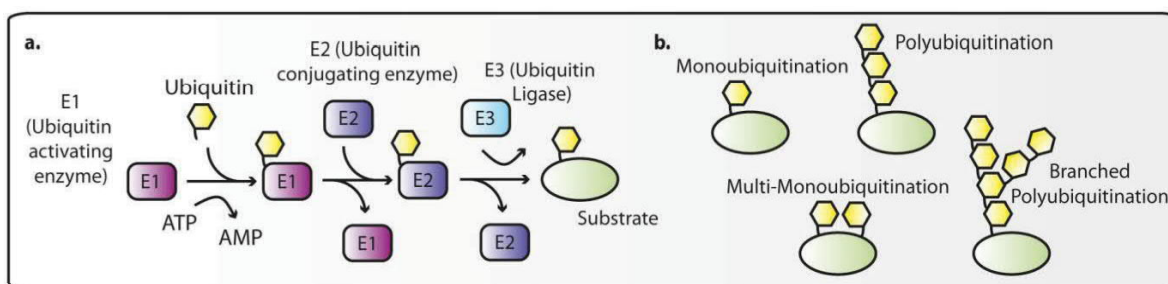


Figure 10. Protein Ubiquitination. (a) The ubiquitination cascade is shown. E1 adenylates ubiquitin which binds the catalytic cysteine of E1. Ubiquitin is then transferred to the cysteine of E2. Finally an E3 ligase binds to the target protein via a substrate recognition domain and initiates the transfer of ubiquitin onto the protein. **(b)** illustrates some of the ways a ubiquitin can accumulate on a protein.

With a few exceptions, these degron tags initiate POI degradation by means of ubiquitination. Ubiquitination describes the post-translational attachment of ubiquitin to a protein via a cascade of enzymatic processes (**Figure 10**). Ubiquitin is first activated by and bound to a ubiquitin-activating (E1) enzyme in an ATP dependent manner. Ubiquitin is then transferred from the catalytic cysteine of the E1 enzyme to that of the ubiquitin conjugating (E2) enzyme. The E2-ubiquitin complex then interacts with an E3 ubiquitin ligase which is responsible for substrate targeting and the transfer of the ubiquitin to the substrate either via the E3 ligase or directly from the E2 enzyme⁴⁰⁶. Most frequently ubiquitin is attached to a lysine on the target protein via an isopeptide bond. Sometimes N-terminal ubiquitination or the ubiquitination of cysteines, serines or threonines can also occur⁴⁰⁷. Ubiquitin has several surface lysines which, following its conjugation to a protein, can be further ubiquitinated. As such, various forms of mono, poly and multi ubiquitination can occur and constitute a ubiquitin code which assists in determining the fate of the protein. Depending upon this patterning, ubiquitin can have a number of effects on a protein including; activation; the stimulation of complex assembly; the facilitation or inhibition of interactions; relocalisation; and protein degradation⁴⁰⁸. Degradation occurs via the Ubiquitin Proteasome pathway (UPP), whereby protein ubiquitination enables proteasome binding and subsequent enzymatic degradation⁴⁰⁹.

In addition to the aforementioned tagging degradation methods, a slew of targeted techniques have been developed which permit protein knockdown without modification of the gene. Each of these methods functions by approximating an E3 ligase to the POI in order to stimulate ubiquitination. Approximations have been demonstrated using both small molecule mediated targeting and protein-E3 ligase fusions that interact with the POI. Proteolysis Targeting Chimeras (PROTACS) are amongst the oldest and most enduring formats for protein degradation. PROTACS are chemically synthesized chimeric small molecules which bind simultaneously to a POI and an E3 ligase domain^{410,411}. Using small molecules for degradation presents several advantages such as; high cell permeability; homogenous diffusive distribution; simplicity of use; and rapid application without the necessity to generate transgenic animals or to introduce nucleic acids. Unfortunately, PROTACS are severely limited by the requirement for chimerisable drugs capable of binding to the POI. Accordingly, though they may become powerful pharmaceuticals, they are poorly suited to widespread use in cell research^{392,412}.

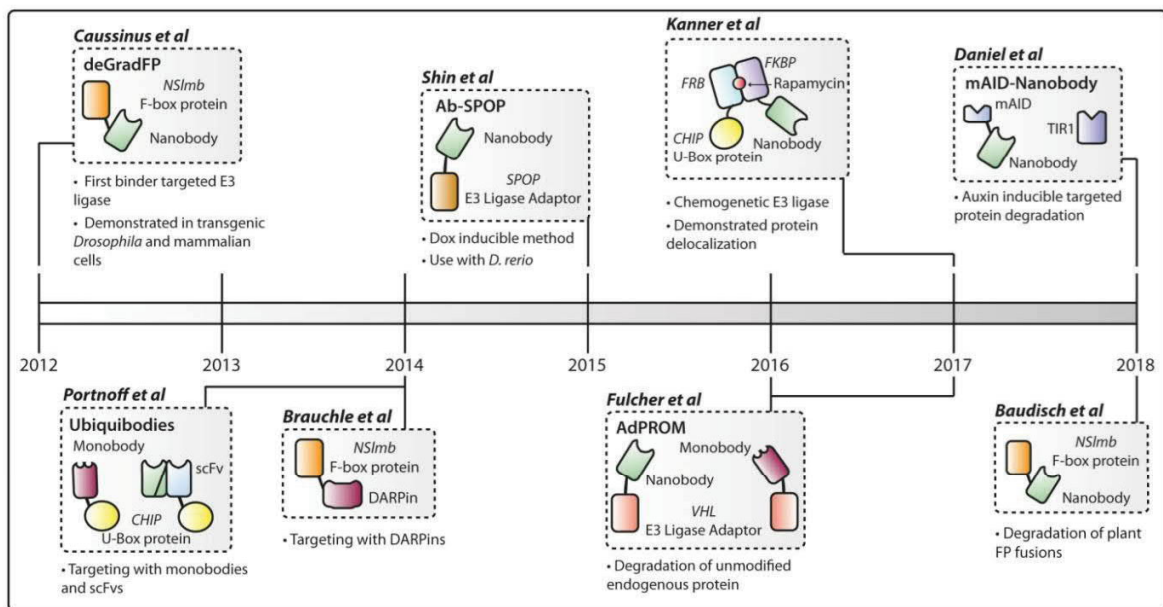


Figure 11. A timeline of binder-E3 ligase methods. This illustration depicts the various binder targeted E3 ligase technologies describes their original contributions

Beginning with work by Zhou et al⁴¹³, numerous researchers developed methods to ubiquitinate and deplete target proteins through the fusion of interacting proteins to E3 ligase machinery. Targeting has been performed using endogenous interactors⁴¹⁴⁻⁴²¹, a viral protein⁴¹³, and both natural⁴²² and recombinant peptide motifs⁴²³. This task is of course highly suited to intrabodies, such as nanobodies,

which can deliver excellent specificity and affinity against almost any target. Caussinus et al developed the first intrabody-E3 ligase technology consisting of a GFP binding nanobody in combination with an F-Box protein⁴²⁴. This method, named deGradFP (degrade Green Fluorescent Protein), was first transiently tested in mammalian cells before use in transgenic *Drosophila*. The system enabled highly effective tissue specific knockdown of the majority of GFP-fused proteins targeted. Similar works soon demonstrated the flexibility of binder-E3 ligase fusions with analogous systems targeted by monobodies, DARPins or scFVs^{69,425}. These experiments show that binder mediated degradation can be simple, effective and rapid. Through the use of fluorescent protein binders these methods are immediately compatible with the many transgenic cell lines and species featuring fluorescent fusions, and through the quantification of fluorescence, protein destruction is easily traceable⁷². As the ubiquitin proteasome pathway (UPP) is highly conserved in eukaryotes, intrabody-E3 ligases have very broad applicability between species^{426,427}. However, each of these systems was expressed in a promoter dependent manner and whilst this approach can deliver a significant degree of control in transgenic animals, the use of constitutive promoters is very limiting in cell culture. If such promoters are used then either transient transfections must be performed, resulting in a high heterogeneity of effect, or stable cell lines can be generated but run the same risks of genetic compensation or lethality associated with knockout. Clearly, mechanisms permitting tighter control over system activation were required to improve usability.

Shin et al generated the first inducible binder-E3 ligase format using a bidirectional doxycycline inducible system⁴²⁸. Induction provides several benefits; it can be used to synchronize whole cell populations in an experiment; it allows for more conditional investigation of a protein; it permits the creation of cell lines from single clones without problems of genetic compensation or lethality; and protein modulation is easily and reproducibly tunable, which may reveal further attributes of the target. Shin et al's method enabled high level degradation of H2B in mammalian cells. Unfortunately, although four further nuclear proteins were tested⁴²⁸, insufficient experiments were undertaken to determine if these additional POI-fusions were degraded as claimed, or whether they were instead relocalized to the cytoplasm. Thus, it is difficult to determine the broader efficacy of this approach. In addition, doxycycline inducible knockdown was demonstrated to be subject to significant delay and intra-population variation using a stable inducible cell line with population-wide degradation taking around 12hours. Following this work Fulcher et al demonstrated a second doxycycline inducible system which enabled significant knockdown after 6 hours, however, too few time points were used and insufficient quantification was undertaken to ascertain maximal knockdown timing⁴²⁹. An advantage of these doxycycline systems is that they ensure that the function of the POI remains untainted by binding prior to induction.

Recently researchers have generated two-part inducible systems for the targeted ubiquitination of protein. Kanner et al produced a rapamycin activated system which was used to displace an ion channel from the surface of cells whilst leaving its concentration unaffected⁴³⁰. Aside from the novel chemogenetic mechanism of activation, this work highlights the variant functional possibilities of ubiquitination⁴³¹ and shows that effects other than degradation can be achieved with engineered E3 ligases. Daniel et al combined the auxin-inducible degron (AID)⁴⁰⁰ into the deGradFP⁴²⁴ approach to form the targeted and inducible mAID-nanobody degradation technology⁴³². The AID tag permits the recruitment of TIR1, a plant F-box protein, to the AID-POI fusion in the presence of the phytohormone auxin. TIR1 complexes with endogenous SCF (Skp1, Cullin, F-box) E3 ligase components and instigates ubiquitination of the AID tag and fused POI. Since auxin is a plant hormone, it is virtually inert in many non-plant species and is therefore a highly appropriate inducer for cell function studies. To deliver a functional nanobody-mAID fusion (mAID is an experimentally determined minimal AID tag⁴³³) which does not simply ubiquitinate and destroy itself, lysines were replaced with arginines on both the GFP targeting VHH and the mAID tag. This rendered the chimera resistant to ubiquitination whilst having no apparent effect on targeting or recruitment functionalities. When co-expressed with TIR1, the mAID-nanobody technology was demonstrated to be a rapid, effective and robust approach to the degradation of GFP and GFP-like proteins. This method has not yet been demonstrated on endogenous proteins, which would show the breadth of its applicability and the requirement for a completely delysinated binder may hinder application in some instances.

Recently, a system utilizing whole antibody targeting for protein depletion has been developed which makes use of the cytosolic FcR/ E3 ligase TRIM21^{434,435}. Endogenously TRIM21 binds to the Fc regions of internalized antibodies bound with antigen and ubiquitinates the complex for degradation via its RING domain⁴³⁶. Through the microinjection of antibodies, TRIM21 can be co-opted to degrade cytosolic antigen in an antibody specific manner. The broad antibody isotype and species binding of TRIM21 enables researchers to select from the massive repertoire of available antibodies to degrade a broad range of antigens⁴³⁷. However, since the method relies upon microinjection, phenotypes must be determined in a single cell specific manner. This method is therefore not applicable with the majority of biochemical protein assay methods nor easily with whole organisms.

Detect and respond systems

Induced approximation is a common mechanism to control protein activation and signal transduction in the cell⁴³⁸⁻⁴⁴⁰. The principle of proximity mediated protein activation has been frequently applied in research to generate constructs capable of indicating protein presence, sensing interactions or eliciting cellular responses^{441,442}. Such constructs use effector proteins which have been either genetically split such that two halves are made which function only upon reunion, or which require enforced dimerisation to function⁴⁴³⁻⁴⁴⁷. Most frequently these techniques are used in the study of protein interactomics and function via the fusion of paired effector protein components to potential interaction partners. Effectors capable of reporter properties such as fluorescence, luminescence or cell survival are utilized and interactions between the POIs are inferred from these phenotypes (Figure 12a).

In an extension of this concept targeting subunits can be incorporated rather than potential interactors. This creates a detection type system whereby the function of two complementing effector-binder fusions is dependent upon their approximation via tandem binding to a tertiary target molecule. Such systems can be generated using nanobodies to detect both intracellular and extracellular antigens with both research and therapeutic aims^{150,151,448,449} (Figure 12b). Tang *et al* created T-DDOG and CRE-DOG, two systems which use nanobodies to bind paired epitopes on GFP to activate transcription factors or a split recombinase. When applied in organisms these systems permit spatial control of reporter gene transcription in a target dependent manner^{150,151}. Work in the Fussenegger laboratory has expanded the use of tandem binding vhh systems through the development of formats dependent upon the small molecules caffeine (C-STAR) and RR120 (GEMS)^{448,449}. These systems can detect antigen both extracellularly and intracellularly and have been shown to function with transcriptional activator pairs in addition to a selection of dimerizing signaling domains. In all, these techniques represent interesting methods for modifying cellular responses in a target dependent manner, they have been demonstrated with a broad selection of effectors and have strong potential to be generalized through the exchange of targeting domains.

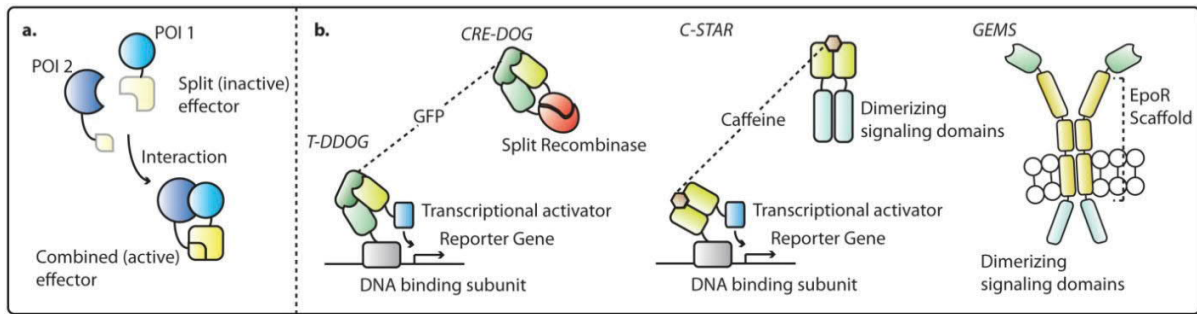


Figure 12. Proximity mediated protein activation. (a) The use of protein complementation technology in protein interactomics is illustrated. Using such systems the presence or absence of interaction between two proteins can be inferred through measurements effector output. (b) A selection of nanobody targeted sense and respond systems.

Diagnostic and Therapeutic Nanobody Applications

Many properties of nanobodies make them highly appealing as therapeutic and diagnostic reagents; their small size permits excellent tissue and tumor penetration^{83,450-452}; high stability allows for multiple routes of administration^{102,105,453-455} and the potential for non-cold chain handling; cleft and active site binding can be highly advantageous^{89,93}; properties including serum half-life and multi-specificity can be readily adjusted via fusions^{456,457}; microbial production is inexpensive; nanobodies can be conjugated or genetically fused with toxins, radionuclides and dyes³⁴¹; intracellular application is possible; and immunogenicity is often low, due both to the high natural analogy to human VH domains and further humanization measures⁷⁸.

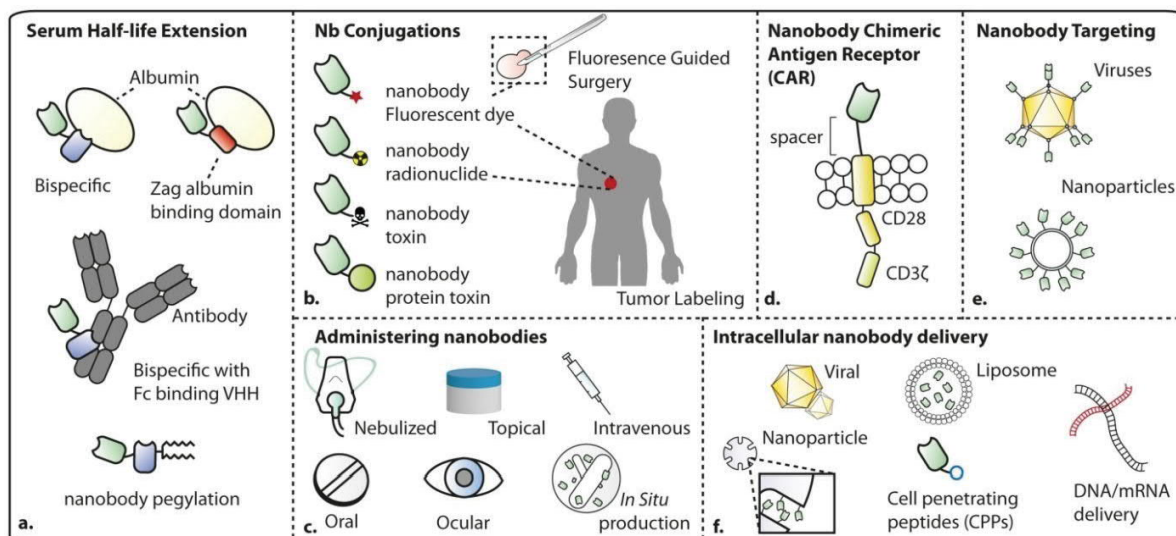


Figure 13. Therapeutic and diagnostic nanobody applications. (a) Technologies to modulate nanobody serum half-life are displayed. (b) Nanobody conjugates and fusions used therapeutically are shown. (c) Several mechanisms for the medicinal administration of nanobodies have been proposed or tested. (d) Nanobodies used in the CAR T-cell approach. (e) Nanobodies used to target large complexes for delivery. (f) Proposed mechanisms for the *in vivo* delivery of nanobodies.

Mechanisms of Nanobody Therapeutics and Diagnostics

Both proposed and realized nanobody therapeutics most frequently function by simple inhibitory modulation of their target. In this way; toxins can be neutralized⁴⁵⁸; receptors, channels and enzymes can be blocked^{361,363,459}; and cell surface interactors can be occupied^{460,461}. Conversely, the stimulation of targets by simple VHH binding, such as when GPCRs (G protein-coupled receptors) are locked in active conformations¹⁴⁸, also has great therapeutic potential. Indeed these mechanisms of agonist and antagonist target regulation have good pharmaceutical pedigree as the basis of the vast majority of small molecule pharmaceuticals.

One significant advantage of large molecule therapeutics over small molecule drugs is the breadth of potential targets. Whereas the current structural simplicity of chemical drugs limits potential drugging to an estimated 22% of human genes⁴⁶² and thereby renders many interesting targets ‘undruggable’⁴⁶³, the macromolecular complexity of protein reagents enables specific and high affinity binding of almost any target, including planar and convex surfaces, as well as the capacity to discriminate between highly similar molecules. This incredible aptitude for target recognition is a primary factor in the massive recent interest and investment in protein pharmaceuticals including monoclonal antibodies (MAbs)⁴⁶⁴.

In addition to inhibitory and stimulatory effects mediatable by single unmodified VHHs, a wealth of therapeutic potentials can be realized by the modular use of nanobodies within larger complexes. For example, nanobodies can act to approximate and activate structures; multivalent nanobodies have been demonstrated to activate cellular pathways through receptor approximation¹¹² and various multispecific formats can be used to re-route immune cells to eliminate targeted tumor cells⁴⁶⁵⁻⁴⁶⁹. VHHs can be applied to target other structures or molecules such as nanoparticles⁴⁷⁰⁻⁴⁷³, viruses^{474,475} and liposomes^{476,477}, as well as fused protein toxins and prodrug converting enzymes^{478,479}. If chemical drugs are conjugated, nanobodies can function as effective and well-defined antibody-drug conjugates⁴⁸⁰. Radionuclide addition forms molecular tracers which may enhance SPECT (single-photon emission computed tomography) or PET (Positron emission tomography) images and permit same-day imaging, such nanobodies can be applied as biomarker specific companion diagnostics, targeted radionuclide therapeutics (TRNT) or combined theranostics^{481,482}. The addition of far-red dyes can similarly facilitate diagnostic imaging, it may be useful for demarcating tumors during surgical excision and can enable photodynamic therapy (PDT)^{452,483-485}. As discussed, nanobodies are also well suited as components within synthetic receptors. One such therapeutic example is the implementation of binders into T cell chimeric antigen receptors (CARs)⁴⁸⁶⁻⁴⁸⁸. CAR T cells are a clinically validated immunotherapy format that use synthetically generated TCR alternatives targeted by antibody derivatives to recruit and activate T-cells in a disease specific manner⁴⁸⁹. Whilst CARs are commonly targeted by scFvs, nanobody targeting also appears to be highly effective and is suggested to be potentially advantageous owing to the high solubility of the VHH, preventing unwanted receptor aggregations, and its reduced gene size, which could be beneficial given the limited capacities of the retroviral vectors typically used to deliver CARs⁴⁹⁰⁻⁴⁹². Lastly, nanobodies do not include an antibody Fc region with which to engage immune machinery, therefore many downstream immune functions, such as ADCC (antibody-dependent cellular cytotoxicity), CDC (complement-dependent cytotoxicity) and ADPh (antibody-dependent phagocytosis), are unachievable. Since it is often therapeutically advantageous to utilize these mechanisms⁴⁹³, many groups have constructed hcAbs chimeras using human components and demonstrated effective restoration of these functions, albeit at the expense of enhanced extravasation and tissue penetration.

Numerous researchers have leveraged the capacity to express potential nanobody therapeutics *in situ* at the disease site. Such approaches could reduce pharmaceutical cost, ensure perpetual administration and assist in therapeutic specificity. Examples include; the use of tumor homing stem cells or bacteria to deliver anti-tumor VHH immunoconjugates or immune checkpoint inhibitors respectively^{455,494} and the

use of modified gut bacteria to express nanobodies against inflammatory disease, bacterial infections, toxins and viruses^{454,495}.

Nanobody Serum Half-life

Owing to their small size unmodified VHHs are rapidly cleared from the blood via glomerular filtration with typical serum half-lives in the order of 3-30 mins^{451,469}. Whilst this trait can be leveraged to assist rapid high contrast tumor labeling for the purposes of imaging⁴⁵¹, in many instances short serum half-life has a negative impact on therapeutic and diagnostic applications. Since the rate of glomerular filtration is strongly influenced by the hydrodynamic radius (HR) of a molecule^{496,497}, nanobody half-lives can be considerably extended by measures which increase this attribute⁴⁹⁸. In this way nanobody fusions, such as those previously discussed (Figure 5), can significantly enhance serum half-life in addition to extending binding capacities^{122,499}. In particular, sequentially fused nanobodies which feature a subunit capable of binding to a long half-life serum protein, such as albumin or an endogenous antibody Fc domain, can be especially effective^{500,501}. Piggybacking on such proteins in this way can extend serum circulation to days^{457,502} by both expanding the VHH HR and by inducing active renal recovery via the neonatal Fc receptor⁵⁰³. This strategy is a sufficiently promising strategy to be included in some nanobody formats currently undergoing clinical trial (ATN-103, ALX-0061, ALX-0761)^{502,504,505}. Pegylation is another highly effective and widely used strategy which can improve not only the serum half-life of a biopharmaceutical but also the solubility and stability^{498,506}. Pegylation called be applied via conjugation to purified nanobody and functions solely by increasing the HR of the protein⁵⁰⁷.

Therapeutic Applications of Nanobodies

Given the massive diversity and flexibility of potential nanobody therapeutic and diagnostic mechanisms, it's perhaps unsurprising that a correspondingly large panel of proposed applications run the gamut of human disease. Indeed nanobodies have been generated against pathogenic components of bacteria^{508,509}, viruses^{510,511}, parasites^{512,513}, prions⁵¹⁴, toxins^{515,516} and venoms^{517,518}, in addition to biomarkers and targets associated with autoimmune, ocular, skeletal, neurological⁵¹⁹⁻⁵²¹, cardiovascular⁵²² and respiratory disorders as well as cancers⁴⁸².

Presently 13 nanobodies are being trialed for therapeutic or diagnostic potential, a single VHH therapeutic has been approved and many more are at the pre-clinical stage (**table 1**)^{113,482,522}. Notably,

despite the large repertoire of SDBs targeting and modifying intracellular disease antigens, no ongoing clinical trial seeks to further these proposals.

	Biologic	Target	Application	Manufacturer	Status
	Cablivi Caplacizumab (ALX-0081)	Von Willebrand Factor (VWF)	Acquired Thrombotic thrombocytopenic purpura (aTTP)	Ablynx (Sanofi)	Approved
	Vobarilizumab (ALX-0061)	IL-6R	Rheumatoid Arthritis	Ablynx (Sanofi)	Phase II
	Ozoralizumab (ATN-103)	TNF- α	Rheumatoid Arthritis	Taisho	Phase II
	ALX-0171	Respiratory Syncytial Virus Fusion Protein	Respiratory Syncytial Virus	Ablynx (Sanofi)	Phase II
Therapeutics	ALX-0761 / M1095	IL-17A/IL-17F	Psoriasis	Merck	Phase I
	ALX-1141 / M6495	ADAMTS-5	Osteoarthritis	Merck	Phase I
	BI836880	VEGF/Ang2	Oncology	Boehringer Ingelheim	Phase I
	BI655088	CX3CR1	Chronic Kidney Disease	Boehringer Ingelheim	Phase I
	ALX-0141	RANKL	Osteoporosis	Ablynx (Sanofi)/ EddingPharm	Phase I
	CAM-H2 (TRNT)	HER2	Oncology	Camel-IDS	Phase I
	Nanobody CAR-T cells	BMCA	Oncology	The Pregene Biotechnology Company	Phase I
	Bispecific Nanobody CAR-T cells	CD19 CD20	Oncology	Henan Hualong Biotechnology Company	Phase I
Diagnostics	⁶⁸ Ga NOTA-Anti-HER2 VHH1	HER2	Oncology	Universitair Ziekenhuis Brussel	Phase II
	^{99m} Tc-NM-01	PD-L1	Oncology	NanoMab	Phase I

Table 1. sdAb clinical trials and approvals.

Protein delivery

The absence of antibody like intracellular biotherapeutics is likely in large part due to difficulties surrounding their cellular delivery. Whilst small molecule drugs can be designed to feature high membrane permeability coefficients^{523,524} and can therefore freely diffuse into cells, proteins and oligonucleotides are both too large and too charged to enter via diffusion. Aside from its potential therapeutic utility, protein delivery is also interesting for cellular research. Delivering protein rather than nucleic acids potentially permits more concise control over the quantity and timing of delivery since it is independent of mechanisms of transcription and translation. Additionally protein delivery can be useful in experiments with non-dividing and hard to transfect cells and is necessary for experiments using chemically modified proteins³¹⁷. Presently, protein delivery into *in vitro* cell populations can be performed using a range of methods including physical methods⁵²⁵ such as microinjection⁵²⁶, electroporation⁵²⁷ and hyperosmolarity⁵²⁸, as well as with commercial reagents which complex the protein with other molecules such as cationic peptides⁵²⁹, liposomes or lipoplexes⁵³⁰. Whilst the efficiencies of these methods in terms of transfection percentages can be above 90%, a degree of cellular toxicity is associated with many of these approaches and their application *in vivo* is significantly more complicated.

Cellular protein delivery *in vivo* is associated with a substantial number of considerations⁵³¹. Firstly, simply navigating the therapeutic to its target cell can be highly problematic. The capacity to reach that cell will be highly dependent upon local histology and may be affected by factors such as cell junction types, the vascularisation of the area, capillary permeability^{532,533}, interstitial pressure gradients⁵³⁴, cell distance to the capillary, and the nature of the intervening connective tissue^{535,536}. If administered intravenously then targeting will be further affected by properties of the protein complex in the blood including; the physicochemical stability of the delivered complex as well as its protease resistance⁵³⁷; and the serum half-life which can be affected by factors such as opsonisation⁵³⁸, kidney extravasation, and removal in the spleen and liver⁵³⁹⁻⁵⁴¹. Potential immune responses can also affect circulation and function as well as lead to harmful reactions⁵⁴². Additionally, a cell-specific targeting strategy may be necessary to reduce off-target loss of the therapeutic into incorrect cell types and decrease potential side effects⁵⁴³. Once a complex is approximated to its target cell it must also be capable of stimulating cellular uptake⁵⁴⁴. If a complex is internalized via endocytosis, then endosomal release of the complex must be triggered such that it reaches the cytoplasm⁵⁴⁵. Lastly, if the delivered protein is in complex with

other molecules a mechanism of intracellular specific dissociation may be also be required to free active protein⁵⁴⁶.

***In vivo* protein delivery technologies**

A large array of technologies has been developed for the purpose of addressing the challenges of *in vivo* cellular protein delivery. Such approaches can be broadly divided into those which permit the delivery of modified protein monomers and those which form larger macromolecular carrier complexes^{530,547}.

Genetically or chemically mediated covalent conjugation of cell penetrating peptides (CPPs), or more recently circular CPPs, to a protein is perhaps the most widely demonstrated method for the delivery of single units^{548,549}. Cationic CPPs utilized for protein delivery, are thought to interact with negatively charged components of the phospholipid bilayer and induce endocytosis of the CPP-POI fusion⁵⁴⁸. Alternatively, positive charge can instead be incorporated into a protein's surface by mutational residue exchange. A 'supercharged' form of the protein is thereby generated, which has been shown to enable membrane translocation presumably via the same mechanism⁵⁵⁰⁻⁵⁵². Lastly, researchers have demonstrated that some proteins are amenable to entry via fusion to certain bacterial pore forming toxins^{553,554}. Whilst such monomeric approaches may benefit from the possibility of high tissue penetration, due to their potentially small size a number of drawbacks may be associated with these approaches. They will for example be subject to serum half-life considerations which due to their simplistic nature they will have little capacity to modulate. In addition, whilst attempts have been made to improve tissue dependent uptake^{555,556}, these methods are generally not tissue specific owing to the ubiquitous nature of the surface molecules with which they interact, this could potentially be problematic both in terms of side effects and the quantity of therapeutic required to dose any given population. Lastly, research suggests that these methods achieve very modest cytoplasmic delivery efficiency due either to poor uptake or poor endosomal release and thus require high concentrations of delivery^{557,558}.

Protein delivery can also be performed using supramolecular complexes loaded with the desired protein. Potentially such complexes can be tailored to diminish some of the drawbacks of monomeric delivery although with the likely unavoidable disadvantage of reduced tissue penetration. Loading proteins into larger complexes allows their hydrophilicity and charge to be overridden by the properties of the overall complex. Complexes can then be constructed to promote desirable interactions with the cell membrane and may additionally be combined with molecules permitting cell targeting⁵⁵⁹,

environment responsive attributes⁵⁶⁰, serum half-life modulation and endosomal rupture⁵⁶¹. Such nanocarriers vary greatly in composition and can be; proteinaceous, including protein polymers⁵⁶² or engineered virus like particles(VLPs)⁵⁶³; formed of synthetic polymers⁵⁶⁴; based on lipids, such as liposomes⁵³⁰; designed carbon structures such as carbon nanotubes⁵⁶⁵; or composed of rigid inorganic frameworks such as gold⁵⁶⁶ or silica⁵⁶⁷.

Mesoporous Silica Nanoparticles

Mesoporous silica nanoparticles (MSNs) are structures of between 30-300 nm permeated by mesopores ranging in size and morphology^{568,569}. MSNs have a range of desirable properties which make them highly promising *in vivo* shuttles for various molecular cargoes and as a result they are presently the most investigated class of inorganic nanocarrier for nanomedicine⁵⁷⁰.

Using porous rather than planar surfaces has a dramatic effect on the surface area of a nanoparticle, surface area determines the quantity of exposed functional groups and thereby the loading capacity. In the case of MSNs, pores impart the silica structures with immense surface areas sometimes surpassing $1000\text{m}^2\text{g}^{-1}$ ⁵⁷¹. This results in exceptional loading capacities and contributes to MSNs carrying drug loads which can be a thousand times in excess of liposomes of equivalent size⁵⁷². In addition to this, molecules loaded into these pores benefit from a shielding effect against immune and protease machinery provided by the architecture of the nanoparticle⁵⁶⁷. A further advantage of silica nanoparticles is that they are biologically well tolerated. Silica is “generally regarded as safe” by the FDA and this safety is corroborated by studies showing MSNs to be highly biocompatible as well as biodegradable and non-immunogenic⁵⁷³⁻⁵⁷⁵. Whilst MSNs are versatile in terms of achievable shape, size and pore properties, careful manufacture delivers highly homogenous products, which is important for potential clinical application^{576,577}. Lastly, due to their flexible surface chemistry MSNs have been extensively combined with other molecules to deliver a large array of attributes making them highly adaptable for various delivery challenges^{571,578-581}.

The versatility of MSNs has led to their use for the delivery of a range of molecules; they have been frequently demonstrated to be amenable to targeted small molecule delivery, including drugs and dyes^{571,582}; the intracellular delivery of nucleic acids has been demonstrated using DNA and siRNA with variant MSNs^{582,583}; and numerous studies have documented cellular and tissue protein delivery with large pore MSNs⁵⁸⁴. *In vitro* cytosolic delivery has been demonstrated including the delivery of functional chromobodies^{317,585} and *In vivo* delivery to the endosomal system has also been performed using mice

^{586,587}. Unfortunately, a systematic optimisation of MSNs for intracellular protein delivery, including variance of morphological and functional traits, is absent from the literature and thus the true potential of the method has been difficult to estimate.


Results

Nanoparticle mediated delivery and small molecule triggered activation of proteins in the nucleus

METHODS



Nanoparticle mediated delivery and small molecule triggered activation of proteins in the nucleus

Hsin-Yi Chiu ^{a*}, Jack A. Bates ^{b*}, Jonas Helma^b, Hanna Engelke^a, Hartmann Harz ^b, Thomas Bein ^a, and Heinrich Leonhardt ^b

^aDepartment of Chemistry and Center for NanoScience (CeNS), Ludwig-Maximilians-Universität München (LMU), Munich, Germany;;

^bDepartment of Biology II and Center for NanoScience (CeNS), Ludwig-Maximilians-Universität München (LMU), Planegg-Martinsried, Germany

ABSTRACT

Protein transfection is a versatile tool to study or manipulate cellular processes and also shows great therapeutic potential. However, the repertoire of cost effective techniques for efficient and minimally cytotoxic delivery remains limited. Mesoporous silica nanoparticles (MSNs) are multi-functional nanocarriers for cellular delivery of a wide range of molecules, they are simple and economical to synthesize and have shown great promise for protein delivery. In this work we present a general strategy to optimize the delivery of active protein to the nucleus. We generated a bimolecular Venus based optical sensor that exclusively detects active and bioavailable protein for the performance of multi-parameter optimization of protein delivery. In conjunction with cell viability tests we maximized MSN protein delivery and biocompatibility and achieved highly efficient protein transfection rates of 80%. Using the sensor to measure live-cell protein delivery kinetics, we observed heterogeneous timings within cell populations which could have a confounding effect on function studies. To address this problem we fused a split or dimerization dependent protein of interest to chemically induced dimerization (CID) components, permitting control over its activity following cellular delivery. Using the split Venus protein we directly show that addition of a small molecule dimerizer causes synchronous activation of the delivered protein across the entire cell population. This combination of cellular delivery and triggered activation provides a defined starting point for functional studies and could be applied to other protein transfection methods.

ARTICLE HISTORY

Received 24 August 2018
Revised 4 September 2018
Accepted 5 September 2018

KEYWORDS

Biomolecular complementation; biosensor; controlled release; mesoporous silica nanoparticles; protein delivery; drug inducibility; small molecule control; split venus; nuclear proteins

Introduction


The cellular delivery of proteins is both a useful method to study cell pathways and a promising possibility for future medicine [1–4]. However, the toolkit for cost-effective and highly functional *in vitro* transfection remains limited, whilst challenges such as short protein serum half-life, inefficient cellular uptake and endosomal entrapment hinder delivery *in vivo*. Thus, advancements in protein delivery would be useful for cell research and are required to remove a major barrier to the implementation of potential therapies.

Mesoporous silica nanoparticles (MSNs) are a versatile nanocarrier format that has been used for the delivery of chemotherapeutic agents[5,6], oligonucleotides[7,8], and proteins[9–11]. MSNs feature a stable framework to load and shelter cargo

from proteases and the immune system and combine high cellular uptake efficiency with flexible surface functionalisation. Diverse surface conjugations permit augmentation of the nanoparticles to enable the modulation of serum half life, selective cell targeting and controlled drug release[12–17]. MSNs can be generated in large volumes at low financial and labor expenditure [18]. Having previously demonstrated the delivery of bioactive proteins using our large pore MSN variant [19] we sought to produce an optimized delivery protocol that maximizes efficiency whilst retaining good biocompatibility, i.e. the integrity and viability of cells. Beside cellular uptake efficiency, the general applicability of MSNs requires that delivered proteins escape the endosomes and retain their function[20].

CONTACT Heinrich Leonhardt  h.leonhardt@lmu.de; Thomas Bein  bein@lmu.de

*These authors have equally contributed to this article

 Supplemental data for this article can be accessed here.

© 2018 The Author(s). Published by Informa UK Limited, trading as Taylor & Francis Group.

This is an Open Access article distributed under the terms of the Creative Commons Attribution License (<http://creativecommons.org/licenses/by/4.0/>), which permits unrestricted use, distribution, and reproduction in any medium, provided the original work is properly cited.

Several techniques have been developed to quantify efficiencies of cellular protein delivery. The methods often exploit pre-existing cytoplasm to endosome differences such as pH[21], enzyme content[22], access to DNA[23], redox status[24–26] or localization[27] and some utilize the physical separation of the compartments to create exploitable distinctions between the two environments[28,29]. However, despite the advantages of each of these methods, many of these techniques do not provide a real-time readout, give a non-linear output due to amplification, transcription or recombination, give no indication of post-endosome protein functionality, rely on endpoint assays on entire batches of cells, or require complex image analysis. Quantifying delivery efficiencies of functional proteins in real-time still remains challenging. Recently, GFP-based bimolecular fluorescence complementation (BiFC) assays have been developed, consisting of two proteins derived from genetic splitting of a fluorescent protein that only fluoresce after complementation. BiFC assays have been successfully employed for the comparison of cell penetrating peptide (CPP) function and the assessment of antibody internalization [30–32]. They deliver a relative fluorescent readout which is ideal for optimization processes.

In this work, we develop a Venus based optical sensor and apply it to investigate and optimize *in vitro* MSN mediated bioactive protein delivery. We demonstrate how the sensor can be easily applied in conjunction with cell viability assays to optimize diverse aspects of delivery including; total protein transfection, population transfection percentages, cell-to-cell variation, biocompatibility and live-cell delivery kinetics. We demonstrate that large cell-to-cell variability can occur in the delivery of bioactive proteins. As functional studies greatly benefit from defined starting points, we aimed to add another level of control to allow for synchronous and tunable activation of proteins upon delivery.

Materials and methods

Materials

Tetraethyl orthosilicate (TEOS, Aldrich, $\geq 99\%$), (3-glycidyloxypropyl) trimethoxysilane (GPTMS,

Fluka, $\geq 97\%$), cetyltrimethylammonium p-toluene-sulfonate (CTATos, Sigma), triethanolamine (TEA, Aldrich, 98%), magnesium sulfate anhydrous (99.9%, Sigma), toluene anhydrous (Sigma), bi-distilled water obtained from a Millipore system (Milli-Q Academic A10). N(alpha),N(alpha)-bis(carboxymethyl)-L-lysine hydrate (NTA-lysine, Aldrich), sodium carbonate (Sigma), sodium bicarbonate (Sigma), nickel chloride hexahydrate (Riedel-de Haen), tris(hydroxymethyl)-aminomethane (TRIS, $\geq 99\%$, ROTH), acetic acid (99% – 100%, ROTH), thiazolyl blue tetrazolium bromide (MTT, $\geq 97.5\%$, Sigma), dimethyl sulfoxide molecular (DMSO, Applichem, biology grade), Dulbecco's Modified Eagle's Medium (DMEM, Sigma), Dulbecco's Phosphate Buffered Saline (PBS, Sigma), FBS Superior (Biochrom, S0615), Gentamycin solution (SERVA, 50 mg/ml), trypsin-EDTA solution (Sigma, T3924), Dulbecco's Modified Eagle's Medium – phenol red free (DMEM, Gibco), ethanol (EtOH, Aldrich, absolute).

Synthesis and functionalization of large pore MSNs

Un-functionalized MSNs were synthesized using a modification of a previously reported procedure [33]. In brief, a mixture of TEA (0.49 g, 3.3 mmol), CTATos (2.73 g, 6 mmol) and H₂O (144 g, 8 mol) was vigorously stirred (1250 rpm) at 80°C in a 250 ml glass flask until the solution became homogeneous. TEOS (20.83 g, 0.1 mol) was then added and the solution was continuously stirred (1250 rpm) at 80°C for another 2 h, afterwards the synthesized particles can be observed as whitening of the solution. The as-synthesized particles were collected by centrifugation (7000 × g, 15 min) and subsequently subjected to organic template extraction. The organic template extraction was carried out by heating particles in an ethanolic solution (150 mL) containing 3 g of ammonium nitrate at 90 °C under reflux for 1 h followed by a second reflux at 90 °C in a 2 M HCl/ethanolic solution (150 mL) for 1 h. The un-functionalized mesoporous silica nanoparticles (un-MSNs) were collected by centrifugation (7000 × g, 20 min) and were washed with water and EtOH after each extraction step.

To attach epoxy groups to the surface of the MSNs, a post-synthetic grafting procedure was performed. 500 mg of un-MSNs were de-hydrated under reflux (130 °C) in 150 mL of toluene in the presence of MgSO₄ for 4 h. GPTMS (190 mg, 0.83 mmol, 10 mol% of total silica) was subsequently added to the toluene solution, and the solution was stirred (500 rpm) at 130 °C for 2 h. After the solution had cooled to room temperature, the toluene was removed by rotary evaporator (77 mbar, 45 °C, 250 rpm). The resulting epoxy group-modified MSNs (MSN-Epoxy) were washed three times with 150 mL of EtOH and preserved in 50 mL of absolute EtOH. Centrifugation (7000 × g, 20 min) was used to collect particles after each washing step.

MSN-Epoxy particles were then modified to yield NTA-functionalized MSNs (MSN-NTA). 360 mg of MSN-Epoxy and 200 mg (0.6 mmol) of NTA-lysine were mixed in 10 ml of carbonate-bicarbonate buffer (100 mM, pH 9) and the mixture was stirred at RT overnight. The functionalized MSN-NTA particles were washed three times with 100 mL of tris-acetate (TA) buffer (pH 8) at RT and re-suspended in 36 mL of EtOH. Centrifugation (7000 × g, 20 min) was used to collect particles after each washing step. To immobilize Ni²⁺ on the surface of MSN-NTAs, 5 mg of MSN-NTA was dispersed in 5 ml of NiCl₂ (50 mM in H₂O) and stirred at RT for 4 h. The un-bound Ni²⁺ was washed out with H₂O (three times with 5 mL) and the particles were collected following centrifugation (17000 × g, 5 min). The final NTA-Ni complex modified MSNs (MSN-Ni) were stored in 5 mL of EtOH (MSN concentration: 1 mg/mL) for further use.

Characterization of MSNs

Scanning electron microscopy (SEM) and scanning-transmission electron microscopy (STEM) were performed at 30 kV on a Helios NanoLab G3 UC instrument (FEI, USA) with a detection system containing a TLD detector and a STEM ADF detector. A drop of EtOH diluted MSN suspension was dried on a carbon-coated copper grid at room temperature for several hours before SEM/STEM observation. Dynamic light scattering (DLS) measurements were performed on a Malvern Zetasizer-Nano instrument equipped with a 4 mW He-Ne laser (633 nm). Nitrogen

sorption analysis was performed on a Quantachrome Instrument NOVA 4000e at 77 K. Samples (15 – 20 mg) were degassed at 120 °C under vacuum (10 mTorr) one day before measurement. Pore size distribution curves were obtained based on non-local density functional theory (NLDFT) procedures provided by Quantachrome, using the adsorption branch of N₂ on silica.

Plasmid construction and deposition

A previously described pCAG mammalian expression vector containing an IRES-Blasticidin selection gene following the ORF was used for creation of the pCAG-FKBP-VN-T2A-mRFP cassette[34] (Figure 1a). The protein expression vector pET28a was used for FRB-VC-Histag expression (Figure 1b). The Gibson assembly method was applied for all cloning [35]. Plasmids have been deposited into the addgene repository (pCAG-FKBP-VN-T2A-mRFP: #100979, pET28a-FRB-VC-Histag: #100980).

FRB-VC protein purification

FRB-VC was expressed in *E. coli* (BL21 strain) and purified via affinity chromatography on a His-trap column. Expression was induced through addition of 0.5 mM of isopropyl beta-D-1-thiogalactopyranoside (IPTG, ROTH) and cells were further cultured at 18 °C overnight. Cells were harvested and lysed in PBS buffer containing 100 µg/ml of lysozyme (Serva, Germany), 2 mM of phenylmethanesulfonyl fluoride (PMSF, sigma) and 25 µg/ml of DNase (Applichem, Germany) followed by sonication (Branson® Sonifier; 16 × 8 sec, 20% amplitude). Cell debris was collected by centrifugation at 20000 × g for 30 min. Protein purification was performed using a manufacturers 8 M Urea purification protocol (Amersham Biosciences[36]) including renaturation of the protein via FPLC (Äkta Purifier Amersham Biosciences, GE Healthcare, USA) on a 1 ml His-trap column (GE Healthcare, USA). Elution was performed using an increasing imidazole gradient rather than the step-wise imidazole increase outlined in the protocol. Eluted protein was desalted using the PD-10 (GE Healthcare, USA) column and concentrated with an Amicon filter column (cut-off 10

kDa, Merck Millipore, Germany). Purified protein in PBS was aliquoted followed by shock-freezing and storage at -80°C .

FRB-VC protein loading to MSN-Ni

1 mg of MSN-Ni was mixed with 500 μg of FRB-VC protein in 500 μl of PBS at 4°C with shaking (400 rpm) for 1.5 h. The resulting MSN-FRB-VC complexes were collected by centrifugation ($3000 \times g$, 3 min), washed with PBS (1 mL per wash) twice, and re-suspended in 100 μl of PBS.

Cell culture and stable cell line

HeLa Kyoto cells[37] (HeLa k, a modified HeLa cell line characterized by little cell motility and thus suitable for live cell time-lapse imaging) were cultured in DMEM medium supplemented with 10% FBS and gentamycin (50 $\mu\text{g}/\text{ml}$ in cell culture medium) under 5% CO_2 at 37°C . To generate a cell line stably expressing the pCAG-FKBP-VN-T2A-mRFP construct, pCAG-FKBP-VN-T2A-mRFP was transfected into HeLa k cells using Lipofectamine 3000 reagent (Invitrogen). Blasticidin (10 $\mu\text{g}/\text{ml}$ in cell culture medium) was used to select cells between 48 h after transfection and 3 weeks. Highly mRFP fluorescent cells were then isolated via flow cytometry (FACS Aria II, BD Biosciences) to produce a monoclonal cell line (HeLa-FKBP-VN).

Intracellular protein delivery for MSN concentration optimization

HeLa-FKBP-VN cells in DMEM culture medium were seeded on either a 2-well ibiTreat slide (ibidi, Germany) or a 6-well plate (Corning, USA) at 50% confluency 12 h before the intracellular protein delivery experiment. MSNs loaded with FRB-VC proteins (MSN-FRB-VCs) in PBS were added to cell culture in a serum free DMEM and incubated with cells at 37°C for 2 h. Afterwards, the residual particles in the medium were washed out using PBS (1.5 mL per well) followed by a short chloroquine shock (0.5 mM in standard DMEM, 1.5 mL per well in cell culture medium, RT, 5 min) to trigger endosomal protein release. Cells were then incubated in fresh cell culture medium (phenol red

free). All the assays (live cell imaging, FACS analysis and fluorescence readout) were performed at 24 h post MSN-FRB-VCs addition. Images were acquired on an UltraVIEW VoX spinning disc system with laser line combiner (PerkinElmer) assembled with an inverted microscope (Axio Observer D1) using a 63x/1.4 NA Plan-Apochromat oil immersion objective (Zeiss). Images were acquired with an EMCCD camera (C9100-50, Hamamatsu). The microscope was equipped with a humidified and heated environmental chamber set to 37°C , 5% CO_2 (PeCon). Image acquisition was controlled by the program Volocity (ver. 6.3, PerkinElmer).

Flow cytometry

Cells were washed with PBS, detached from a 6-well plate using 0.25% Trypsin-EDTA and finally re-suspended in PBS (3 mL per well) prior to flow cytometry (FACS Aria II, BD Biosciences). Data were analyzed using FlowJo (8.1) software. Non-MSN treated HeLa-FKBP-VN-RFP cells were used to gate out dead cells and aggregates and to calibrate appropriate Venus (using FITC settings) and mRFP gating. Venus +ve and -ve cells were analyzed from the RFP +ve group. 10,000 cells were measured per sample. Experiments were triplicated. Error bars represent standard deviations. P values were obtained through application of two-tailed T-tests with unequal variances.

Microplate reader for cell fluorescence readout

Cells were detached from a 6-well plate using 0.25% Trypsin-EDTA, harvested and washed with PBS. After centrifugation ($150 \times g$, 5 min), cells were re-suspended in 100 μl of PBS and pipetted into a 96-well microplate (Greiner Bio-One, Germany). Fluorescence was measured using a microplate reader (Infinite[®] M1000 PRO, TECAN) with 515 nm excitation and 528 nm emission for Venus measurements and 556 nm excitation and 586 nm emission for RFP measurements. Four readings were taken per well. Background fluorescence in the Venus channel was measured using the stable cell line without addition of the complementing protein and subtracted from other readings. Measurements were

normalized against the RFP channel to account for variations in cell number. Experiments were performed in six biological repeats. Error bars represent standard deviations. P values were obtained through application of two-tailed T-tests with unequal variances.

MTT assay

One day prior to MTT assay HeLa Kyoto cells were plated on a 96-well microplate (5×10^3 cells per well) in DMEM and incubated at 37 °C. After removal of culture medium, cells were exposed to 100 µl of MSN-DMEM solution per well (serum free) with various concentrations, while the control group was incubated with 100 µl of serum-free DMEM. Following 2 h incubation, the cells were washed with PBS three times to remove the residual particles. Freshly prepared MTT solution (0.5 mg/ml in DMEM) was added to the cells (100 µl/well) and the cells were incubated at 37 °C for another 4 h. The purple crystals metabolized from healthy cells were then dissolved in 100 µl of DMSO and the absorbance was measured at 570 nm, while the reference absorbance was measured at 655 nm using a microplate reader (Infinite® M1000 PRO, TECAN). Experiments were triplicated. Error bars represent standard deviations. P values were obtained through application of two-tailed T-tests with unequal variances.

Protein delivery rate experiments

Rapamycin-primed sample

HeLa-FKBP-VN-RFP cells were seeded onto a 2-well ibi-Treat slide 12 h before the experiment. For the rapamycin-primed protein release tracking experiment, 1 µl of rapamycin (from 250 µM stock solution) and 100 µg of MSN-FRB-VC were mixed in 1 mL of serum-free DMEM, and the mixture was added to the cells before the first image was acquired. After 2 h, particles were washed away using PBS, followed by a chloroquine shock (0.5 mM of chloroquine in standard DMEM, 1.5 mL/well) at RT for 5 min triggering endosomal protein release. Cells were tracked at indicated time points for 24 h. Microscopic images were acquired with a Nikon TiE microscope equipped with perfect focus, Yokogawa CSU-W1

spinning disk unit (50 µm pinhole size), Andor ALC600 laser-beamcombiner: 405nm/488nm/561nm/640nm, Yokogawa CSU-W1 dichroic mirror 405/488/561/640 LD Quad, Andor Borealis illumination unit and Andor IXON 888 Ultra EMCCD camera using a Nikon CFI P-Apo 100x Lambda oil immersion objective NA 1.45. The setup was equipped with an environmental chamber (Okolab BIO 1, Bold Line CO₂ and temperature module, gas chamber and humidifying module) and controlled by software from Nikon (NIS elements, version 4.51.01). The environmental conditions during the experiment were set to 37 °C, 5 % CO₂ and humidified atmosphere. Focus drifts during the long-term experiments were compensated by the Nikon perfect focus system. Tiled images (10x10 image fields, 15 % overlap, stitched by NIS elements) were acquired throughout this study to investigate many cells per experiment. 4 color tiles (488 nm, 561 nm, 640 nm and differential interference contrast) were acquired with a frequency of 3 images per hour. On chip binning (2x2) was used throughout to reduce the data amount and to improve the signal to noise ratio. Fluorescence images were acquired with an exposure time of 1 s and an EM gain setting of 160. For the population protein delivery tracking analysis, a single large field area with 200 – 300 cells was assessed at each interval.

Rapamycin-delayed sample

For the Venus reconstitution kinetics tracking (rapamycin-delayed sample), 100 µg of MSN-FRB-VC were mixed in 1 mL of serum-free DMEM, and the mixture was added to the cells before the first image was acquired. After 2 h, particles were washed away using PBS, followed by a chloroquine shock. Cells were tracked at indicated time points using confocal microscopy (an UltraVIEW Vox spinning disc confocal system, PerkinElmer, UK). Rapamycin (1 µl, final conc. 250 nM in standard DMEM) was added to the sample 22 h after chloroquine shock. Live cell images were acquired at randomly chosen areas to prevent Venus fluorescence bleaching. 200 – 300 cells were imaged and counted at each time point. Venus positive cells were counted visually. Venus positive cells in % correspond to the number of nuclei with Venus

fluorescence divided by the number of cells with RFP fluorescence * 100.

Single cell fluorescence tracking

Tracking of fluorescent intensity within single cells was performed on images acquired using a Nikon TiE microscope utilized as outlined above. Rapamycin-primed (250 nM rapamycin applied with MSNs) and delayed experiments (250 nM rapamycin added 24 hs after MSNs) were performed. Fiji software was used to analyze images. A circular ROI of consistent size was used to measure fluorescence in cell nuclei. The ROI was positioned in the nucleoplasm excluding the darker nucleoli. Measurements were taken until mitosis of the cell occurred or imaging ended.

Results

To develop a controllable BiFC sensor we used the chemically inducible dimerization (CID) components FKBP/FRB[38] that form a heterodimer in the presence of rapamycin[39]. For BiFC we selected the split Venus fluorescent protein (split 154/155) based on its high fluorescence signal, rapid maturation at 37 °C and low auto-complementation[40,41]. Our overall approach is outlined in Figure 1. In brief, we fused the N-terminal portion of Venus (VN) with FKBP and added a c-Myc nuclear localization signal (NLS)[42] to facilitate subsequent image analyses (Figure 1(a)). For expression control and calibration we added an mRFP which follows a T2A peptide[43]. The T2A induces ribosomal skipping which enables the synthesis of two proteins (FKBP-VN and mRFP) from one transcript. A blasticidin resistance gene was included to assist in the selection and maintenance of a monoclonal stable cell line (HeLa-FKBP-VN), which was used for all subsequent studies. The complementary half of the BiFC/CID complex (Figure 1(b)), consisting of a His-tagged FRB domain fused to the C-terminal half of Venus (VC), was bacterially expressed, purified by affinity chromatography and loaded into the MSNs for cellular delivery (Figure 1(c)).

Following endocytosis of FRB-VC loaded MSNs (MSN-FRB-VC)[44], carrier and cargo proceed through the endosomal system where decreasing

pH causes dissociation of His-tagged FRB-VC from the MSN. Endosomal rupture is triggered using chloroquine[19] and FRB-VC is released to the cytosol. FRB-VC diffuses to the nucleus and interacts with FKBP-VN, which is primed for dimerization with pre-bound rapamycin. This ternary complex formation (FKBP-rapamycin-FRB) approximates the two Venus halves, promotes complementation and enables chromophore maturation. Thus, successful protein delivery can then be monitored as Venus fluorescence in the nucleus, which concentrates the signal, facilitates automated image analysis and improves the signal to noise ratio.

Large-pore MSNs were surface-functionalized with NTA-Ni complexes (MSN-Ni) through a series of modifications (Figure 2(a)) to accommodate pH dependent binding and release of the His-tagged FRB-VC[10,11,19]. STEM and SEM images (Figure 2(b)) indicated that the resulting nitrilotriacetic acid-modified MSNs (MSN-NTAs) exhibit uniform particle size and coral surface morphology with irregular pore shape (pore size ranging from 10 – 40 nm) consistent with the structure of the un-functionalized form (Figure S1). These particle characteristics were confirmed by dynamic light scattering (DLS) (Figure 2(c)) and N₂ sorption analyses (Figures 2(d,e)) and are summarized in Table S1.

To optimize protein delivery we first tested different particle concentrations. As expected, the HeLa-FKBP-VN cell line by itself and the addition of unloaded MSNs did not yield any Venus fluorescence while MSN-FRB-VC complexes led to clear nuclear signals (Figure 3(a), Figure S2). Successful protein delivery can be conveniently quantified in cell populations with microplate fluorometry, as the formation of Venus fluorescence requires endosomal escape and release of functional proteins. Whilst a significant increase ($p = 0.004$) in protein delivery is seen between the 50 µg/ml and 100 µg/ml concentrations, the fluorescent signal plateaued at higher concentrations (Figure 3(b)). We then measured protein transfection rates, i.e. the fraction of cells with a clear fluorescence signal, by flow cytometry and again found a significant increase from 50 µg/ml to 100 µg/ml concentrations ($p = 0.016$) indicating some dose dependency, with higher concentrations having no further positive effect (Figure 3(c)). MTT

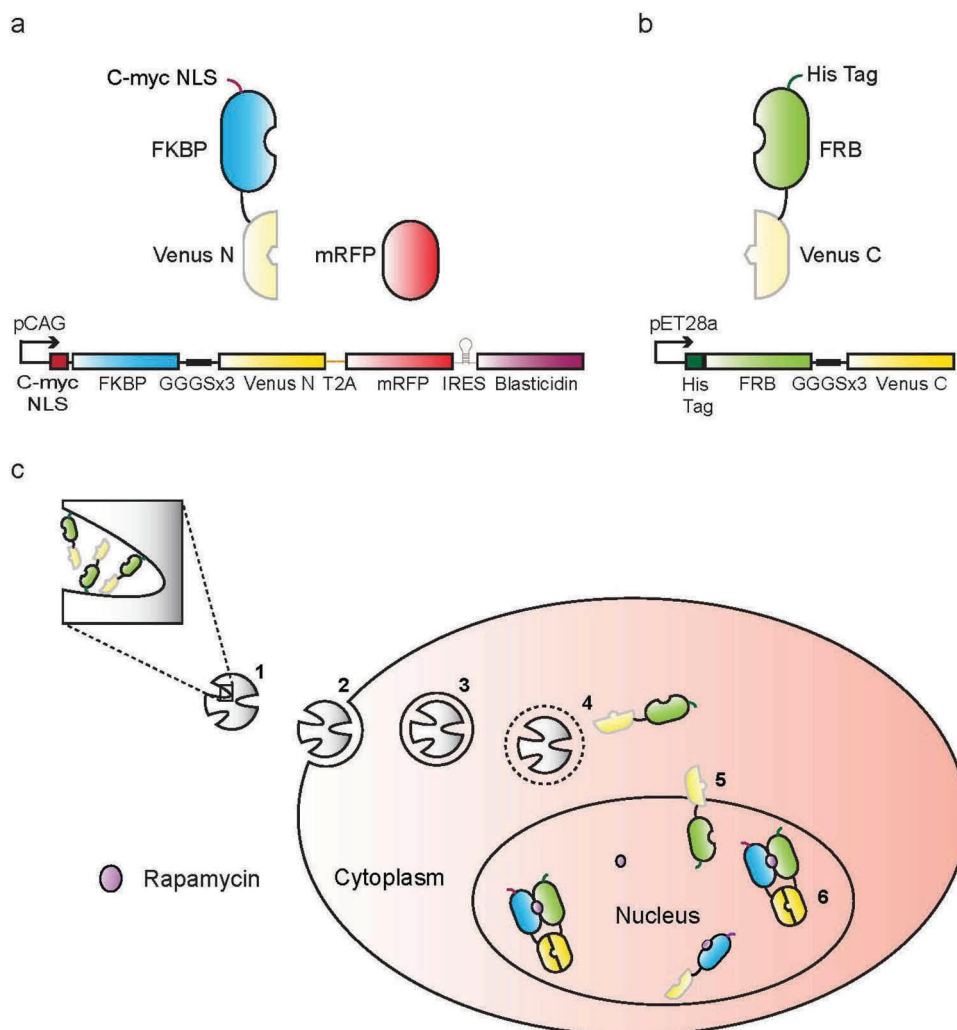


Figure 1. A two-component protein delivery sensor. Layouts of the: **a** mammalian expression cassette and **b** bacterial expression cassette are shown. **c** MSN-mediated protein delivery sensing. **1** His-tagged FRB-VC proteins are loaded into MSNs via surface Ni-NTA complexes. **2** Charged MSN-FRB-VCs bind to HeLa-FKBP-VN cell surfaces and are **3** endocytosed. Lower pH in the endosomal system causes accelerated FRB-VC dissociation from the MSN. **4** Chloroquine shock triggers endosomal protein release followed by **5** free diffusion of FRB-VCs into the nucleus. **6** Addition of rapamycin leads to the formation of FRB/rapamycin/FKBP ternary complexes driving Venus complementation and fluorophore maturation.

assays were performed in parallel to assess possible cytotoxicity. Results indicated that nanoparticle additions up to 100 $\mu\text{g/ml}$ did not affect cell viability. However, increased cytotoxicity was observed with higher particle concentrations of 150 $\mu\text{g/ml}$ and 200 $\mu\text{g/ml}$ (Figure 3(d)). Based on these three data sets, we selected 100 $\mu\text{g/ml}$ as the optimal MSN concentration to obtain high protein delivery efficiency with low cytotoxicity.

To monitor protein delivery in single cells, we imaged live cell populations with spinning disc microscopy over time. We first incubated rapamycin primed HeLa-FKBP-VN cells with MSN-FRB-VC complexes (100 $\mu\text{g/ml}$) and imaged

before and after chloroquine shock. While no Venus fluorescence was detected before the chloroquine shock, first signals became visible in nuclei of about 1% of the cells within 30 min after chloroquine mediated endosome rupture, surpassed 50% after 5.5 h and reached 85% at 9 h (Figure 4(a)). A live cell image of protein release taken 10 h post chloroquine shock shows yellow fluorescent nuclei, i.e. successful protein delivery, in most cells (Figure 4(c)). Time-lapse videos covering the entire time course of protein delivery into hundreds of cells show this cell-to-cell temporal variability of nuclear fluorescence onset over 24 h (movie 1).

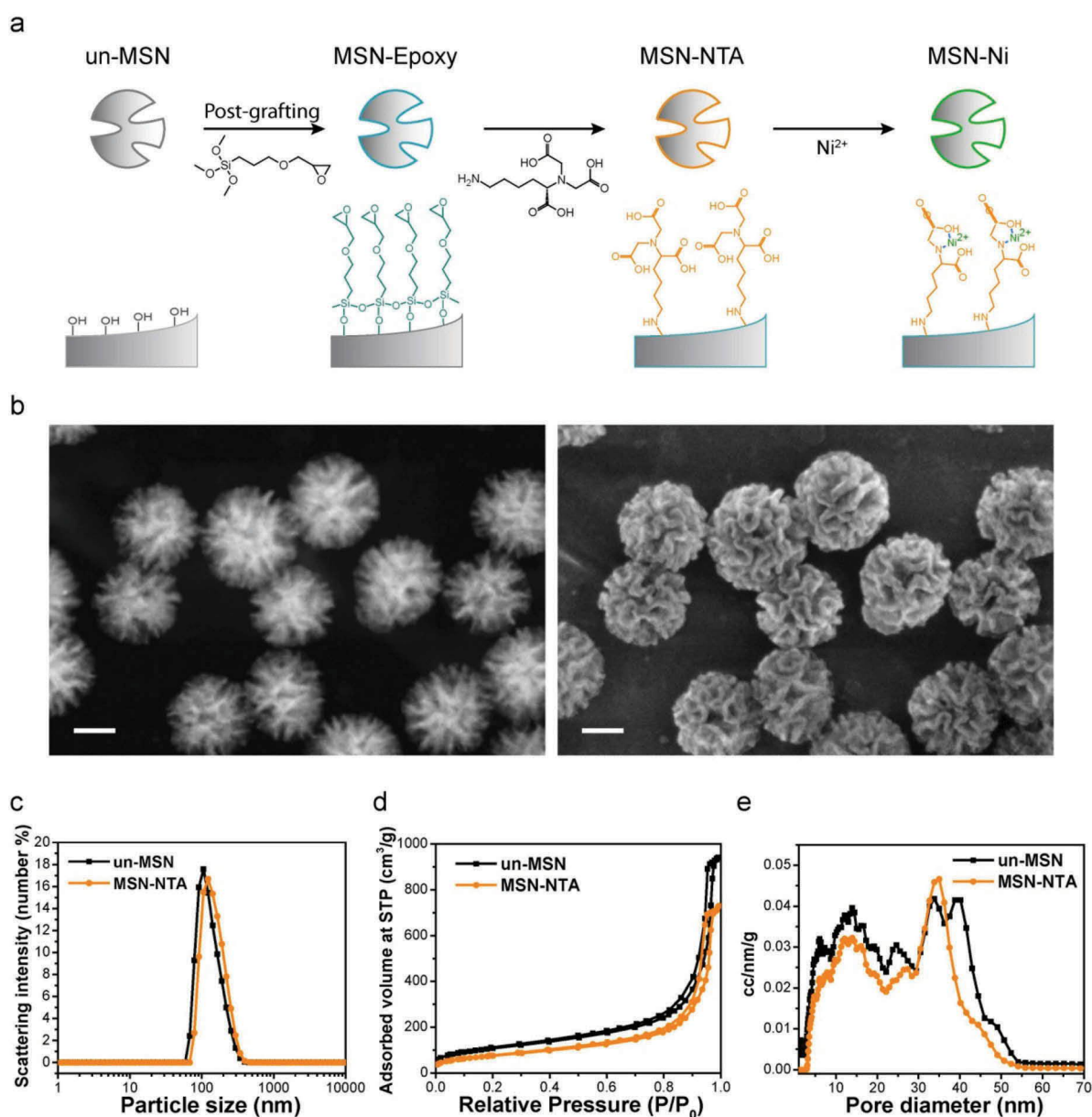


Figure 2. Synthesis and characterization of MSNs for controlled binding and release of His-tagged protein. **a** Surface modification series of un-functionalized MSNs (un-MSNs) to MSN-Ni. **b** STEM (left) and SEM (right) images of MSN-NTAs, scale bar: 50 nm. Characterization of un-MSNs and MSN-NTAs: **c** dynamic light scattering, **d** N₂ sorption isotherms and **e** pore size distribution calculated via NLDFT mode.

To address this cell-to-cell temporal variability we incubated cells with MSN-FRB-VC and added rapamycin (250 nM) 22 h after chloroquine shock (Figure 4(b)). We reasoned that at this point the protein was likely already released in the majority of the cells and therefore the timing of Venus fluorescence should represent sensor complex formation and maturation rather than protein release. The comparison of both experimental conditions shows that while in rapamycin primed cell populations the onset of nuclear fluorescence occurred

over a period of 10 hours, the later addition of rapamycin caused a synchronous onset within 1–2 h within the majority of cells monitored by live cell microscopy (Figures 4(a,b)). Also, the quantification of fluorescence in single cells over time shows the heterogeneity in fluorescence increase in the rapamycin primed cells as opposed to the synchronous increase of fluorescence in the cells with delayed rapamycin addition (Figures 4(d,e)). The heterogeneous fluorescence onset and increase in the rapamycin primed cells suggests

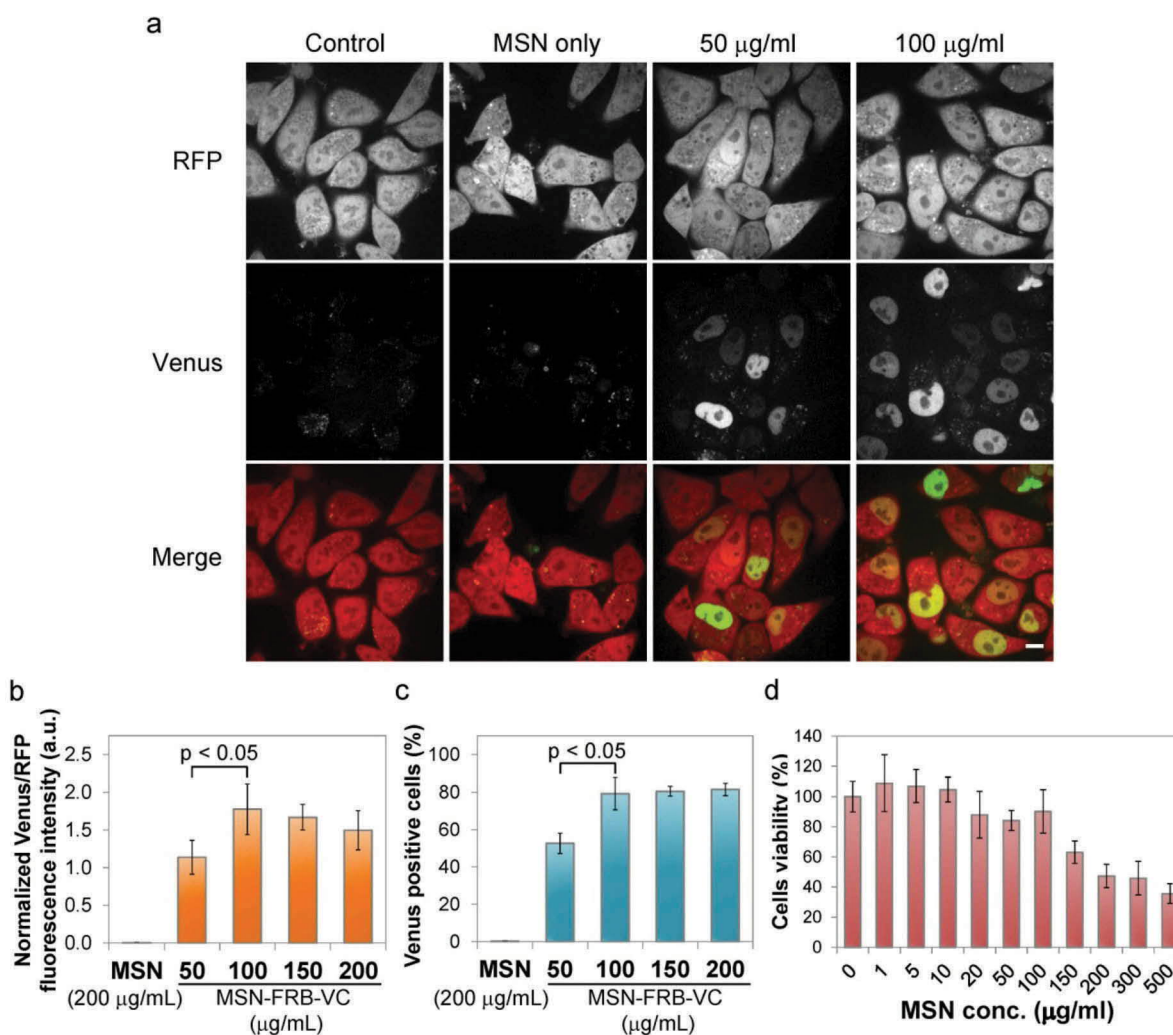


Figure 3. Optimization of MSN-mediated protein delivery. Different MSN-FRB-VC concentrations were incubated with HeLa-FKBP-VN cells. **a** Live-cell images were taken 20 h post endosomal protein release induction. *Scale bar: 10 µm.* **b** Population fluorescence was measured using a microplate reader. **c** Flow cytometry measured protein transfection rate. **d** MTT assays assessed cytotoxicity of un-MSNs. Error bars represent SDs.

that endosomal rupture may continuously occur even several hours after transient chloroquine shock. Consistently, we observe enlarged endosomes even 15 h after chloroquine shock indicating prolonged endosomal rupture over many hours (Figure S3). Unlike sensors that rely upon transcription or other amplification mechanisms, the ratio-metric nature of the BiFC sensor enables cell-to-cell variation measurements not only between but also within populations (Figure 4(f)). With image analysis, parameters such as the range of protein released within a cell population as well as means and standard deviations can be determined. Clearly, the combination of protein delivery with subsequent activation methods, like the

bimolecular complementation triggered here by rapamycin, provides a defined starting point for functional studies.

Discussion

The BiFC sensor described in this study makes it possible to simultaneously monitor the time course of protein delivery and cellular responses in thousands of cells over hours and days. The lack of any signal amplification mechanism limits the maximal sensitivity of the BiFC sensor, but due to its ratio-metric nature enables cell-to-cell variation measurements. In consideration of the significance of cellular protein stoichiometry this should be a

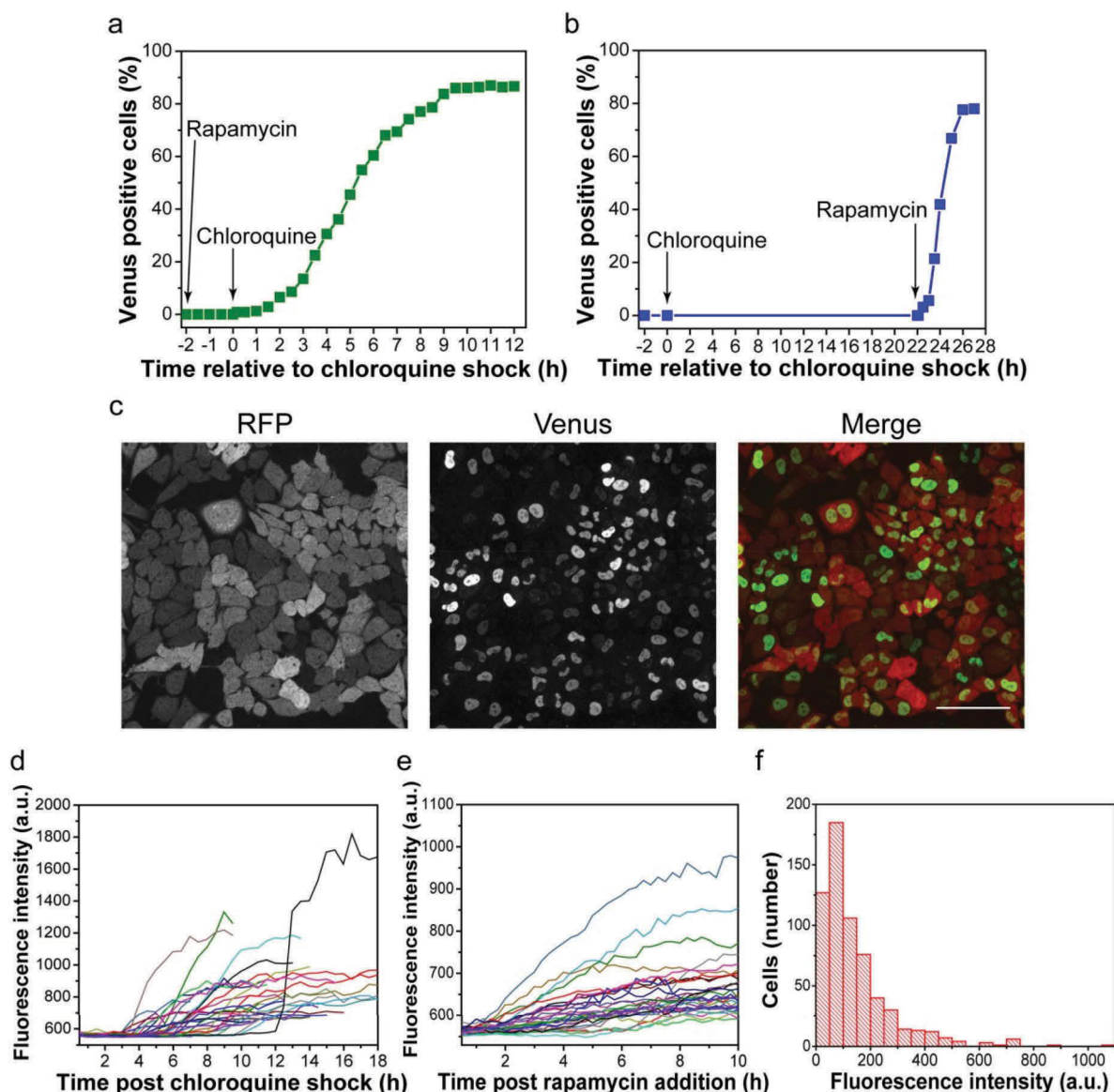


Figure 4. Live cell tracking of protein release. **a** MSN-FRB-VCs were added to rapamycin primed HeLa-FKBP-VN cells at time point -2 h and live cell imaging began. Following chloroquine shock at 0 h cells were imaged and analyzed for Venus nuclear fluorescence rates for a further 12 h. **b** MSN-FRB-VCs and chloroquine were applied as above. Delayed rapamycin addition (22 h after chloroquine shock) triggered synchronous activation of delivered protein, cell imaging and analysis of Venus fluorescence continued for 5 h. **c** A live cell image of the rapamycin-primed sample 10 h after chloroquine shock. Scale bar: $100\ \mu\text{m}$. Fluorescence intensity tracking from 30 cells in **d** rapamycin-primed and **e** rapamycin-delayed samples. **f** Fluorescence intensity distribution among 625 cells in a rapamycin-primed sample analyzed at 15 h post chloroquine shock.

useful attribute for understanding and adapting nanocarriers for various tasks.

Fluorescent live cell delivery tracking revealed a variable timing of bioavailability upon addition of MSNs, indicating that cellular uptake and intracellular release of functional proteins varies from cell to cell by several hours. This temporal heterogeneity in direct protein delivery experiments complicates

functional studies. One possible solution is protein splitting and addition of controllable dimerization modules that allows for delivery of inactive protein halves over longer time intervals and subsequent activation by chemical induction across cell populations. Our results show that the delivery of inactive protein halves in combination with the chemically inducible dimerization components FKBP/FRB allow for

rapamycin triggered functional complementation and thus provide a defined starting point for functional studies and enable the controlled manipulation of cellular functions.

The focus of this study was on the delivery process and therefore only one half of the split protein was delivered and the other half was produced by genetic means in the recipient cells, but as single MSNs can carry multiple molecules and single cells can uptake multiple MSNs, also mixtures of proteins can be delivered. To be able to quantify the rate and efficiency of delivery we used a split fluorescent protein (Venus) which is only one of a rapidly growing list of proteins that can be split and then functionally complemented. Therefore, this approach could easily be extended to a large number of proteins through either trial and error or based on structural information and should be applicable to single globular domains as well as multidomain proteins [45,46].

Conclusions

In summary, we have developed an inducible two-component fluorescent live cell sensor to track and optimize protein delivery with respect to efficiency, bioavailability and biocompatibility. We propose that the system described here is well suited for multi-parameter optimization and the comparison of different protein nanocarriers. We demonstrate that large pore MSN-Nis are capable of non-toxic nuclear delivery in up to 80% of a cell population whilst requiring only a his-tag for protein loading. In light of these properties as well as the prevalent use of his-tags for protein purification we suggest that MSN-Nis are good candidates for widespread cell research use. Finally, we have shown that small molecule controlled bimolecular complementation can be used for synchronous activation of delivered proteins in cell populations and provide a defined start point for functional studies.

Acknowledgments

The authors thank Dr. Steffen Schmidt for technical assistance with the STEM/SEM microscopy.

Disclosure statement

No potential conflict of interest was reported by the authors.

Funding

Financial support from the Deutsche Forschungsgemeinschaft (SFB 1032 and SPP1623/LE721/13), the Center for Nano Science (CeNS) and the Excellence Cluster Nanosystems Initiative Munich (NIM) is gratefully acknowledged.

Availability of data and materials

All data generated or analyzed during this study are included in this published article and the Additional information files.

Plasmids for the production of sensor proteins and cell lines are available through addgene repository (pCAG-FKBP-VN-T2A-mRFP: #100979, pET28a-FRB-VC-Histag: #100980).

ORCID

Hsin-Yi Chiu  <http://orcid.org/0000-0002-2922-2606>
 Jack A. Bates  <http://orcid.org/0000-0003-2910-6485>
 Hartmann Harz  <http://orcid.org/0000-0003-1218-2107>
 Thomas Bein  <http://orcid.org/0000-0001-7248-5906>
 Heinrich Leonhardt  <http://orcid.org/0000-0002-5086-6449>

References

- [1] Mitragotri S, Burke PA, Langer R. Overcoming the challenges in administering biopharmaceuticals: formulation and delivery strategies. *Nat Rev Drug Discov.* 2014 Sep;13(9):655–672. .PubMed PMID: 25103255; PubMed Central PMCID: PMC4455970.
- [2] Leader B, Baca QJ, Golan DE. Protein therapeutics: a summary and pharmacological classification. *Nat Rev Drug Discov.* 2008 Jan;7(1):21–39. .PubMed PMID: 18097458.
- [3] Herce HD, Schumacher D, Schneider AFL, et al. Cell-permeable nanobodies for targeted immunolabelling and antigen manipulation in living cells. *Nat Chem.* 2017 Aug;9(8):762–771. . PubMed PMID: 28754949.
- [4] Roder R, Helma J, Preiss T, et al. Intracellular delivery of nanobodies for imaging of target proteins in live cells. *Pharm Res.* 2017 Jan;34(1):161–174. PubMed PMID: 27800572.
- [5] Xu R, Zhang G, Mai J, et al. An injectable nanoparticle generator enhances delivery of cancer therapeutics. *Nat Biotechnol.* 2016 Apr;34(4):414–418. PubMed PMID: 26974511.
- [6] van Rijt SH, Bolukbas DA, Argyo C, et al. Protease-mediated release of chemotherapeutics from mesoporous silica nanoparticles to ex vivo human and mouse

- lung tumors. *ACS Nano*. 2015 Mar 24;9(3):2377–2389. .PubMed PMID: 25703655.
- [7] Moller K, Muller K, Engelke H, et al. Highly efficient siRNA delivery from core-shell mesoporous silica nanoparticles with multifunctional polymer caps. *Nanoscale*. 2016 Feb 21;8(7):4007–4019. PubMed PMID: 26819069.
- [8] Dengler EC, Liu J, Kerwin A, et al. Mesoporous silica-supported lipid bilayers (protocells) for DNA cargo delivery to the spinal cord. *J Control Release*. 2013 Jun 10;168(2):209–224. PubMed PMID: 23517784; PubMed Central PMCID: PMC4013798.
- [9] Kilpelainen M, Riikonen J, Vlasova MA, et al. In vivo delivery of a peptide, ghrelin antagonist, with mesoporous silicon microparticles. *J Controlled Release: off J Controlled Release Soc*. 2009 Jul 20;137(2):166–170. PubMed PMID: 19345247.
- [10] Han DH, Na HK, Choi WH, et al. Direct cellular delivery of human proteasomes to delay tau aggregation. *Nat Commun*. 2014;5:5633. .PubMed PMID: 25476420.
- [11] Chen YP, Chen CT, Hung Y, et al. A new strategy for intracellular delivery of enzyme using mesoporous silica nanoparticles: superoxide dismutase. *J Am Chem Soc*. 2013 Jan 30;135(4):1516–1523. PubMed PMID: 23289802.
- [12] Slowing II, Vivero-Escoto JL, Wu CW, et al. Mesoporous silica nanoparticles as controlled release drug delivery and gene transfection carriers. *Adv Drug Deliv Rev*. 2008 Aug 17;60(11):1278–1288. PubMed PMID: 18514969.
- [13] Lu J, Liang M, Li Z, et al. Biocompatibility, biodistribution, and drug-delivery efficiency of mesoporous silica nanoparticles for cancer therapy in animals. *Small*. 2010 Aug 16;6(16):1794–1805. PubMed PMID: 20623530; PubMed Central PMCID: PMC4013798.
- [14] Vivero-Escoto JL, Slowing II, Trewyn BG, et al. Mesoporous silica nanoparticles for intracellular controlled drug delivery. *Small*. 2010 Sep 20;6(18):1952–1967. PubMed PMID: 20690133.
- [15] Heidegger S, Gossel D, Schmidt A, et al. Immune response to functionalized mesoporous silica nanoparticles for targeted drug delivery. *Nanoscale*. 2016 Jan 14;8(2):938–948. PubMed PMID: 26659601.
- [16] Watermann A, Brieger J. Mesoporous silica nanoparticles as drug delivery vehicles in cancer. *Nanomaterials (Basel)*. 2017 Jul 22;7(7). DOI:10.3390/nano7070189. PubMed PMID: 28737672; PubMed Central PMCID: PMC5535255.
- [17] Shi J, Hou S, Huang J, et al. An MSN-PEG-IP drug delivery system and IL13Ralpha2 as targeted therapy for glioma. *Nanoscale*. 2017 Jul 6;9(26):8970–8981. PubMed PMID: 28443896.
- [18] Chiu H-Y, Leonhardt H, Bein T. Synthesis and functionalization of ordered large-pore mesoporous silica nanoparticles for biomedical applications. *Chemie Ingenieur Technik*. 2017;89(7):876–886.
- [19] Chiu HY, Deng W, Engelke H, et al. Intracellular chromobody delivery by mesoporous silica nanoparticles for antigen targeting and visualization in real time. *Sci Rep*. 2016;6:25019. .PubMed PMID: 27173765; PubMed Central PMCID: PMC4865863.
- [20] Varkouhi AK, Scholte M, Storm G, et al. Endosomal escape pathways for delivery of biologicals. *J Controlled Release: off J Controlled Release Soc*. 2011 May 10;151(3):220–228. PubMed PMID: 21078351.
- [21] Qian Z, Martyna A, Hard RL, et al. Discovery and mechanism of highly efficient cyclic cell-penetrating peptides. *Biochemistry*. 2016 May 10;55(18):2601–2612. PubMed PMID: 27089101.
- [22] Loison F, Nizard P, Sourisseau T, et al. A ubiquitin-based assay for the cytosolic uptake of protein transduction domains. *Mol Therapy: Journal Am Soc Gene Ther*. 2005 Feb;11(2):205–214. PubMed PMID: 15668132.
- [23] D'Astolfo DS, Pagliero RJ, Pras A, et al. Efficient intracellular delivery of native proteins. *Cell*. 2015 Apr 23;161(3):674–690. PubMed PMID: 25910214.
- [24] Cheung JC, Kim Chiaw P, Deber CM, et al. A novel method for monitoring the cytosolic delivery of peptide cargo. *J Controlled Release: off J Controlled Release Soc*. 2009 Jul 1;137(1):2–7. PubMed PMID: 19285529.
- [25] Eiriksdottir E, Mager I, Lehto T, et al. Cellular internalization kinetics of (luciferin-)cell-penetrating peptide conjugates. *Bioconjug Chem*. 2010 Sep 15;21(9):1662–1672. PubMed PMID: 20684543.
- [26] Hallbrink M, Floren A, Elmquist A, et al. Cargo delivery kinetics of cell-penetrating peptides. *Biochim Biophys Acta*. 2001 Dec 01;1515(2):101–109. PubMed PMID: 11718666.
- [27] Holub JM, Larochelle JR, Appelbaum JS, et al. Improved assays for determining the cytosolic access of peptides, proteins, and their mimetics. *Biochemistry*. 2013 Dec 17;52(50):9036–9046. PubMed PMID: 24256505; PubMed Central PMCID: PMC4006873.
- [28] Verdurmen WP, Luginbuhl M, Honegger A, et al. Efficient cell-specific uptake of binding proteins into the cytoplasm through engineered modular transport systems. *J Controlled Release: off J Controlled Release Soc*. 2015 Feb 28;200:13–22. . PubMed PMID: 25526701.
- [29] Chao TY, Raines RT. Fluorogenic label to quantify the cytosolic delivery of macromolecules. *Mol Biosyst*. 2013 Mar;9(3):339–342. .PubMed PMID: 23340874; PubMed Central PMCID: PMC4013798.
- [30] Milech N, Longville BA, Cunningham PT, et al. GFP-complementation assay to detect functional CPP and protein delivery into living cells. *Sci Rep*. 2015;5:18329. .PubMed PMID: 26671759; PubMed Central PMCID: PMC4680871.

- [31] Kim JS, Choi DK, Park SW, et al. Quantitative assessment of cellular uptake and cytosolic access of antibody in living cells by an enhanced split GFP complementation assay. *Biochem Biophys Res Commun.* 2015 Nov 27;467(4):771–777. PubMed PMID: 26482850.
- [32] Schmidt S, Adjobo-Hermans MJ, Wallbrecher R, et al. Detecting cytosolic peptide delivery with the GFP complementation assay in the low micromolar range. *Angewandte Chemie.* 2015 Dec 7;54(50):15105–15108. PubMed PMID: 26515694.
- [33] Zhang K, Xu LL, Jiang JG, et al. Facile large-scale synthesis of monodisperse mesoporous silica nanospheres with tunable pore structure. *J Am Chem Soc.* 2013 Feb 20;135(7):2427–2430. PubMed PMID: 23363241.
- [34] Chen T, Ueda Y, Dodge JE, et al. Establishment and maintenance of genomic methylation patterns in mouse embryonic stem cells by Dnmt3a and Dnmt3b. *Mol Cell Biol.* 2003 Aug;23(16):5594–5605. PubMed PMID: 12897133; PubMed Central PMCID: PMC36327.
- [35] Gibson DG, Young L, Chuang RY, et al. Enzymatic assembly of DNA molecules up to several hundred kilobases. *Nat Methods.* 2009 May;6(5):343–345. PubMed PMID: 19363495.
- [36] Hancock K, Biosciences A Life science news, cited 2015 Dec 8. Available from: https://www.gelifesciences.com/gehcls_images/GELS/Related%20Content/Files/1314729545976/litdoc18115403p14_16_20161013210347.pdf
- [37] Landry JJ, Pyl PT, Rausch T, et al. The genomic and transcriptomic landscape of a HeLa cell line. G3 (Bethesda). 2013 Aug;3(8):1213–1224. PubMed PMID: 23550136; PubMed Central PMCID: PMC3737162.
- [38] Choi J, Chen J, Schreiber SL, et al. Structure of the FKBP12-rapamycin complex interacting with the binding domain of human FRAP. *Science.* 1996 Jul 12;273(5272):239–242. PubMed PMID: 8662507.
- [39] Banaszynski LA, Liu CW, Wandless TJ. Characterization of the FKBP.rapamycin.FRB ternary complex. *J Am Chem Soc.* 2005 Apr 6;127(13):4715–4721. . PubMed PMID: 15796538.
- [40] Nagai T, Ibata K, Park ES, et al. A variant of yellow fluorescent protein with fast and efficient maturation for cell-biological applications. *Nat Biotechnol.* 2002 Jan;20(1):87–90. PubMed PMID: 11753368.
- [41] Shyu YJ, Liu H, Deng X, et al. Identification of new fluorescent protein fragments for bimolecular fluorescence complementation analysis under physiological conditions. *Biotechniques.* 2006 Jan;40(1):61–66. PubMed PMID: 16454041.
- [42] Dang CV, Lee WM. Identification of the human c-myc protein nuclear translocation signal. *Mol Cell Biol.* 1988 Oct;8(10):4048–4054. PubMed PMID: 3054508; PubMed Central PMCID: PMC365473.
- [43] Donnelly ML, Hughes LE, Luke G, et al. The ‘cleavage’ activities of foot-and-mouth disease virus 2A site-directed mutants and naturally occurring ‘2A-like’ sequences. *J Gen Virol.* 2001 May;82(Pt 5):1027–1041. PubMed PMID: 11297677.
- [44] Oh N, Park JH. Endocytosis and exocytosis of nanoparticles in mammalian cells. *Int J Nanomedicine.* 2014;9(Suppl 1):51–63. .PubMed PMID: 24872703; PubMed Central PMCID: PMC4024976.
- [45] Shekhawat SS, Ghosh I. Split-protein systems: beyond binary protein-protein interactions. *Curr Opin Chem Biol.* 2011 Dec;15(6):789–797. .PubMed PMID: 22070901; PubMed Central PMCID: PMC3237955.
- [46] Stynen B, Tournu H, Tavernier J, et al. Diversity in genetic in vivo methods for protein-protein interaction studies: from the yeast two-hybrid system to the mammalian split-luciferase system. *Microbiol Mol Biol Rev.* 2012 Jun;76(2):331–382. PubMed PMID: 22688816; PubMed Central PMCID: PMC3372256.

Supplemental: Nanoparticle mediated delivery and small molecule triggered activation of proteins in the nucleus

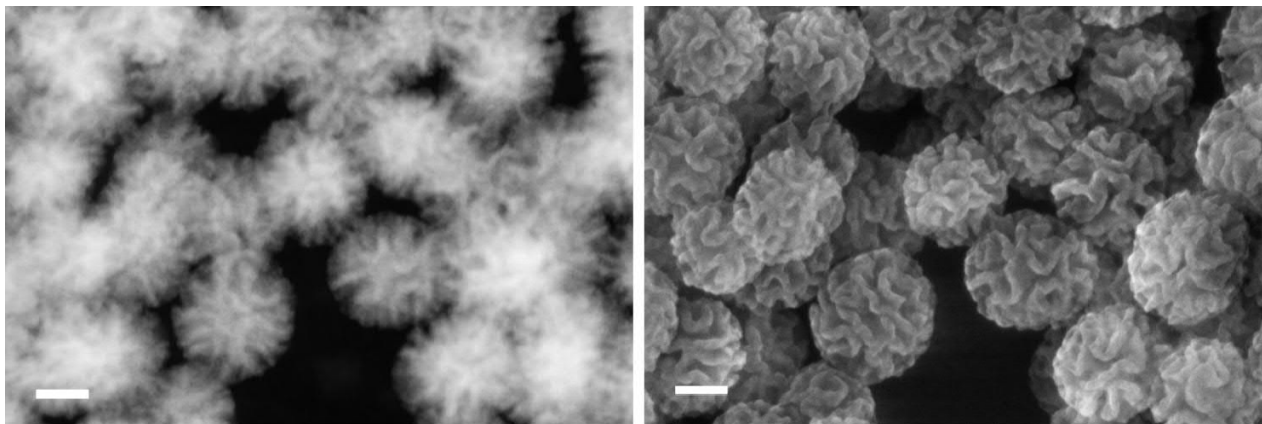


Figure S1. STEM (left) and SEM (right) images of un-functionalized MSNs. *Scale bar: 50 nm.*

Sample	Particle size (nm)	Pore size distribution (nm)	Pore volume (cm ³ /g)	Surface area (m ² /g)
Un-MSN	133 ± 50	4 - 45	1.4	390
MSN-NTA	152 ± 54	4 - 40	1.1	275

Table S1. Summary of characterization data of un-MSNs and MSN-NTAs.

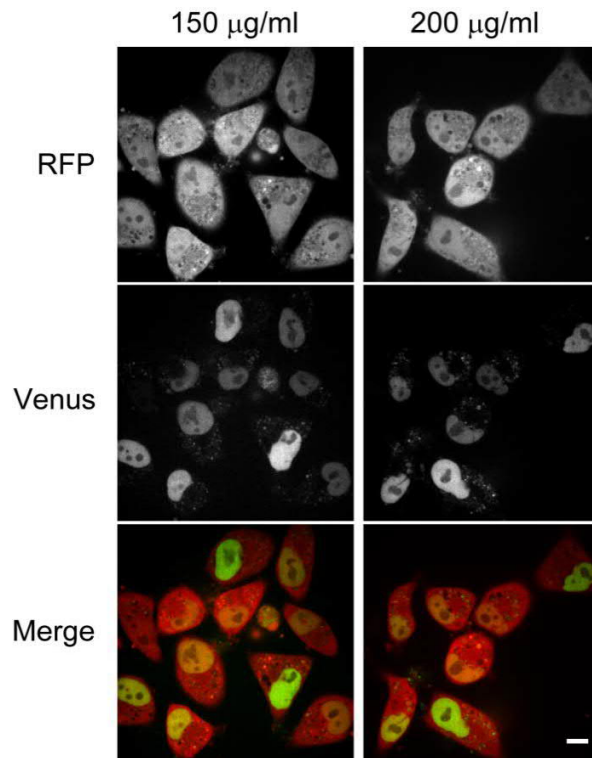


Figure. S2 Live cell confocal imaging of MSN-mediated intracellular protein delivery in the cytosolic protein delivery detection system. HeLa-FKBP-VN cells were incubated with 150 $\mu\text{g/ml}$ and 200 $\mu\text{g/ml}$ of MSN-FRB-VC, respectively, and images were taken 20 h post endosomal release trigger (chloroquine shock). *Scale bar: 10 μm .*

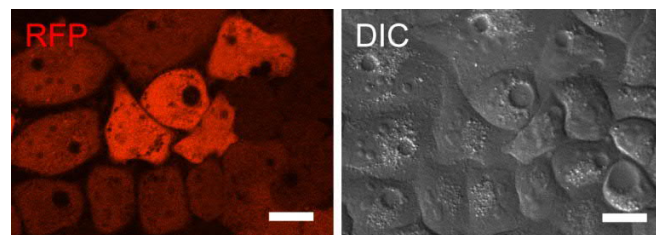


Figure. S3 Live cell images at 15 h post chloroquine shock. Swollen vesicles can be observed in cells after 15 h of chloroquine shock. *Scale bar: 10 μm .*

Tunable light and drug induced depletion of target proteins

ARTICLE

<https://doi.org/10.1038/s41467-019-14160-8>

OPEN

Tunable light and drug induced depletion of target proteins

Wen Deng ¹, Jack A. Bates¹, Hai Wei¹, Michael D. Bartoschek ¹, Barbara Conrad¹ & Heinrich Leonhardt ^{1*}

Biological processes in development and disease are controlled by the abundance, localization and modification of cellular proteins. We have developed versatile tools based on recombinant E3 ubiquitin ligases that are controlled by light or drug induced heterodimerization for nanobody or DARPIn targeted depletion of endogenous proteins in cells and organisms. We use this rapid, tunable and reversible protein depletion for functional studies of essential proteins like PCNA in DNA repair and to investigate the role of CED-3 in apoptosis during *Caenorhabditis elegans* development. These independent tools can be combined for spatial and temporal depletion of different sets of proteins, can help to distinguish immediate cellular responses from long-term adaptation effects and can facilitate the exploration of complex networks.

¹Department of Biology II, Ludwig-Maximilians-Universität München, Munich, Germany. *email: h.leonhardt@lmu.de

The cellular abundance of proteins is determined by transcription, translation and degradation, each of which may be targeted for functional studies. Genetic methods, including the recent variants of gene editing, are precise and versatile but not dynamic, which may over time provoke cellular adaptations and complicate functional analyses¹. In contrast, the transient and tunable methods targeting specific mRNAs, mostly by RNA interference, are less efficient and not suited for stable proteins with little natural turnover² or maternally provided proteins. Therefore, current protein knockdown techniques, directly target proteins of interest (POIs) with the cellular ubiquitin-proteasome system (UPS), mainly using two strategies. Degradation domains or degrons, which are protein fragments mediating degradation of protein, were genetically fused to POIs to control their stabilities^{3–12}. Alternatively, the mammalian F-box protein, which is a component of the SCF E3 ubiquitin ligase complex, was directed with a GFP binding vhh4 nanobody¹³ to degrade fluorescent fusion proteins¹⁴. Recently, the auxin-induced protein degradation system was generalized by combining the auxin-induced degron (AID) and GFP binding nanobody to degrade GFP fusion protein controllably¹⁵. In these cases, the stability of POIs can be dynamically controlled with small molecules (like auxin or Shield-1), but targeted destruction requires prior genetic engineering to render POIs susceptible.

Targeting endogenous proteins has been demonstrated with the Trim-Away method^{16,17}, which is based on the TRIM21 E3 ubiquitin ligase. TRIM21 binds antibodies and ubiquitinates their bound antigens marking them for proteasomal degradation. Here the need for genetic manipulations is replaced by physical microinjection of purified antibodies, which requires specialized equipment and sustained depletion requires repeated injections. Alternatively, ubiquitin ligases and POIs may be bound and connected with bi-functional small molecules named proteolysis targeting chimera (PROTAC)¹⁸, which bypasses the need for genetic engineering but requires selection and chemical engineering of cell permeable small molecules with dual binding specificity.

The goal of this study is to develop versatile toolsets for efficient and controlled depletion of tagged as well as untagged endogenous target proteins in cells and organisms. To study complex cellular systems it is desirable to have inducible tools for defined starting points and reversibility to monitor the response to transient interference. Any system should be tunable to gradually control protein levels, to probe stoichiometric requirements and to define rate-limiting levels. To address redundancies and interdependencies it would be helpful to target sets of proteins in freely selectable temporal and spatial combinations. Here, we present light and drug-controlled depletion tools that can be used in combination to control cellular levels of two or more sets of proteins.

Results

Screening E3 ubiquitin ligases for protein depletion. For ubiquitination, proteins are recognized and bound by the substrate binding part of specific E3 ubiquitin ligases, which ligate ubiquitin to the substrate proteins via their catalytic domain. As a general strategy we replaced the native substrate binding domain of E3 ubiquitin ligases with recombinant binding modules to direct the ubiquitin ligase activity to selected target proteins and mark them for depletion. For optimal efficiency we first tested and compared the catalytic activity of different types of E3 ubiquitin ligase domains, including F-box, BTB, RING, and HECT domains. To be able to directly monitor depletion efficiency we chose a green fluorescent fusion protein (GFP-CXXC4, GFP fused to the N-terminus of CXXC-type zinc finger protein 4) as a test

target and fused the ligase domains with the GFP binding nanobody GBP1 (GFP binding protein 1)¹³. Ligase fusions were introduced into HeLa cells stably expressing the target (GFP-CXXC4) and fluorescence was monitored by microscopy or FACS. The side-by-side comparison of ubiquitin ligase constructs showed varying reductions in fluorescence intensities with the RING domain of LNX1 protein (RING^{Lnx1}) functioning most effectively and reaching depletion efficiencies of more than 95% (Supplementary Fig. 1a, b). Similarly, a second target protein (GFP-PCNA, GFP fused to Proliferating Cell Nuclear Antigen protein) was also most efficiently depleted with the RING^{Lnx1} (Supplementary Fig. 1c). Based on sequence alignments and the crystal structure of the TRAF6 RING domain¹⁹, we tried to further shorten the RING^{Lnx1} domain; however, the shorter construct (RING^{Lnx1 sh}) failed to degrade the target (GFP-PCNA), indicating that the RING^{Lnx1} domain is optimal for protein depletion (Supplementary Fig. 1d, e). Compared to other tested domains, RING^{Lnx1} was the smallest and most efficient (Supplementary Fig. 1f); therefore, we chose this E3 ubiquitin ligase domain for further tool development.

Development of a light induced protein depletion tool. To be able to control and finetune the targeted ubiquitination, we separated target binding from catalytic activity and fused them to light sensitive heterodimerization modules. Upon short exposure to blue light the conformation of the light responsive protein changes and thereby triggers heterodimer formation. This light induced heterodimerization brings together the target binding nanobody and the ubiquitin ligase domain to mark proteins of interest (POIs) for degradation (Fig. 1a). For the implementation of light induced protein depletion (LiPD), we tested two protein pairs, iLID/SspB²⁰ and CIBN/CRY2²¹, which dimerize upon blue light triggered conformational change. As the kinetics of light induced dimerization (LiD) and especially the dissociation rate might be critical for specific applications, we measured these parameters with live cell microscopy. In brief, one half (iLID or CIBN) was anchored at a defined subcellular site, the cell membrane or focal nuclear replication sites via a GFP binding nanobody, and the enrichment of the corresponding other half (SspB or CRY2, respectively) was monitored over time (Supplementary Fig. 2). In comparison, the CIBN/CRY2 pair seemed more efficient in the recruitment of proteins at the cell membrane with dissociation half times of about 5 min (Supplementary Fig. 2a, b). We further tested the CIBN/CRY2 dimerization pair in the nucleus using replication protein PCNA as anchoring structures (Supplementary Fig. 2c). The fine punctate pattern of these PCNA-labeled replication foci clearly shows the rapid recruitment of the PHR domain of CRY2 (PHR^{CRY2}) within a few seconds after light exposure (Supplementary Fig. 2d and Movie 1). Quantitative analysis of several cells showed a slow dissociation of PHR^{CRY2}-mCh with a half time of about 6 min (Supplementary Fig. 2e). While the short-lived iLID/SspB dimer might be of advantage for some applications, we chose the more efficient and stable CIBN/CRY2 dimerization pair for subsequent protein depletion experiments.

We then tested different configurations and combinations of the CIBN/CRY2 dimerization pair and the protein targeting/depletion modules to optimize the LiPD system. We found that the GBP1-PHR^{CRY2}/RING^{Lnx1}-CIBN combination showed the best depletion of GFP-PCNA upon light induction (Supplementary Fig. 3a, b). Of the tested GFP binding nanobodies, GBP1 performed best in depletion of GFP-PCNA (Supplementary Fig. 3c) and was chosen for subsequent experiments. Transient co-expression of these optimized components enabled rapid depletion of GFP-PCNA after light induction and caused a GFP

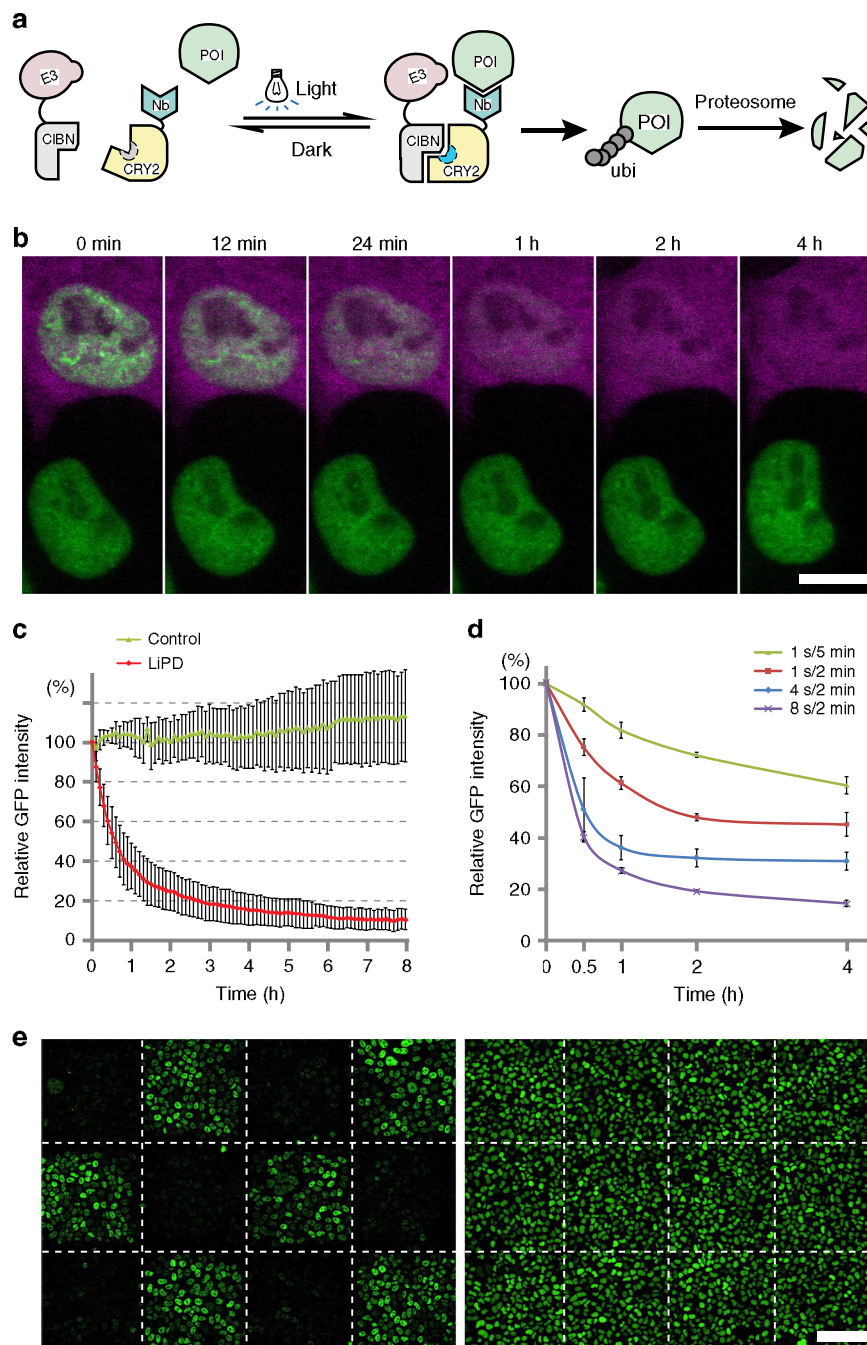


Fig. 1 Light induced protein depletion. **a** Schematic representation of the light induced protein depletion tool. Short light pulses trigger a conformational switch in Cryptochrome 2 (CRY2) and thus allow heterodimerization with CIBN (cryptochrome-interacting basic-helix-loop-helix 1 N-terminus). The light induced heterodimerization brings together the nanobody bound protein of interest (POI) and the E3 ubiquitin ligase (E3) causing ubiquitination and depletion of the target protein. E3 RING domain of E3 ubiquitin ligase, Nb Nanobody, POI protein of interest, ubi ubiquitin. **b** Light treatment induced rapid depletion of the target protein (in green) in cells containing the LiPD system (magenta) but not in control cells. Scale bar is 10 μm . **c** Depletion kinetics of GFP-CXXC4 with the LiPD system. For LiPD cells, $n = 27$; for control cells, $n = 16$. Intensity values are shown as mean \pm SD. **d** Tunable regulation of GFP-CXXC4 abundance across a whole-cell population with diverse illuminating programs using an LED lightbox. Biological triplicates were measured; Intensity values are shown as mean \pm SD. **e** Spatial control of protein depletion with the LiPD system. Stable LiPD/GFP-CXXC4 cells were exposed to a chess board pattern of light, leading to depletion of GFP-CXXC4 in the illuminated squares (left). GFP-CXXC4 cells without LiPD system were treated using the same lightening program to exclude loss of fluorescence due to photobleaching (right). Scale bar is 100 μm .

signal decrease to about 20% of the initial intensities within 4 h (Supplementary Fig. 3d, e and Movie 2).

To enhance the efficiency of the LiPD, we aimed for a stable and balanced stoichiometry between the two components by expressing them with similar promoters (mouse and rat EF1a promoters) on a single vector, which can easily be integrated into

the genome via the piggyBac transposon (Supplementary Fig. 3f). We inserted the LiPD system into the GFP-CXXC4-expressing cell line. Without light induction, stable expression of the LiPD system caused only a slight reduction (about 3%) of the fluorescence, which might be due to ambient light during cell culture and spontaneous heterodimer formation (Supplementary

Fig. 3g, h). After light induction, GFP-CXXC4 levels decreased quickly, but not in cells without the LiPD system (Fig. 1b, and Supplementary Movie 3). Quantitative imaging showed that depletion of the GFP fusion protein was rapid and could be observed immediately after light induction, with a half depletion time of about 30 min (Fig. 1c). GFP-CXXC4 was depleted to a level below 10% in cells with the LiPD (Fig. 1c), indicating a fast and efficient regulation of protein abundance in living cells. To apply this LiPD technology to other cellular targets, we generated a LiPD cell line and inserted GFP at the endogenous *CENPA* locus by a CRISPR/Cas9 mediated gene editing and recombineering technology²² (Supplementary Fig. 4a, b). Also in this case, live cell imaging showed a fast and almost complete depletion of GFP-CENPA after light illumination (Supplementary Fig. 4c, d and Movie 4). Since the GFP knock-in was heterozygotic, only half of the cellular CENPA was GFP-tagged and depleted after light induction, thus no mitotic defect was observed during the whole imaging period.

To control proteostasis across large cell populations, we constructed a simple LED lightbox, which can be programmed to expose cells in culture dishes to 470 nm light at defined time intervals (Supplementary Fig. 5a). The lightbox was first tested by monitoring the induction of dimerization between the LiD protein pairs (Supplementary Fig. 5b, c) and then the depletion of GFP-CENPA protein (Supplementary Fig. 5d, e). To test whether the GFP fusion protein levels can be tuned and continuously regulated with light, the LiPD/GFP-CXXC4 cell line was treated with different illumination programs (Supplementary Fig. 5f), and fluorescence intensities of the whole-cell populations were measured with a fluorescence reader at different time points. With these illumination programs, the GFP fusion protein was depleted with different kinetics down to amounts ranging from 20 to 70% of the initial values, indicating a dose-dependent regulation of proteostasis across the cell population (Fig. 1d).

Besides this dose and time control, the physical nature of the LiPD system also offers spatial control. To explore this option, light induction was applied in a chess board pattern to the GFP-CXXC4 cells with stably integrated LiPD. This patterned illumination resulted in a local depletion of the targeted GFP fusion protein, which demonstrates efficient spatial control of protein levels and allows the direct side-by-side comparison with neighboring non-depleted cells (Fig. 1e).

Development of drug-induced protein depletion. To obtain a second tool that can be used independently or in combination with this LiPD system, we developed a drug-induced protein depletion (DiPD) tool. We utilized a chemically induced dimerization (CID) pair to bring the targeting and destruction modules into close proximity. Similar to the LiPD, the POI is contacted by a specific targeting module that is fused with one half of the CID pair. Upon drug addition, this targeting module heterodimerizes with the destruction module via the complementary CID half causing the POI to be ubiquitinated and thus marked for proteasomal degradation (Fig. 2a). Three CID pairs, induced with abscisic acid (ABA)²³, gibberellic acid (GA-3)²⁴, or rapamycin²⁵, were tested but only the rapamycin induced FKBP/FRB pair showed efficient depletion of the POI (Supplementary Fig. 6a). To optimize the efficiency of the FKBP/FRB-based DiPD system we tested different configurations and linker lengths. The direct comparison showed that the target (GFP-PCNA) was most efficiently depleted by the GBP5-FKBP connected via a 2× or 3× GGGS linker (Supplementary Fig. 6b, c). Analogous to the LiPD, the two optimized DiPD parts were placed in a piggyBac transposon vector for efficient transposase mediated genome

integration (Supplementary Fig. 6d). To control for possible protein depletion caused by the single components, the E3 ligase or rapamycin, GFP-PCNA cells were transfected with the E3FRB catalytic construct (without the FKBP part) and then treated with rapamycin. The comparison shows that all three components for catalysis, targeting, and induction are required for efficient protein depletion (Supplementary Fig. 6e). To systematically test the performance of the DiPD, the DiPD piggyBac vector was integrated in a HeLa cell line stably expressing GFP-PCNA. Firstly, we examined whether the stably expressed DiPD system itself disturbs the abundance of cellular GFP-PCNA. The GFP-PCNA cells with DiPD were mixed with cells lacking the system, and imaged for high-throughput analysis. The comparison with control cells shows that in the absence of rapamycin induction the stable expression of DiPD does not affect GFP-PCNA levels (Supplementary Fig. 6f).

To test the dose dependency of protein depletion, we incubated the cells with different rapamycin concentrations for 12 h and then measured average GFP-PCNA intensities in bulk with a fluorescence plate reader. Already 10 nM rapamycin was sufficient to deplete the target protein below 50% and higher concentrations (50 and 250 nM) achieved a depletion to less than 10% of the original protein levels (Fig. 2b). As no adverse side-effects, such as cell death, cell cycle arrest, or abnormal morphological changes, were observed, we chose 250 nM for subsequent applications and the corresponding time course images showed no detectable target protein after 8 h (Fig. 2c).

Next, we tested the DiPD with a stable protein and chose nuclear LaminA (LMNA), which has a reported half-life of about 4 d in cultured cells²⁶. In mouse embryonic fibroblast (MEF) cells, the stably expressed GFP-LMNA was rapidly degraded with a half depletion time of about 1 h and within 4 h more than 95% of the target protein was depleted while no loss was detected in cells without DiPD (Fig. 2d, e and Supplementary Movie 5).

To evaluate the sustainability and reversibility of DiPD, we tracked GFP fluorescence intensities in cells cultured in the presence of rapamycin or with rapamycin withdrawn after 24 h. The cellular GFP-PCNA could be maintained at the barely detectable level of below 10% in the presence of rapamycin and gradually recovered after removal of rapamycin, demonstrating both sustainable and reversible depletion of the POI (Fig. 2f).

Besides nuclear proteins, we also tested the DiPD system for depletion of cytosolic proteins like the Isocitrate dehydrogenase 1 (IDH1) which catalyzes the decarboxylation of isocitrate. We generated a HeLa cell line expressing GFP-IDH1 together with the DiPD system. Upon rapamycin induction, a rapid depletion of the cytosolic GFP-IDH1 was observed (Supplementary Fig. 7). Similarly, another cytoplasmic enzyme adenosylhomocysteinase (AHCY) could be depleted via the DiPD system within an even shorter time period, demonstrating efficient degradation of cytoplasmic proteins with the DiPD system. Likewise, we tested different type of transmembrane proteins for depletion with the DiPD system. We could show inducible depletion of the C-terminal GFP fusion of three-prime repair exonuclease 1 (TREX1) protein, which localizes on the endoplasmic reticulum (ER) membrane via a single transmembrane helix and of the inner nuclear membrane MAN1 protein, which utilizes a double transmembrane helices. In addition, we demonstrated depletion of the Lamin B receptor (LBR) protein, which is anchored in the ER and nuclear membrane via eight transmembrane helices (Supplementary Fig. 7). In comparison to nonmembrane proteins, depletion of integral transmembrane proteins was slower, which likely reflects their retention from proteasomal degradation. An accelerated degradation of these membrane proteins could be observed after cell division, suggesting that the

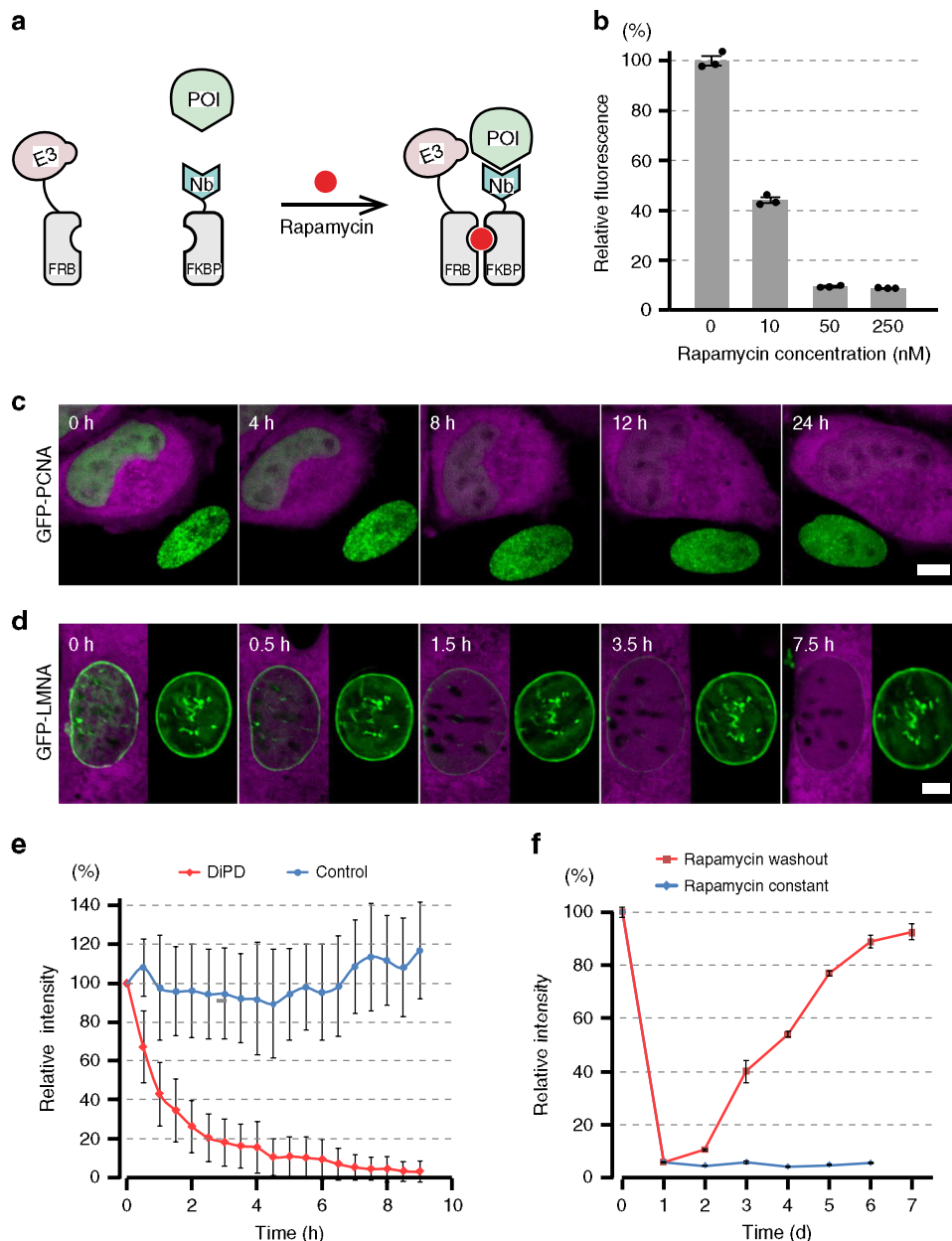


Fig. 2 Drug-induced depletion of GFP fusion proteins. **a** Principle of drug-induced protein depletion. The destruction module (E3, ubiquitin E3 ligase) and the targeting module (Nb, Nanobody) are fused to FRB and FKBP, respectively. Upon addition of rapamycin FRB and FKBP heterodimerize triggering the ubiquitination and depletion of the POI (protein of interest). **b** Dose dependency of GFP-PCNA depletion. Biological triplicates were measured and results are shown as mean \pm SD. **c, d** Snapshots of GFP-PCNA (**c**) and GFP-LMNA (**d**) depletion after rapamycin treatment. GFP fusion proteins are shown in green and the DiPD system is marked with DsRed (in magenta). Scale bars are 5 μ m. **e** Kinetics of GFP-LMNA depletion after rapamycin treatment. Measured DiPD cells $n = 15$ and controls without DiPD $n = 11$, error bar stands for SD. **f** The recovery of protein levels after rapamycin removal. Biological triplicates were measured and results are shown as mean \pm SD.

accompanying reorganization of cellular membranes partially mobilizes transmembrane proteins and increases chances for their proteasomal degradation.

To expand the general applicability of DiPD, we designed a versatile DiPD vector for the simple insertion of any targeting modules. We validated this vector system with a GFP binding designed ankyrin repeat protein (DARPin, 3G124nc)²⁷ and an mCherry-binding nanobody LaM4²⁸ (Supplementary Fig. 8a) to target GFP- and mCherry- fusion proteins, respectively. Both, nanobody and DARPin based, DiPD constructs allowed for efficient and rapamycin dependent depletion of GFP- or mCherry- fusion proteins as demonstrated with GFP-PCNA

(Supplementary Fig. 8b, c) or mCherry-LMNA (Supplementary Fig. 8d).

Drug-induced depletion of endogenous proteins. In all protein depletion experiments thus far we targeted fluorescent fusion proteins, which allows direct monitoring of depletion efficiency and provides a quantitative, temporal and spatial correlation of target protein levels with cellular phenotypes at single cell resolution. However, the insertion of artificial sequences coding for fluorescent fusion proteins can affect gene expression and/or protein function and requires lengthy genetic engineering procedures including selection and passaging of cells, which are not

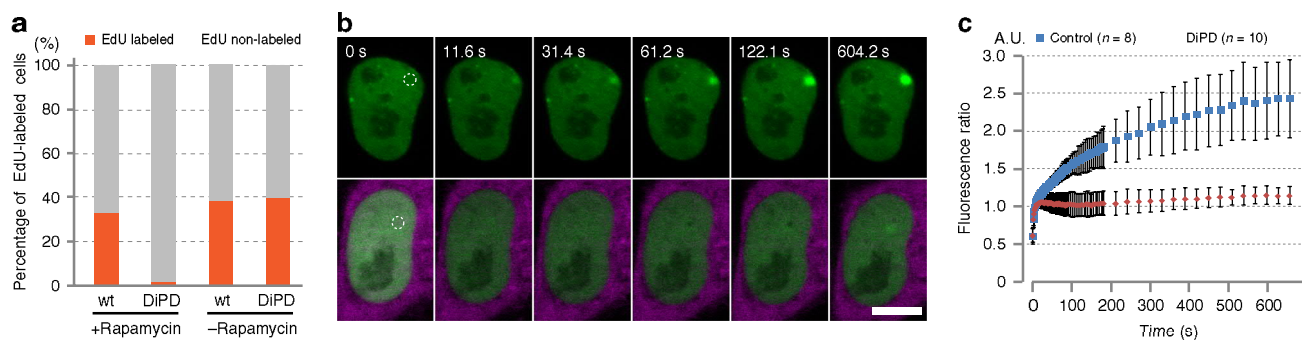


Fig. 3 Transient depletion of an essential protein with DiPD. **a** EdU labeling of DNA synthesis in cells after endogenous PCNA depletion. Practically no EdU incorporation was detected in induced DiPD expressing cells, while around 1/3 of cells without DiPD (wt) and/or without rapamycin induction were EdU positive. For each group, around 1200 to 6000 cells were analyzed. **b** Recruitment of GFP-tagged DNA LIG1 to DNA damage repair sites in the presence and absence of PCNA. Recruitment of DNA LIG1 (green) to the DNA damage repair site (dashed circle) was abolished after PCNA depletion (lower panel, DiPD shown in magenta), but not in cells with PCNA (upper panel). Scale bar equals to 10 μm . **c** DNA LIG1 recruitment kinetics in cells with and without PCNA. Results are shown as mean \pm SD.

suitable for the study of primary cells or organisms without genetic modifications.

To deplete endogenous proteins, we generated DiPD vectors with nanobodies binding to nuclear LaminA/C (LMNA/C) and PCNA protein (Supplementary Fig. 9a). Immunofluorescence showed that the endogenous LMNA/C protein was efficiently depleted from the nuclear envelope in cells containing the DiPD after rapamycin induction (Supplementary Fig. 9b). PCNA is an interesting target as it is a central and essential DNA replication factor and knockout cells are not viable. HeLa cells with and without the PCNA targeting DiPD system were mixed and jointly treated with rapamycin for side-by-side comparison. Immunostaining after overnight incubation (12 h) demonstrated that the endogenous PCNA was efficiently depleted to background levels in a DiPD and rapamycin dependent manner (Supplementary Fig. 9c, d).

This transient depletion of the essential protein PCNA now permits direct functional studies. As PCNA is the central loading platform for a number of factors at nuclear replication foci²⁹, we monitored DNA synthesis with an EdU (5-ethynyl-2'-deoxyuridine) labeling assay. EdU is a nucleotide analog, which is readily incorporated into newly synthesized DNA at nuclear replication sites. However, upon rapamycin induced PCNA depletion no EdU incorporation could be detected (Fig. 3a and Supplementary Fig. 9e).

Besides its essential role in DNA replication, PCNA also participates in DNA damage repair (DDR) pathways building a dynamic loading platform for other factors like, DNA ligase 1 (LIG1), which ligates DNA strands during DNA replication and damage repair^{30,31}. The role of PCNA in recruitment of cellular factors to nuclear repair sites has mostly been investigated by mutating the PCNA binding domains (PBDs) of these factors³¹. To directly study the role of the essential PCNA, we applied our DiPD system and measured the recruitment of LIG1. We inflicted DNA damage at defined nuclear spots by laser microirradiation and monitored the recruitment of GFP-LIG1 in cells with and without PCNA depletion. While in undepleted cells LIG1 is rapidly recruited to DDR sites within minutes, practically no accumulation was detected in cells upon rapamycin induced depletion of PCNA (Fig. 3b and Supplementary Movie 6). The quantification shows an accumulation of GFP-LIG1 at DDR sites starting a few seconds after microirradiation and increasing during the following minutes, while only minor GFP-LIG1 recruitment was detected upon depletion of the endogenous PCNA (Fig. 3c). These results demonstrate how the DiPD system enables the study of

essential proteins as illustrated with these functional studies of PCNA in DNA replication and repair.

Multiple and combinatorial depletion of proteins. As most cellular processes involve multiple redundant proteins or alternative pathways, we set out to expand the range of our protein depletion systems. Since the destruction module of the DiPD system is an independent component, it can be easily combined with multiple targeting domains. To test the feasibility of such a multi-DiPD system we combined three different targeting modules binding LMNA/C, PCNA, and GFP (Fig. 4a). While the abundance of these targeted proteins was not affected in the absence of rapamycin, all three POIs were depleted after rapamycin treatment (Fig. 4b and Supplementary Fig. 10a, b).

While the multi-DiPD tool allows simultaneous depletion of multiple proteins, some biological questions may require the selective and combinatorial or sequential depletion of distinct target proteins. Towards this goal we combined our DiPD and LiPD systems to selectively deplete different sets of proteins with rapamycin and/or light induction. With LiPD we targeted the stably expressed GFP-CXXC4 and with DiPD the endogenous LMNA/C protein (Fig. 4c). We selectively applied the chemical and physical inducers (rapamycin and/or light) and obtained specific and combinatorial depletion of GFP-CXXC4 and LMNA/C (Fig. 4d and Supplementary Fig. 11). These results show that the combination of LiPD and DiPD allow the selective, spatial, and temporal depletion of different sets of proteins.

Protein depletion in *C. elegans*. Next we applied targeted protein depletion to study protein function in the context of an entire organism. Genetic and physical manipulation by itself can easily impair cellular function and even cause death. Therefore, we aimed with our DiPD for the opposite i.e., the rescue of cells from programmed cell death. Since the ubiquitin-proteasome system exists in all eukaryotes, we picked *Caenorhabditis elegans*, which is a well-established model for apoptosis^{32,33}. As a target, we chose the caspase CED-3, which is essential for triggering apoptosis in defined cells during *C. elegans* development. In animals with a *ced-3* loss of function (*lf*) mutation, cells that normally undergo apoptosis inappropriately survive causing an extracellular phenotype.

Importantly, for targeted protein depletion to work, the RING domain of the mammalian E3 ligase has to functionally interact with an endogenous E2 enzyme of the host. Sequence comparison showed that Ube2d2, one of the ubiquitin conjugating E2 enzymes for the mouse RING^{Lnx1}, is ubiquitously expressed

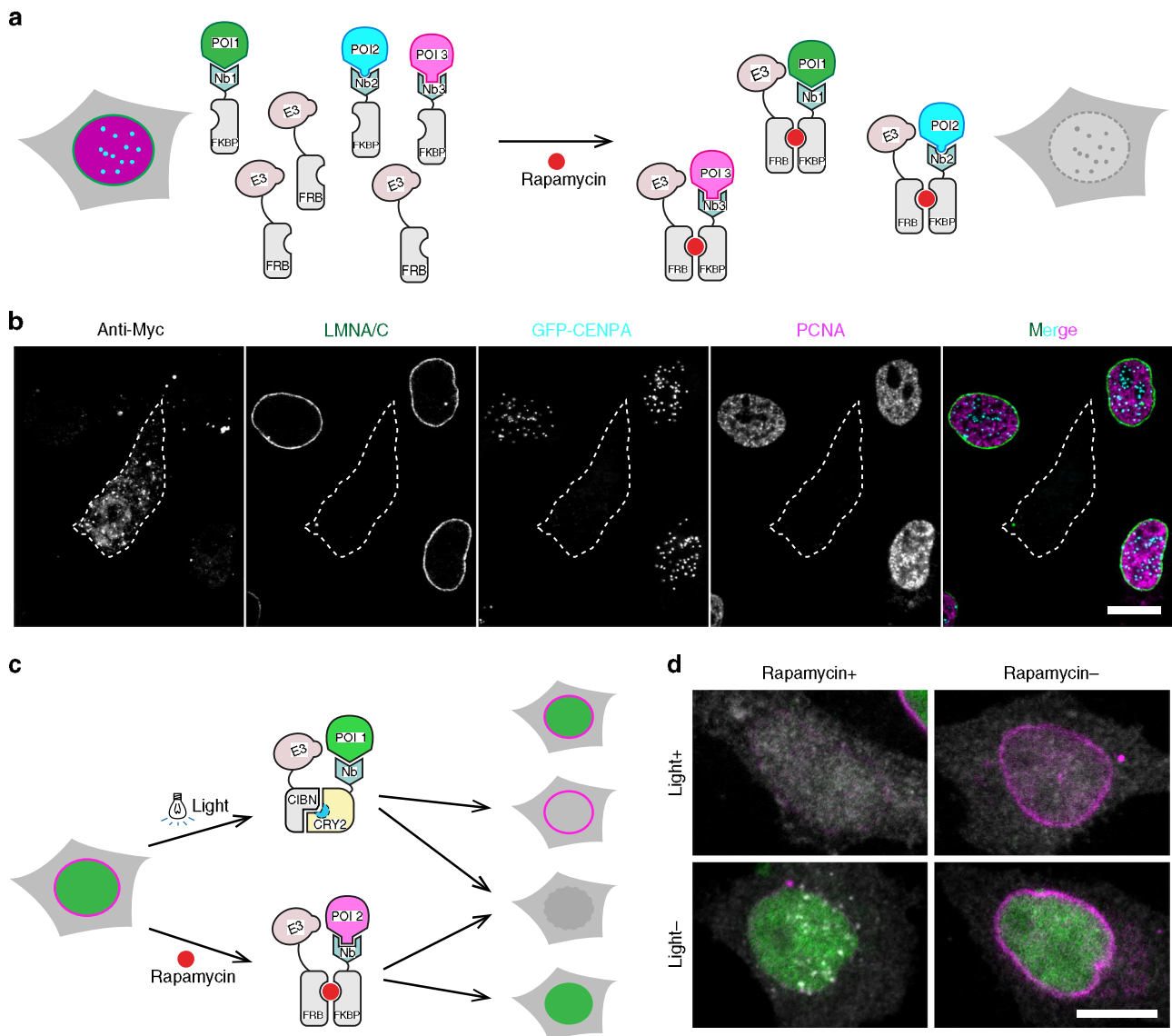


Fig. 4 Combinatorial depletion of different sets of multiple proteins. **a** Schematic outline of the multi-protein targeting DiPD system. Multiple POIs (proteins of interest, POI1-3) are targeted by distinct protein specific targeting modules (Nanobodies, Nbs), which are embedded in the DiPD system. Upon induction with rapamycin the POIs are ubiquitinated and degraded. E3 ubiquitin E3 ligase. **b** Triple depletion of endogenous LMNA/C, PCNA and GFP-CENPA proteins. GFP-CENPA cells were transfected with DiPD constructs targeting LMNA/C, PCNA and GFP. Proteins were detected by immunostaining or GFP fluorescence after rapamycin treatment. A triple depletion of targeted proteins could be observed in the presence of rapamycin. **c** Principle of combinatorial light and drug-induced depletion of two independent proteins (POI1 and POI2). **d** Combinatorial depletion of a nucleoplasmic (GFP-CXXC4, in green) and a nuclear envelope protein (LMNA/C, in magenta). Cells with the light and drug inducible protein depletion tools express DsRed as marker (in gray). Scale bars are 10 μ m. Extended versions of this figure including uninduced controls are shown in Supplementary Fig5. 10 and 11.

and highly conserved from *C. elegans* to human (Supplementary Fig. 12a). To adapt DiPD for *C. elegans* we optimized the codon usage of the targeting and destruction components and used the ubiquitous *eft-3* promoter together with the *gpd-2/gpd-3* intergenic region for proper stoichiometric expression (Supplementary Fig. 12b).

To be able to directly monitor the efficiency and biological effect of protein depletion in developing animals we generated transgenic animals where the endogenous CED-3 was functionally replaced by a GFP-tagged CED-3 (CED-3::GFP). The optimized GBP nanobody based DiPD system was then added as extrachromosomal array (*bcEx1328*). Rapamycin treatment (Fig. 5a) led to an almost complete depletion of CED-3::GFP in embryos within 6 h, which was not observed with the DMSO solvent control (Fig. 5b). The CED-3::GFP signal gradually

recovered after 6–30 h (Fig. 5b, c), which might be due to inactivation of rapamycin in *C. elegans*.

To resolve protein depletion kinetics, we monitored CED-3::GFP levels in the first 6 h after induction (Supplementary Fig. 13a). Quantitative analyses showed a clear reduction of CED-3::GFP already at the first time point (1 h) and maximal depletion between 4 and 6 h after induction (Supplementary Fig. 13b). We also tested two higher concentrations of rapamycin and found a dose-dependent protein depletion efficiency (Supplementary Fig. 13c, d).

Next, we wanted to investigate whether the rapamycin-mediated depletion of CED-3::GFP protein affects apoptosis and causes an extracellular phenotype. To that end, we allowed the CED-3::GFP embryos to develop into larvae and analyzed their anterior pharynxes where the ‘extra cells’ phenotype can easily be

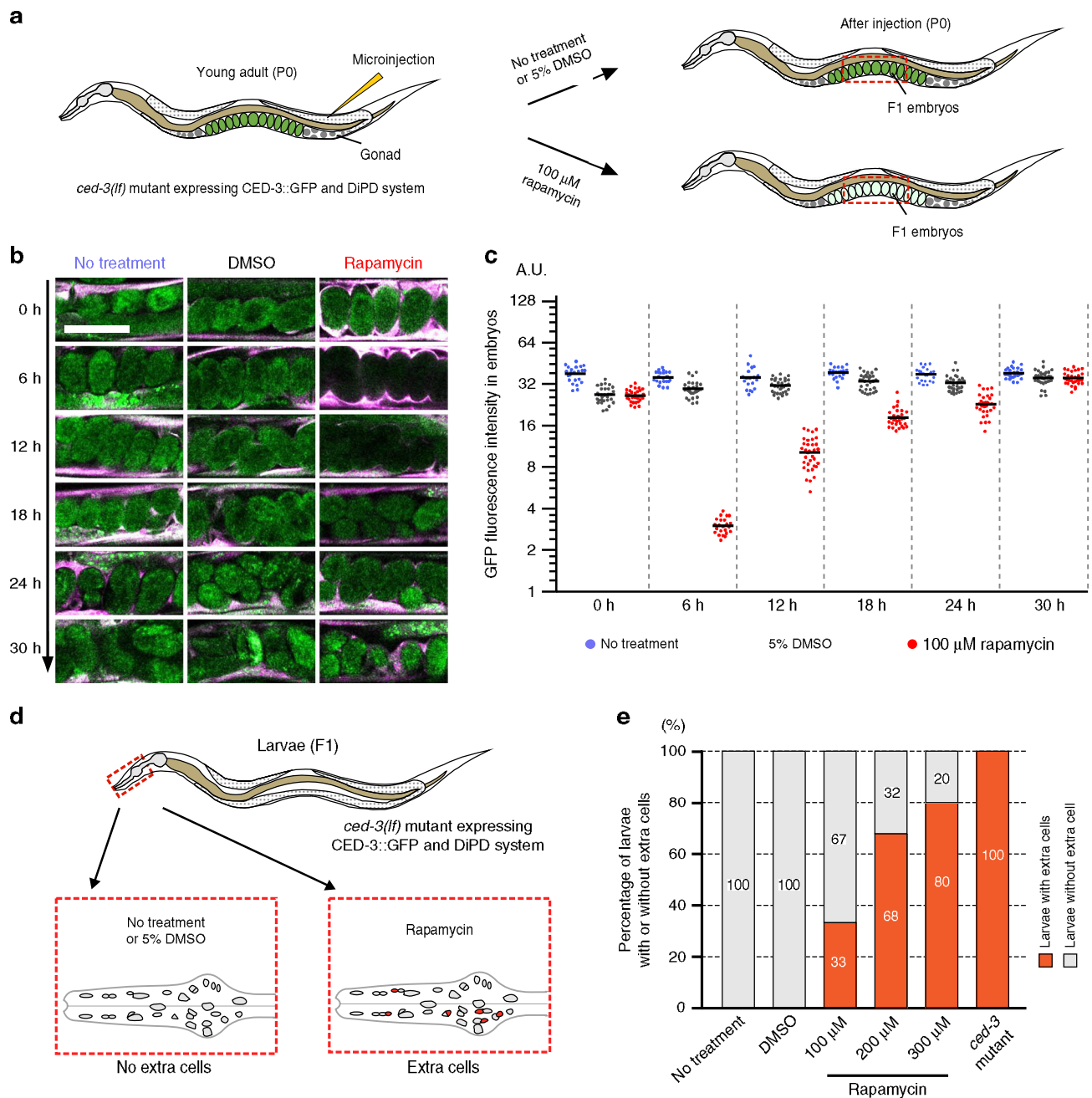


Fig. 5 Transient depletion of CED-3::GFP transforms cell fate. **a** Schematic for drug-induced depletion of CED-3::GFP in *ced-3(lf)* embryos carrying the DiPD system. Rapamycin (100 μ M) or DMSO (5%; control) was administered to adults (P0 generation) and CED-3::GFP fluorescence signal was monitored in embryos (F1 generation) over time. **b** Images of CED-3::GFP signal (in green) in embryos at different time points after rapamycin treatment. Scale bar 50 μ m. **c** Quantification of CED-3::GFP signal in embryos. Data points and the mean values are shown. $n = 19$ –34, biological replicates (embryos). **d** Schematic of rescue assay of extracells phenotype in the pharynx of *ced-3(lf)* mutants. **e** Rapamycin-mediated depletion of CED-3::GFP results in larvae (F1 generation) with extra cells. For each group 15–25 larvae were analyzed.

scored (Fig. 5d). We found that none of the larvae from untreated or DMSO-treated embryos exhibited an ‘extra cells’ phenotype. In contrast, we found that depending on the concentration of rapamycin, from 33 to 80% of larvae from rapamycin-treated embryos exhibited an extracells phenotype, indicating that in these animals, CED-3::GFP was depleted below the level required for apoptosis (Fig. 5e). These results demonstrate that DiPD is well suited to study protein function in an intact, developing organism and can even be used to achieve positive outcomes such as the rescue of cells from apoptotic death.

Discussion

A comprehensive understanding of cellular processes requires an inventory of all cellular components and studies to identify their function in the context of cells and organisms. Genetic methods to inactivate or mutate target genes typically feature high precision and complete penetrance but tend to be rather static. In contrast, knockdown methods targeting mRNA or protein levels are by nature less precise but far more dynamic. While siRNA and shRNA based methods have been enhanced for specificity and efficiency, they still depend on the natural turnover of

the corresponding proteins, which may take days and weeks until any effect can be seen.

Here we present a versatile toolset for the direct depletion of cellular proteins. The goal was to combine the flexibility to target virtually any cellular structure with temporal and spatial control. For many applications it is desirable to work with fluorescently tagged proteins as long as the genetic manipulation does not affect expression or function. The use of fluorescent tags permits monitoring of cellular protein levels and their subcellular localization over cell division cycles and in response to external stimuli. Therefore, we started with existing cell lines expressing fluorescent fusions to directly monitor and optimize our protein depletion strategies (DiPD and LiPD), which has the additional advantage that the validated targeting constructs described here will cover a large share of future applications and alleviate the need to develop new binders or constructs.

In many cases, it is, however, necessary or desirable to directly target the endogenous proteins without the need for prior genetic engineering and lengthy selection procedures, which are often not possible or perturbing in studies of primary cells. Here we demonstrate that our inducible protein depletion strategy can be applied to endogenous proteins and that different binders like nanobodies and DARPins may be used for targeting. Until recently, the intracellular application of recombinant binders has been hampered by their limited availability but the development of new screening technologies and the establishment of complex synthetic libraries now allow for rapid identification of new binders including nanobodies, monobodies, affimers, and DARPins^{28,34–40}. Over the past years, there has been a steep increase in binders against cellular target structures including post-translational modifications as well as alternative protein conformations and activity states^{37,41–43}. In addition, naturally occurring protein-binding domains could be repurposed. The modular design of our vectors accommodates and facilitates the use of all kinds of binding domains to target in principle any cellular structure.

The transient nature of this targeted protein depletion enables studies of essential proteins as we demonstrated with PCNA, which is strictly required for DNA replication in S phase. With rapamycin induced depletion of the endogenous PCNA we opened a window for functional studies and could analyze the role of PCNA in DNA repair. The ability to gradually tune protein levels with DiPD and LiPD also provides quantitative data for model refinements, to identify rate-limiting steps and protein levels and to explore genetic phenomena like haploinsufficiency.

As the ubiquitin-proteasome system exists in all eukaryotes, archaea and also in some bacteria (*Actinomycetales* and *Nitrospirales*)⁴⁴, our toolset for targeted protein depletion should be broadly applicable. As one example, we successfully used the DiPD to test the role of CED-3 in the control of apoptosis in *C. elegans* and could show that transient depletion of CED-3 rescues daughter cells from programmed cell death. For chemical induction we used rapamycin as it binds with high affinity and efficiently induced protein depletion. In our cellular systems we did not observe any adverse side effects and used even higher concentrations up to 500 nM. To reduce or avoid mTOR inhibition also rapamycin derivatives (rapalogs) could be used⁴⁵ to control dimerization and targeted protein depletion.

Our protein depletion toolsets use light and rapamycin as inducer and can therefore be combined with auxin driven AID or PROTAC systems allowing for independent control of three or more sets of proteins. Also, in our first tests the plant hormones ABA and GA-3 were far less efficient inducers for targeted protein depletion. However, these small molecules had been successfully used to induce heterodimerization in mammalian cells^{23,24,46}, suggesting that the respective fusion constructs we

had used for DiPD might be less active due to steric constraints. Therefore, with a systematic optimization of linker lengths, fusion points and domain sizes also these plant hormones should function in DiPD. Altogether, our light and rapamycin induced protein depletion toolsets in combination with auxin, ABA and GA-3 driven depletion tools allow independent control of multiple sets of proteins and should help to elucidate the interplay or co-dependence of proteins and cellular pathways.

The modular design of these toolsets also allows for an easy exchange of the catalytic domain to switch from ubiquitin ligation to other post-translational modifications like e.g., targeted phosphorylation, acetylation or methylation to name only a few. In other words, these toolsets for protein depletion could easily be expanded to control practically any post-translational modification and its removal. To avoid any genetic alterations, the protein depletion or modification tools could also be introduced as mRNA or directly as proteins using either cell penetrating peptides, mesoporous beads or other protein delivery methods^{47,48}. In this study we target proteins for basic research, but viral or pathogenic proteins or oncoproteins could also be targeted for therapeutic purposes.

In summary, we present versatile toolsets for light and drug-controlled targeted protein depletion, which enables the independent temporal and spatial control of two or more sets of proteins in cells and organisms.

Methods

Cell culture. HeLa (WT and transgenic) cells and BHK cells⁴⁹ were cultured in DMEM (Sigma) supplemented with 10% FBS (Fetal Bovine Serum, Sigma), mouse embryonic fibroblast cells (MEFs) were cultured in DMEM with 15% FBS. All cells were cultured under 5% CO₂ at 37 °C. For live cell imaging, cells were cultured in phenol-red free DMEM supplemented with FBS. The microscope stage was warmed up to 37 °C and supplied with humidified air containing 5% CO₂.

Plasmid construction. Gene fragments, encoding FBW1A, FBW1B, KEAP1, and LNX1 functional domains, were cloned from cDNA derived from mouse J1 embryonic stem cells. The HECT domain of NEDD4 was amplified from pCI-neo-mCherry-NEDD4⁵⁰. The E3 ligase fragments together with GBPs⁴¹ were cloned into pIRES2-DsRed Express plasmid (Clontech). For fluorescent fusion proteins, coding sequences for LaminA, Man1, Lbr, Ahcy, and IDH1, were amplified from mouse cDNA, and fused to the C-terminus of eGFP or mCherry. TREX1-GFP and GFP-CXXC4 constructs were published before^{51,52}. Sequences encoding mCherry-binding nanobody LaM4 and GFP binding DARPIn 3G124nc were synthesized (Eurofins Genomics) according to published data^{27,28}.

The plasmid pBC1661 (*P_{ced-3}ced-3::gfp*) used to express CED-3::GFP in vivo was generated by dividing the full length of *ced-3* rescuing fragment into two fragments (~6 kb + 7 kb) and amplifying both fragments from genomic DNA using PCR. The two fragments were ligated into the pCFJ909 (miniMos vector) using the Gibson assembly kit (New England Biolabs). To construct the pDiPD-GBP5_worm (*P_{eft-3}ring::frb::ha::gpd-2/gpd-3::gfp5::fkbp::myc_3'UTR*) plasmid, codon optimized gene fragments encoding RING^{LNX1}, GBP5, FKBP and FRB with artificial introns were synthesized (Eurofins Genomics) and cloned using the Gibson assembly kit (New England Biolabs).

All primers used in this study are listed in Supplementary Table 1; all plasmids used are listed in Supplementary Table 2.

Cell lines and worm strains. HeLa GFP-PCNA cells were from Chagin et al.⁵³, MEF cells expressing GFP-LaminA were from Chiu et al.⁵⁴. To establish HeLa stably expressing GFP fusion proteins, cells were transfected with pCAG-GFP-CXXC4-IB plasmids with Lipofectamine 3000 (Thermo Fisher Scientific) following manufacturer's instruction, selected with blasticidin S (Sigma-Aldrich) at the concentration of 6 µg/ml for 7 days, and purified with FACS (FACSAria II, BD Biosciences). MEF cells expressing mCh-LaminA were established by random integration after transfection of pPGK-mCh-LaminA plasmid, positive cells were purified by FACS.

For generating a GFP-CENPA knock-in cell line, a MIN-tagged CENPA HeLa cell line was firstly generated by insertion of an *atp* recombination site (MIN-tag)²² after the start codon of *CENPA* gene. Plasmids encoding pSpCas9A (pSpCas9 (BB)-2A-GFP, addgene #48138)⁵⁵ and an sgRNA targeting to *CENPA* start codon (5'-GCACCCTCTGCGGCGTGTCA-3') together with a synthesized 200 nt ssDNA repair template, which contains homology arms centered around the MIN-tag were transfected into HeLa cells. Transfected cells (marked by GFP expression) were enriched by FACS (Aria II, BD Biosciences), and seeded into a P100 plate. After 8 days, single colonies were manually picked and transferred into a 96-well plate and

expanded. Genomic DNA from each colony was isolated and screened by PCR using the MIN-external primers (primer sequences in Supplementary Table 1). To recombine GFP-CENPA into the genome, the MIN-CENPA cell line was transfected with the attB-GFP-CENPA plasmid together with the BXB1 integrase plasmid⁵⁶. GFP-positive cells were selected 24 h after transfection with G418 (1 mg/ml, Sigma–Aldrich) and sorted by FACS. Enriched GFP-positive cells were seeded into P100 dish and expanded. GFP-positive colonies were picked manually under a fluorescence microscope, then expanded and characterized by screening PCR using the primers shown in Supplementary Fig. 4 and Table 1. The GFP-CENPA HeLa Kyoto cell line was further verified by Sanger sequencing of the recombined locus.

To generate DiPD and LiPD stable lines, the piggyBac-DiPD or piggyBac-LiPD plasmid was co-transfected with piggyBac transposase expression plasmid in a ratio of 3:1, and cells were selected with 150 µg/ml hygromycin (Sigma–Aldrich) for 7 days followed by FACS. Expression of the DiPD and LiPD units were confirmed by immunostaining with antibodies against the HA (3F10, Sigma–Aldrich, 1:200) and Myc-tag (9E10, Thermo Fisher Scientific, 1:200).

C. elegans strains were maintained at 20 °C. The following *C. elegans* strains were used and maintained at 20 °C: LGIV *ced-3(n717)*⁵⁷; LGV *bcSi36* and *bEx1328* (this study, Supplementary Table 3).

Germline transformation was performed as described⁵⁸. For the miniMos injection, plasmid PBC1611 was injected at a concentration of 10 ng/µl together with the co-injection markers pCFJ601 at 50 ng/µl, pGH8 at 10 ng/µl, pCFJ90 at 2.5 ng/µl, pCFJ104 at 5 ng/µl into the miniMos strain HT1593 as described before⁵⁵. A single copy of the *ced-3::gfp* transgene was integrated on chromosome V (LGV *bcSi36*) and the site of insertion was mapped and sequenced using inverse PCR⁵⁹. For the extra-chromosome array injection, plasmid pDiPD-GBP5_worm (*P_{efp-3::ring::fwb::ha::gpd-2/gpd-3::gfp5::fkbp::myc_3'UTR}*) was injected at a concentration of 50 ng/µl together with the co-injection markers *P_{efp-3::mkate2}* and pRF4 at 150 ng/µl into LGV *bcSi36*(*P_{ced-3::gfp}*) strain to generate a stable extrachromosomal array *bEx1328*.

All cell lines used are listed in Supplementary Table 3.

Fixed sample slides preparation for confocal microscopy. To prepare sample slides for confocal microscope, cells were seeded on coverslips in 6-well plates. After transfection, induction or other treatments, cells were fixed with 4% formaldehyde in PBS (phosphate buffer solution) for 10 min at room temperature (RT), then washed three-times with PBST (PBS with 0.02% Tween). To permeabilize the cell, fixed samples were treated with PBS containing 0.5% Triton X-100 for 5 min at RT, followed by three-times washing with PBST.

For samples with immunostaining, primary antibodies were diluted in blocking buffer (3% BSA in PBST), and incubated with the sample for 1 h at RT. Samples were washed three times with PBST, and incubated with fluorescein labeled secondary antibodies that are diluted in blocking buffer. One hour later, cells were washed three times with PBST to remove the unbound secondary antibodies.

Cell nuclei were stained with DAPI (4',6-diamidino-2-phenylindole, 200 ng/ml in PBS) for 10 min at RT. Coverslips were mounted with Vectashield antifade mounting medium (Vector Laboratories) and sealed with clear fingernail polish on glass slides.

Testing the depletion efficiency of E3 ligases. HeLa cells stably expressing GFP-CXXC4 or GFP-PCNA were seeded on 18 × 18 mm² coverslips and transfected with pFBW1A-GBP1-IR, pFBW1B-GBP1-IR, pKEAP1-GBP1-IR, pLNX1-GBP1-IR, pGBP1-NEDD4-IR, and pGBP1-IR with Lipofectamine 3000 (Thermo Fisher Scientific). Cells were fixed and sample slides prepared. Image acquisition was performed with a spinning disc confocal microscope (UltraView VoX, Perkin Elmer) using a ×63 objective and an EMCCD camera (1000 × 1000 pixels, Hamamatsu). For the analysis, cells were segmented according to the DAPI stained nuclei, and the intensities of GFP and DsRed signals in the nuclear segment of each cell were determined and average gray values calculated. The background signal was subtracted and the average GFP intensity of transfected cells (~20 cells) for each construct was calculated and plotted with RStudio program. pGBP1-IR transfected cells served as negative control.

Association and dissociation of different LID pairs. BHK cells were seeded in 8-well µslides (ibidi GmbH) and transfected with plasmids encoding fluorescent proteins fused to the LID components SspB/iLID²⁰ or PHR/CIBN²¹. A spinning disc confocal microscope (UltraView VoX, Perkin Elmer) was used for live cell imaging and a 488 nm laser (600 ms, 10% of a 2.5 mW power) was used for heterodimers induction. Association and dissociation of the mCherry tagged LID components to and from the cell membrane anchored components was imaged with a 561 nm laser.

To check the association and dissociation of the PHR/CIBN heterodimer in the nucleus, BHK cells were seeded in 8-well µslides (ibidi GmbH), and triple transfected with pNLSGFP-iRFP670-PCNA, pCIBN-GBP and pCRY2PHR-mCherry plasmids. Fluorescence excited with 488 nm (for eGFP illumination and induction), 561 nm and 640 nm lasers was recorded at maximum imaging speed of the microscope. For the dissociation assay, only 561 nm laser and 640 nm lasers were used, and images were recorded using a preset program (maximum speed for 1 min, then 5 s intervals for 2 min, then 10 s intervals for 2 min, and 30 s intervals

for 10 min). For data analysis, PCNA foci were segmented according to iRFP670 intensity ($I_{PCNA}^{iRFP670}$) and the PHR-mCh intensity at these foci was measured and average mCherry intensity values were calculated for each cell (I_{PCNA}^{mCh}). For each time point, the PHR-mCh associated with PCNA foci was calculated with Eq. (1).

$$I = \frac{I_{PCNA}^{mCh} - I_{NUC}^{mCh}}{I_{PCNA}^{iRFP670} - I_{NUC}^{iRFP670}} \quad (1)$$

I_{NUC}^{mCh} and $I_{NUC}^{iRFP670}$ was the nuclear average intensity of mCherry and iRFP670, respectively.

Optimization of the LiPD system. To test the different combinations for LiPD, HeLa cells stably expressing GFP-PCNA were seeded in 8-well µslides (ibidi GmbH) and co-transfected with three combinations for LiPD (GBP1-PHR/CIBN-RING, CIBN-GBP1/RING-PHR, GBP1-PHR/RING-CIBN). To test the efficiency of different GBPs for the LiPD, LiPD constructs using GBP1, GBP2, and GBP4 were transfected into GFP-PCNA cells. Cells were then imaged with a spinning disc confocal microscope (UltraView VoX, Perkin Elmer). Four hundred and eighty-eight nanometer laser (10% of 2.5 mW for 0.6 s) was used for light induction and imaging GFP simultaneously. Five hundred and sixty-one nanometer laser was used to excite DsRed for identifying transfected cells. Image stacks were taken every 10 min (six frames per hour).

For data analysis, image stacks were projected with maximum intensity, and the GFP-PCNA intensity in the nuclear area was measured at time 0 min and 120 min for each group. Average intensity and the standard deviation were calculated and histograms were made in Excel (Microsoft).

Testing the conditions for DiPD. HeLa GFP-PCNA cells were seeded on coverslips in 6-well plates and transfected with DiPD plasmid or E3FRB-GBP5 plasmid. About 24 h after transfection, the cells were treated with 250 nM rapamycin or DMSO only overnight. Cells were then fixed and HA was detected by immunostaining with anti-HA antibody (3F10, 1:200, Sigma–Aldrich) and sample slides were prepared.

Sample slides were imaged with a spinning disc confocal microscope (Eclipse Ti, Nikon). GFP and Alexa Fluor 594 were excited with a 488 nm and 594 nm laser, respectively. 16-bits digital images were recorded with an EMCCD camera. Images were processed and quantified with imageJ. Measured fluorescence intensities for each group were plotted in boxplot format with R (Rstudio).

Test of background depletion for LiPD and DiPD. For LiPD background depletion control, GFP-CXXC4 cells stably expressing LiPD were mixed with cells lacking the LiPD and seeded on coverslips. For testing of DiPD background control, GFP-PCNA cells with and without stably expressed DiPD were mixed and seeded on coverslips. Cells were fixed and HA was stained, microscopic slides were prepared as described before.

For high-content analysis, samples were imaged with an automatic fluorescence microscope (Operetta, Perkin Elmer). DAPI, GFP and Alexa Fluor 594 (anti-HA) were excited with correspondent lasers using a ×40 high NA objective. For each coverslip 121 fields were imaged (an 11 × 11 fields square area). Image analysis was performed with the Harmony analysis software (Perkin Elmer). In brief, cell nuclei were recognized and segmented in the DAPI channel and correspondent GFP and anti-HA fluorescence intensities were measured for each cell nucleus. The cells then were divided into two groups (LiPD or DiPD group versus control group) according to the anti-HA fluorescence intensity. The GFP intensity of each group was plotted in boxplot format with R (Rstudio).

Depletion of transmembrane and cytoplasmic proteins. HeLa cells were transfected with the DiPD plasmid together with a plasmid encoding a PiggyBac transposase (System Biosciences) using Lipofectamine 3000 (Thermo Fisher Scientific). Cells stably expressing DiPD were selected with hygromycin at 150 µg/ml followed by purification with FACS (FACSaria II, BD Biosciences). To deplete the GFP fused membrane or cytoplasmic proteins, the stable DiPD cells were transiently transfected with a plasmid encoding the GFP fusion. Cells were cultured and selected with antibiotics (blasticidin S: 6 µg/ml; G418: 150 µg/ml), then cell mixtures were seeded into 8-well or 2-well µslides (ibidi GmbH). Cells were treated with 250 nM rapamycin and imaged immediately with a spinning disc confocal microscope (Eclipse Ti, Nikon) equipped for live cell culture (with heating and humidified CO₂ supply). GFP and DsRed were excited with 488 nm and 561 nm lasers, respectively, and cells were imaged every 30 min for about 24 h. Acquired images were processed and organized with imageJ.

Detection of endogenous PCNA depletion by immunostaining. HeLa cells expressing the DiPD-aPCNA-IR (with DsRed marker) were mixed with wt HeLa cell at a 1:1 ratio and seeded onto coverslips in a 6-well plate. Cells were cultured in medium containing 250 nM rapamycin for about 12 h, and then fixed with 4% formaldehyde in PBS for 10 min. Cells were permeabilized in PBS with 0.5% TritonX-100 for 5 min and blocked in the blocking solution (PBS with 3% BSA, 0.2% Tween) for 1 h at room temperature. Rat anti-PCNA (16D10, 1:10) supernatant and mouse anti-myc (1:200, 9E10, Thermo Fisher Scientific, MA1-980) were

diluted in the blocking solution and incubated with the samples for 1 h at RT. Alexa Fluor 488 labeled donkey anti-rat (Life Technology, A21208) and Alexa Fluor 647 labeled donkey anti-mouse (Life Technology, A31571) secondary antibodies were diluted in the blocking solution at a ratio of 1:200. Secondary antibody incubation was performed at RT for 1 h. Cell nuclei were stained with DAPI (200 ng/ml in PBS), and the coverslips mounted in Vectashield antifade medium (Vector Laboratories) and sealed with clear nail polish.

EdU labeling of DNA synthesis in HeLa cells. HeLa cells expressing the DiPD-aPCNA-IR were mixed with wt HeLa cell at a 1:1 ratio and seeded onto coverslips in 6-well plates. Then the cells were treated with 250 nM rapamycin for 24 h and incubated in pre-warmed medium containing 10 μ M EdU (5-ethynyl-2'-deoxyuridine) for 15 min, then gently washed twice with PBS and fixed with PBS containing 4% formaldehyde. The fixed cells were permeabilized with 0.5% Triton-X-100 in PBS and blocked with 3% BSA in PBST (PBS with 0.2% Tween). Click chemistry on the incorporated EdU was performed in the reaction cocktail (4 mM CuSO₄, 50 nM sodium ascorbate and Alexa Fluor 488 labeled azide dye in 0.1 M Tris/HCl pH 7) for 1 h in a humidified dark chamber, then washed three times with PBST (PBS with 0.2% Tween). HA-tagged DiPD components were detected with rat anti-HA (3F10, 1:200, Sigma-Aldrich) monoclonal antibodies and the goat anti-rat Alexa Fluor 594 secondary antibody (1:200, Life Technology, A11007). The samples were incubated with the diluted antibodies for 1 h at RT in a humidified chamber. DNA was stained with 200 ng/ml DAPI in PBS. Coverslips were mounted in Vectashield antifade mounting medium (Vector Laboratories) and sealed with clear nail polish.

Quantitative high-throughput assay of EdU labeling. Slides with mounted coverslips were imaged with the Operetta high-content imaging system (Perkin Elmer). DAPI, Alexa Fluor 488 dye and Alexa Fluor 594 dye were excited with correspondent lasers using a $\times 40$ high NA objective. For each coverslip, 121 fields were imaged (an 11 \times 11 fields square area). Image analysis was performed with the Harmony analysis software (Perkin Elmer). Cell nuclei were segmented according to the DAPI staining and then the average signal intensities obtained with 488 nm (EdU staining) and 594 nm (HA staining) excitation was quantified in these segmented areas of all cells. Based on their Alexa Fluor 594 signal, cells treated with or without rapamycin were divided into DiPD and control (wt) groups. Replicating cells in each group were identified by EdU-labeling.

Light induced depletion of GFP-PCNA and GFP-CXXC4. HeLa cells stably expressing GFP-PCNA were seeded in 8-well μ slides (ibidi GmbH) and transfected with the pViro-LiPD-GBP1-IR plasmid. HeLa cells stably expressing GFP-CXXC4 and the LiPD were mixed with cells without LiPD system, and seeded in 8-well μ slides (ibidi GmbH). Cell culture medium was changed to phenol-red free medium and balanced for CO₂ in the incubator before imaging. The 488 nm laser was used to excite the GFP (600 ms, 10% of a 2.5 mW power) and induce the protein depletion simultaneously, 561 nm laser was used to detect the co-expressed DsRed signal. The induction and imaging frequency was 10 frames per hour (6 min interval between two frames), and cells were imaged for about 5 h. Z-stacks of the image were acquired to avoid a loss of focus during the long-term imaging process.

To quantify the GFP signal, z-stack projection with maximum intensity was performed and the average intensity of the cell nucleus was determined after background subtraction. To exclude potential GFP fluorescence loss due to photobleaching, all ratios were compared to non-transfected control cells in the same imaging field.

Drug-induced depletion of GFP-PCNA and GFP-LaminA. Cells stably expressing GFP fusion proteins together with the DiPD were mixed with cells only expressing GFP fusion proteins (serving as control) and seeded in 2-well μ slides (ibidi GmbH). Attached cells were imaged after addition of the inducer (250 nM rapamycin) with a spinning disc confocal microscope (Eclipse Ti, Nikon) equipped for live cell culture (with heating and humidified CO₂ supply). GFP and DsRed were excited with 488 nm and 561 nm lasers, respectively, and cells were imaged every 20 or 30 min.

For image analysis, cell nuclei (for GFP-PCNA quantification) or nuclear envelope (for GFP-LaminA quantification) were segmented manually and the fluorescence intensities measured with ImageJ. The average gray values in these segmented areas of cells at each time point were plotted in Excel (Microsoft).

Sustained or reversible depletion of GFP-PCNA. HeLa cells stably expressing both GFP-PCNA and the DiPD-GBP5-IR were cultured in 60 mm culture dishes. Cells were treated with 250 nM rapamycin for 24 h, then split into two wells, maintained in medium with rapamycin (rapamycin constant, for sustained DiPD) or without rapamycin (rapamycin washout, for reversible DiPD) for 7 d. Every 24 h, cells were trypsinized and collected for measurement of the GFP-PCNA fluorescence intensity. To measure the GFP and DsRed fluorescence, cells were trypsinized and spun down at 180 g for 5 min, washed twice with PBS, resuspended in 100 μ l PBS and transferred to 96-well microplates (μ CLEAR, black, Greiner Bio-one) for measuring the fluorescence intensity with a fluorescence plate reader (Infinite M1000, Tecan). For data analysis, fluorescence intensities of GFP-PCNA

were normalized by the intensity of DsRed to adjust the cell number differences, then the GFP-PCNA intensity at each time points was plotted in Excel (Microsoft). Biological triplicates were performed.

Laser induced DNA damage and LIG1 recruitment assay. HeLa cells expressing the DiPD-aPCNA-IR (with DsRed marker) were mixed with wt HeLa cell at a 1:1 ratio, and seeded in 2-well μ slides (ibidi GmbH). Cell mixtures were transfected with GFP-LIG1 expression plasmid. Cells were incubated with 250 nM Rapamycin for 12 h to deplete cellular PCNA. Before laser microirradiation, the culture medium was changed to phenol-red free medium and cell mixtures were incubated with 10 μ g/ml Hoechst 33342 for 10 min to sensitize the cell for DNA damage induction. Cells were imaged with an Ultraview Vox spinning disc confocal microscope, and DNA damage was induced with a 405 nm laser (spot irradiation with 50% laser intensity). GFP-LIG1 (excited by 488 nm laser) and DsRed (excited by 561 nm laser) were imaged at maximum speed with 2 s intervals between frames for 2 min, then 5 s intervals for 1 min followed by 30 s intervals for 10 min. Images were recorded with a frame size of 1000 \times 1000 pixels and 109 nm per pixel.

For quantification of local enrichment at DNA damage sites, the mean intensity of GFP-LIG1 at the irradiated region (ROI) was measured as I_{ROI} , and compared to the GFP-LIG1 intensity of the whole nucleus I_{nuc} . The enrichment of GFP-LIG1 at the ROI equals $I_{ROI} - I_{nuc}$. To compensate for potential photobleaching during image acquisition, the reduction of whole nuclear GFP-LIG1 intensity at time point T_n ($I_{nuc T_n}$) was compared to the intensity at the start point T_0 ($I_{nuc T_0}$). The accumulation of GFP-LIG1 at the DNA damage site at time point T_n (I_{T_n}) was normalized and calculated with Eq. (2).

$$I_{T_n} = \frac{I_{ROI T_n} - I_{nuc T_n}}{I_{ROI T_0} - I_{nuc T_0}} \times \frac{I_{nuc T_0}}{I_{nuc T_n}} \quad (2)$$

Dose-dependent depletion of GFP-CXXC4 with a lightbox. For light induced depletion of GFP-CXXC4 across large cell populations, HeLa cells stably expressing GFP-CXXC4 and LiPD-GBP1-IR were seeded in p35 dishes and induced with an LED lightbox using four different induction programs (program 1-4) with alternating light and dark phases of different duration (program 1: $t_1 = 1$ s, $t_2 = 5$ min; program 2: $t_1 = 1$ s, $t_2 = 2$ min; program 3: $t_1 = 4$ s, $t_2 = 2$ min; program 4: $t_1 = 8$ s, $t_2 = 2$ min. t_1 is the duration of light induction, and t_2 is the interval in the dark between inductions, as shown in Supplementary Fig. 5f). For each program, at time points 0, 0.5, 1, 2, and 4 h after induction, cells were trypsinized, washed and collected, then GFP and DsRed fluorescence was measured with a fluorescence plate reader (Infinite M1000, Tecan), and plotted in Excel. The constitutive DsRed signals were used to normalize for cell numbers. Biological triplicates were performed for each program and each time point.

Construction of the lightbox. A 470 nm LED light bulb (3 W, 30 lm, 10°, Ledxon) and a digital timer (Tempatron UDT, Eltime Controls) were used to build a lightbox, which could illuminate the cells programmably. The distance from the light bulb to cultured cells (30 cm) was chosen to ensure even sample illumination.

Spatially controlled LiPD. Cells stably expressing GFP-CXXC4 and the LiPD system or without the LiPD (control) were seeded in 4-well μ slides (ibidi GmbH) and cultured till full confluency. The cells were illuminated and imaged with a spinning disc confocal microscope (Eclipse Ti, Nikon) using a $\times 60$ oil objective. Imaging fields arranged in a chess board pattern were illuminated with a 488 nm laser (300 ms, 0.7 mW per cm²) to achieve a spatial controlled depletion of GFP-CXXC4 in cells. Cells were induced repeatedly every 6 min for 4 h. After the four hours induction, the final fluorescence overview image was collected as a 7 \times 7 large image field. The GFP-CXXC4 cells without the LiPD system were induced and imaged with the identical experimental setup to control for loss of fluorescence due to photobleaching.

Multi-protein targeting DiPD. HeLa GFP-CENPA cells were seeded on coverslips in 6-well plates and triple transfected with DiPD-aLamin, DiPD-aPCNA, and DiPD-GBP plasmids (3 μ g plasmid DNA per well, at the ratio of 1:1:1). Cells were cultured overnight and treated with rapamycin (250 nM) for 24 h and fixed with formaldehyde. Immunostaining was performed to detect the LaminA/C (with rabbit anti-LMNA/C antibodies, Millipore, 1:500), PCNA (with monoclonal rat anti-PCNA antibody, 16D10, supernatant, 1:10) and Myc-tagged nanobodies (with antibody mouse anti-Myc, 9E10, 1:200, Thermo Fisher Scientific). Alexa Fluor 405 labeled goat anti-mouse (A31553), Alexa Fluor 594 labeled goat anti-rabbit (A11034) and Alexa Fluor 647 labeled goat anti-rat (A21247) were used as secondary antibodies (all from Life Technology, 1:200). Coverslips were mounted on slides and fluorescence images were acquired with the spinning disc confocal microscope (Ultraview VoX, Perkin Elmer) as described before.

Combinatorial depletion of multiple proteins. HeLa GFP-CXXC4 cells were cultured on coverslips in 35 mm culture dishes and co-transfected with LiPD-GBP1 and DiPD-aLamin constructs. 24 h after transfection, rapamycin was added into the culture medium to a concentration of 250 nM overnight (for rapamycin

treatment group). Next, cells were put into the lightbox and induced with the 470 nm LED light for 4 s repeatedly every 2 min for light induced depletion of GFP-CXXC4. After 4 h of induction, cells were fixed and permeabilized, then stained with antibody against LaminA/C (rabbit anti-LMNA/C antibodies, Millipore, 1:500) and HA tag (3F10, 1:200, Sigma–Aldrich) to detect the LiPD or DiPD components. Cell nuclei were stained with DAPI and the coverslips were mounted on slides and sealed with clear nail polish. Cells were imaged with a spinning disc confocal microscope (Ultraview VoX, Perkin Elmer) as described above.

Phenotype analysis and microscopy for worm experiments. Rapamycin and DMSO microinjections were performed as described⁶⁰. Once adults were injected with different reagents (5% DMSO and 100 μ M, 200 μ M, 300 μ M rapamycin or without injection), they were imaged using a Leica TCS SP5 II confocal microscope at 0, 1, 2, 3, 4, 5, 6, 12, 18, 24, and 30 h after injection. The slide preparation and all settings of the confocal to record GFP fluorescence signal were performed as described⁶¹. Briefly, a Z-stack volume of \sim 20–25 μ m with a step size of 2.0 μ m was setup to record the GFP fluorescent signal of the embryos in each injected adult (laser power was 15% for 488 nm and 1% for 561 nm). For all the confocal images, a noise reduction function was applied by using the Leica Application Suite (LAS) software to remove the cytoplasmic noise background.

Following confocal acquisition of CED-3::GFP fluorescence signal in the embryos of injected adults, for every Z-slice in which a distinct whole embryo boundary could be seen, the mean intensity of the CED-3::GFP fluorescent within the whole embryo boundary was determined by drawing the region of interest (ROI) around the boundary of the whole embryo in ImageJ.

To observe extra cells in anterior pharynx, injected adults (P0 generation) were maintained at 20 °C to recover treated F1 embryos. Once F1 embryos had developed into L4 stage larvae, the number of extra cells in the anterior pharynx was determined using Nomarski Optic as described⁶².

Reporting summary. Further information on research design is available in the Nature Research Reporting Summary linked to this article.

Data availability

The data that support the findings of this study are available upon reasonable request.

Received: 6 May 2019; Accepted: 12 December 2019;

Published online: 16 January 2020

References

- El-Brolosy, M. A. & Stainier, D. Y. R. Genetic compensation: a phenomenon in search of mechanisms. *PLoS Genet.* **13**, e1006780 (2017).
- Liu, Y., Beyer, A. & Aebersold, R. On the dependency of cellular protein levels on mRNA abundance. *Cell* **165**, 535–550 (2016).
- Banaszynski, L. A., Chen, L.-c., Maynard-Smith, L. A., Ooi, A. G. L. & Wandless, T. J. A rapid, reversible, and tunable method to regulate protein function in living cells using synthetic small molecules. *Cell* **126**, 995–1004 (2006).
- Armstrong, C. M. & Goldberg, D. E. An FKBP destabilization domain modulates protein levels in *Plasmodium falciparum*. *Nat. Methods* **4**, 1007–1009 (2007).
- Herm-Gotz, A. et al. Rapid control of protein level in the apicomplexan *Toxoplasma gondii*. *Nat. Methods* **4**, 1003–1005 (2007).
- Maynard-Smith, L. A., Chen, L.-c., Banaszynski, L. A., Ooi, A. G. L. & Wandless, T. J. A directed approach for engineering conditional protein stability using biologically silent small molecules. *J. Biol. Chem.* **282**, 24866–24872 (2007).
- Pratt, M. R., Schwartz, E. C. & Muir, T. W. Small-molecule-mediated rescue of protein function by an inducible proteolytic shunt. *Proc. Natl Acad. Sci. USA* **104**, 11209–11214 (2007).
- Nishimura, K., Fukagawa, T., Takisawa, H., Kakimoto, T. & Kanemaki, M. An auxin-based degron system for the rapid depletion of proteins in nonplant cells. *Nat. Methods* **6**, 917–922 (2009).
- Neklesa, T. K. et al. Small-molecule hydrophobic tagging-induced degradation of HaloTag fusion proteins. *Nat. Chem. Biol.* **7**, 538–543 (2011).
- Renicke, C., Schuster, D., Usherenko, S., Essen, L.-O. & Taxis, C. A LOV2 domain-based optogenetic tool to control protein degradation and cellular function. *Chem. Biol.* **20**, 619–626 (2013).
- Bonger, K. M., Rakhit, R., Payumo, A. Y., Chen, J. K. & Wandless, T. J. General method for regulating protein stability with light. *ACS Chem. Biol.* **9**, 111–115 (2014).
- Hermann, A., Liewald, J. F. & Gottschalk, A. A photosensitive degron enables acute light-induced protein degradation in the nervous system. *Curr. Biol.* **25**, R749–R750 (2015).
- Rothbauer, U. et al. Targeting and tracing antigens in live cells with fluorescent nanobodies. *Nat. Methods* **3**, 887–889 (2006).
- Caussinus, E., Kanca, O. & Affolter, M. Fluorescent fusion protein knockout mediated by anti-GFP nanobody. *Nat. Struct. Mol. Biol.* **19**, 117–121 (2012).
- Daniel, K. et al. Conditional control of fluorescent protein degradation by an auxin-dependent nanobody. *Nat. Commun.* **9**, 3297 (2018).
- Clift, D. et al. A method for the acute and rapid degradation of endogenous proteins. *Cell* **171**, 1692–1706.e1618 (2017).
- Chen, X. et al. Degradation of endogenous proteins and generation of a null-like phenotype in zebrafish using Trim-Away technology. *Genome Biol.* **20**, 19 (2019).
- Sakamoto, K. M. et al. Protacs: Chimeric molecules that target proteins to the Skp1–Cullin–F box complex for ubiquitination and degradation. *Proc. Natl Acad. Sci. USA* **98**, 8554–8559 (2001).
- Yin, Q. et al. E2 interaction and dimerization in the crystal structure of TRAF6. *Nat. Struct. Mol. Biol.* **16**, 658–666 (2009).
- Guntas, G. et al. Engineering an improved light-induced dimer (iLID) for controlling the localization and activity of signaling proteins. *Proc. Natl Acad. Sci. USA* **112**, 112–117 (2015).
- Kennedy, M. J. et al. Rapid blue-light-mediated induction of protein interactions in living cells. *Nat. Methods* **7**, 973–975 (2010).
- Mulholland, C. B. et al. A modular open platform for systematic functional studies under physiological conditions. *Nucleic Acids Res.* **43**, e112–e112 (2015).
- Liang, F.-S., Ho, W. Q. & Crabtree, G. R. Engineering the ABA plant stress pathway for regulation of induced proximity. *Sci. Signal.* **4**, rs2 (2011).
- Miyamoto, T. et al. Rapid and orthogonal logic gating with a gibberellin-induced dimerization system. *Nat. Chem. Biol.* **8**, 465–470 (2012).
- Banaszynski, L. A., Liu, C. W. & Wandless, T. J. Characterization of the FKBP-rapamycin-FRB ternary complex. *J. Am. Chem. Soc.* **127**, 4715–4721 (2005).
- Schwanhauser, B. et al. Global quantification of mammalian gene expression control. *Nature* **473**, 337–342 (2011).
- Hansen, S. et al. Design and applications of a clamp for Green Fluorescent Protein with picomolar affinity. *Sci. Rep.* **7**, 16292 (2017).
- Fridy, P. C. et al. A robust pipeline for rapid production of versatile nanobody repertoires. *Nat. Methods* **11**, 1253–1260 (2014).
- Sporbert, A., Gahl, A., Ankerhold, R., Leonhardt, H. & Cardoso, M. C. DNA polymerase clamp shows little turnover at established replication sites but sequential de novo assembly at adjacent origin clusters. *Mol. Cell* **10**, 1355–1365 (2002).
- Levin, D. S., McKenna, A. E., Motycka, T. A., Matsumoto, Y. & Tomkinson, A. E. Interaction between PCNA and DNA ligase I is critical for joining of Okazaki fragments and long-patch base-excision repair. *Curr. Biol.* **10**, 919–922 (2000).
- Mortusewicz, O., Rothbauer, U., Cardoso, M. C. & Leonhardt, H. Differential recruitment of DNA Ligase I and III to DNA repair sites. *Nucleic Acids Res.* **34**, 3523–3532 (2006).
- Conradt, B., Wu, Y. C. & Xue, D. Programmed cell death during *Caenorhabditis elegans* development. *Genetics* **203**, 1533–1562 (2016).
- Horvitz, H. R. Worms, life, and death (Nobel lecture). *ChemBioChem* **4**, 697–711 (2003).
- Schlehuber, S. & Skerra, A. Tuning ligand affinity, specificity, and folding stability of an engineered lipocalin variant—a so-called ‘anticalin’ - using a molecular random approach. *Biophys. Chem.* **96**, 213–228 (2002).
- McMahon, C. et al. Yeast surface display platform for rapid discovery of conformationally selective nanobodies. *Nat. Struct. Mol. Biol.* **25**, 289–296 (2018).
- Tiede, C. et al. Affimer proteins are versatile and renewable affinity reagents. *eLife* **6**, e24903 (2017).
- Zimmermann, I. et al. Synthetic single domain antibodies for the conformational trapping of membrane proteins. *eLife* **7**, e34317 (2018).
- Gilbreth, R. N. et al. Isoform-specific monobody inhibitors of small ubiquitin-related modifiers engineered using structure-guided library design. *Proc. Natl Acad. Sci. USA* **108**, 7751–7756 (2011).
- Dreier, B. & Pluckthun, A. Rapid selection of high-affinity binders using ribosome display. *Methods Mol. Biol.* **805**, 261–286 (2012).
- Moutel, S. et al. NaLi-H1: A universal synthetic library of humanized nanobodies providing highly functional antibodies and intrabodies. *eLife* **5**, e16228 (2016).
- Kirchhofer, A. et al. Modulation of protein properties in living cells using nanobodies. *Nat. Struct. Mol. Biol.* **17**, 133–138 (2009).
- Kummer, L. et al. Structural and functional analysis of phosphorylation-specific binders of the kinase ERK from designed ankyrin repeat protein libraries. *Proc. Natl Acad. Sci. USA* **109**, E2248–E2257 (2012).
- Koide, A., Abbatiello, S., Rothgery, L. & Koide, S. Probing protein conformational changes in living cells by using designer binding proteins: Application to the estrogen receptor. *Proc. Natl Acad. Sci. USA* **99**, 1253–1258 (2002).

44. Striebel, F., Imkamp, F., Özcelik, D. & Weber-Ban, E. Pupylation as a signal for proteasomal degradation in bacteria. *Biochim. Biophys. Acta* **1843**, 103–113 (2014).
45. Bayle, J. H. et al. Rapamycin analogs with differential binding specificity permit orthogonal control of protein activity. *Chem. Biol.* **13**, 99–107 (2006).
46. Gao, Y. et al. Complex transcriptional modulation with orthogonal and inducible dCas9 regulators. *Nat. Methods* **13**, 1043–1049 (2016).
47. Erazo-Oliveras, A. et al. Protein delivery into live cells by incubation with an endosomolytic agent. *Nat. Methods* **11**, 861–867 (2014).
48. Herce, H. D. et al. Cell-permeable nanobodies for targeted immunolabelling and antigen manipulation in living cells. *Nat. Chem.* **9**, 762–771 (2017).
49. Tsukamoto, T. et al. Visualization of gene activity in living cells. *Nat. Cell Biol.* **2**, 871–878 (2000).
50. Nabhan, J. F., Pan, H. & Lu, Q. Arrestin domain-containing protein 3 recruits the NEDD4 E3 ligase to mediate ubiquitination of the β 2-adrenergic receptor. *EMBO Rep.* **11**, 605–611 (2010).
51. Wolf, C. et al. RPA and Rad51 constitute a cell intrinsic mechanism to protect the cytosol from self DNA. *Nat. Commun.* **7**, 11752 (2016).
52. Liu, N. et al. Intrinsic and extrinsic connections of Tet3 dioxygenase with CXXC zinc finger modules. *PLoS ONE* **8**, e62755 (2013).
53. Chagin, V. O. et al. 4D Visualization of replication foci in mammalian cells corresponding to individual replicons. *Nat. Commun.* **7**, 11231 (2016).
54. Chiu, H. Y. et al. Intracellular chromobody delivery by mesoporous silica nanoparticles for antigen targeting and visualization in real time. *Sci. Rep.* **6**, 25019 (2016).
55. Ran, F. et al. Genome engineering using the CRISPR-Cas9 system. *Nat. Protoc.* **8**, 2281–2308 (2013).
56. Hermann, M. et al. Binary recombinase systems for high-resolution conditional mutagenesis. *Nucleic Acids Res.* **42**, 3894–3907 (2014).
57. Ellis, H. M. & Horvitz, H. R. Genetic control of programmed cell death in the nematode *C. elegans*. *Cell* **44**, 817–829 (1986).
58. Mello, C. & Fire, A. DNA transformation. *Methods Cell Biol.* **48**, 451–482 (1995).
59. Frøkjær-Jensen, C. et al. Random and targeted transgene insertion in *Caenorhabditis elegans* using a modified Mos1 transposon. *Nat. Methods* **11**, 529–534 (2014).
60. Zeilich, J., Mangal, S., Zanin, E. & Lambie, E. J. Establishment of a CRISPR/Cas9-based strategy for inducible protein dimerization. *microPublication Biology*. <https://doi.org/10.17912/W2208R> (2018).
61. Wei, H., Yan, B., Gagneur, J. & Conrath, B. *Caenorhabditis elegans* CES-1 Snail represses pig-1 MELK expression to control asymmetric cell division. *Genetics* **206**, 2069–2084 (2017).
62. Schwartz, H. T. & Horvitz, H. R. The *C. elegans* protein CEH-30 protects male-specific neurons from apoptosis independently of the Bcl-2 homolog CED-9. *Genes Dev.* **21**, 3181–3194 (2007).

Acknowledgements

The authors would like to thank Dr. Hartmann Harz for help with microscopy, Andrew G. Bates for building the lightbox, Dr. Congdi Song for GFP-Man1 and GFP-Lbr, Carina

Trummer for GFP-Idh1, Dr. Elisabeth Karg for GFP-Ahcy plasmids and Dr. Eric Lambie for advice on worm expression vectors. We are grateful to Dr. M. Cristina Cardoso for providing the TREX1-GFP plasmid and discussions. This work was supported by funds from the Deutsche Forschungsgemeinschaft (DFG, SFB 1243-A01 and 1064-A17), the Bayerische Forschungsförderung (AZ-1286-17), and Center for Integrated Protein Science Munich (CIPSM, EXC114). M.D.B. is a fellow of the International Max Planck Research School for Molecular Life Sciences (IMPRS-LS).

Author contributions

W.D. and H.L. conceived the project and wrote the manuscript. W.D., J.A.B. and H.W. performed the experiments. M.D.B. generated and characterized the MIN- and GFP-tagged CENPA HeLa cell line. W.D., J.A.B., H.W., B.C. and H.L. designed the experiments and interpreted results. All authors read, discussed, and approved the manuscript.

Competing interests

The authors declare no competing interests.

Additional information

Supplementary information is available for this paper at <https://doi.org/10.1038/s41467-019-14160-8>.

Correspondence and requests for materials should be addressed to H.L.

Peer review information *Nature Communications* thanks Markus Affolter, Matthias Wymann and the other, anonymous, reviewer(s) for their contribution to the peer review of this work.

Reprints and permission information is available at <http://www.nature.com/reprints>

Publisher's note Springer Nature remains neutral with regard to jurisdictional claims in published maps and institutional affiliations.



Open Access This article is licensed under a Creative Commons Attribution 4.0 International License, which permits use, sharing, adaptation, distribution and reproduction in any medium or format, as long as you give appropriate credit to the original author(s) and the source, provide a link to the Creative Commons license, and indicate if changes were made. The images or other third party material in this article are included in the article's Creative Commons license, unless indicated otherwise in a credit line to the material. If material is not included in the article's Creative Commons license and your intended use is not permitted by statutory regulation or exceeds the permitted use, you will need to obtain permission directly from the copyright holder. To view a copy of this license, visit <http://creativecommons.org/licenses/by/4.0/>.

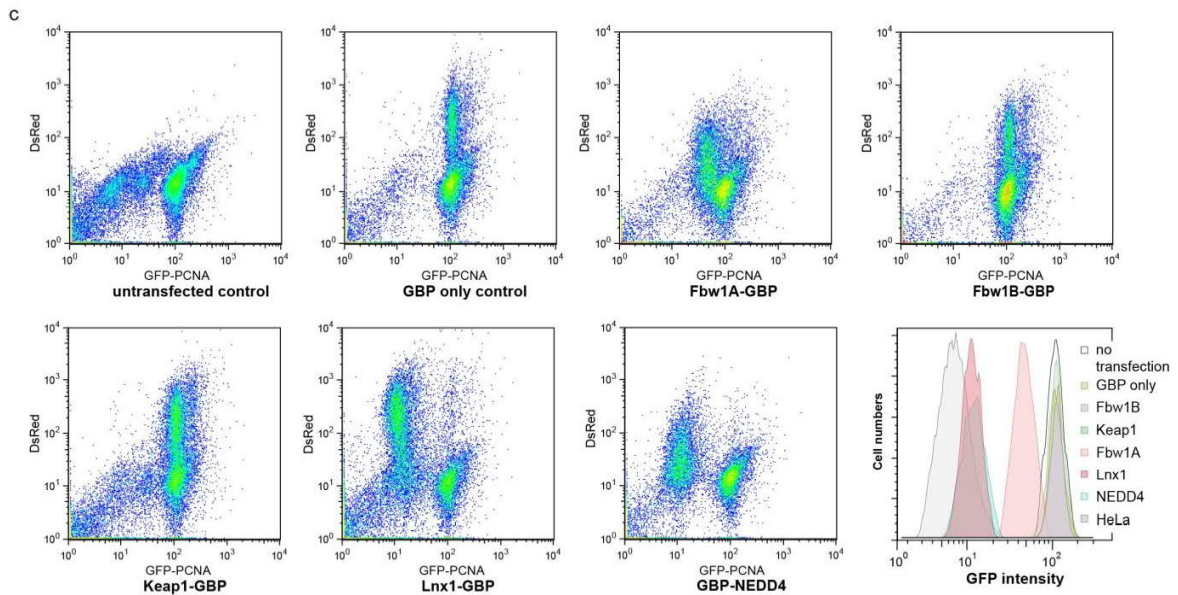
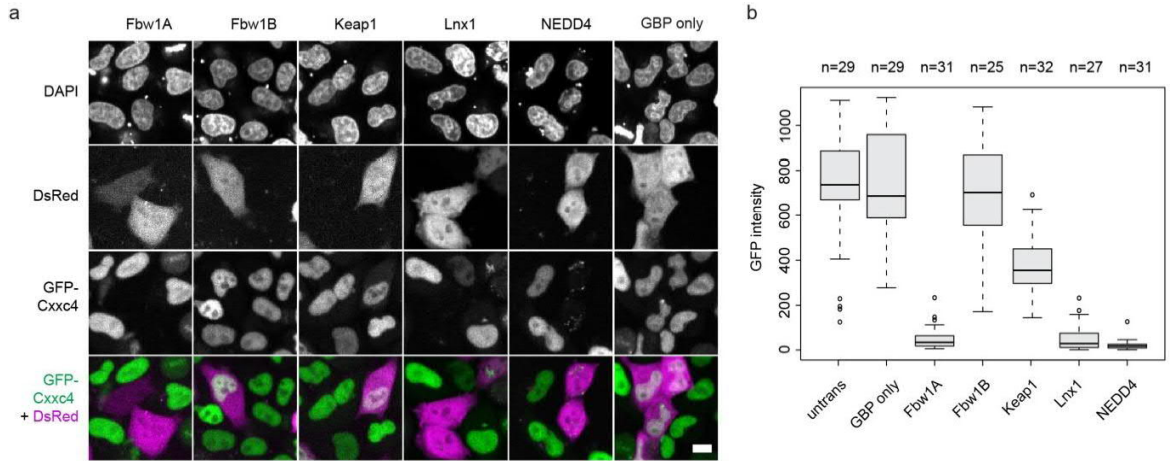
© The Author(s) 2020

Supplemental: Tunable light and drug induced depletion of target proteins

Supplementary information

Tunable light and drug induced depletion of target proteins

Deng *et al.*



d

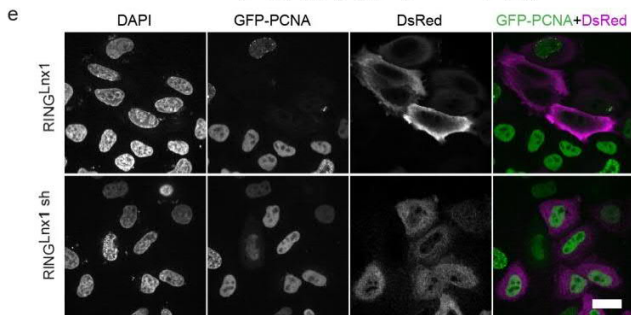
RING finger motif

SP | O70263 | LNX1_MOUSE YTEDVDDLICHICLQALLDPLDTPCGHTYCTLCLTNFLVE-KDFCFVDRKPVVLQHCCKSSILVNLKLLVTCFTE----- 114
 SP | Q8TBB1 | LNX1_HUMAN YFEEVDDLICHICLQALLDPLDTPCGHTYCTLCLTNFLVE-KDFCFVDRKPVVLQHCCKSSILVNLKLLVTCFTE----- 110
 SP | Q9Y4K3 | TRAF6_HUMAN FDPPLSKYECPCICLALREAVQTPCGHRFCACIIKSLRDAGHKCEVDNELLLENQLFPDN-FAKREILSLMVKCENEGCLHKMELRLLEDHQACEFALMDCP 164
 SP | Q8N448 | LNX2_HUMAN YQNEVDDLICHICLQALLDPLDTPCGHTYCTLCLTNFLVE-KDFCFVDRKPVVLQHCCKSSILVNLKLLVTCFTE----- 119
 SP | Q91XL2 | LNX2_MOUSE YQGEVDDLICHICLQALLDPLDTPCGHTYCTLCLTNFLVE-KDFCFVDRKPVVLQHCCKSSILVNLKLLVTCFTE----- 120

..... * * * * * : : : * * * * * : * : : : : : * * * : : : : : * * * *

SP | O70263 | LNX1_MOUSE HCTEVLQRCDLQHHFQTSCKGASHY-----GLTKDRKRRSQDQCPD---G--CASL-MATTLG--PEVSAAA 172
 SP | Q8TBB1 | LNX1_HUMAN HCTQVLQRCDLEHHEFTSKGASHY-----GLTKDRKRRSQDQCPD---G--CASL-TATAPS--PEVSAAA 168
 SP | Q9Y4K3 | TRAF6_HUMAN CQQRPFQKPHINIHILKDCPRQVSCDNCAASMAFEDKEIHQDNCPLANVICYCNITLIREQMPNHYLDLDCPT 237
 SP | Q8N448 | LNX2_HUMAN VCKDVMQRCDLEAHLKNCRCPGASHR-----RVALERKRTSRTQAEIENENG--PTLLDPAGTLS--PEADCLG 182
 SP | Q91XL2 | LNX2_MOUSE VCKDVMQRCDLEAHLKNCRCPGASHR-----RVDLERRKTSQTQIEGETG--STVIDPPGTLE--PETDCSG 183

* : * : : * : * : : : : * : : : : : * : : : : : * : : : : : * : : : : : * : : : : *

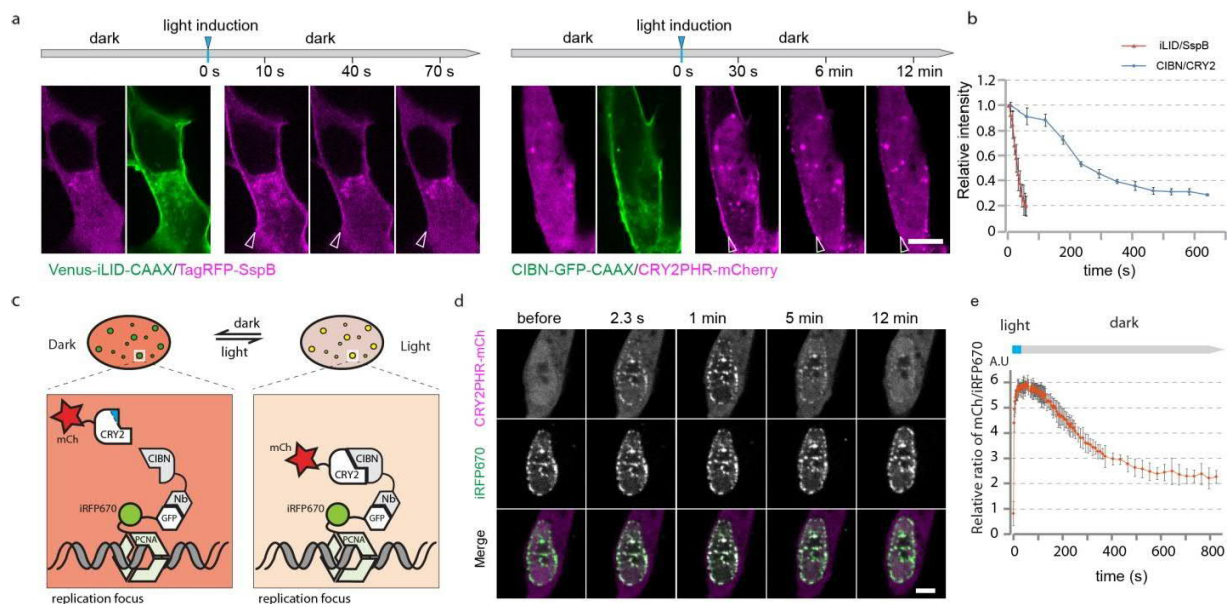


f

Protein	Efficiency	Fragments size (AAs)	Type of domain
Fbw1A	middle	239 (1-239)	F-box (Cullin-dependent)
Fbw1B	not work	228 (1-228)	F-box (Cullin-dependent)
Keap1	low	323 (1-323)	F-box (Cullin-dependent)
Lnx1	high	171 (1-171)	RING
NEDD4	high	283 (921-1303)	HECT

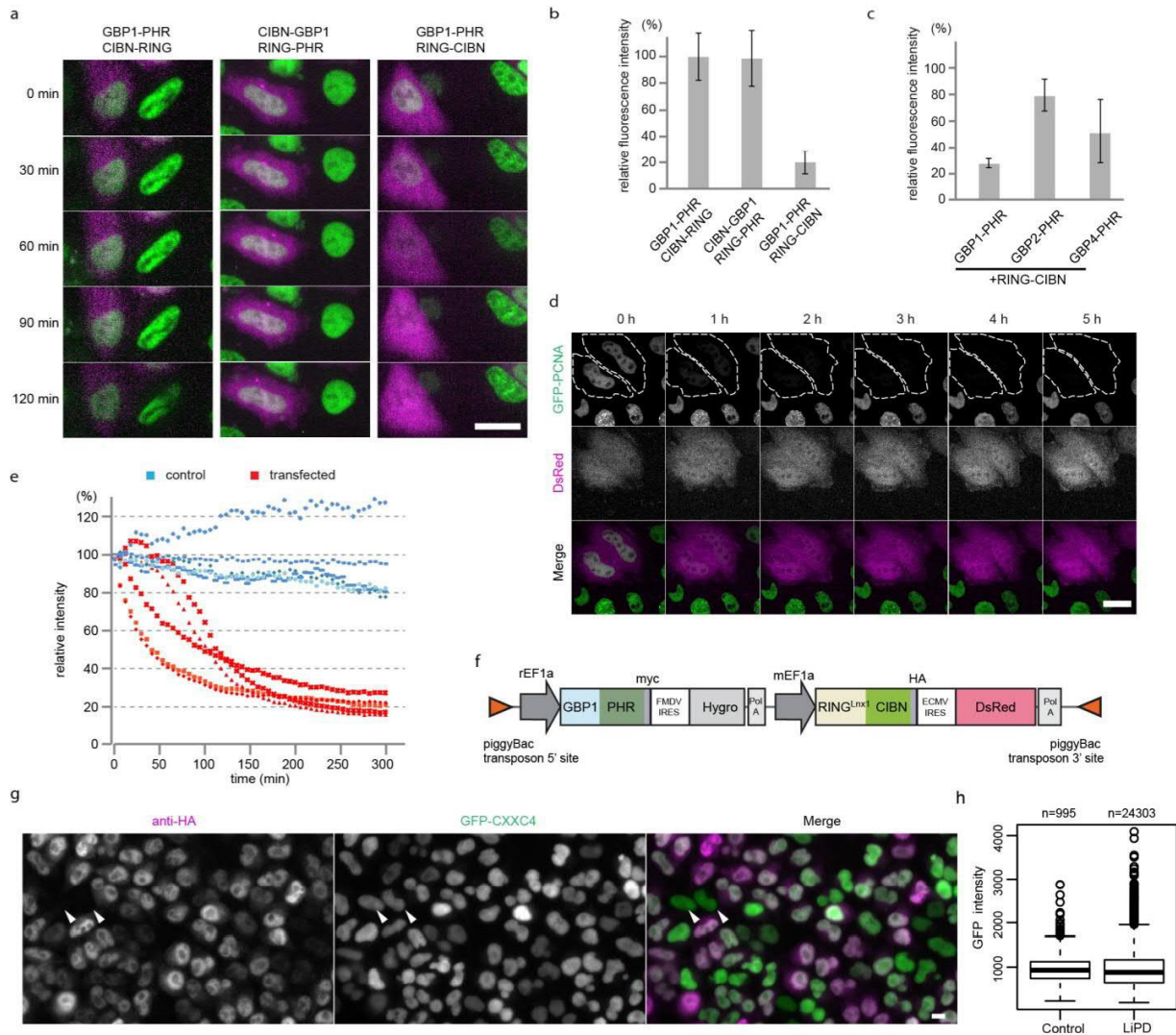
Supplementary Figure 1 Screening E3 ligase domains for efficiency in protein depletion.

a, depletion of GFP-CXXC4 with candidate E3 ligase domains fused with a GFP binding nanobody (GBP1). DsRed expression is linked via an IRES with expression of the respective E3 ligase fusion to mark cells transiently expressing the E3 ligase fusion. Scale bar represents 10 μm . **b**, Image analysis based quantification of GFP-CXXC4 fluorescence in cells expressing the different E3 ligase fusions. Boxes show the 25th to 75th percentile range (interquartile range, IQR), and the whiskers indicate 1.5 times IQR, outliers are the values higher than 1.5 times IQR above the third quartile or values lower than 1.5 times IQR below the first quartile, medians are shown as lines in the boxes. **c**, Flow cytometry profiles of GFP-PCNA HeLa cells expressing the five different E3 ligase nanobody fusions in comparison to nanobody only or untransfected GFP-PCNA HeLa cells and to HeLa wild-type cells. The GFP-PCNA intensity of (DsRed positive) cells are displayed in the histogram. **d**, Protein sequence alignment of RING domains from closely related LNX proteins and TRAF6. **e**, The efficiency in protein depletion of the long RING (RING^{Lnx1}) and short RING (RING^{Lnx1 sh}) fragments was compared as in part **a**. Scale bar is 20 μm . **f**, Features list of the E3 ligases tested in this study.



Supplementary Figure 2 Association and dissociation dynamics of light induced heterodimer components.

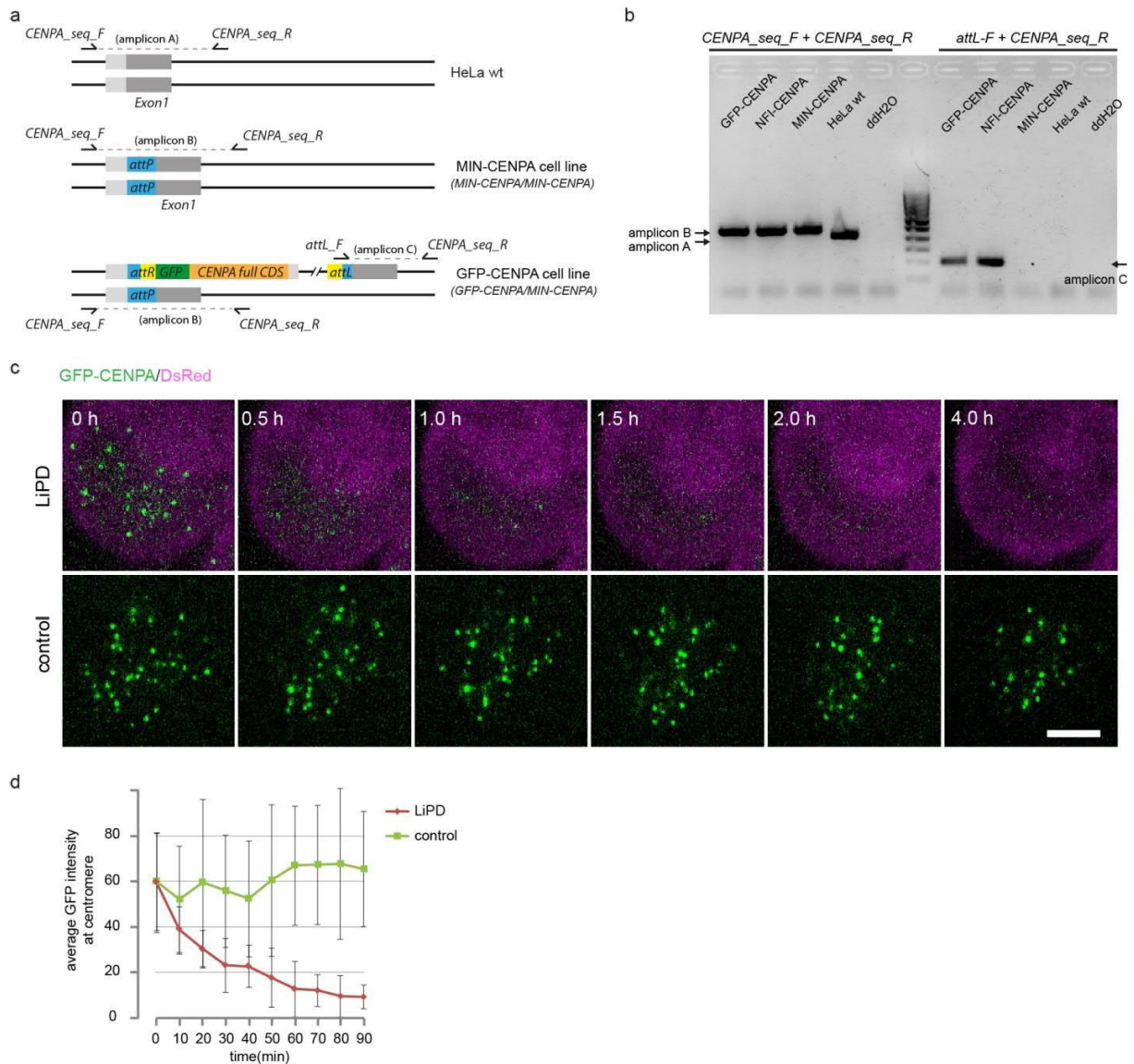
a, Two LID pairs, iLID/SspB and CIBN/CRY2PHR, were tagged with different fluorescent proteins and tested by live cell imaging. One component of each LID heterodimer (iLID and CIBN) was anchored at the cell membrane by fusion with the K-RAS4b CAAX isoprenylation sequence (KKKKKSKTKCVIM) at the C-termini of the two proteins. Light induced heterodimer formation at the cell membrane (marked with arrows) was monitored by fluorescence microscopy; please note the different time intervals indicated above. **b**, The heterodimer formation was quantified as enrichment of the second component (TagRFP-SspB and CRY2PHR-mCherry) at the membrane over time. The direct comparison shows that the CIBN/CRY2PHR heterodimer has a longer half-time (about 5 min) and was therefore chosen for subsequent experiments. For each group, five cells were measured, and results are shown as mean value \pm SD. The CIBN/CRY2PHR heterodimer formation was also tested with another cellular anchor as outlined in **c**. Here, the CIBN part was recruited to replication foci via a GFP binding nanobody (GBP1) that binds the GFP-PCNA fusion protein, which was in addition fused with near-infrared FP iRFP670 for imaging. **d**, The enrichment of CRY2PHR-mCh at replication foci after light induced dimerization was monitored with fluorescence microscopy over time. **e**, Quantification of enrichment at replication foci reveals a similar dissociation dynamics as for the membrane recruitment in **b** with half-times of about 5 min. Error bars are defined as SD., number of analyzed cells = 9. For **a** - **e**, Heterodimer formation was induced with a 488 nm laser (10% of 2.5 mW for 0.6 s); scale bars represent 10 μ m.



Supplementary Figure 3 Optimization of light induced protein depletion (LiPD).

a, For LiPD the more stable CIBN/PHRCRY2 heterodimer pair (see Supplementary Fig. 2) was chosen and different orientations for the functional domain fusions were tested. We compared N- and C-terminal fusions with the targeting nanobody (GBP1) and the RING ubiquitin ligase domain (RING). Cells expressing the LiPD construct were identified by the co-expressed DsRed marker shown in magenta. The capacity of these different LiPD constructs to deplete a cellular GFP-tagged protein (GFP-PCNA stably expressed in HeLa cells) was monitored over 120 min with repeated light induced dimerization using a 488 nm laser (10% of 2.5 mW for 0.6 s) every 10 min. **b**, The efficiency of different LiPD constructs to deplete GFP-PCNA was evaluated at the 120 min time point by comparing the average nuclear fluorescence intensity at 0 min and 120 min. The direct comparison shows that the GBP1-PHR/RING-CIBN combination was by far the most efficient in depleting the cellular target protein. Error bars are defined as SD. **c**, Two more GFP binding nanobodies (GBP2 and GBP4) were tested using this LiPD orientation and the same experimental set-up but found to be less efficient. Error bars are defined as

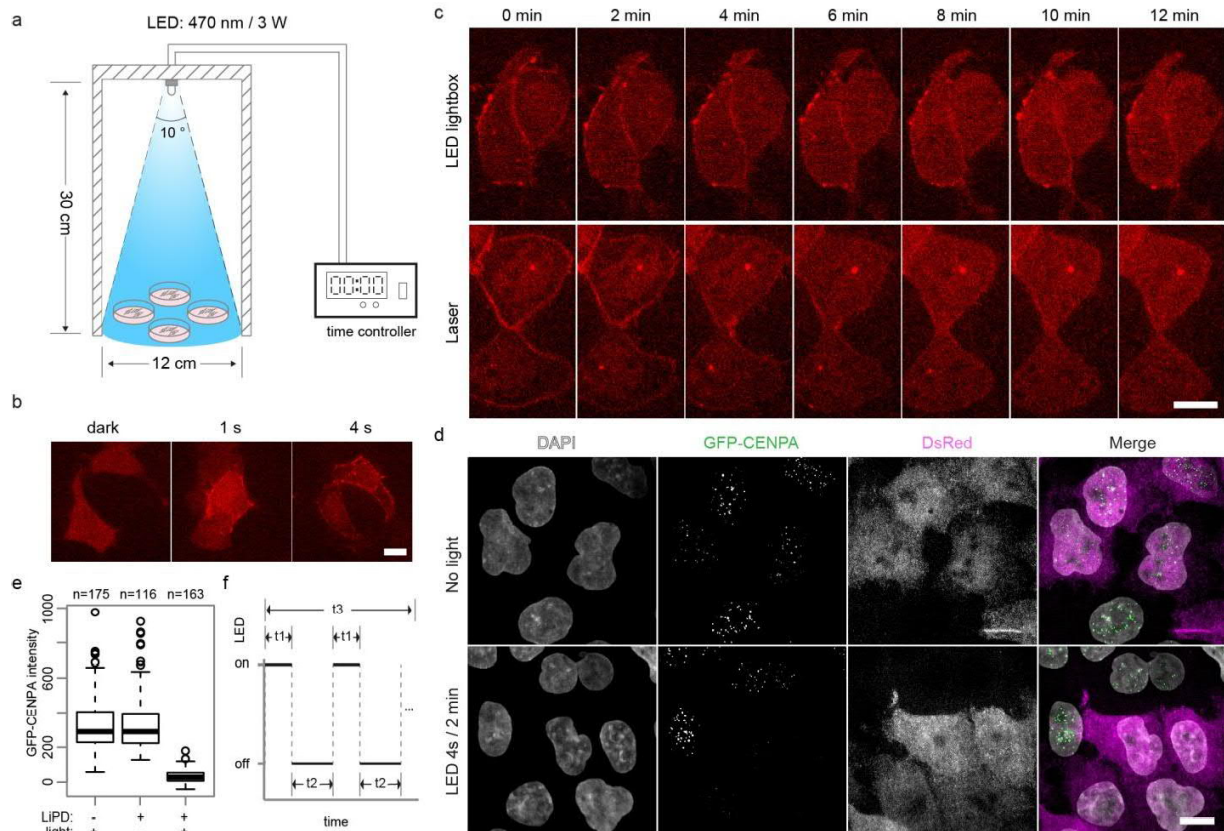
SD. **d**, The optimized LiPD construct (GBP1-PHR/RING-CIBN) was used to deplete the stably expressed GFP-PCNA and cells were monitored over 5 h. Cells expressing the LiPD construct were identified by the co-expressed DsRed and are marked with a dashed line. **e**, Relative nuclear fluorescence intensities of five cells for each group were measured every 10 min and plotted. **f**, The optimal LiPD combination (GBP1-PHR/RING-CIBN) identified in this study was placed in a piggyBac vector for further applications (see Fig. 1 and Supplementary Fig. 4). A single two promoter cassette was generated for constant stoichiometric expression of LiPD system components including a drug resistance gene (hygro, hygromycin B phosphotransferase) for selection and a fluorescent marker (DsRed) to identify cells expressing the LiPD components. Transposon 5' and 3' inverted terminal repeats (ITRs) are incorporated enabling highly efficient piggyBac transposase mediated cell line generation. **g**, Images of GFP-CXXC4 cells stably expressing the LiPD system. GFP-CXXC4 cells expressing the LiPD system (anti-HA positive cells) and control cells without the LiPD (arrowhead, anti-HA negative) were mixed and imaged for detection of background protein depletion caused by the system under these experimental conditions. **h**, GFP intensities of cells with and without the LiPD were quantified and plotted, showing on average only a weak (~3%) background degradation of the target protein GFP-CXXC4. Boxes show the 25th to 75th percentile range (interquartile range, IQR), and the whiskers indicate 1.5 times IQR, outliers are the values higher than 1.5 times IQR above the third quartile or values lower than 1.5 times IQR below the first quartile, medians are shown as lines in the boxes. Scale bars stand for 10 μ m.



Supplementary Figure 4 Light induced depletion of tagged endogenous proteins.

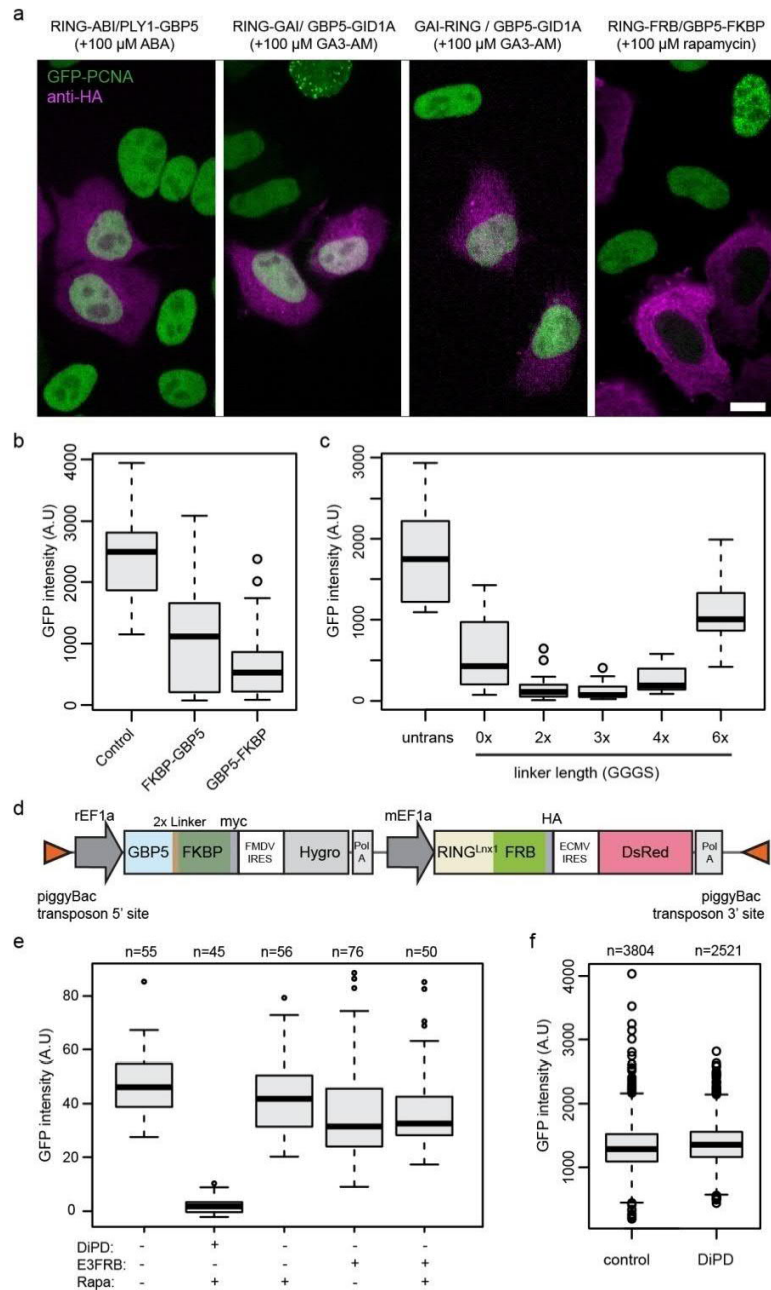
a, A GFP-CENPA knock-in cell line was generated using a two step protocol. First, *attP* (MIN-tag) sites were introduced using CRISPR/Cas9 at the 5' end of the *CENPA* ORF after the start codon (MIN-CENPA). Second, the *GFP-CENPA* was integrated into the *attP* site by the Bxb1 mediated recombination and thereby placed under the transcriptional control of the endogenous *CENPA* promoter (GFP-CENPA). **b**, Characterization of the GFP-CENPA endogenous knock-in cell line by PCR. Two pairs of primers as shown in **a** were used to amplify the recombinant *GFP-CENPA* locus, one primer pair detects the *attP* site inserted at the *CENPA* locus (amplicon B), while the other pair detects the Bxb1 mediated insertion (*attL*) of GFP-CENPA at the locus (amplicon C). Both primer pairs together indicate that the GFP-CENPA cell line is heterozygotic with one allele containing the GFP-CENPA knock-in and the other allele harboring the original MIN-tag at the endogenous *CENPA* locus. HeLa wt cells were used as negative control and heterozygotic NFI-CENPA (N-terminally FLAG-tagged CENPA) as positive control for amplicon C. **c**, Light induced depletion of GFP-CENPA by the LiPD system. GFP-CENPA was degraded quickly after

exposure to blue light (same protocol as in Supplementary Fig. 3a). Scale bar is 10 μ m. **d**, Quantification of GFP-CENPA at centromeres after light induction. For each time point 26 to 57 centromeres were identified and measured. Average GFP intensity at recognized centromere is shown; error bars are defined as SD. However, as progressing protein depletion reduced the fluorescent label and left less recognizable centromeres we systematically underestimated the overall protein depletion.



Supplementary Figure 5 Population-wide light induced protein depletion.

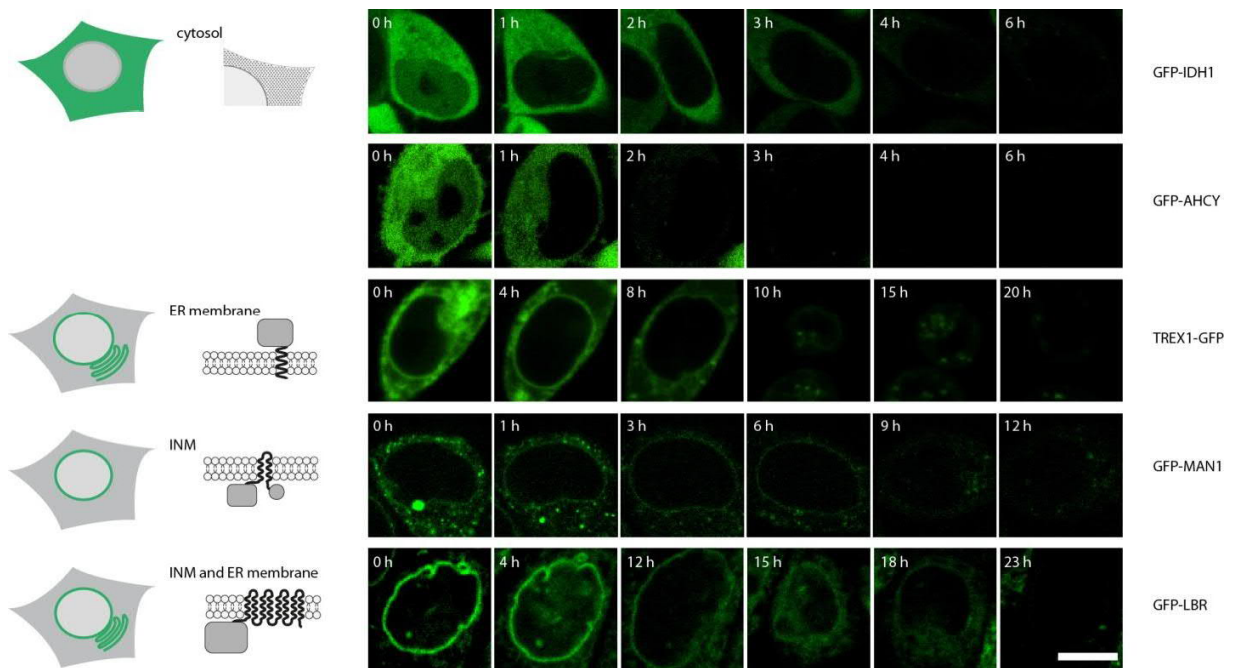
a, Schematic outline of the LED lightbox. **b**, LED light induced hetero-dimerization of Venus-CIBN-CAAX and mCh-CRY2PHR. LED lightbox induced heterodimerization of mCherry tagged CRY2PHR with Venus-CIBN-CAAX at the cell membrane following 1 or 4 s of illumination. **c**, Heterodimers as in **b** were induced with laser (488 nm, 10% of 2.5 mW for 0.6 s) and LED lightbox (4 s). The dissociation of heterodimers was monitored over time revealing a similar half life time of about 6 min for LED and laser induced dimers. **d**, Stable LiPD/GFP-CENPA cells (DsRed expressing) were mixed with GFP-CENPA HeLa cells (serving as internal controls) and examined for LED light induced depletion of GFP-CENPA. After 4 h no GFP-CENPA signal was detected in LED illuminated cells expressing the LiPD (DsRed positive shown in magenta) while little to no depletion was observed in neighboring cells without the LiPD or in cells that were not illuminated (no light). Scale bars represent 10 μm . **e**, Quantification of the LED light induced depletion of GFP-CENPA in cells. Boxes show the 25th to 75th percentile range (interquartile range, IQR), and the whiskers indicate 1.5 times IQR, outliers are the values higher than 1.5 times IQR above the third quartile or values lower than 1.5 times IQR below the first quartile, medians are shown as lines in the boxes. **f**, Scheme of the binary program for light induced dimerization with the LED lightbox. In this set-up the duration of the illumination periods (t_1), the dark intervals (t_2) and the entire process (t_3) can be defined and optimized. Scale bars are 10 μm .



Supplementary Figure 6 Optimization of the drug induced protein depletion (DiPD) system.

a, Representative fluorescent images of directed protein depletion by three different chemically induced protein interaction pairs. Among the tested combinations, only the FKBP-FRB pair, and not the ABI-PLY1 or GAI-GID1A systems, showed efficient depletion of the POI (GFP-PCNA, in green) after treatment with the corresponding inducers. The expression of the respective system was detected with antibodies recognizing the HA tag (in magenta). Scale bar represents 10 μ m. **b**, Testing different GBP/FKBP orientations for the DiPD. GBP5 at both, the N- and C- terminus, of the FKBP unit reduced GFP-PCNA levels upon induction, whereby the N-terminal GBP5 fusion of FKBP showed a better efficiency. **c**, Effects

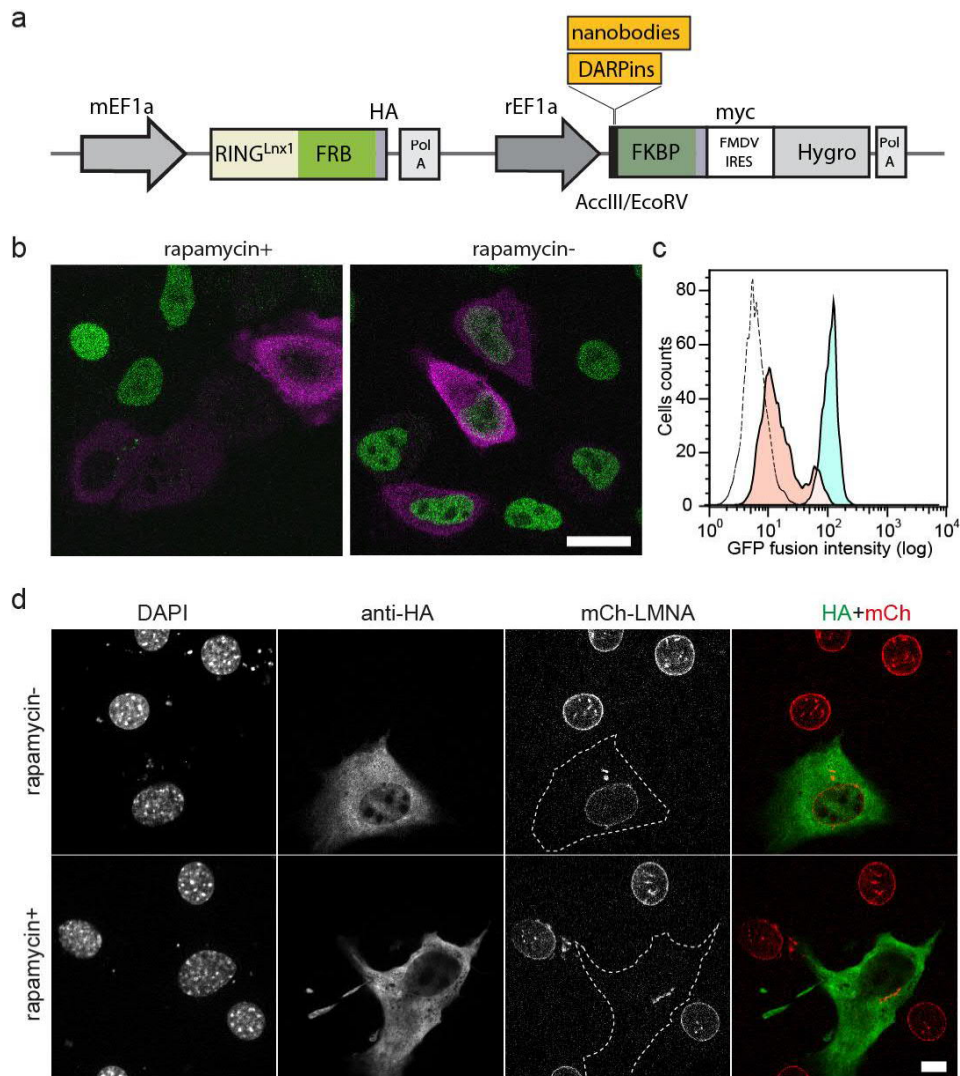
of the flexible linker on the efficiency of the DiPD system. Linkers with different length were tested for their effect on the drug induced depletion of GFP-PCNA protein. While DiPD constructs with the 2× and 3× GGS linkers showed the best depletion efficiencies, the longer 6× GGS linker seemed to impair protein depletion. The experiments were repeated with biologically independent samples (cell cultures): untransfected control (n = 13), 2× linker (n = 17), 3× linker (n = 16), 4× linker (n = 15), 6× linker (n = 14). Arbitrary units of GFP fluorescence are shown in box plots. **d**, Outline of the DiPD cassette compatible with piggyBac transposon system for stable genome integration. **e**, Control for E3 ligase expression and rapamycin treatment. GFP-PCNA cells were transfected to express either DiPD or E3FRB and treated with or without rapamycin. The comparison shows that all three components are required for efficient protein depletion. **f**. GFP-PCNA intensity is not affected by stable expression of the DiPD in the absence of rapamycin. The GFP-PCNA intensities of cells expressing (DiPD) or without DiPD (control) were quantified by high throughput imaging analysis. (**b**, **c**, **e** and **f**) Boxes show the 25th to 75th percentile range (interquartile range, IQR), and the whiskers indicate 1.5 times IQR, outliers are the values higher than 1.5 times IQR above the third quartile or values lower than 1.5 times IQR below the first quartile, medians are shown as lines in the boxes.



Supplementary Figure 7 Depletion of cytoplasmic and transmembrane proteins with the DiPD system.

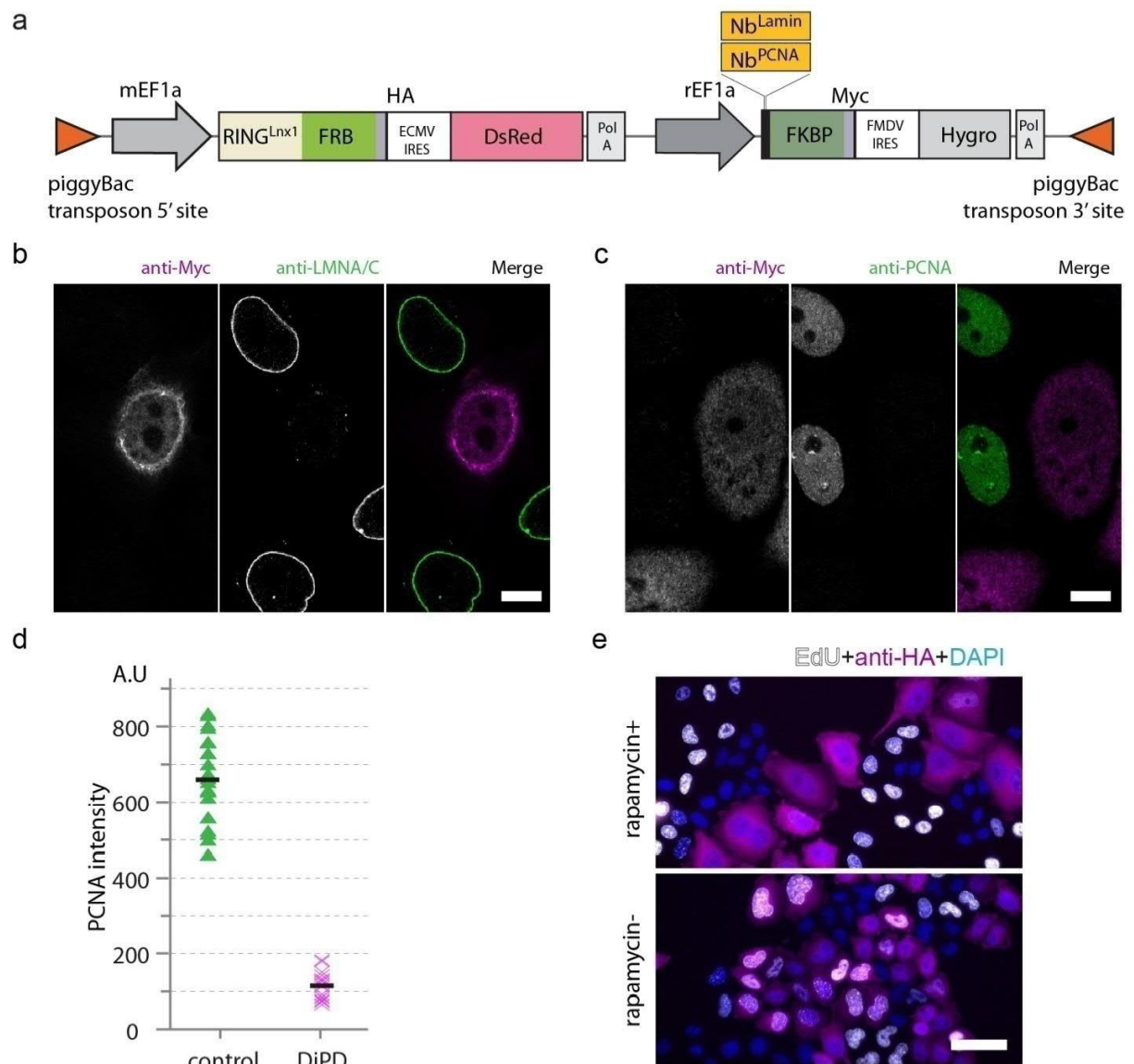
Cytosolic proteins, IDH1 and AHCY (first two rows), were rapidly depleted with the DiPD system.

Transmembrane proteins with single (TREX1), double (MAN1) or multiple (LBR) transmembrane helices were fused to GFP, and depletion of the GFP fusions by the DiPD system was induced by the addition of rapamycin (last three rows). ER, endoplasmic reticulum; INM, inner nuclear membrane. Scale bar stands for 10 μm .



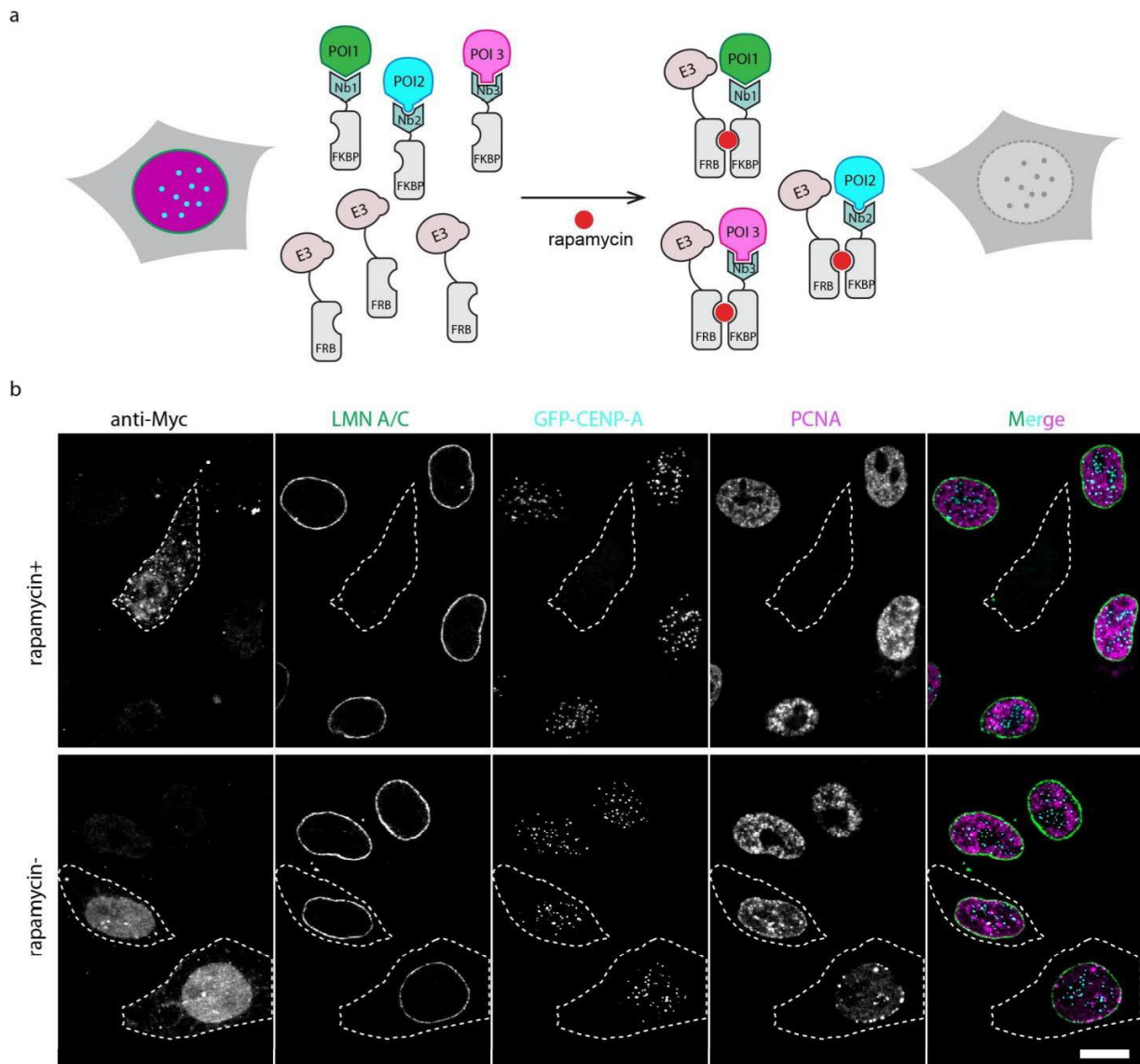
Supplementary Figure 8 Generalization of the DiPD system with different targeting modules.

a, Schematic outline of the DiPD vector accommodating different types of binding domains. To widen the application of the DiPD, a GFP binding DARPIn and mCherry binding nanobody were used. **b**, GFP-PCNA was depleted inducibly in cells transfected with the DARPIn based DiPD vector (in magenta). **c**, GFP-PCNA fluorescence in cells expressing the DARPIn based DiPD was analyzed by flow-cytometry. Untreated cells showed a clear fluorescence signal (in blue) compared to wt HeLa cells (transparent peak with dashed line). Rapamycin treatment caused a roughly tenfold reduction in mean fluorescence distribution (in brown). For each group, about 10,000 cells were analyzed. **d**, Depletion of mCherry fusion protein with an mCherry binding nanobody by the DiPD system. MEF cells stably expressing mCherry tagged LaminA (mCh-LMNA) were transfected with the mCherry binding nanobody DiPD construct (marked with dashed line). The mCh-LMNA protein was efficiently depleted upon rapamycin induction. Scale bars are 10 μ m.



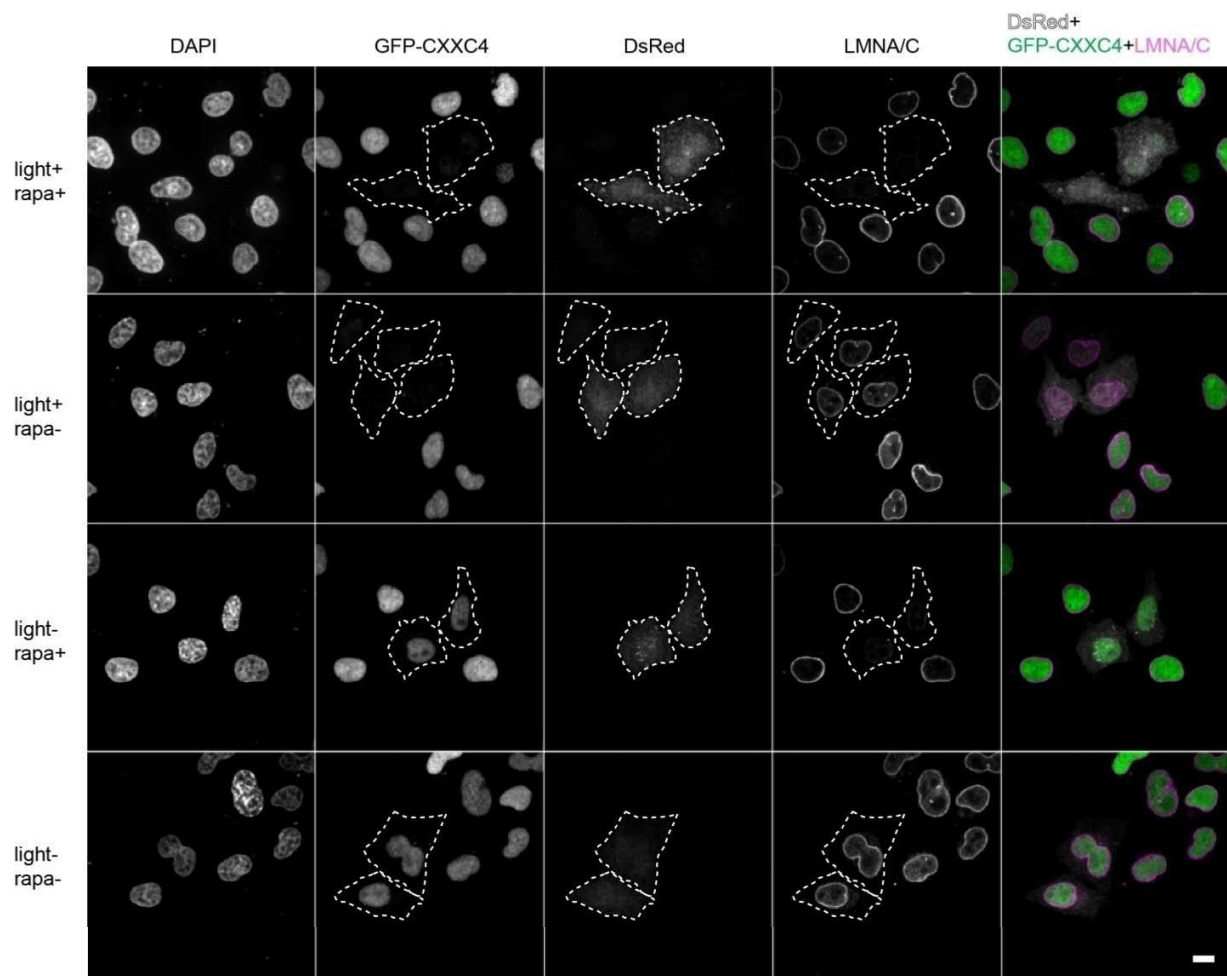
Supplementary Figure 9 Depletion of endogenous LMNA/C and PCNA with the DiPD system.

a, Schematic outline of LaminA and PCNA nanobodies (Nb) mediated DiPD for depletion of endogenous proteins. **b,c**, Depletion of endogenous LMNA/C (**b**) and PCNA (**c**) in HeLa cells with the stably integrated DiPD system. Endogenous proteins (detected by antibody) were depleted by the DiPD system (identified by anti-myc antibody) in the presence of rapamycin, but not in the co-cultured cells without the DiPD. Scale bar is 10 μm . **d**, Quantification of PCNA in cells with (DiPD) and without (control) the nanobody mediated DiPD (control group: n=22; and DiPD cells: n=17). **e**, No nuclear EdU labeling was detected in PCNA depleted cells (upper panel, rapamycin induced and DiPD expressing cells were identified with anti-HA staining in magenta). Without rapamycin induction (lower panel) EdU labeling was detected in cells independent of presence or absence of the DiPD system. Quantification is shown in Fig. 3a. Scale bar represents 50 μm .



Supplementary Figure 10 Simultaneous depletion of multiple proteins by the DiPD system.

a, Schematic outline of the multi-protein targeting DiPD system. Multiple POIs were targeted by different protein specific targeting modules (Nbs) which were embedded in the DiPD system. Upon induction with rapamycin the POIs are ubiquitinated and degraded. **b**, Triple depletion of endogenous LMNA/C, PCNA and GFP-CENPA proteins. GFP-CENPA cells were transfected with DiPD constructs targeting LMNA/C, PCNA and GFP. Proteins were detected by immunostaining or GFP fluorescence after rapamycin treatment. A triple depletion of targeted proteins could be observed in the presence of rapamycin (upper panel), but not in cells without rapamycin induction (lower panel). Scale bar represents 10 μm .

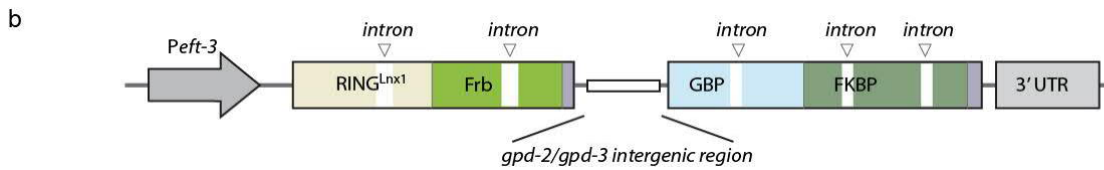


Supplementary Figure 11 Combinatorial depletion of two different proteins.

Combinatorial depletion of a nucleoplasmic (GFP-CXXC4) and a nuclear envelope protein (LMNA/C). Cells with the light- and drug- inducible protein depletion tools express DsRed as marker while surrounding DsRed negative cells serve as negative control. Scale bar is 10 μ m.

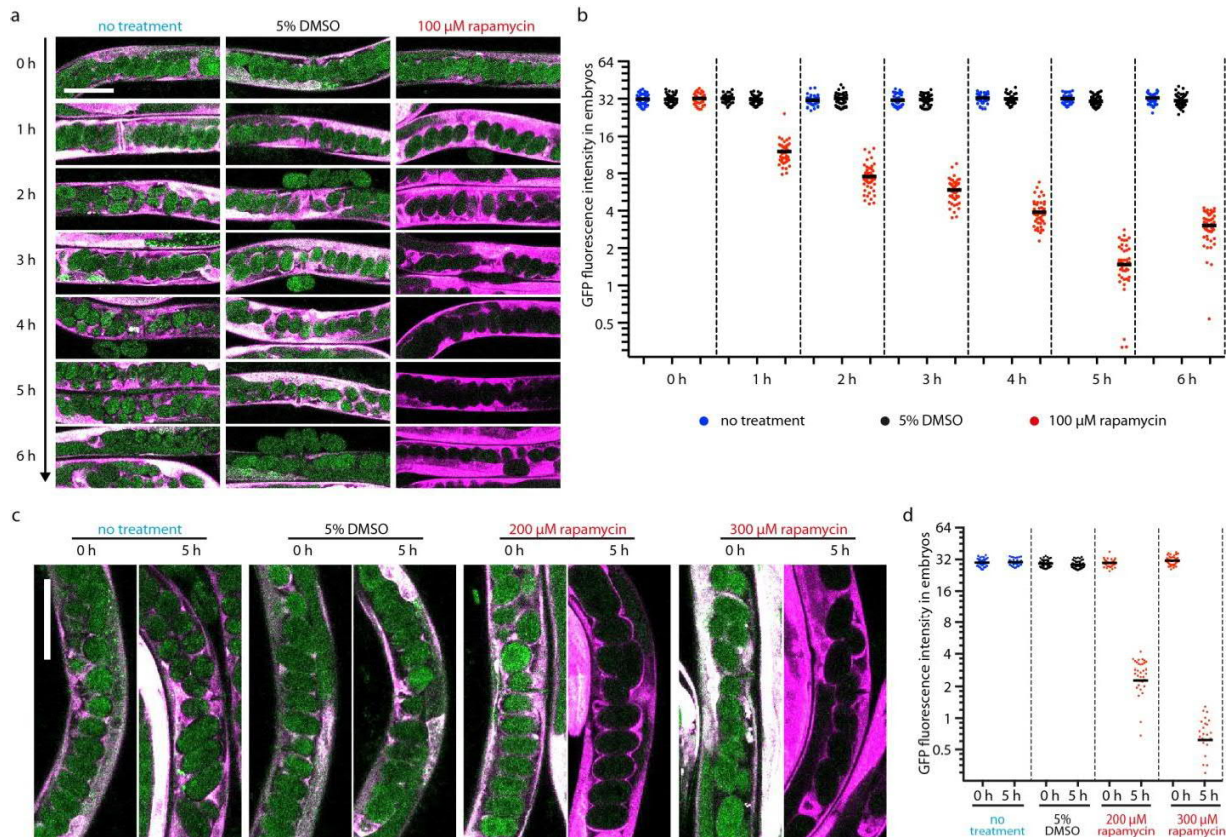
a

Mouse	1	-MALKRIHKELNDLARDPPAQC	SAGPVGDDMFHWQATIMGPNDS	PYQGGVFFLTIHFPTDYPFKPPKVAFTTRIY	74
Human	1	-MALKRIHKELNDLARDPPAQC	SAGPVGDDMFHWQATIMGPNDS	PYQGGVFFLTIHFPTDYPFKPPKVAFTTRIY	74
Worm	1	-MALKRIQKELQDLGRDPPAQC	SAGPVGDDLFHWQATIMGPES	PYQGGVFFLTIHFPTDYPFKPPKVAFTTRIY	74
Fruit fly	1	-MALKRINKELQDLGRDPPAQC	SAGPVGDDLFHWQATIMGPPDS	PYQGGVFFLTIHFPTDYPFKPPKVAFTTRIY	74
Yeast	1	MSSSKRIAKELSDLERDPPTSC	SAGPVGDDLYHWQASIMGPADS	PYAGGVFFLSIHFPDYPFKPKISFTTKIY	75
		: *** ***.** *****: .*****: :*****:****	:*** *****:*****:*****: :***:***		
Mouse	75	HPNINSNGSICLDILRSQWSPALTISKVLLSICSLLCDPNPDDPLVPEIARIYKTDREKYNRIAREWTQKYAM			147
Human	75	HPNINSNGSICLDILRSQWSPALTISKVLLSICSLLCDPNPDDPLVPEIARIYKTDREKYNRIAREWTQKYAM			147
Worm	75	HPNINSNGSICLDILRSQWSPALTISKVLLSICSLLCDPNPDDPLVPEIARIYKTDREKYNQLAREWTQKYAM			147
Fruit fly	75	HPNINSNGSICLDILRSQWSPALTISKVLLSICSLLCDPNPDDPLVPEIARIYKTDREKYNELAREWTRKYAM			147
Yeast	76	HPNINANGNICLDILKQWSPALTLSKVLLSICSLTLDANPDDPLVPEIAHIYKTDREPKYEATAREWTRKYAV			148
		*****:*.*****: .*****:*****:***** * *****:***** :*: *****:***:			



Supplementary Figure 12 Application of the DiPD system in *C. elegans*.

a, Alignment of the E2 ubiquitin conjugation enzyme UBE2D2 homologs shows high sequence conservation, which indicates a similar mechanism for protein ubiquitination and suggests that the mouse derived E3 RING^{Lnx1} ligase should function with the conserved *C. elegans* E2 enzyme. Protein sequences were taken from UniProt database (sequence IDs are: P62838 (mouse); P62837 (human); P35129 (worm); P25867 (fruit fly); P15731 (yeast)). **b**, Construction of a DiPD vector for expression in *C. elegans*. The DiPD system was codon-optimized for expression in *C. elegans* and placed under the transcriptional control of the ubiquitous *eft-3* promoter. Artificial introns were used to enhance the expression and a *gpd-2/gpd-3* intergenic region was inserted to achieve equal expression levels of both parts.



Supplementary Fig. 13 Time and dose dependent depletion of CED3::GFP in worm embryos.

a, Images of CED3::GFP in *C. elegans* embryos for the first 6 h after rapamycin induction. Untreated or DMSO treated worms serve as control. **b**, Quantitative analysis of CED3::GFP in worm embryos. Depletion of CED3::GFP could already be detected at the first time point (1h), and reached maximal depletion between 4 to 6 h. For each time point, 29 to 53 embryos were quantified. **c**, **d**, Rapamycin dose dependent depletion of the CED3::GFP in worms. Compared to **a** and **b**, two higher concentrations of rapamycin (200 μ M and 300 μ M) were administrated to worms, and the CED3::GFP in worm embryos was imaged (**c**) and analyzed (**d**) 5 h after treatment, showing a dose dependent depletion of the target protein. For each time point, 31 to 53 embryos were quantified. Scale bar is 50 μ m.

Supplementary Table 1. Primers used in this study.

name	sequences
Fbxw1A-F	AAGCTAGCATGGACCCGGCAGAGG
Fbxw1A-R	CTAGATCTCACTCCGGCAGTGGATTCTC
mFbxw11-F	TAGCTAGCATGGAGCCCCGACTCGGT
mFbxw11-R	TCCAAGCTGCTTTTATCCCAGATCTTG
Keap1-F	GGGCTAGCATGCAGCCCGAACCCAA
Keap1-R	GCAGATCTTGGGCGCGCGGAG
LnX1up	GCGCTAGCCATGAACCAACCGGACC
LnX1down	AAGAGATCTTGGCGGCTGCAGAAACC
LnXSTOPdown	CGAGATCTTAGGCGGCTGCAG
NEDD4-F	AACTCGAGCTACTCCAGGGATTACAAAAG
NEDD4-R	AAGTCGACCTAATCAACTCCATCAAAGCCC
Nb-F	AAAGATCTCGATGGCTCAGGTGCAGCTGC
Nb-R	TTGTGCGACTCAGGAGACGGTGACCTGG
ShRING-GBP-F	CGTTCACGGGGAGCGGATGGCATGAAGGCCTGGAAGA
ShRING-R	TCCGCTCCCCGTGAACGGGCAGGTGAC
CIBN-Nb-F	GCGCTAGCATGAATGGAGCTATAGGAG
CIBN-Nb-R	GCGAAGATCTCATGAATATAATCCGTTTTTC
CRY2-F	GAGAGCTCCATGAAGATGGACAAAAAGA
CRY2-R	TGGTCGACTTATGCTGCTCCGATCATG
Nb-CIBN-F	GCGAGCTCCATGAATGGAGCTATAGGAG
Nb-CIBN-R	CGAGTCGACTTAATGAATATAATCCGTTTTTC
E3-F	CCATGAACCAACCGGACCTTGC
E3-R	GGCGGCTGCAGAAACCT
rEF1aGib-F	GAAAGCCACCGCTAATCAAAGCAA
E3-Gibson-F	AAGCAACCGGTGCCACCATGAACCAACCGGACCTTGC
E3-CIBN-F	AGAGGTTTCTGCAGCCGCCATGAATGGAGCTATAGGAGGTGACCT
CIBN-HA-R	TCTTATCATGTCTGGCCAGCTAGCTGTACATTACGCGTAGTCTGGCACGTCGTAGGGGT AATGAATATAATCCGTTTTCTCCAATTCC
Nb-Gibson-F	GAAAGCCACCGCTAATCAAAGCAATCCGGACCGCCATGGCTCAGGTGCAGCTGGTG
Nb-Gibson-R	TCCCACCACCTGAGGAGACGGTGACCTG
linker-CRY2-F	TCACCGTCTCCTCAGGTGGTGGGAGCATGAA
CRY2-myc-R	TGCTCCTAGGCGTACGGGATCCTTAAAGCAGGTCTCCTCTGAGATCAGCTTCTGCATT GCTGCTCCGATCATGATC
pVitro-ORF2-R	TTGGGGAAACCTGCTCCTAGGCGTACGGGATCC
LnXRING-F	ACCTTAATGGAGGCTCCATGAACCAACCGGA
LnXRING-R	GGCACGTCGTAGGGGTAGGCGGCTGCAGAAAC
HA-R	GGGCGCTAGCTGTACATTACGCGTAGTCTGGCACGTCGTAGGGGT
GID1A-F	TGGTGGGAGCATGCTCGAGGCTGCGAGCGATGAA
GID1A-R	TTAAAGCAGGTCTCCTCTGAGATCAGCTTCTGCTCACATTCCGCGTTTACAAAC
E3-R2	CTTCATGGAGGCGGCTGCAGAAACCT
GAI-F	AGCCGCCTCCATGAAGAGAGATCATCATCATC
GAI-R	GGCACGTCGTAGGGGTAAATTAAGGTCGGTGAGCATAG
PLY-F	GGAACCGCCATGCTCGAGACTCAAGACGAATTCACCC

PLY-R	ATGCTGCCTCCTCCGTCGACGTTTCATAGCTTCAGTGATCG
ABI-F	GCCGCCTCCATGAAGGTGCCTTTGTATGGTTTTACTTC
ABI-R	TGGTGGTGGTTGATTTGAAGTACCCCTACGACGTGCC
ABI-R2	GGCACGTCGTAGGGGTACTTCAAATCAACCACCACCA
GAI1N-F	CACCGCTAATCAAAGCAACCGGTGCCACCATGAAGAGAGATC
GAI1N-R	GGAGCCTCCATTAAGGTCGGTGAGCATAG
Vect-GBP-F	GCAATCCGGAACCGCCATGGCTCAGGTGCAGCT
GBP-L-R	GAGCATGCTCCCACCACCTGAGGAGACGGTGACCTG
GBP-L-F	TCCTCAGGTGGTGGGAGCATGCTCGAGGGCGTGCA
FK-myc-V-R	TACGGGATCCTTAAAGCAGGTCTCCTCTGAGATCAGCTTCTGCATGTCGACTTCCAGTT TTAGAAGCTC
Vect-FK-F	GCAATCCGGAACCGCCATGCTCGAGGGCGTGCA
FK-L-GBP-R	CCTGAGCCATGCTGCCTCCTCCGTCGAC
L-GBP-F	AGGAGGCAGCATGGCTCAGGTGCAGCTG
myc-Vect-R	ACGGGATCCTTAAAGCAGGTCTCCTCTG
2xlinker-F	TCCTCAGGAGGAGGCTCCGGTGGTGGGAGCATGCTCG
2Xlinker-R	GGAGCCTCCTCCTGAGGAGACGGTGACCTGG
3xlinker-F	CGGTGGCTCTGGAGGAGGCTCCGGTGGTGGGAGCATGCTC
3xlinker-R	CCTCCTCCAGAGCCACCGCCTGAGGAGACGGTGACCTGG
4xlinker-F	GAGCATGCTCCCACCACCGGAGCCTCCTCCAGAGCCACCG
4xlinker-R	GGACCCACCTCCTGAGGAGACGGTGACCTGGG
6xlinker-F	GGCGGCGGCAGTGCCGGAGGATCAGGAGGTGGGTCCGGCGG
6xlinker-R	CCTCCGCCACTGCCGCCGCTGAGGAGACGGTGACCTGGG
rEF1-F	GAAAGCCACCGCTAATCAAAGCAA
rEF1-Nb-F	GCAATCCGGAACCGCCATGGCTCAGGTGCAGCT
Nb-R	TGAGGAGACGGTGACCT
Nb-linker-R	CACCGGAGCCTCCTCCGATTGAGGAGACGGTGACCTGG
Nb-Gibson-R	GCTCCCACCACCGGAGCC
FKBP-F	ATGCTCGAGGGCGTGACAGGTGG
FKBP-Gibson-F	CTCCGGTGGTGGGAGCATGCTCGAGGGCGTGCA
FKBP-R	GTCGACTTCCAGTTTTAGAAGCTCCA
FKBP-myc-R	TACGGGATCCTTAAAGCAGGTCTCCTCTGAGATCAGCTTCTGCATGTCGACTTCCAGTT TTAGAAGCTC
FKBP-Gibson-R	CTGCTCCTAGGCGTACGGGATCCTTAAAGCAGGTCTCCTCT
mEF1E3-F	AAGCAACCGGTGCCACCATGAACCAACCGGACCTTGC
E3-Gibson-R	CTTCATGCCAGGCGGCTGCAGAAACCT
Frb-Gibson-F	TGCAGCCGCCTGGCATGAAGGCCTGGAA
Frb-HA-R	GCCAGCTAGCTGTACATTACGCGTAGTCTGGCACGTCGTAGGGGTAGAACTGCTTTGA GATTCGTCGG
EcoV-FKBP	CACCGCTAATCAAAGCAATCCGGAGATATCGGAGGAGGCTCCGGTGGTG
DARPin-F	GCCACCATGGGACCTGGTTCCGATTTGG
DARPin-R	AGCGGCTTTTTGAAGTACCTCG
Nb-F1	ATCAAAGCAATCCGGAGATGCCACCATGGCTCAGGTGCAGCTGGT
Nb-F2	ATCAAAGCAATCCGGAGATGCCACCATGGCTCAGGTGCAGCTG
NbLamin-R	CACCGGAGCCTCCTCCGATTGAGGAGACGGTGACCTGG
LaM4-R	CACCGGAGCCTCCTCCGATTGAGCTAACTGTCACCTGAGT

Peft3-GBP-F	TTCAGTTGGGAAACACTTTGCTCTAGAAAAAATGGCTCAAGTTCAGCTCCA
HA-Peft3-R	GCTTGAAAGGATTTTGCATTTATCACTAGTTTACGCGTAATCAGGCACGTC
inter-GBP-F	GGGAAACTGCTGTACCGGTAGAAAAAATGGCTC
inter-GBP-R	CTACCGGTACAGCAGTTTCCCTGAATTTAAAATTAG
Peft3-E3-F	TTCAGTTGGGAAACACTTTGCTCTAGAAAAAATGGCGTCTGAAACTAAAGCC
myc-Peft3-R	GCTTGAAAGGATTTTGCATTTATCACTAGTTTAAAGCAAATCTTCTCTGATAT
LmnA-F	GGGCGATCGCATGGAGACCCCGCTACA
LmnA-R	AGTCGCGGCCGCTTTACATGATGCTGC
MINexternal-F	CAGAAGCCAGCCTTTTCGCTCCC
MINexternal-R	CCTGCGAGCCTCGGTTTTCTCC
CENPA-seq-F	TCTACGTAAGGGGCGTTCCA
CENPA-seq-R	GGATCGGGACTCGGGAGAT
attL_F	CCGGCTTGTGACGACG
MIN-tag DNA donor oligo	GGCCGGGGGTCTGGGGTCTGGGCTCGGGCTGCGCCTCCTCGGGCCTCGGGCTTTGCGC TCCGGCGGCGGGCCGGTTTGTACCGTACACCACTGAGACCGCGGTGGTTGACCAGA CAAACCGAGCATGACACGCCGAGAGGGTGCTGGCGCCCGGTCCCACGGCTCCTGCTC GGGCTGCCGGGTCCGGGAGCGAAAGGC

Supplementary Table 2. Plasmids used in this study.

name	prokaryotic resistance	internal number	used in	reference
pFbx1A-GBP1-IR	Kana	pc4209	SF.1	this study
pFbx1B-GBP1-IR	Kana	pc4211	SF.1	this study
pKeap1-GBP1-IR	Kana	pc4212	SF.1	this study
pLnx1-GBP1-IR	Kana	pc4213	SF.1	this study
pGBP1-Nedd4-IR	Kana	pc4214	SF.1	this study
pGBP1-IR	Kana	pc4215	SF.1	this study
pRINGsh-GBP1-IR	Kana	pc4216	SF.1	this study
pLL7.0: Venus-iLID-CAAX	Amp	Addgene Plasmid #60411	SF.2	Guntas et al. 2016
pLL7.0: hITSN1(1159-1509)-tgRFPT-SSPB WT	Amp	Addgene Plasmid #60419	SF.2	Guntas et al. 2016
pCRY2PHR-mCherryN1	Kana	Addgene Plasmid #26866	SF.2, SF.5	Kennedy et al. 2010
pCIBN(deltaNLS)-pmGFP	Kana	Addgene Plasmid #26867	SF.2, SF.5	Kennedy et al. 2010
pNLSGFP-iRFP670-PCNA	Kana	pc4222	SF.2	this study
pCIBN-GBP1-IR	Kana	pc4223	SF.2, SF.3	this study
pGBP1-CIBN-IR	Kana	pc4224	SF.3	this study
pRING-PHR-IR	Kana	pc4225	SF.3	this study
pGBP1-PHR-IR	Kana	pc4226	SF.3	this study
pCIBN-RING-IR	Kana	pc4227	SF.3	this study
pVitro-LiPD-GBP1-IR	Hyg	pc4228	SF.3	this study
pVitro-LiPD-GBP2-IR	Hyg	pc4229	SF.3	this study
pVitro-LiPD-GBP4-IR	Hyg	pc4231	SF.3	this study
Piggybac-LiPD-GBP1-IR	Amp/Hyg	pc4232	Fig.1, 4 , SF.5, 11	this study
pSpCas9(BB)-2A-GFP (PX458)	Amp	Addgene Plasmid #48138	SF.4	Ran et al., 2013
pCAG-NLS-HA-Bxb1	Amp	Addgene Plasmid #51271	SF.4	Hermann et al. 2014
pattb-EGFP-CENPA	Kana	pc4233	SF.4, 5, 10	this study
pCAG-EGFP-Cxxc4	Amp	pc2311	Fig. 1, 4; SF.11	Liu et al. 2013
piggyBacRING-ABI1/PLY1-GBP5-IR	Amp/Hyg	pc4235	SF.6	this study

piggyBacRING-GAI/GBP5-GID1A-IR	Amp/Hyg	pc4236	SF.6	this study
piggyBacGAI-RING/GBP5-GID1A	Amp/Hyg	pc4237	SF.6	this study
pRING-FRB-HA /FKBP-GBP5-myc	Hyg	pc4238	SF.6	this study
pVitro-DiPD0L	Hyg	pc4242	SF.6	this study
pVitro-DiPD2L	Hyg	pc4243	SF.6	this study
pVitro-DiPD3L	Hyg	pc4244	SF.6	this study
pVitro-DiPD4L	Hyg	pc4245	SF.6	this study
pVitro-DiPD6L	Hyg	pc4246	SF.6	this study
pVitro-DiPD-GBP5-IR	Hyg	pc4247	Fig.4, SF.11	this study
Piggybac-DiPD-GBP5-IR	Amp/Hyg	pc4248	Fig.4, SF.6	this study
pVitro-E3FRB-GBP5	Hyg	pc4234	SF.6	this study
pCAG-EGFP-Lbr-IB	Amp	pc2631	SF.7	this study
pEGFP-N1_hTrex1-WT	Kana	-	SF.7	Wolf et al. 2016
pCAG-EGFP-IDH1-IB	Amp	pc3492	SF.7	this study
pCAG-EGFP-Ahcy-IB	Amp	pc3688	SF.7	this study
pCAG-EGFP-Man1-IB	Amp	pc3081	SF.7	this study
pVitro-DiPD base	Hyg	pc4249	SF.7	this study
pVitro-DiPD-DARPin-IR	Hyg	pc4251	SF.7	this study
pVitro-DiPD-LaM4	Hyg	pc4252	SF.7	this study
pPGK-mCh-LaminA	Amp	pc4253	SF.7	this study
Piggybac-DiPD-aLamin-IR	Amp/Hyg	pc4254	Fig.4, SF.9, 10,11	this study
Piggybac-DiPD-aPCNA-IR	Amp/Hyg	pc4255	Fig.3,4; SF.9,10	this study
pGFP-LIG1	Kana	pc613	Fig.3	Mortusewicz et al. 2006
<i>P_{eft-3}ring::frb::ha::gpd-2/gpd-3::gfp5::fkbp::myc_3'UTR</i>	Amp	pc4257	Fig.5	this study
<i>P_{ced-3}ced-3::gfp</i>	Amp	-	Fig.5	this study
<i>P_{eft-3}mkate2</i>	Amp	-	Fig.5	this study

Kana: kanamycin; Amp: ampicillin; Hyg: hygromycin B; SF: Supplementary Figure

Supplementary Table 3. Cell lines and worm strains used in this study.

cell line	species	cell type	reference
HeLa Kyoto	human	cervical adenocarcinoma cells	RRID:CVCL_1922
MEF	mouse	embryonic fibroblast cells	ATCC
HeLa MIN-CENPA	human	cervical adenocarcinoma cells	this study
HeLa GFP-CENPA	human	cervical adenocarcinoma cells	this study
HeLa GFP-CENPA LiPD	human	cervical adenocarcinoma cells	this study
HeLa GFP-CENPA DiPD	human	cervical adenocarcinoma cells	this study
MEF GFP-LaminA	mouse	embryonic fibroblast cells	Chiu et al. 2016
MEF GFP-LaminA DiPD	mouse	embryonic fibroblast cells	this study
MEF mCh-LaminA	mouse	embryonic fibroblast cells	this study
HeLa GFP-PCNA	human	cervical adenocarcinoma cells	Chagin et al. 2016
HeLa GFP-CXXC4	human	cervical adenocarcinoma cells	this study
HeLa GFP-CXXC4 LiPD	human	cervical adenocarcinoma cells	this study
HeLa DiPD	human	cervical adenocarcinoma cells	this study
BHK	hamster	kidney cells	Tsukamoto et al. 2000

worm strain	description	reference
LGIV <i>ced-3</i> (n717)	<i>ced-3(lf)</i> loss of function	Ellis and Horvitz. 1986
LGV <i>bcSi36</i> (derived from <i>ced-3</i> (n717)) ($P_{ced-3}ced-3::gfp$)	<i>ced-3(lf)</i> loss of function <i>ced-3::gfp</i> transgene	this study
<i>bcEx1328</i> (derived from <i>bcSi36</i>) ($P_{eft-3}ring::frb::ha::gpd-2/gpd-3::gfp5::fkbp::myc_3'UTR$; $P_{eft-3}mkate2$)	<i>ced-3(lf)</i> loss of function <i>ced-3::gfp</i> transgene and DiPD system on extrachromosomal array	this study

Engineering binder-guided apoptotic proteins responsive to intracellular antigens

Engineering binder-guided apoptotic proteins responsive to intracellular antigens

Jack A. Bates, Weihua Qin, Jonas Helma, Heinrich Leonhardt

Nanobodies, BiFC, Split proteins, Viral proteins, HIV, HBV, complementation, synthetic biology, VHH, sdAb, Gene therapy, undruggable drug targets

Bridging target recognition to endogenous response is a highly effective natural and biopharmaceutical mechanism for disease control. However, the antigen-specific machinery enabling these processes are restricted to the extracellular environment. Thus, a vast proportion of potential targets remain unreachable within the intracellular space. Using the modularization principles of synthetic biology, we have generated a nanobody directed 'detect and eliminate' format that targets pathogenic proteins intracellularly. We applied a fluorescent screen to identify nanobody pairs that spatially coincide on intracellular disease targets, before functionalizing these nanobodies with cell death effector proteins. Tandem binding of the fusion proteins to an antigen approximates and activates the effector, killing the target cell. Using a dual nanobody format we have generated both highly selective antigen sensors and potent apoptosis inducing chimeras, responsive to the capsid proteins of HIV-1 and Hepatitis B. Viewed in the context of contemporary biomolecule delivery, cell targeting technologies, and therapeutic gene regulation, we believe that these target responsive apoptotic proteins (TRAPs) provide a promising new approach to tackle previously undruggable intracellular pathogens.

Introduction

Targeted biotherapeutics, such as monoclonal antibodies and modified T-cells, represent a rapidly growing share of contemporary medicine¹⁻³. Mimicking adaptive immune mechanisms, these highly selective therapeutics often functionally converge with endogenous immune machinery to exert cytotoxic effects against cells harbouring their target⁴⁻⁷. Such cell killing approaches have proven to be highly effective medicines with particular utility in cancer care⁸. However, despite the abundance of disease proteins that manifest inside cells, analogous intracellular cytotoxic approaches have not come of age.

Whilst innate mechanisms of intracellular immunity can induce cell death in response to some foreign molecules⁹, the receptors of these pathways only recognise and respond to more general patterns or structures associated with pathogens. As such, they cannot be so readily reprogrammed as the antibodies or T cell receptors of the extracellular space. As such, the induction of cell death in response to precise intracellular proteins requires new molecules to be designed which are capable of combining the functions of antigen detection and cell killing response.

Implementing modularization principles of synthetic biology^{10,11}, several groups have demonstrated various "detect and respond" systems using paired two part chimeras¹²⁻¹⁶. These fusions consist of two binding modules that align adjacently on the target, coupled to effector proteins that are only active upon induced approximation. In the presence of the target, the two binding subunits form a ternary complex with the antigen and this unites and activates the attached effector subunits. This induced proximity mechanism of protein regulation occurs naturally several times within the cell death pathways¹⁷⁻²⁰ and we therefore reasoned that numerous pathways components may be appropriate for use as effectors in two-part "detect and kill" formats. Whilst this concept has previously been demonstrated using caspase-3^{21,22}, a systematic optimisation of components, including binding subunit considerations and the assessment of numerous cell death effectors, is absent from the literature. To meet this need, we aimed to construct highly optimised two-part

targeted cell killing molecules, designed in line with key criteria we deem likely essentials for downstream pharmaceutical application; high potency; high selectivity; rapid action and low probable immunogenicity.

Our chimeras are targeted by nanobodies (Nbs), a mature class of antibody derivative notable for their high stability, low immunogenicity, intracellular solubility, compact structure (~15 kDa), and high binding affinities²³. In combination, these characteristics make nanobodies highly attractive for use in synthetic biology and pharmacology^{24,25}. We demonstrate the optimization of nanobody pairings using a bimolecular fluorescence complementation (BiFC) based assay and test our output combinations with cell killing effectors. Seven human programmed cell death effectors have been tested in this work, selected from the apoptotic and pyroptotic pathways. Ultimately, a truncated caspase-9²⁶ effector subunit is chosen for further application and fused to our optimised nanobodies. We show the efficacy and adaptability of our finalised target responsive apoptotic protein (TRAP) format against the viral capsid proteins of HIV-1 and hepatitis B, in addition to utilising a DARPIn²⁷ binder to target GFP.

Results

Viral proteins as molecular scaffolds

We selected proteins of the human immunodeficiency virus (HIV-1) and the Hepatitis B virus (HBV) against which to target our fusion proteins. These viruses continue to be very prevalent on a global level with high associated mortality^{28,29} and have the capacity to cause incurable chronic infection. For these reasons both viruses have received extensive attention from gene therapy researchers^{30,31} and are interesting diseases for TRAP application.

We reasoned that the capsid proteins of these viruses would likely make good targets for our chimeras. Both capsid proteins are highly expressed relative to other components of the viruses and both are accessible in the cytosol^{32,33}. We used six nanobodies generated in-house via alpaca inoculation and phage display to target the HIV-1 p24 capsid protein. Five of these nanobodies bind the C-terminal domain of p24 (CTD1_{Nb}, CTD2_{Nb}, CTD9_{Nb}, CTD12_{Nb}, CTD19_{Nb})³⁴ and a single binder interacts with the N-terminal domain (NTD1)³⁵. To enable targeting of the HBV capsid protein HBcAg, three previously reported nanobodies were synthesised using published sequences³⁶ (HB2_{Nb}, HB4_{Nb}, HB6_{Nb}).

Screening for compatible nanobody pairs

Although numerous *in vitro* methods exist to determine both the affinity of single nanobodies and whether multiple nanobodies can simultaneously bind an antigen³⁷⁻³⁹, these techniques are both insufficient to account for all variables present *in vivo* and non-inclusive of some conditions required for complementation. For example, unique *in vivo* difficulties may include: epitope competition with an antigen interactor, differences in nanobody expression, binding, stability and solubility in the cytosol, differences in target folding intracellularly and non-specific binding to endogenous targets, whilst effective complementation will occur only if antigen epitopes are both spaced and aligned appropriately.

We therefore created an *in vivo* screen for the determination of compatible nanobody pairs able to mediate effector complementation. The screen combines bimolecular fluorescence complementation (BiFC)⁴⁰, a split protein technique that uses fluorescence from a re-forming fluorescent protein to indicate interaction, with antigen-nanobody mediated approximation (Fig. 1c). This method delivers a fluorescent read-out when compatible nanobody pairs combine on the antigen. As the fluorescence increases in a complex dependent manner, once normalised, higher

fluorescence is indicative of more efficient chimera pairing on an antigen. The yellow fluorescent protein Venus (split 158/159) was selected for the screen due to its high brightness, rapid and efficient maturation at 37 °C and good signal-to-noise ratio (SNR)⁴¹. The SNR was further improved through incorporation of the Venus V150A mutation⁴² to reduce noise due to spontaneous complementation of the split protein.

The screen utilizes three vectors (Fig. 1a and 1b); two containing the Venus N-terminal (VN) or C-terminal (VC) portions, in fusion with the nanobodies to be tested; and a cassette containing the antigen of interest. Restriction sites have been inserted into the constructs to accommodate the rapid transfer of antigen and nanobody fragments. A pre-selected panel of candidate nanobodies is inserted into each of the two Venus fragment fusion cassettes and the various nanobody containing vectors can be systemically combined both in the presence of and without the antigen, through triple transfection. An mRFP is expressed on the Nb-VC cassette which detaches via a T2A protein and is used for the normalisation of transfection efficiency.

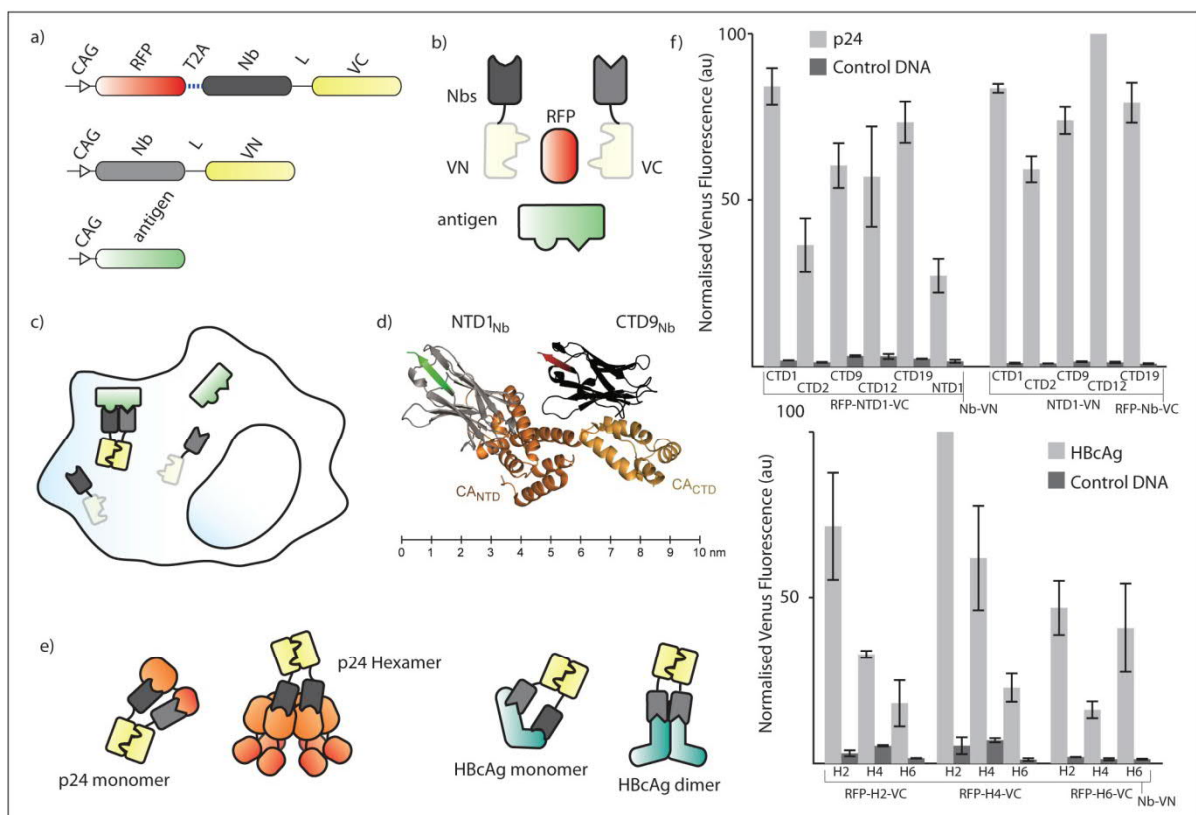


Figure 1. Screening for compatible nanobody pairs. (a) Schematic of the 3 cassettes used to fluorescently screen for adjacent Nb pairs (Venus C (VC), Venus N (VN), Nanobody (Nb)). (b) Proteins expressed from the screening plasmids. (c) Intracellular complex formation on an antigen is illustrated with resulting Venus activation. (d) Crystal structure alignment of the HIV-1 p24 antigen with two p24 nanobodies (created in pymol through alignment of PBD 2XV6, PDB 3H4E and an internal crystal structure of NTD1_{Nb}). (e) Illustration depicts the various ways chimeras may successfully bind to the two viral proteins and induce effector complementation. (f) Normalised Venus fluorescent output upon combination of different Nb-BIFC chimeras with and without viral antigen. Biological triplicates are shown. Error bars depict standard error.

We reasoned that our nanobody-fluorescence complementation (Nb-FC) chimeras could dimerise in either of two ways: through tandem adjacent binding to a single antigen, or through binding to multimerising antigens (Fig. 1e). *In vitro* epitope mapping data indicated that each of the p24 CTD targeting Nbs bound epitopes within a narrow range (178-206aa) and likely overlap³⁴. Furthermore, prior experimentation revealed that the transfection of each of the five CTD Nbs with p24 inhibits polymerization of the HIV-1 capsid protein (unpublished work). The NTD1 Nb does not inhibit capsid

assembly³⁵. We therefore screened the five CTD Nbs against the single NTD nanobody, to assess for tandem binding to the antigen, in addition to screening the NTD1 nanobody against itself, to assess for complementation due to antigen multimerisation. No data was available regarding the epitopes of the three HBcAg binders and so we screened each of the Nbs against itself and each of the other nanobodies.

Venus fluorescence was measured using a microplate reader and normalised against signal in the mRFP channel. Since these experiments were transient transfections, which often vary significantly between replicates, we further normalised each round of transfections against the signal of a selected pairing. All combinations of nanobodies tested against p24 and seven of the nine against HBcAg, produced statistically significant levels of signal when transfected with the antigen versus a no antigen control (Fig. 1f).

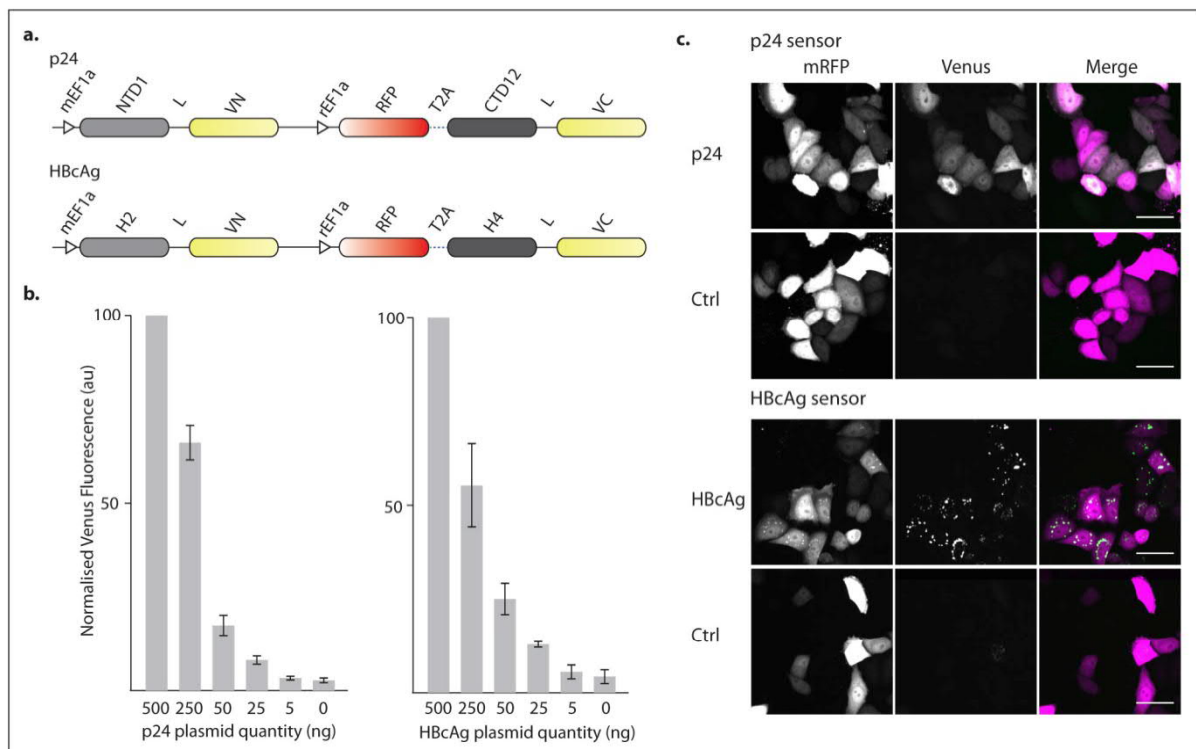


Figure 2. Constructing nanobody-BiFC sensors. (a) Single cassette nb-BiFC antigen sensors (2x Nb-Fcs) incorporating the p24 and HBcAg Nbs are depicted. (b) The dose dependent fluorescent output of the two viral protein sensors is evidenced through transfection of varying quantities of antigen DNA. Biological triplicates are shown. (c) Images demonstrate sensor fluorescence in response to antigen and control at 24 h post transfection (scale bar 30 μm). Error bars depict standard error.

Developing Nb-FC sensor cassettes

Using the optimal nanobody combinations and orientations discovered through screening (as defined by the highest Venus fluorescent output), we produced single vector dual promoter cassettes to function as sensors for the viral proteins (2xNb-FC) (Fig. 2a). We reasoned that a single vector would likely improve the function of the sensors through more balanced expression of Nb-FC components.

We wanted to demonstrate that the mechanism of induced approximation used in these sensors delivers signal which correlates to antigen quantity. We therefore examined the dose dependency relationship between antigen and fluorescent output by transfecting varying amounts of antigen DNA with fixed amounts of 2xNb-FC (Fig. 2b). When we analysed the normalised Venus fluorescence at 48 hs, we saw a clear relationship between antigen load and sensor output. The maximum amount of antigen transfected (500 ng, or 20% of the total transfection) delivered impressive SNRs of 37:1

and 23:1 for the p24 and HBcAg sensors. Both sensors continued to yield significantly higher signal than the control when just 1% of the transfection was antigen DNA (p24 $p=0.0158$, HBcAg $p=0.016$). Live cell imaging of sensor transfected Hela Kyoto cells sensors with and without antigen was also performed (S. movies 1 and 2, Fig. 2c) and further demonstrates the robust, selective signal achievable using the 2xNb-FC method.

Combining antigen induced activation with antigen dependent stabilisation

Since intracellular Nb solubility would likely affect the function our chimeras, we fused each of our optimal Nbs to GFP to assess their distribution following transfection. Whilst generally the Nbs appeared to be homogenously distributed across the cells, we discovered a slight tendency towards aggregation for NTD1_{Nb} (Fig 3a). Interestingly, we also observed a substantial increase in fluorescence when NTD1_{Nb}-GFP was co-transfected with antigen rather than control DNA (~7.5x) (Fig 3b). We interpreted this to be indicative of antigen-dependent stability (ADS), a phenomenon whereby a binder's stability increases when in complex with its antigen⁴³.

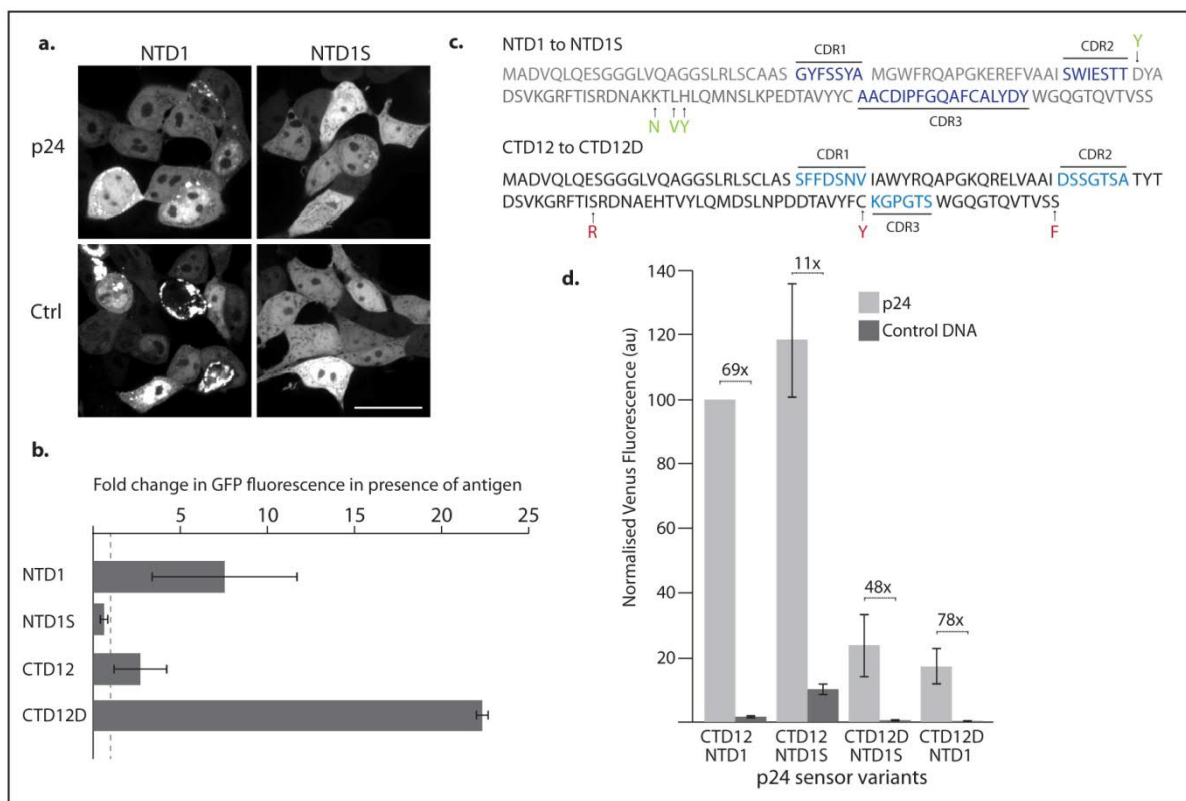


Figure 3. Engineering Nb solubility and introducing ADS into 2xNb-Fc (a) The intracellular distributions of NTD1_{Nb}-GFP and NTD1S_{Nb}-GFP with and without p24 antigen are shown (scale bar 30 μ m). The images are adjusted individually to maximise the visualisation of distribution. (b) The fold difference in cellular fluorescence of various Nb-GFP fusions with antigen versus a no antigen control. (c) The point mutations utilised to create NTD1S_{Nb} and CTD12D_{Nb} from their parent molecules are depicted (CDR(complementarity determining region)). (d) The NTD1Nb, NTD1sNb, CTD12Nb, CTD12DNb binders are exhaustively combined into the 2xNb-FC cassettes to assess their function as p24 sensors. Biological triplicates are shown. All error bars depict standard deviations.

To improve the solubility and intracellular stability of NTD1_{Nb}, we combined extensive comparative sequence analysis and a deductive Nb splicing approach, to isolate four NTD1_{Nb} amino acids which were irregular for their position and could be affecting solubility (S.note. 1). When we engineered the Nb via a series of point mutations at these sites (forming NTD1S_{Nb}), the intracellular solubility of the Nb greatly improved (S.Fig.1a, Fig.3a). Furthermore, the ADS effect, observed for the NTD1_{Nb} parent, was entirely absent (Fig 3b). We then inserted this NTD1S_{Nb} binder into the p24 sensor cassette for

comparison with NTD1_{Nb} variant. Testing revealed that whilst the NTD1S_{Nb} delivered the highest overall Venus output in the presence of p24, the NTD1_{Nb} sensor had a far superior SNR (Fig. 3d). We therefore hypothesised that ADS and our induced proximity mechanism were functioning synergistically to reduce unwanted effector activation in the absence of antigen, by degrading unbound Nb and effector (S. Fig. 1d).

To test this further we selectively destabilised CTD12_{Nb} by mutation, according to the work of Tang et al⁴³ (CTD12D_{Nb}) (Fig. 3c). Much like NTD1_{Nb}, CTD12D_{Nb}-GFP formed aggregates when expressed intracellularly (S.Fig.1b), but also exhibited an extraordinary shift in stability when p24 antigen was added to the transfection (Fig. 3b, S.Fig.1c). When combined into the p24 sensor cassette with NTD1_{Nb}, CTD12D_{Nb} had a remarkable effect on system background and SNR. Background fluorescence became indiscriminable in the majority of cells when examined by spinning disk confocal microscope and the SNR rose to 78:1 (Fig. 3d). Comparison of SNRs between cassettes containing the most and least stable variants clearly shows that ADS and induced proximity can be multiplexed to deliver extremes of regulation on the protein level.

Selecting cell death effectors

Successful natural detection of an intracellular pathogen typically results in elimination of the infected cell through programmed cell death processes such as apoptosis and pyroptosis⁴⁴⁻⁴⁶. Numerous components of the cell death machinery have been demonstrated to be amenable to activation through artificial proximity induced activation¹⁷⁻²⁰. We selected seven of these effectors to test for the capacity to elicit antigen dependent cell death when fused to our proximity inducing nanobodies. Four of these effectors (caspase-1 (C1), caspase-8 (C8), caspase-9 (C9) and Bax) are activatable via the approximation of monomers, caspase-3 (C3) can be activated through forced proximity of two homodimers, and FADD, as well as APAF-1, depend upon interaction with endogenous caspase-8 and caspase-9 respectively prior to forming their active dimers (S.Fig. 2a). Caspase-1 (C1) is an effector of the pyroptotic pathway, while the remaining six effectors are components of the apoptotic pathways.

Each effector was used in fusion with HB2_{Nb}, which we have demonstrated to be suitable for effector approximation when expressed with HBcAg (Fig. 1f). A vector containing the mouse PGK promoter was created to allow expression of the fusions at lower, more physiological levels than the EF1a and CAG vectors used earlier in the work (Fig. 4a)⁴⁷. As both pyroptosis and apoptosis permit annexin V binding of phosphatidylserine^{48,49}, we measured cell death activation using a commercial luciferase assay that tracks this process (RealTime-Glo™ annexin apoptosis assay, Promega). Transfections included the rapidly maturing mNeon green protein⁵⁰ to enable visualization of transfected cells. Additionally, we produced 18 hour time-lapse videos of transfections with and without antigen, prior to luminescence measurements, to enable visual corroboration of findings.

Our luminescence data (Fig. 4b) revealed that the Nb-Bax fusion was highly cytotoxic even in the absence of antigen, suggesting that Bax concentrations were well in excess of tolerable limits. Neither the Apaf-1 CARD domain (aa 1-97), the FADD Death effector domain (DED) (aa 1-90), nor the truncated caspase-8 (aa 207-479) instigated cell death in either the presence or absence of antigen. Failure of the Apaf-1 and FADD components to initiate cell death, despite previous reports to the contrary^{17,20,51}, may be associated with the requirement for heterodimerisation with endogenous caspases prior to activation, which adds a further level of complexity and stoichiometric constraint to the interactions necessary to form an active complex. The absence of any apparent background cell death upon transfection of Caspase-8 contradicts reports of the high basal cytotoxicity published by others¹⁷. We therefore believe that the inactivity of our H2-Caspase 8 protein is most likely due to

inactivation due to Nb fusion, though it remains possible that extensive anti-apoptotic machinery is limiting caspase-8 function in this cell line.

Caspase-1, Caspase-3 and Caspase-9 all generated varying amounts of antigen dependent cell death. The truncated Caspase-9 fusion appeared to be the most cytotoxic of the three whilst retaining

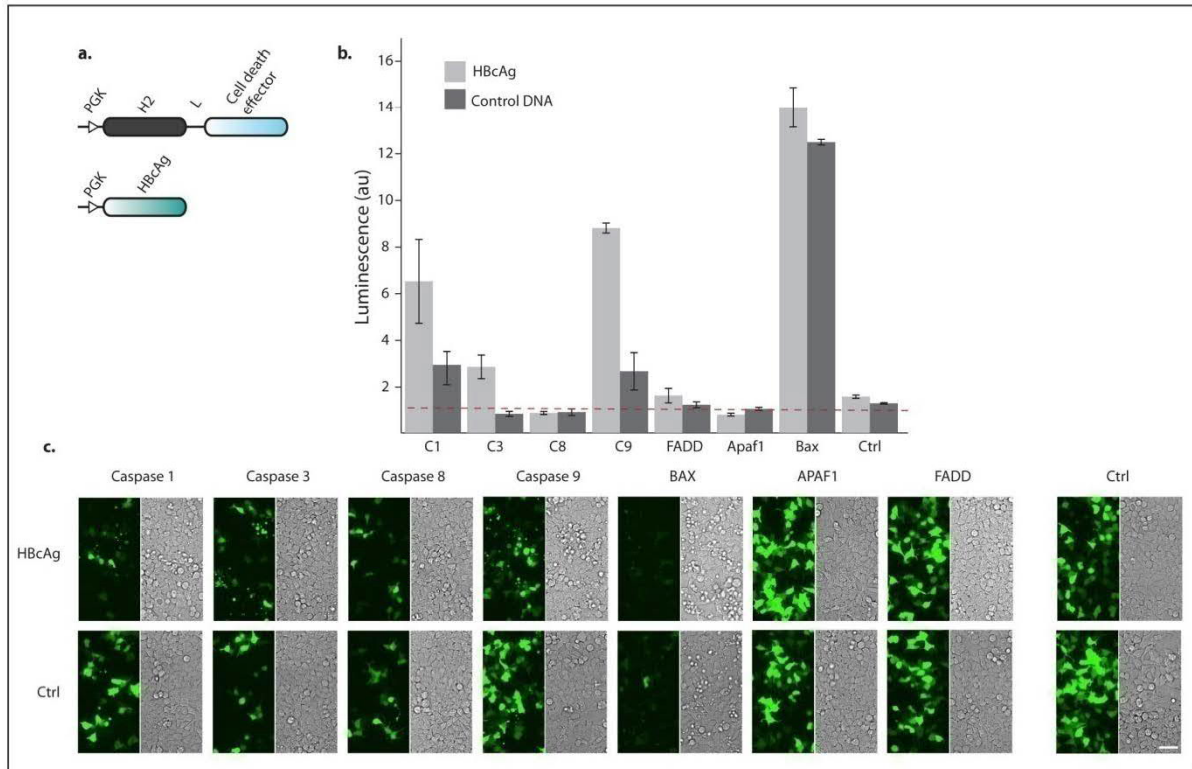


Figure 4. Screening cell death effectors. (a) mPGK promoter driven cassettes for antigen expression and effector testing are illustrated. (b) Luminescence data, reporting on apoptotic or pyroptotic cell death, is presented for each Nb-effector fusions with and without antigen at a time point of 24 hs. The red dotted line represents untransfected control cell luminescence. (c) Live-cell imaging was used to track each of the nanobody-effector transfections, the 18 h time point is shown (scale bar 50 μM). (Error bars depict standard deviations). (Ctrl) Control readings and images represent cells transfected with mNeon and control DNA only.

imperfect but good selectivity. Caspase-3 exhibited no apparent background cell killing although we also saw only moderate levels of cell death when transfected with antigen. Since caspase-3 has previously been utilised in targeted cell death constructs^{21,22}, we attempted to determine whether the difference might be concentration dependent. We therefore cloned the fusion onto a high expression CAG promoter driven vector and co-transfected it with our CAG HBcAg construct (supplementary Fig. 3a). Upon microscopic inspection the higher level of expression appeared to very significantly increase the efficacy of targeted cell killing (supplementary Fig. 3b and 3c) and also to lead to only minimal off target cell death.

Since caspase-9 exhibited higher selective toxicity than caspase-1, we decided to discontinue experimentation with caspase-1. Although caspase-3 was less potent than caspase-9, Nb-C3 fusions generated only very minimal off-target cell death, even when expressed at very high levels, and we therefore decided to continue testing them.

HIV capsid protein responsive cell death

Before trialling the Nb-C9 and Nb-C3 fusions against the p24 antigen, we sought to generate a highly reproducible experimental set-up, which was more emulative of the treatment of an infected cell. We decided that a stable cell line expressing the p24 antigen would be somewhat representative of

an in situ infection and would also allow us to test the fusions against lower levels of antigen. In addition this set up removes some of the experimental variation due to transient transfection. To generate the cell line we utilised a combination of CRISPR genome editing and BXB1 recombinase mediated cassette integration⁵². Using this method, we obtained a stable HEK cell line containing a single copy of a CAG-p24 gene in the AAVS1 genetic “safe harbour” (HEK-p24)⁵³. We included a Blasticidin resistance gene to assist in maintenance of the cell line (Fig. 5a).

NTD1_{Nb} and CTD12_{Nb} were cloned into the PGK caspase-3 and caspase-9 cassettes for testing with the HEK-p24 cell line. Testing revealed that while the caspase-3 fusions displayed no apparent apoptosis promoting activity within either cell lines, nb-Caspase-9 chimeras initiated highly selective cell death in the HEK-p24 cells (Fig. 4b). The failure of the caspase-3 constructs to instigate cell death under these low antigen conditions is unsurprising given our prior results when testing at lower levels. Furthermore, our data demonstrating the superior toxicity of caspase-9 upon forced approximation are consistent with apoptotic effector research performed by others¹⁷.

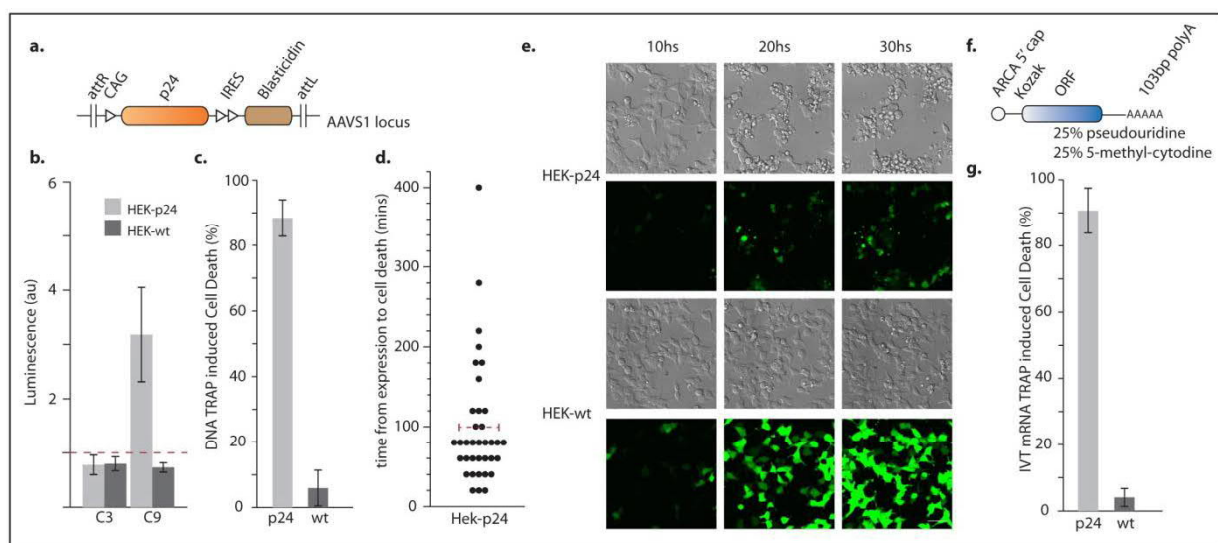


Figure 5. TRAPs in application against HIV-1 p24 antigen (a) Scheme illustrates a single pCAG-p24 cassette recombined into the AAVS1 locus. (b) Caspase-3 and Caspase-9 Nb chimeras are tested for activity against HEK wt and HEK p24 cell lines. Luminescence correlates to apoptosis. The red dotted line represents untransfected control cell luminescence. (c) Cell tracking is used to measure the percentage of TRAP induced cell death in HEK-wt and HEK-p24 cell lines (TRAPs are expressed from DNA). (d) The timing between the start of mNeon expression, indicating TRAP co-expression, and cell death, is shown. The red dotted line depicts the mean. (e) Time point Images following co-transfection of DNA TRAP constructs and mNeon into HEK-p24 and HEK-wt cells are displayed. Scale bar 50 μ m. (f) The composition of the generated IVT mRNAs is shown. (g) Cell tracking is used to measure the percentage of IVT mRNA TRAP induced cell death in HEK-wt and HEK-p24 cell lines. Biological triplicates are shown. (All error bars depict standard deviations)

Following the selection of caspase-9 as an effector, we sought to optimise elements of our *target responsive apoptotic proteins* (TRAPs). We first performed linker length comparison experiments using NTD1_{Nb} and CTD12_{Nb} (S.Fig. 3b) to determine the ideal format for complementation. In these experiments we transfected low amounts of TRAP DNA into HEK-p24 and HEK-wt cells, and analysed time-lapse recordings for apoptosis. Ultimately, we opted to continue development with 2x GGGs linkers. We also tested each of the stability variants of the NTD1 and CTD12 Nbs to assess for an effect on background activation. As we knew that higher DNA doses of the TRAPs were quite cytotoxic, we transfected large quantities of each TRAP into HEK-wt cells to study their off-target activity. Theoretically, the ADS Nbs should lead to greatly reduced TRAP concentrations in the absence of antigen, which should in turn lower background activation. However, when we analysed live cell imaging of the transfections we saw that ADS did not improve background for the NTD1 variants and that CTD12_{Nb} directed TRAPs were significantly more cytotoxic than those containing

CTD12_{Nb} (S.Fig 3c). This is likely due to the aggregation incurred by the two ADS Nbs, which may have activated the fused caspase-9. We postulate that such background is not seen in the split Venus sensors due to a requirement for heterodimers in that case.

When we tested our fully optimised TRAP chimeras in the HEK-p24 and HEK-wt cell lines, we saw that they were highly potent and selective (Fig. 5e) activators of apoptosis. Cell tracking of transfected cells imaged over an 18 h period post transfection revealed that 88.4% (SD 5.8%) of the transfected HEK-p24 cells underwent apoptosis whilst this was only true of 5.9% (SD 5.6%) in the HEK wt control (Fig. 5c). When we analysed the time between the emergence of mNeon signal, indicating likely TRAP co-expression, and cell death, we observed a mean time to cell death of 99 minutes. By 2 hs over 80% of antigen expressing cells reactive to the TRAPs had undergone apoptosis, demonstrating that TRAPs function rapidly to eradicate the target cells (Fig. 5d). 30 h time lapse recordings of TRAP transfections are attached and demonstrate the potency and selectivity of our chimeras (Movie. 1).

Delivery of IVT mRNA encoded TRAPs

Whilst DNA delivery could provide lasting protection to a cell population, it may in some instances be desirable to ensure that TRAPs are only transiently expressed. Transient expression may be less taxing to cell physiology and would likely reduce the risk of immunogenicity. We propose that IVT (*in vitro* transcribed) mRNA could be a particularly good transient format for TRAP delivery^{54,55}. IVT mRNA can be cost effectively and reliably synthesised, it cannot lead to oncogenesis through genomic insertion, and due to translation mediated amplification, relatively low amounts must be delivered when compared to protein. Lastly, numerous technologies are presently under development for the delivery of such RNAs⁵⁵.

We therefore generated optimised TRAP IVT mRNAs for transfection (Fig 5f). We incorporated Pseudouridine (25%) and 5-methyl-cytidine (25%) to improve mRNA stability and reduce potential innate immune responses to the mRNAs⁵⁶⁻⁵⁸. Transfection of the mRNA TRAPs resulted in highly efficacious and selective cell killing over the 18h window of analysis (Fig. 5g, S. Movie 3). 91% (SD 7%) of transfected HEK-p24 cells were successfully eliminated whilst only 7% (SD 4%) of the control HEK-wt cells were killed.

DARPin targeted TRAPs

The TRAPs concept should be compatible with a range of targeting subunits. To demonstrate its versatility in this regard, we incorporated a GFP binding DARPin (designed ankyrin repeat protein)⁵⁹ in place of a Nb (DP-C9) (S. Fig 4a). A tandem GFP fusion (GFP-GFP) was also formed to act as an antigen upon which the DP-C9 TRAP could bind twice. We produced time-lapse recordings of DP-C9 + GFP-GFP and DP-C9 +no antigen control co-transfections. Much like the Nb directed versions DP-C9 TRAPs showed great potency and specificity against their target (S. movie 4) (S. Fig. 4c). Interestingly, the high affinity of the DP-C9 (300 pM) allowed us to deliver very low amounts of the TRAP without a meaningful loss of potency, which appeared to decrease off-target cell killing.

Discussion

Despite the obvious desirability of such a mechanism, intracellular methods eliciting the antigen dependent elimination of cells remain underdeveloped. In this work we outline an adaptable pipeline for the production of targeted proteins appropriate for this task. The resulting TRAPs have been designed and tested to consist of probable best-in-class components with respect to potency, specificity, speed of action and immunogenicity. Testing against three targets revealed a clear therapeutic window, at which TRAP concentrations were suitable to selectively eliminate the

appropriate cells. Furthermore, since apoptotic effector components have been used, *in vivo* target cell death should be both highly contained and non-inflammatory⁴⁴.

Production of TRAPs begins with the selection of targeting subunits. Targeting intracellular antigens using standard antibodies derivatives, such as scFvs, is frequently plagued by folding and solubility issues due to the reducing environment of the cytoplasm⁶⁰. In addition, the larger gene size of these derivatives could be a significant limitation where viral delivery is planned⁶¹. We therefore worked to develop TRAPs using more compact binders with greater intracellular stability. Both nanobodies and DARPins were demonstrated in this work but we suggest that other single domain binding formats, such as Anticalins⁶² or Monobodies⁶³, should also be compatible.

The Nb-FC fusion method demonstrated here delivers an easily quantifiable output that directly correlates with the number of fluorescent complexes formed. In addition to being a highly practical approach to the discovery of adjacent binders for other effector applications, the resulting Nb-FC combinations can themselves be directly used within antigen sensors. We anticipate Nb-FCs could be employed not only in foreign antigen detection, such as infection studies, but also to investigate endogenous targets. Here they could perhaps be used to study protein expression as well as events that introduce or reorient epitopes such as posttranslational modifications, alternative splice forms, conformational rearrangements and complex formations.

In the course of this work we used fluorescent effectors to demonstrate that ADS and induced proximity are pairable mechanisms for protein regulation. In light of the difficulty in delivering nucleic acids or proteins homogeneously into the cell, having mechanisms capable of such SNRs could prove extremely useful for intracellular protein pharmaceuticals. Unfortunately, the attendant reduction in solubility with our ADS Nbs was ultimately counterproductive when they were applied as TRAP targeting modules. However, since a continuum of solubilities was reported when mutating multiple nanobodies⁴³, it may be possible to remove this obstacle, which could be particularly useful when applying TRAPs to antigens with very high concentrations.

Aside from foreign molecules, TRAPS may also be usefully directed to targets created due to alterations in protein profile as a consequence of cancer. Such exploitable variations could include; oncofusion proteins⁶⁴; misfolded proteins⁶⁵; splice variants⁶⁶; single mutations²²; and proteins erroneously expressed within a cell type. However, when selecting a target to be addressed by TRAPs, antigen concentration should be carefully considered. This is because the efficacy of the TRAP mechanism is contingent upon the concentration of active complexes formed. If the concentration of antigen is too low, it may not be possible to form sufficient caspase-9 dimers to trigger apoptosis. If target concentration is too high, then TRAP components could be sequestered away from each other on separate antigen molecules. We further anticipate that the exact limits of the therapeutic window will vary from cell to cell depending upon the balance of apoptotic and anti-apoptotic machinery. The half-life of the antigen should also be considered since it may also affect TRAP functionality, with shorter half-lives having a detrimental effect on the capacity of TRAPs to elicit selective cell death. Lastly, the binder used to target the antigen should be carefully selected since the affinity of the targeting subunit used with the TRAP will have a considerable effect on the efficacy of the TRAP. Using higher affinities should deliver superior rates of complex formation. Effectively, this should stretch the therapeutic window in both directions and also allow lower, less cytotoxic, concentrations of TRAP to be effective.

Conclusion

To our knowledge, with our original chimera species we have demonstrated the first proximity activated fusions to complex with viral proteins. With fast developing multidisciplinary efforts to make *in vivo* cellular biomolecule delivery safe and efficient^{55,67-69}, the stage is set for synthetic biologists and others to find selective, effective and non-immunogenic solutions to tackle disease intracellularly. TRAP chimeras, which coupling a capacity to disrupt target function through binding with selective activation of cell death, are a promising new prospect.

Methods

Cloning Procedures

Phusion polymerase (Thermoscientific) was used to perform all cloning PCRs. Restriction enzymes, Ligase (Thermoscientific) and Hifi assembly mix (NEB) were used for cloning procedures. Chemically competent *E. coli* JM109 bacteria, produced in-house, were used for transformation. Selection of transformed cells was performed using 1% LB-Agar supplemented with 100 µg/ml ampicillin (Roth) or 200 µg/ml hygromycin B (Sigma-Aldrich). The HBcAg capsid and HBcAg binder sequences were synthesized as geneblocks (IDT). Supplementary note 3 outlines plasmids created including backbones. IVT mRNA was generated using the HiScribe™ T7 ARCA mRNA Kit (without tailing). A 103bp poly A tail was introduced via primer to the template DNA.

Mammalian Cell Culture, Transfection

All microscopy performed in supplementary figure 1, in addition to those images shown in figures 2c and 3a, utilized HeLa Kyoto cells. The remaining experiments were performed using either wild type HEK-293T cells or HEK-293T cells modified to stably express p24 (HEK-p24). All cell lines were cultured in 10% FCS DMEM (Sigma Aldrich). HEK-p24 cells were periodically cultured with Blasticidin hydrochloride 10 µg/ml (Sigma-Aldrich) to maintain the purity of the cell line. Blasticidin was removed from the medium at least 3 days prior to transfection experiments to minimize possible blasticidin effects on cell health. Transfections for BiFC and nanobody-GFP fusion experiments were performed using Lipofectamine 3000™ (Invitrogen) according to the manufacturers protocol with cell confluency at around 70%. The minimum recommended Lipofectamine volume outlined in the manufacturers protocol was used for transfection. Empty Bacterial vector was used as control DNA for transfections. All cell death effector experiments were performed using Fugene HD™ (Promega) at a Fugene reagent:DNA ratio of 2.5:1 with a cell confluency of around 70%. 5 µl of transfection mixture was used per well for 96-well transfections and volume was scaled with well growing area for larger formats. Transfected DNA amounts can be found in supplementary note 1. RNA transfections were performed using Lipofectamine MessengerMax™ Transfection Reagent (Invitrogen). Cells were tested for mycoplasma contamination using an in-house procedure. Wild type cell lines were not authenticated.

HEK-p24 Cell line Construction

CRISPR Cas9 technology was used to insert a CAG promoter with BXB1 attP recombination site into the AAVS1 locus of HEK293T cells using “ggagccacattaaccggccct”⁷⁰ as a gRNA targeting sequence⁷¹. A combined gRNA Cas-9 plasmid was used with a double stranded DNA plasmid template using 750bp overlaps in both directions for the integration. The gRNA was calculated using the Zhang lab guide design program (no longer available online). Homozygous insertion of CAG-attP into the AAVS1 locus was confirmed via genomic PCR (primers “tctcttcgcattggagtcg” , “atcctctctggctccatcgt” and “attaaccggccctgggaatataag”)and sequencing. The pCAG-NLS-HA-Bxb1 plasmid was co-transfected with the pCAG-p24-IRES-Blast cassette at a ratio of 1:1 for integration. Immunostaining (mouse anti-HIV-1 p24 ab9071 Abcam: Donkey anti mouse alexa 594 invitrogen R37115) was used in addition to genomic PCRs (“ctgtggattcgggtcacctc” , “atcctctctggctccatcgt” and “tcacgctcgtcgtttggat”) to ensure heterozygous recombination into the AAVS1 locus.

Microplate Fluorometry

For nanobody screening experiments (Fig. 1f), as well as antigen dosing experiments (Fig. 2b), Nb variant sensor testing experiments (Fig. 3d) and Nb variant GFP fusion testing (Fig 3b), cells were

washed using PBS and detached from either 12-well plates (screening and variant experiments) or 6-well plates (dosing experiments) via scraping 48 hours after transfection. Cells were then centrifuged and washed once more using 1ml PBS before being resuspended in 100 μ l (screening and variants) or 200 μ l (dosing) of PBS. 100 μ l of each sample was then transferred into a 96-well microplate (Greiner bio-one, Germany). Fluorescence was measured with a microplate reader (Infinite[®] M1000 PRO, TECAN). Measurements were taken using Venus signal (515 nm excitation and 528 nm emission), RFP(556 nm excitation and 586 nm), GFP (488 nm excitation 509 nm emission). Four readings were taken per well. Untransfected cells were also measured to determine background fluorescence in the two channels. Background fluorescence was subtracted from the readings. All readings were normalized for transfection against the RFP channel. In the nanobody screening experiments each replicate was further normalized against a given nanobody combination within the group which was arbitrarily given the value of 100 (N1-VN+R-C12-VC for p24; H2-VN+R-H4-VC for HBcAg). In antigen dosing experiments each replicate was normalized against the highest antigen dose. Normalisations in the variant Nb sensor testing experiments were against the NTD1_{Nb} and CTD12_{Nb} pairing. T tests were performed to assess significance. Experiments were performed as biological triplicates.

Measuring cell death with Luminescence

Cells were transfected in triplicate in a 96-well plate using Fugene HD and imaged for 18 hs. Following imaging Staurosporine (2 μ M) was added to mock cells (timepoint 18 h) to initiate apoptosis and act as a positive control. RealTime-Glo™ Annexin V apoptosis assay (Promega) reagents, applied according to the manufacturer's protocol, were added to wells at a time point of 20h. A 4 h incubation time was used for substrate activation and luminescence was subsequently measured in each of the wells (timepoint 24 h) (Infinite[®] M1000 PRO, TECAN). Measurements of wells containing only medium and assay reagents were used to deduct background luminescence. Samples were normalized against untransfected and untreated HEK-wt and HEK-p24 wells, which were given the value of 1.

Imaging

Spinning Disk microscopy

A Nikon TiE microscope equipped with perfect focus was used for all live cell imaging. The microscope was used in combination with a Yokogawa CSU-W1 spinning disk unit and CSU-W1 dichroic mirror, as well as an ALC600 laser-beamcombiner, IXON 888 Ultra EMCCD camera and Borealis illumination unit manufactured by Andor. An environmental chamber (Okolab BIO 1, Bold Line CO₂ and temperature module, gas chamber and humidifying module) maintained experimental conditions at 37 °C, 5 % CO₂ and humidified atmosphere. All experiments used either a 100x oil immersion objective or a 40x air objective. An overlap of 15% was used where image tiling was applied. Venus and GFP were excited using the 488 nm laser, RFP was imaged after excitation with the 561 nm laser.

Immunofluorescence imaging

Confocal microscopy (TCS SP5, Leica) was used following immunostaining to confirm the presence of p24 antigen in the HEK p24 cell line. A 63x 1.4 numerical aperture Plan-Apochromat oil immersion objective was used for imaging. DAPI and Alexa 594 were excited by 405 nm diode laser and 591 nm diode pumped solid-state laser respectively.

Image analysis and cell death quantification

All images were analysed using Image J software. Live-cell tracking apoptosis experiments were analysed in the following way. A 6x6 tiled region of each well was recorded for a period of 18hs using

a 40x air objective. Each video was gridded into four non-contiguous boxes. The first 10 cells to express mNeon green in each quadrant were analysed, if more than 10 cells simultaneously expressed mNeon by the same time point then all cells were counted. A cell was determined to have survived if it had not detached completely before the end of the video and/or formed apoptotic bodies and is not rounded at the end point. Additionally, if the cell undergoes mitosis and neither daughter cell dies until 18 h it was considered to have survived. A cell's death was recorded if; the cell detached and fragmented into apoptotic bodies; if the cell rounded and underwent significant cell shrinkage for the remainder of the video (minimum 2 hs); or if the cell mitosed and both daughter cells underwent apoptosis before 18 h. If a cell could not be tracked with a reasonable degree of certainty due to proximity to neighbouring cells or a cell leaves the image the cell was discounted from the analysis. Rounded cells that did not form apoptotic bodies or undergo significant shrinkage and cells that mitosed and only 1 daughter cell died within 1 h of mitotic completion were considered ambiguous and a further cell was selected in their place. All death effector TRAP experiments were performed in triplicate.

Immunostaining

HEK-p24 and HEK 293T wt control cells were fixed on coverslips, permeabilised and stained using DAPI in addition to mouse anti-p24 antibody (Abcam ab9071) (1:100). Secondary staining was performed using donkey anti-mouse Alexa 594 (Invitrogen R37115).

References

- 1 Moorkens, E. *et al.* The Market of Biopharmaceutical Medicines: A Snapshot of a Diverse Industrial Landscape. *Frontiers in pharmacology* **8**, 314, doi:10.3389/fphar.2017.00314 (2017).
- 2 Baybutt, T. R., Flickinger, J. C., Jr., Caparosa, E. M. & Snook, A. E. Advances in Chimeric Antigen Receptor T-Cell Therapies for Solid Tumors. *Clinical pharmacology and therapeutics* **105**, 71-78, doi:10.1002/cpt.1280 (2019).
- 3 Elgundi, Z., Reslan, M., Cruz, E., Sifniotis, V. & Kayser, V. The state-of-play and future of antibody therapeutics. *Adv Drug Deliv Rev* **122**, 2-19, doi:10.1016/j.addr.2016.11.004 (2017).
- 4 Rogers, L. M., Veeramani, S. & Weiner, G. J. Complement in monoclonal antibody therapy of cancer. *Immunol Res* **59**, 203-210, doi:10.1007/s12026-014-8542-z (2014).
- 5 Lo Nigro, C. *et al.* NK-mediated antibody-dependent cell-mediated cytotoxicity in solid tumors: biological evidence and clinical perspectives. *Ann Transl Med* **7**, 105, doi:10.21037/atm.2019.01.42 (2019).
- 6 Gul, N. & van Egmond, M. Antibody-Dependent Phagocytosis of Tumor Cells by Macrophages: A Potent Effector Mechanism of Monoclonal Antibody Therapy of Cancer. *Cancer research* **75**, 5008-5013, doi:10.1158/0008-5472.CAN-15-1330 (2015).
- 7 Benmebarek, M. R. *et al.* Killing Mechanisms of Chimeric Antigen Receptor (CAR) T Cells. *International journal of molecular sciences* **20**, doi:10.3390/ijms20061283 (2019).
- 8 Redman, J. M., Hill, E. M., AlDeghaither, D. & Weiner, L. M. Mechanisms of action of therapeutic antibodies for cancer. *Mol Immunol* **67**, 28-45, doi:10.1016/j.molimm.2015.04.002 (2015).
- 9 Tam, J. C. H. & Jacques, D. A. Intracellular immunity: finding the enemy within--how cells recognize and respond to intracellular pathogens. *Journal of leukocyte biology* **96**, 233-244, doi:10.1189/jlb.4RI0214-090R (2014).
- 10 Silver, P. A., Way, J. C., Arnold, F. H. & Meyerowitz, J. T. Synthetic biology: Engineering explored. *Nature* **509**, 166-167, doi:10.1038/509166a (2014).
- 11 Auslander, S., Auslander, D. & Fussenegger, M. Synthetic Biology-The Synthesis of Biology. *Angewandte Chemie* **56**, 6396-6419, doi:10.1002/anie.201609229 (2017).
- 12 Tang, J. C. *et al.* A nanobody-based system using fluorescent proteins as scaffolds for cell-specific gene manipulation. *Cell* **154**, 928-939, doi:10.1016/j.cell.2013.07.021 (2013).
- 13 Tang, J. C. *et al.* Cell type-specific manipulation with GFP-dependent Cre recombinase. *Nat Neurosci* **18**, 1334-1341, doi:10.1038/nn.4081 (2015).
- 14 Scheller, L., Strittmatter, T., Fuchs, D., Bojar, D. & Fussenegger, M. Generalized extracellular molecule sensor platform for programming cellular behavior. *Nature chemical biology* **14**, 723-729, doi:10.1038/s41589-018-0046-z (2018).
- 15 Bojar, D., Scheller, L., Hamri, G. C., Xie, M. & Fussenegger, M. Caffeine-inducible gene switches controlling experimental diabetes. *Nature communications* **9**, 2318, doi:10.1038/s41467-018-04744-1 (2018).
- 16 Stains, C. I. *et al.* A general approach for receptor and antibody-targeted detection of native proteins utilizing split-luciferase reassembly. *ACS chemical biology* **5**, 943-952, doi:10.1021/cb100143m (2010).
- 17 Fan, L., Freeman, K. W., Khan, T., Pham, E. & Spencer, D. M. Improved artificial death switches based on caspases and FADD. *Human gene therapy* **10**, 2273-2285, doi:10.1089/10430349950016924 (1999).
- 18 MacCorkle, R. A., Freeman, K. W. & Spencer, D. M. Synthetic activation of caspases: artificial death switches. *Proceedings of the National Academy of Sciences of the United States of America* **95**, 3655-3660 (1998).

- 19 Gray, D. C., Mahrus, S. & Wells, J. A. Activation of specific apoptotic caspases with an engineered small-molecule-activated protease. *Cell* **142**, 637-646, doi:10.1016/j.cell.2010.07.014 (2010).
- 20 Rider, T. H. *et al.* Broad-spectrum antiviral therapeutics. *PLoS one* **6**, e22572, doi:10.1371/journal.pone.0022572 (2011).
- 21 Tse, E. & Rabbitts, T. H. Intracellular antibody-caspase-mediated cell killing: an approach for application in cancer therapy. *Proceedings of the National Academy of Sciences of the United States of America* **97**, 12266-12271, doi:10.1073/pnas.97.22.12266 (2000).
- 22 Chambers, J. S., Brend, T. & Rabbitts, T. H. Cancer cell killing by target antigen engagement with engineered complementary intracellular antibody single domains fused to pro-caspase3. *Scientific reports* **9**, 8553-8553, doi:10.1038/s41598-019-44908-7 (2019).
- 23 Helma, J., Cardoso, M. C., Muyldermans, S. & Leonhardt, H. Nanobodies and recombinant binders in cell biology. *The Journal of cell biology* **209**, 633-644, doi:10.1083/jcb.201409074 (2015).
- 24 Lecocq, Q. *et al.* Theranostics in immuno-oncology using nanobody derivatives. *Theranostics* **9**, 7772-7791, doi:10.7150/thno.34941 (2019).
- 25 Chanier, T. & Chames, P. Nanobody Engineering: Toward Next Generation Immunotherapies and Immunoimaging of Cancer. *Antibodies* **8**, 13 (2019).
- 26 Straathof, K. C. *et al.* An inducible caspase 9 safety switch for T-cell therapy. *Blood* **105**, 4247-4254, doi:10.1182/blood-2004-11-4564 (2005).
- 27 Pluckthun, A. Designed ankyrin repeat proteins (DARPs): binding proteins for research, diagnostics, and therapy. *Annu Rev Pharmacol Toxicol* **55**, 489-511, doi:10.1146/annurev-pharmtox-010611-134654 (2015).
- 28 Fetting, J., Swaminathan, M., Murrill, C. S. & Kaplan, J. E. Global epidemiology of HIV. *Infect Dis Clin North Am* **28**, 323-337, doi:10.1016/j.idc.2014.05.001 (2014).
- 29 MacLachlan, J. H. & Cowie, B. C. Hepatitis B virus epidemiology. *Cold Spring Harbor perspectives in medicine* **5**, a021410, doi:10.1101/cshperspect.a021410 (2015).
- 30 Herrera-Carrillo, E. & Berkhout, B. Bone Marrow Gene Therapy for HIV/AIDS. *Viruses* **7**, 3910-3936, doi:10.3390/v7072804 (2015).
- 31 Gebbing, M., Bergmann, T., Schulz, E. & Ehrhardt, A. Gene therapeutic approaches to inhibit hepatitis B virus replication. *World J Hepatol* **7**, 150-164, doi:10.4254/wjh.v7.i2.150 (2015).
- 32 Engelman, A. & Cherepanov, P. The structural biology of HIV-1: mechanistic and therapeutic insights. *Nat Rev Microbiol* **10**, 279-290, doi:10.1038/nrmicro2747 (2012).
- 33 Liang, T. J. Hepatitis B: the virus and disease. *Hepatology* **49**, S13-21, doi:10.1002/hep.22881 (2009).
- 34 Schmidthals, K. *Generation and characterization of heavy chain antibodies derived from Camelids* Doctorate thesis, LMU Munich, (2013).
- 35 Helma, J. *et al.* Direct and dynamic detection of HIV-1 in living cells. *PLoS one* **7**, e50026, doi:10.1371/journal.pone.0050026 (2012).
- 36 Serruys, B., Van Houtte, F., Farhoudi-Moghadam, A., Leroux-Roels, G. & Vanlandschoot, P. Production, characterization and in vitro testing of HBcAg-specific VHH intrabodies. *The Journal of general virology* **91**, 643-652, doi:10.1099/vir.0.016063-0 (2010).
- 37 Malmqvist, M. Surface plasmon resonance for detection and measurement of antibody-antigen affinity and kinetics. *Current opinion in immunology* **5**, 282-286 (1993).
- 38 Wienken, C. J., Baaske, P., Rothbauer, U., Braun, D. & Duhr, S. Protein-binding assays in biological liquids using microscale thermophoresis. *Nature communications* **1**, 100, doi:10.1038/ncomms1093 (2010).
- 39 Hengerer, A. *et al.* Determination of phage antibody affinities to antigen by a microbalance sensor system. *BioTechniques* **26**, 956-960, 962, 964 (1999).
- 40 Hu, C. D., Chinenov, Y. & Kerppola, T. K. Visualization of interactions among bZIP and Rel family proteins in living cells using bimolecular fluorescence complementation. *Molecular cell* **9**, 789-798 (2002).

- 41 Shyu, Y. J., Liu, H., Deng, X. & Hu, C. D. Identification of new fluorescent protein fragments for
bimolecular fluorescence complementation analysis under physiological conditions.
BioTechniques **40**, 61-66 (2006).
- 42 Nakagawa, C., Inahata, K., Nishimura, S. & Sugimoto, K. Improvement of a Venus-based
bimolecular fluorescence complementation assay to visualize bFos-bJun interaction in living
cells. *Bioscience, biotechnology, and biochemistry* **75**, 1399-1401 (2011).
- 43 Tang, J. C. *et al.* Detection and manipulation of live antigen-expressing cells using
conditionally stable nanobodies. *Elife* **5**, doi:10.7554/eLife.15312 (2016).
- 44 Elmore, S. Apoptosis: a review of programmed cell death. *Toxicologic pathology* **35**, 495-516,
doi:10.1080/01926230701320337 (2007).
- 45 Barber, G. N. Host defense, viruses and apoptosis. *Cell death and differentiation* **8**, 113-126,
doi:10.1038/sj.cdd.4400823 (2001).
- 46 Man, S. M., Karki, R. & Kanneganti, T. D. Molecular mechanisms and functions of pyroptosis,
inflammatory caspases and inflammasomes in infectious diseases. *Immunological reviews*
277, 61-75, doi:10.1111/imr.12534 (2017).
- 47 Qin, J. Y. *et al.* Systematic comparison of constitutive promoters and the doxycycline-
inducible promoter. *PloS one* **5**, e10611, doi:10.1371/journal.pone.0010611 (2010).
- 48 Miao, E. A., Rajan, J. V. & Aderem, A. Caspase-1-induced pyroptotic cell death. *Immunological
reviews* **243**, 206-214, doi:10.1111/j.1600-065X.2011.01044.x (2011).
- 49 Bratton, D. L. *et al.* Appearance of phosphatidylserine on apoptotic cells requires calcium-
mediated nonspecific flip-flop and is enhanced by loss of the aminophospholipid translocase.
The Journal of biological chemistry **272**, 26159-26165 (1997).
- 50 Shaner, N. C. *et al.* A bright monomeric green fluorescent protein derived from
Branchiostoma lanceolatum. *Nature methods* **10**, 407-409, doi:10.1038/nmeth.2413 (2013).
- 51 Hu, Y., Ding, L., Spencer, D. M. & Nunez, G. WD-40 repeat region regulates Apaf-1 self-
association and procaspase-9 activation. *The Journal of biological chemistry* **273**, 33489-
33494 (1998).
- 52 Mulholland, C. B. *et al.* A modular open platform for systematic functional studies under
physiological conditions. *Nucleic acids research* **43**, e112, doi:10.1093/nar/gkv550 (2015).
- 53 Sadelain, M., Papapetrou, E. P. & Bushman, F. D. Safe harbours for the integration of new
DNA in the human genome. *Nat Rev Cancer* **12**, 51-58, doi:10.1038/nrc3179 (2011).
- 54 Kowalski, P. S., Rudra, A., Miao, L. & Anderson, D. G. Delivering the Messenger: Advances in
Technologies for Therapeutic mRNA Delivery. *Molecular therapy : the journal of the American
Society of Gene Therapy* **27**, 710-728, doi:10.1016/j.ymthe.2019.02.012 (2019).
- 55 Kaczmarek, J. C., Kowalski, P. S. & Anderson, D. G. Advances in the delivery of RNA
therapeutics: from concept to clinical reality. *Genome Med* **9**, 60, doi:10.1186/s13073-017-
0450-0 (2017).
- 56 Kormann, M. S. *et al.* Expression of therapeutic proteins after delivery of chemically modified
mRNA in mice. *Nature biotechnology* **29**, 154-157, doi:10.1038/nbt.1733 (2011).
- 57 Uchida, S., Kataoka, K. & Itaka, K. Screening of mRNA Chemical Modification to Maximize
Protein Expression with Reduced Immunogenicity. *Pharmaceutics* **7**, 137-151,
doi:10.3390/pharmaceutics7030137 (2015).
- 58 Kauffman, K. J. *et al.* Efficacy and immunogenicity of unmodified and pseudouridine-modified
mRNA delivered systemically with lipid nanoparticles in vivo. *Biomaterials* **109**, 78-87,
doi:10.1016/j.biomaterials.2016.09.006 (2016).
- 59 Brauchle, M. *et al.* Protein interference applications in cellular and developmental biology
using DARPins that recognize GFP and mCherry. *Biol Open* **3**, 1252-1261,
doi:10.1242/bio.201410041 (2014).
- 60 Tanaka, T. & Rabbitts, T. H. Protocol for the selection of single-domain antibody fragments by
third generation intracellular antibody capture. *Nature protocols* **5**, 67-92,
doi:10.1038/nprot.2009.199 (2010).

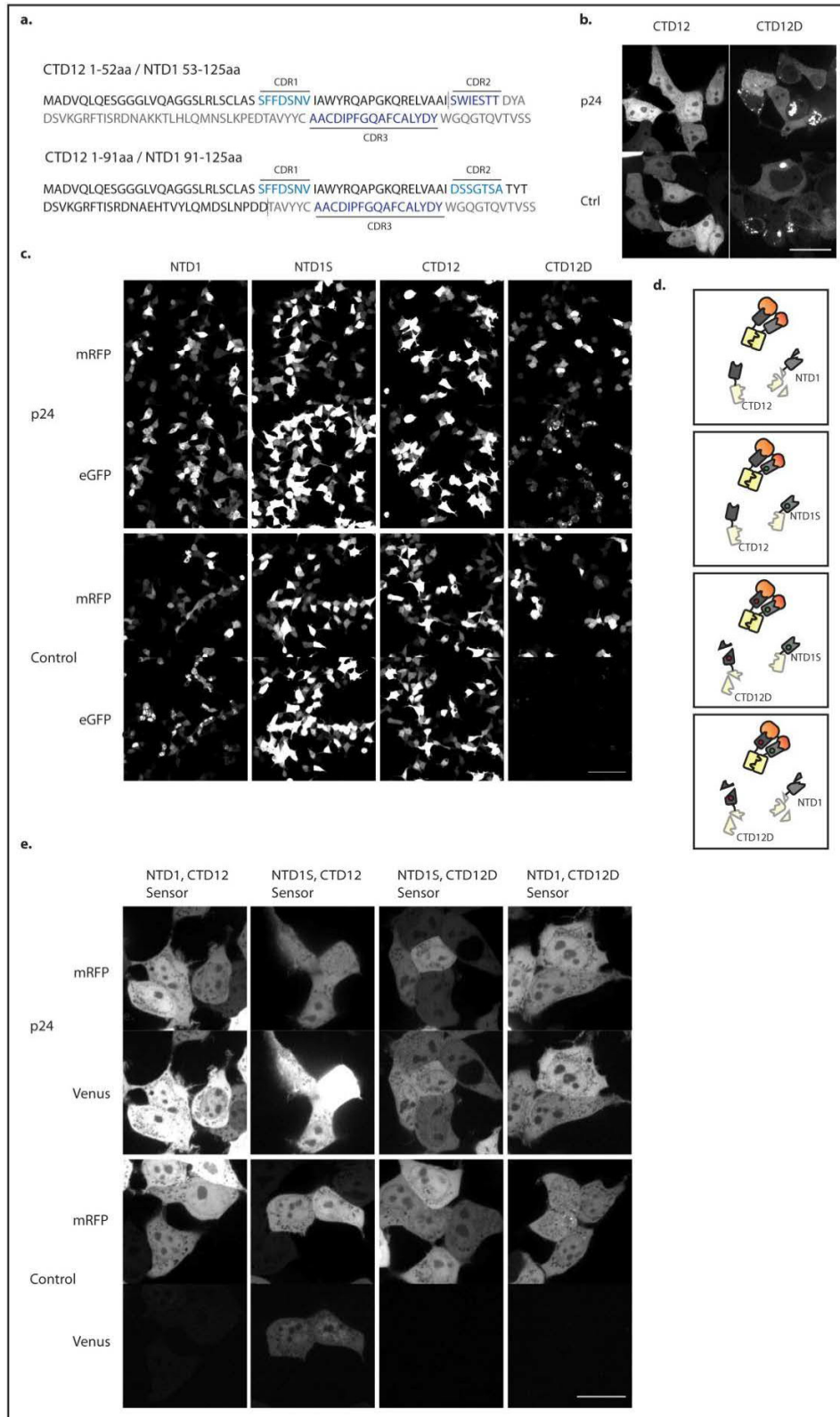
- 61 Grieger, J. C. & Samulski, R. J. Packaging capacity of adeno-associated virus serotypes: impact of larger genomes on infectivity and postentry steps. *Journal of virology* **79**, 9933-9944, doi:10.1128/JVI.79.15.9933-9944.2005 (2005).
- 62 Richter, A., Eggenstein, E. & Skerra, A. Anticalins: exploiting a non-Ig scaffold with hypervariable loops for the engineering of binding proteins. *FEBS letters* **588**, 213-218, doi:10.1016/j.febslet.2013.11.006 (2014).
- 63 Sha, F., Salzman, G., Gupta, A. & Koide, S. Monobodies and other synthetic binding proteins for expanding protein science. *Protein science : a publication of the Protein Society* **26**, 910-924, doi:10.1002/pro.3148 (2017).
- 64 Mitelman, F., Johansson, B. & Mertens, F. The impact of translocations and gene fusions on cancer causation. *Nat Rev Cancer* **7**, 233-245, doi:10.1038/nrc2091 (2007).
- 65 Bruning, A. & Juckstock, J. Misfolded proteins: from little villains to little helpers in the fight against cancer. *Front Oncol* **5**, 47, doi:10.3389/fonc.2015.00047 (2015).
- 66 Eswaran, J. *et al.* RNA sequencing of cancer reveals novel splicing alterations. *Scientific reports* **3**, 1689, doi:10.1038/srep01689 (2013).
- 67 Bolhassani, A., Jafarzade, B. S. & Mardani, G. In vitro and in vivo delivery of therapeutic proteins using cell penetrating peptides. *Peptides* **87**, 50-63, doi:10.1016/j.peptides.2016.11.011 (2017).
- 68 Finer, M. & Glorioso, J. A brief account of viral vectors and their promise for gene therapy. *Gene therapy* **24**, 1-2, doi:10.1038/gt.2016.71 (2017).
- 69 Moghimi, S. M. & Wagner, E. Nanoparticle Technology: Having Impact, but Needing Further Optimization. *Molecular therapy : the journal of the American Society of Gene Therapy* **25**, 1461-1463, doi:10.1016/j.ymthe.2017.06.007 (2017).
- 70 Mali, P. *et al.* RNA-guided human genome engineering via Cas9. *Science* **339**, 823-826, doi:10.1126/science.1232033 (2013).
- 71 Ran, F. A. *et al.* Genome engineering using the CRISPR-Cas9 system. *Nature protocols* **8**, 2281-2308, doi:10.1038/nprot.2013.143 (2013).

Supplemental: Engineering binder-guided apoptotic proteins responsive to intracellular antigens

Engineering binder-guided apoptotic proteins responsive to intracellular antigens

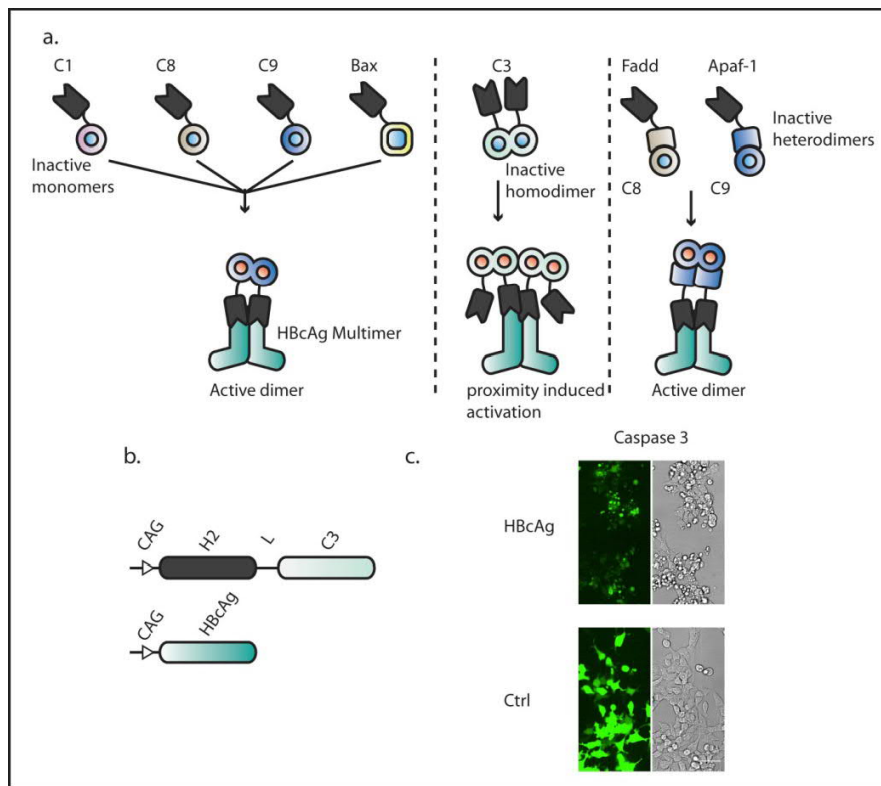
Jack A. Bates, Weihua Qin, Heinrich Leonhardt and Jonas Helma

Supplementary Information

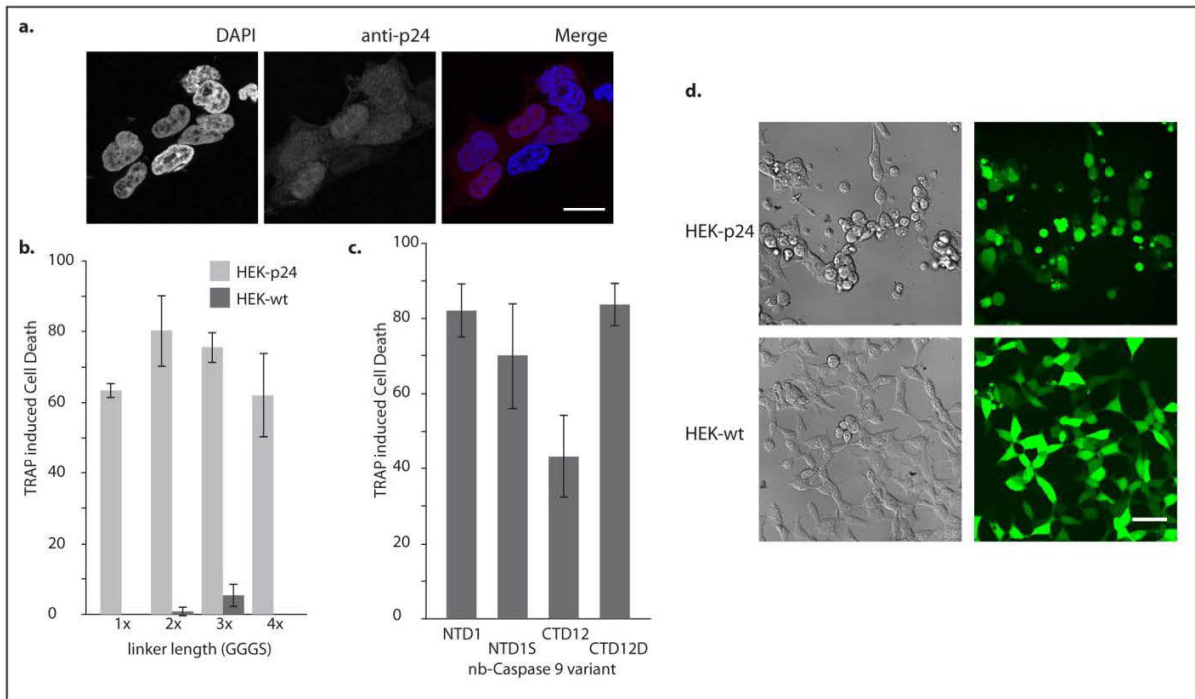


S. Figure 1. Modifying nanobody stability and solubility. (a) Spliced fusions of NTD1_{Nb} and CTD12_{Nb} Nb portions. (b) CTD12_{Nb} and CTD12_{Nb} are expressed in HeLa Kyoto with and without p24. Images are individually adjusted to improve the visualization of

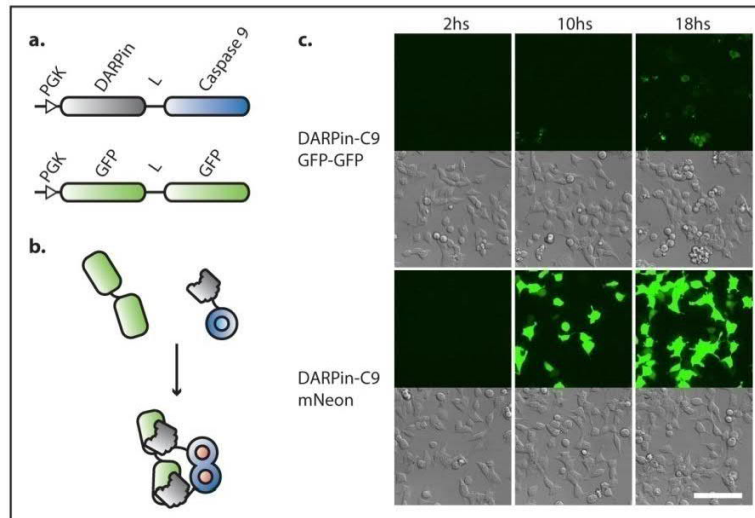
distribution (scale bar 30 μ m). **(c)** GFP fused p24 binding Nb variants are expressed in HeLa Kyoto cells with mRFP and imaged at 24 h for the comparison of GFP signal levels. Images recorded and adjusted identically. (scale bar 100 μ M). **(d)** The synergistic function of ADS and proximity induced activation are illustrated. **(e)** Sensor fluorescence generated both in the presence and absence of p24 antigen is shown for each of the 2xNb-FC p24 sensors at 24s. Images recorded and adjusted identically (scale bar 20 μ m).



S. Figure 2. Cell Death Effectors and high level Caspase 3 expression. (a) The variant mechanisms of proximity induced activation for the tested effectors are illustrated. (b) CAG promoter driven expression cassettes of the H2 nanobody-Caspase 3 and HBcAg are displayed (c). 18 h timepoint image following transfection of H2-Caspase 3 in HEK cells with and without antigen (scale bar 50 μ m).



S. Figure 3. Optimisation and application of TRAPs against HIV-1 p24 antigen. (a) Immunostaining of the p24 antigen in the HEK-p24 cell line. Scale bar 20 μ m. (b) 18 h cell tracking apoptosis analysis comparing variant TRAP linker lengths using NTD1_{NB} and CTD12_{NB}. Lower amounts are transfected to assess for higher potency. (c) Non-specific apoptosis is studied by transfecting high TRAP DNA amounts in the absence of antigen. 18h cell tracking is used to analyse apoptosis caused by TRAPs using ADS and classic stable p24 Nb variants. (d) Live-cell imaging 24 hs after co-transfection of RNA TRAP constructs and mNeon into HEK-p24 and HEK-wt cells are displayed. Scale bar 50 μ m. (Error bars depict standard deviations).



S. Figure 4. DARPin targeted TRAPs. (a) Cassettes used for the validation of DARPins in the TRAP format are shown and corresponding proteins are also displayed (b). The mechanism of DP-C9 TRAP activation on GFP-GFP is depicted. (c) Time points taken from live-cell imaging TRAPs with and without GFP-GFP antigen are shown (scale bar 100 μ m).

Supplementary note 1.

In order to help isolate regions of NTD1_{Nb} potentially affecting its intracellular solubility, we systematically spliced the Nb together with CTD12_{Nb} (Supplementary Figure 1a). Since CTD12_{Nb} is soluble intracellularly, we reasoned that if a single region were responsible for the lower solubility of NTD1_{Nb}, we may be able to determine which it is by observing the intracellular distribution of the spliced Nbs. When we fused each of the new Nbs to GFP we observed that, whilst the *CTD12 1-52aa / NTD1 53-125aa* Nb retained the poor solubility of NTD1_{Nb}, the *CTD12 1-91aa / NTD1 91-125aa* appeared to diffuse evenly throughout the cell. We therefore reasoned that the region affecting solubility laid most likely within CDR2 or FR3 (framework region 3). Since the modification of CDRs is more likely to result in negative effects on affinity, we focused on determining potential problematic regions in FR3. We aligned the amino acid sequence of NTD1_{Nb} to those of 150 other nanobodies (sequences were obtained both from online databases or from Nbs developed in-house). Using this method we determined 4 amino acids which were unusual in their position. We then mutated each of these residues to match those of a nanobody scaffold known to have excellent biophysical properties (sdAb^{D10})¹. Further testing in fusion with GFP revealed that the modified binder (named NTD1S_{Nb}) exhibited greatly improved intracellular solubility.

Supplementary note 2

Transfection compositions

DNA

Screening Assay (Fig. 1f)

Nb-VN	33%	RFP-Nb-VC	33%	pCAG-Antigen	33%
Nb-VN	33%	RFP-Nb-VC	33%	Control DNA	33%

Nb-FC sensor with antigen variation (Fig. 2b)

Nb FC sensor	80%	pCAG-Antigen	20%	X	
Nb FC sensor	80%	pCAG-Antigen	10%	Control DNA	10%
Nb FC sensor	80%	pCAG-Antigen	2%	Control DNA	18%
Nb FC sensor	80%	pCAG-Antigen	1%	Control DNA	19%
Nb FC sensor	80%	pCAG-Antigen	.2%	Control DNA	19.8%
Nb FC sensor	80%	X		Control DNA	20%

Nb-FC sensor Imaging (Fig. 2c)

Nb FC sensor	80%	pCAG-Antigen	20%
Nb FC sensor	80%	Ctrl DNA	20%

Nb variant-GFP imaging and measurement (Fig. 3a,b and S. Fig. 1b,c)

CAG Nb variant-GFP	40%	CAG-p24	40%	CMV mRFP	20%
CAG Nb variant-GFP	40%	Control DNA	40%	CMV mRFP	20%

Nb-FC p24 sensor variant imaging and measurement (Fig. 3d and S. Fig. 1e)

pVitro p24 sensor variant	70%	CAG-p24	30%
pVitro p24 sensor variant	70%	Control DNA	30%

Cell Death effector screening HBcAg (Fig. 4b,c and S.Fig. 2c)

PGK H2-Cell death effector	45%	PGK Antigen	45%	mNeon	10%
PGK H2-Cell death effector	45%	Control DNA	45%	mNeon	10%
x		Control DNA	90%	mNeon	10%
PGK Antigen	45%	Control DNA	45%	mNeon	10%

CAG H2-Caspase 3	45%	CAG Antigen	45%	mNeon	10%
CAG H2-Caspase 3	45%	Control DNA	45%	mNeon	10%

Cell Death effector screening p24 cell line (Fig. 5b)

PGK CTD12-Caspase 9	22.5%	PGK NTD1-Caspase 9	22.5%	Control DNA	45%	mNeon	10%
PGK CTD12-Caspase 3	22.5%	PGK NTD1-Caspase 3	22.5%	Control DNA	45%	mNeon	10%

Nb-Caspase 9 nanobody variant screening (S.Fig.3c)

CTD12-Caspase 9	90%	mNeon	10%
CTD12D-Caspase 9	90%	mNeon	10%
NTD1-Caspase 9	90%	mNeon	10%
NTD1S-Caspase 9	90%	mNeon	10%

Nb-Caspase 9 linker length screening (S.Fig.3b)

CTD12-Caspase 9 Linker variant	12.5%	NTD1S-Caspase 9 Linker variant	12.5%	Control DNA	65%	mNeon	10%
-----------------------------------	-------	-----------------------------------	-------	----------------	-----	-------	-----

Optimised Nb-Caspase 9 p24 testing (Fig. 5c,d,e)

CTD12-Caspase 9	20%	NTD1S-Caspase 9	20%	Control DNA	50%	mNeon	10%
-----------------	-----	-----------------	-----	-------------	-----	-------	-----

Darpin-Caspase 9 testing (S.Fig. 4c)

Darpin-C9	25%	GFP-GFP	20%	Control DNA	55%
Darpin-C9	25%	mNeon	10%	Control DNA	65%

IVT RNA

Nb-Caspase 9 p24 testing (Fig 5 f,g)

CTD12-Caspase 9	40%	NTD1S-Caspase 9	40%	mNeon	20%
-----------------	-----	-----------------	-----	-------	-----

Supplementary note 3

Plasmids

Pre-existing plasmids used for transfection or cloning

Plasmid name	Manufacturer/Author	Addgene no.
CMV mNeon green	Allele Biotechnology	X
pCAG GFP	Matsuda et al ²	11150
pVITRO1-Trastuzumab-IgG1/κ	Invivogen	61883
PCAG IRES Blast	Chen et al	X
pCAG-NLS-HA-Bxb1	Hermann et al ³	51271

Constructed plasmids

Plasmid name	Base Plasmid	Eukaryotic Resistance	Bacterial Resistance
pCAG H2-Venus N	pCAG GFP	X	Amp
pCAG H4-Venus N	pCAG GFP	X	Amp
pCAG H6-Venus N	pCAG GFP	X	Amp
pCAG NTD1-Venus N	pCAG GFP	X	Amp
pCAG CTD1-Venus N	pCAG GFP	X	Amp
pCAG CTD2-Venus N	pCAG GFP	X	Amp
pCAG CTD9-Venus N	pCAG GFP	X	Amp
pCAG CTD12-Venus N	pCAG GFP	X	Amp
pCAG CTD19-Venus N	pCAG GFP	X	Amp
pCAG RFP-H2-Venus C	pCAG GFP	X	Amp
pCAG RFP-H4-Venus C	pCAG GFP	X	Amp
pCAG RFP-H6-Venus C	pCAG GFP	X	Amp
pCAG RFP-NTD1-Venus C	pCAG GFP	X	Amp
pCAG RFP-CTD1-Venus C	pCAG GFP	X	Amp
pCAG RFP-CTD2-Venus C	pCAG GFP	X	Amp
pCAG RFP-CTD9-Venus C	pCAG GFP	X	Amp
pCAG RFP-CTD12-Venus C	pCAG GFP	X	Amp
pCAG RFP-CTD19-Venus C	pCAG GFP	X	Amp
pCAG p24	pCAG GFP	X	Amp
attB pCAG p24	pCAG IRES Blast	Blast	Amp
pCAG HA-HBcAg	pCAG IRES Blast	Blast	Amp
pCAG CTD12-GFP	pCAG GFP	X	Amp
pCAG CTD12D-GFP	pCAG GFP	X	Amp
pCAG NTD1-GFP	pCAG GFP	X	Amp
pCAG NTD1S-GFP	pCAG GFP	X	Amp
pVITRO1 p24 Nb-FC sensor CTD12 NTD1	pVITRO1-Trastuzumab-IgG1/κ	Hyg	Hyg

pVITRO1 p24 Nb-FC sensor CTD12D NTD1	pVITRO1-Trastuzumab- IgG1/κ	Hyg	Hyg
pVITRO1 p24 Nb-FC sensor CTD12 NTD1S	pVITRO1-Trastuzumab- IgG1/κ	Hyg	Hyg
pVITRO1 p24 Nb-FC sensor CTD12D NTD1S	pVITRO1-Trastuzumab- IgG1/κ	Hyg	Hyg
pVITRO1 HBcAg Nb-FC sensor	pVITRO1-Trastuzumab- IgG1/κ	Hyg	Hyg
PGK NTD1-C9 3XGGGS Sacl	pCAG GFP- Promoter switched for PGK	X	Amp
PGK CTD12-C9 3XGGGS Sacl	pCAG GFP- Promoter switched for PGK	X	Amp
PGK H2-C1 3XGGGS Sacl	pCAG GFP- Promoter switched for PGK	X	Amp
PGK H2-C3 3XGGGS Sacl	pCAG GFP- Promoter switched for PGK	X	Amp
pCAG H2-C3 3xGGGS Sacl	pCAG GFP	X	Amp
PGK H2-C8 3XGGGS Sacl	pCAG GFP- Promoter switched for PGK	X	Amp
PGK H2-C9 3XGGGS Sacl	pCAG GFP- Promoter switched for PGK	X	Amp
PGK H2-APAF1 3XGGGS Sacl	pCAG GFP- Promoter switched for PGK	X	Amp
PGK H2-BAX 3XGGGS Sacl	pCAG GFP- Promoter switched for PGK	X	Amp
PGK H2-FADD 3XGGGS Sacl	pCAG GFP- Promoter switched for PGK	X	Amp
PGK NTD1S-C9 3XGGGS Sacl	pCAG GFP- Promoter switched for PGK	X	Amp
PGK CTD12D-C9 3XGGGS Sacl	pCAG GFP- Promoter switched for PGK	X	Amp
PGK NTD1S-C9 1XGGGS	pCAG GFP- Promoter switched for PGK	X	Amp
PGK NTD1S-C9 2XGGGS	pCAG GFP- Promoter switched for PGK	X	Amp
PGK NTD1S-C9 3XGGGS	pCAG GFP- Promoter switched for PGK	X	Amp
PGK NTD1S-C9 4XGGGS	pCAG GFP- Promoter switched for PGK	X	Amp
PGK CTD12-C9 1XGGGS	pCAG GFP- Promoter switched for PGK	X	Amp
PGK CTD12-C9 2XGGGS	pCAG GFP- Promoter switched for PGK	X	Amp
PGK CTD12-C9 3XGGGS	pCAG GFP- Promoter switched for PGK	X	Amp
PGK CTD12-C9 4XGGGS	pCAG GFP- Promoter switched for PGK	X	Amp

PGK DARPIN-C9	pCAG GFP- Promoter switched for PGK	X	Amp
PGK GFP-GFP	pCAG GFP- Promoter switched for PGK	X	Amp

References

- 1 Moutel, S. *et al.* NaLi-H1: A universal synthetic library of humanized nanobodies providing highly functional antibodies and intrabodies. *Elife* **5**, doi:10.7554/eLife.16228 (2016).
- 2 Matsuda, T. & Cepko, C. L. Electroporation and RNA interference in the rodent retina in vivo and in vitro. *Proceedings of the National Academy of Sciences of the United States of America* **101**, 16-22, doi:10.1073/pnas.2235688100 (2004).
- 3 Hermann, M. *et al.* Binary recombinase systems for high-resolution conditional mutagenesis. *Nucleic acids research* **42**, 3894-3907, doi:10.1093/nar/gkt1361 (2014).

Discussion

Protein Delivery

Optimizing *in vitro* protein delivery

A very broad range of parameters and characteristics should be considered in the design of an MSN for protein delivery^{584,588}. These include the shape of the nanoparticle, as well as its size, both of which have been shown to affect cellular uptake⁵⁸⁹⁻⁵⁹², extravasation rates⁵⁹³, and serum half-life properties^{594,595}. The gross morphology further combines with pore size and structure to determine the loading potential of a given particle. Tuning pore size and architecture is important to maximize surface area for a given cargo size and furthermore, it affects the rate of release from a nanoparticle^{596,597}. Beyond these structural considerations MSNs can also be formulated with a large variety of functional groups which will affect the charge, uptake and toxicity of the particle^{598,599}, as well as the molecules with which it can be bound. The nature of these groups will further determine the efficacy of cell specific protein release, as well as the leakiness of the particle. The addition of molecules via these functional groups provides attributes to the complex which are essential for protein delivery and not inherent to the MSN. For example, despite claims that MSNs can themselves elicit endosomal disruption⁶⁰⁰, this is not something that was witnessed to any significant degree in our work. Efficient protein delivery will then likely require an additional mechanism for endosomal escape to be incorporated onto the nanoparticle such as fusogenic peptides⁶⁰¹ or polymers eliciting a possible proton sponge effect⁶⁰². The serum half-life of the nanoparticle may also be unsatisfactory for a given application and so further molecules may be required to modulate this such as PEG or a lipid coat^{603,604}. Lastly, MSNs may require targeting moieties to direct them to the region of interest^{571,605}.

Clearly, a very substantial amount of optimisation must be undertaken to discover the most effective MSN variants for protein delivery. This is particularly important as, despite good compatibility at lower doses, both in our work and the work of others MSNs exhibit toxicity at higher doses⁶⁰⁶ and it is therefore desirable to administer the minimum effective dose. Since the adjustment of many of these parameters will ultimately seek to further the end goal of improved cytosolic delivery, much of this optimisation work could be undertaken using variants of the Venus sensor demonstrated by us. Indeed, our sensor should be suitable for the optimisation of a great range of protein delivery options⁶⁰⁷.

Importantly, the sensor would also be of great use for comparisons between these technologies, something which to our knowledge has only been minimally undertaken to date⁵⁵⁷.

Optimizing *in vivo* protein delivery

Whilst promising therapeutic candidates can be determined using *in vitro* investigation, nanoparticle parameters must ultimately be investigated *in vivo* where factors such as serum half-life, serum protein adsorption⁶⁰⁸, and cellular accessibility complicate delivery. Here too we propose that our Venus based sensor could be an interesting candidate. We expect that such a sensor could be incorporated into an organism, such as a mouse with relative ease. This would allow for visual assessment of protein delivery across the organism. Alternatively, cancer cell lines used for cell line xenograft⁶⁰⁹ could be modified prior to introduction into the mouse to enable the monitoring of tumor uptake.

One advantage of our method is that the level of fluorescent signal correlates with the amount of protein delivered, this is untrue of some popular techniques that permanently alter the transcription of the cell, such as recombinase based sensor methods⁵²⁸. However, this more quantifiable output comes at the cost of sensitivity. Additionally, unless the target cell population is optically accessible, such that it can be repeatedly visualized without sacrificing the animal, or it is found in the blood and can be assessed by blood sampling, then time point based sampling could be difficult with this Venus system. Time point sampling could be important in understanding delivery kinetics and overall delivery during optimisation. This is especially true since complexes with extended physiological half-lives may be more likely to reach their target cell and thus future delivery methods could take place over protracted timeframes of days.

One method by which one could obtain a time course is by having the delivered protein trigger the expression of a secreted protein which could then be measured in the blood. Ideally this would be a reversible process so that researchers would be able to obtain estimations of delivery timings. Since it should be reversible, recombinase based methods are not ideal and the delivery of a transcriptional activator could be preferable. However, because it is also desirable to differentiate between specific and non-specific delivery, the delivery of a transcription factor alone is too simple. To this end the split delivery concept could perhaps be repurposed and combined with tissue specific promoters to meet these requirements in a manner outlined in figure 14.

It may be most profitable to combine numerous protein delivery sensors to assess a range of delivery traits. For example; a highly sensitive system, such as a recombinase based method, might deliver the best approximation of the overall pattern of delivery; fluorescent complementation could assist in measuring the relative quantities and homogeneity of protein delivery; and a split transcription system such as is outlined in figure 14 could be a tool to optimize delivery specificity and understand its timing.

MSNs for protein delivery

Owing to the many parameters assessed and the high efficiency of protein delivery, our work is arguably amongst the clearest to date regarding the potential of MSNs for *in vitro* protein delivery⁵⁶⁷. The delivery of bioactive and bioavailable protein into around 80% of HeLa cells was demonstrated using the Venus sensor and flow cytometry and a more sensitive sensor may have revealed a higher rate still. This delivery rate is comparable to those given for numerous commercially available PTD based or cationic lipid reagents (e.g. 60-95% Chariot™, Active Motif; Pierce™ Protein Transfection Reagent, ThermoFisher Scientific 40%-90%). This of course raises the question of whether this large-pore MSN variant might be suitable for broader use and several features of the particle arguably support that notion. For example; particle synthesis utilizes highly affordable materials and should be readily scalable^{577,610}; The Ni-NTA surface chemistry incorporated into this MSN³¹⁷ would be widely convenient due to the high prevalence of his-tag mediated purification; and both the optimal MSN dose and the Chloroquine ‘shock’ method applied for endosomal release were experimentally shown to be minimally cytotoxic in this work and a previous work respectively³¹⁷.

The production of a one size fits all protein transduction reagent is complicated greatly by the variance exhibited between proteins in terms of size, shape and charge. In order to determine if MSNs exhibit the necessary generality to be considered as a reagent for broad spectrum use, a selection of proteins with these variant parameters must first be tested. Bearing in mind that the proteins coat the nanoparticle and therefore could substantially alter its surface properties, the protein loaded could significantly affect delivery performance. Inversely however, having the interaction between the protein and MSN dependent only upon the presence or otherwise of a his-tag rather than the surface chemistry of the protein, such as is the case with some other transfection reagents, could prove to be advantageous in terms of generality provided the attributes of the MSN override those of the loaded protein. The large pore MSNs tested by us exhibit a ridged coral-like surface morphology with dimensions varying typically

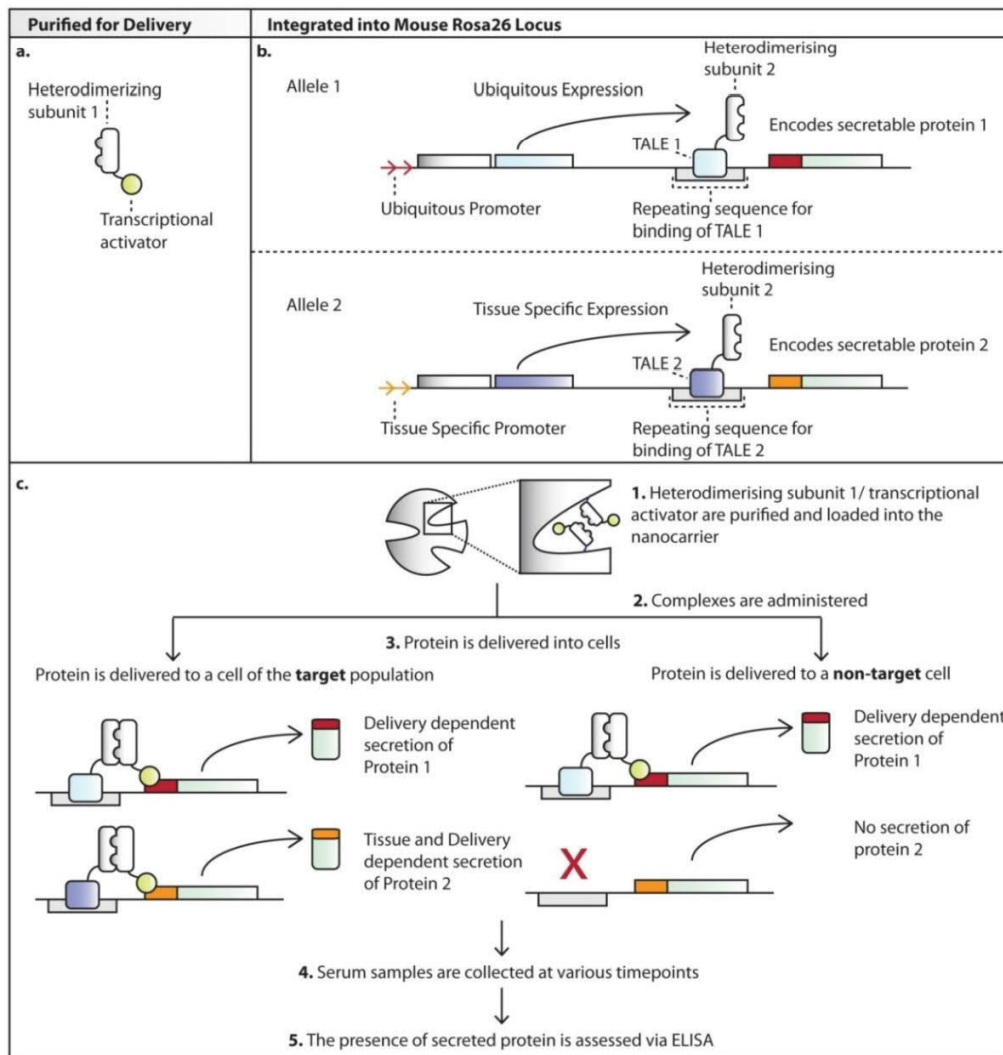


Figure 14. A Potential *in vivo* Protein Delivery Sensor. A two-hybrid system which uses split delivery to optimize tissue specific delivery over time. **(a)** A heterodimerizing subunit (HS1) is fused to a transcriptional activator (TA) for purification. **(b)** Sensor mice are genetically modified to express two cassettes. Allele 1 ubiquitously expresses heterodimerizing subunit 2 (HS2) and TALE 1 (T1) in fusion. This fusion then binds to sequences upstream of the coding sequence for secretable protein 1 (SP1). Allele 2 uses tissue specific promoters (which could be exchanged by recombination) to selectively express HS2 and TALE 2 (T2) in fusion. This fusion then binds to sequences upstream of the coding sequence for secretable protein 2 (SP2). **(c)** **1.** The purified sensor half is loaded into nanocarrier and subsequently **2.** the nanocarrier is administered to the animal. **3.** All cells secrete Protein 1 in response to nuclear protein delivery. This occurs because the delivered HS1-TA binds to the ubiquitously expressed HS2-T1 allowing TA to drive the expression of SP1. In cells of the correct tissue type HS2-T2 is expressed and can interact with the delivered protein such that they also express SP2. **4.** Serum is collected at numerous time points following the administration of the nanoparticles. **5.** SP1 and SP2 are measured in the serum samples via ELISA and represent overall protein delivery and tissue specific protein delivery respectively. A recombinase could also be expressed after the tissue specific promoter to excise HS2-T1 tissue specifically so that targeted delivery only results in SP2 secretion. Readings can be used for specific protein delivery optimization by seeking to increase SP2 and decrease SP1.

between 10 nm and 40 nm. We tested these particles using a relatively small delivered protein of just 22 kDa which measures approximately 3x12 nm when elongated. However, given the dimensions of the surface pores, it should also be possible to efficiently load much larger proteins. We therefore expect

these nanoparticles to be quite broadly applicable in their present morphology. If however future work determines that this is not the case, then a repertoire of particles could potentially be synthesized for the delivery of proteins of various molecular weights. Lastly, different cell lines differ significantly in their ease of protein transfection, testing function on a variety of cell lines would therefore also be very important for determining general applicability.

Due to the many complications of *in vivo* delivery already discussed^{532,536}, it is difficult to imagine the near-future broad application of MSNs for *in vivo* cytosolic delivery. A good nearer-term prospect for MSN mediated protein delivery could be the delivery of vaccine proteins and peptides⁵³¹. Using nanocarriers to deliver protein subunits for the purpose of vaccination can lead to substantial increases in uptake by APCs (Antigen Presenting Cells) and subsequently improved antigen display⁶¹¹. Delivery to APCs is relatively simple due to the highly phagocytic nature of the cells. Indeed, a common problem of nanoparticle delivery is their rapid uptake into the mononuclear phagocytic system (MPS)⁶¹² rather than into target tissues, in this instance this is however advantageous. The nature of protein delivery for vaccines is also less demanding. When proteins are required for presentation on MHCII molecules they do not require endosomal escape as they will be processed within the membrane system. Whilst cytosolic delivery is required for Class I presentation, the protein is not required to be either functional or correctly folded since it will ultimately be digested and used in peptide form⁶¹³. Researchers have already demonstrated successful immune stimulation using large pore MSNs in this way and this represents a promising avenue for the particles^{586,587,614}.

Targeted Apoptosis

Considerations for TRAPs

In the attached work we developed an approach to pathogenic intracellular antigens which elicits apoptosis of the host cell. In this way, TRAPs mirror the action of endogenous cellular defense mechanisms in that they induce cell death upon pathogen detection⁶¹⁵. However, whilst natural pathogen detection is naturally either very generic or occurs with significant delay⁶¹⁶ TRAPs utilize nanobody targeting to act with a high degree of specificity and convergence with apoptotic machinery to rapidly eliminate cells. Importantly, unlike endogenous machinery which will not respond to self antigen, synthetic targeting mechanisms including TRAPs can be programmed to do so. The capacity to

target self antigens has proven highly useful for numerous cancer and autoimmune immunotherapies and we anticipate that it may also be useful for TRAPs⁴⁶⁴.

A further advantage of TRAPs is their capacity to be formed of human or human analogous components which we believe should result in minimal immune activation upon application. In instances where TRAPs are incorporated into the cell for expression over an extended duration, or where repeated applications are intended, low immunogenicity is particularly important since reactions could result in the T cell mediated elimination of cells containing the TRAP components. Although we did not employ mutational measures to humanize our nanobodies⁷⁸ this is a clear next step for the technology.

In this study, we also demonstrated a BiFC based solution to the problem of very high background when utilizing intrabodies for the live cell imaging of intracellular targets. We showed that through the use of BiFC in combination with ADS, SNRs of 78:1 could be demonstrated. However, since the method was only demonstrated on very high levels of antigen the extent of its generality is unknown. Use of this method with lowly expressed targets may necessitate a reduction in one or both components of the system. We suggest that the approach could deliver more visually impressive results when applied with non-diffusive antigens as is typically necessary with chromobody type techniques.

When testing our TRAPS we encountered various conditions under which they did not function. To account for these it is helpful to think of factors affecting TRAP function in terms of three parameters; the concentration of complex components, including TRAPs and antigens; the affinities of these components, between the binders and antigen and at the caspase-9 interface; and the potency of the activated caspase-9, i.e. how many complexes are required to initiate a successful apoptotic cascade.

Since the potency of TRAPs is related to the number of active complexes, stoichiometric considerations governing the likelihoods of complex concentrations are important. The concentration of components and the affinity between them determine the final concentration of active complex. Whilst the level of target antigen cannot be altered, antigen epitope saturation, and thereby complex formation, can be increased by introducing more TRAP or via improvements to TRAP affinity for the antigen. Having a good rate of epitope binding is particularly important for TRAP function because they are active as ternary (two TRAPs binding to a single antigen) or quaternary (a single TRAP binding twice to a homomultimerising antigen) complexes, as opposed to standard binary antibody-antigen complexes. Because the TRAPs are only active in these complete complexes, inefficiencies in the interactions involved in complex formation amplify. For example, if only 20% of cellular antigen epitope 1 is bound by TRAP 1

and a further 20% is bound by TRAP 2, then only 4% (20% of 20%) of antigen is part of a fully formed ternary complex.

Insufficient complex formation for apoptosis can occur if; the antigen level is too low to accommodate enough complexes; if low TRAP affinity or concentration affects binding; or if antigen concentration is too high to be effectively targeted without expressing concentrations of TRAP which induce cell death by autodimerisation. In the last instance TRAP components could bind well but be sequestered on separate antigens and fail to form sufficient active complexes.

We expect that higher affinities could have a remarkable effect on the potency and background activity of TRAPs. The affinities of widely utilized binders span a huge range, with dissociation constants in the high femtomolar to low micromolar range and care should be taken to select more affine molecules for TRAP formation. Low to mid nanomolar p24 nanobodies were used in this work and some toxicity was seen even when transfections were somewhat optimized. Higher affinities should expand the therapeutic window in both directions by allowing more complete saturation of lowly or highly expressed antigens without higher expression of the TRAP and subsequent autoactivation. In addition, besides the saturation of the antigen and formation of higher complex numbers, lower dissociation rates could hugely benefit TRAPs by giving complexes more time to form and function.

Lastly, variances in cellular susceptibility to apoptosis should be considered. These could include the activity and levels of relevant pro and anti apoptotic components in addition to any relevant mutations which may be present⁶¹⁷.

Delivering TRAPs

Since caspase-9 has the capacity to auto-dimerize at higher concentrations we anticipated that it may be difficult to handle and deliver in its purified protein form, we therefore delivered DNA and mRNA forms of the system. Delivery as DNA could be advantageous since it is potentially amenable to AAV (adeno associated virus) or lentiviral gene delivery, which are perhaps the two most progressed intracellular delivery formats. AAV delivered gene therapies have been approved for 3 genetic diseases and are presently under investigation in a large number of clinical trials⁶¹⁸ due in part to their good safety profile relative to other methods⁶¹⁹. Whilst AAVs may not presently deliver to the breadth of cells required to see TRAPs be optimally effective, improving the quality of AAV delivery, for example through recombinant capsid screening⁶²⁰, is an area of intense research that could see significant advancement.

Lentiviral vectors could also be used in incidences where *ex vivo* delivery can be performed and have been repeatedly used in HIV gene therapy attempts⁶²¹. The delivery of DNA cassettes rather than protein should also improve the longevity of the technology in the cell. Use of DNA also permits more conditional control over system expression via mechanisms such as promoter selection or endogenous RNA interference mechanisms^{622,623}.

In some instances transient expression of the TRAP is desirable. This could mitigate potential negative impacts in the longer term, including the reduction of immune repercussions, a decrease in potential cytotoxicity through background activation and also a decrease in the physiological burden of expressing the system. One disadvantage of DNA delivery is the danger of genomic integrations leading to cellular transformation a risk which can be avoided by delivering mRNA. We were able to demonstrate highly effective TRAP function using delivered via IVT mRNA. Since delivered mRNAs can lead to the activation of cellular immune mechanisms we implemented modified RNA bases (25% pseudouridine, 25% 5-methylcytosine) to minimize this effect and improve the intracellular durability of the molecules⁶²⁴. Whilst DNA may be more appropriate for the creation of sentinel cell lines, where the system is incorporated into the cell to await infection, mRNA may be preferred in other scenarios since the short term expression elicited should lower the physiological burden of the technology on target cells.

The direct cellular delivery of TRAPs as proteins could be an interesting approach to administration since it would avoid problems of innate nucleic acid immune receptor activation and expression prolonged beyond the useful window. However, the purification of TRAPs for this purpose could be problematic due to the tendency of caspase-9 to dimerize and activate at higher concentrations⁶²⁵. One approach to preventing Caspase-9 dimerization during expression and purification is to fuse a peptide to the protein which functions to occupy the dimer interface⁶²⁶. Potentially such tags could be designed such that they are cleaved away at a later time point. For example, the peptides could be removed via endogenous proteases in the blood, cytosol, tumor microenvironment or endosomal system where the concentrations should be sufficiently low to prevent spontaneous autodimerisation^{627,628}.

System improvements

Modulating caspase activity

It may be possible to improve the TRAP system through modifications of the caspase-9 effector protein. Generally, a caspase-9 of lower background complementation and comparable or improved activity would be desirable since it would decrease background and increase the therapeutic window of the method. A lower complementation rate would allow higher expression of the components which could in some instances be important for achieving sufficient complexes on the target. This could be achieved through adjustments to the affinity at the dimer interface. Protein engineering of this kind has previously been applied to improve both the split Venus variant used in this work⁶²⁹ as well as in very early split protein work involving ubiquitin⁴⁴³.

The caspase-9 interface consists centrally of a stretch of 5 amino acids aligned in an anti-parallel fashion⁶²⁵. At the midpoint of this interface is a Phenylalanine residue (Phe404) which contributes greatly to dimer interaction via the hydrophobic effect. Experimentally the necessity of this residue for interaction has been demonstrated through its substitution with a highly hydrophilic aspartic acid residue^{626,630}. In an attempt to reduce erroneous dimerisation of caspase-9 at higher concentrations without compromising the efficacy of the protein, we explored a series of Phe404 mutants with a focus upon altering the hydrophobicity of this region (Figure 15). Caspase-9 Mutants with valine, tyrosine, alanine or glycine were generated. These residues were selected as points on a continuum of amino acid hydrophobicity⁶³¹.

Timelapse microscopy was used in preliminary experiments to examine the effect of the various mutations on caspase-9 dimerisation in the context of an H2nb fusion and with or without HBcAg. Image analysis was incomplete but appeared to show that it is possible to modulate the potency of the caspase-9 in a non-binary way through exchange of this phenylalanine. In brief, more hydrophobic residues such as valine and tyrosine appeared to still permit target induced apoptosis whilst less hydrophobic residues (alanine and glycine) affected the potency of the caspase-9 very significantly. Unfortunately we did not witness a clear improvement in the ratio of specific and non-specific dimerization with any of these mutants. However, this work is clearly not exhaustive of the possible mutations at the interface and further testing, perhaps utilizing saturation mutagenesis of surface exposed side chains within the central pentamer may yield a more desirable outcome.

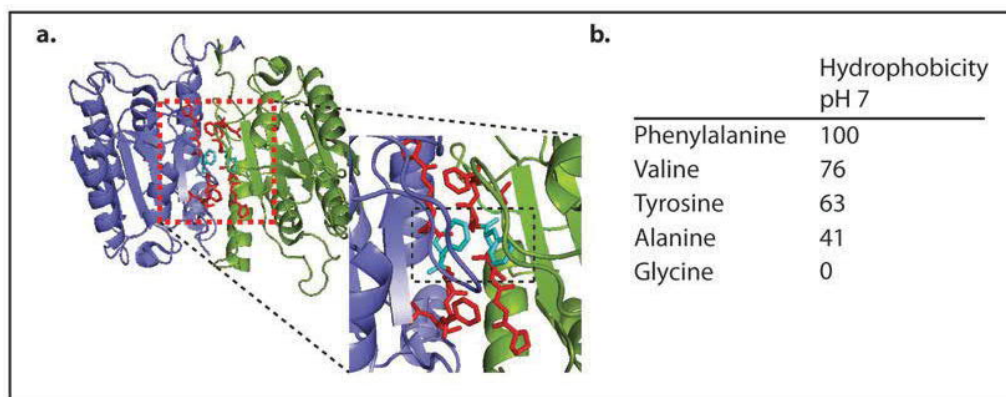


Figure 15. Modifying Caspase-9 dimer interface residues. (a) A Caspase-9 dimer crystal structure is depicted (PDB1JXQ) with interface residues highlighted in red and Phe404 in turquoise. (b) the relative hydrophobicities of phenylalanine and four other residues trialed as substitutions position 404 of caspase-9.

As a further mechanism to reduce background caspase-9 activation we explored the use of antigen dependent selectively stable nanobodies. The use of such nanobodies within the TRAP could reduce background Caspase-9 activity by lowering its concentration in the absence of the antigen. As evidence that this concept of pairing selective stability with proximity induced activation could reduce background in an additive manner we were able to show a significant reduction in the background pairing of split venus halves. This resulted in great improvements in our signal to noise ratios for our fluorescent p24 sensor. Unfortunately, when selectively stable nanobodies were then paired with caspase-9, background activation (as determined by cell death in the absence of antigen) increased. This is likely due to the ADS Nbs' propensity towards aggregation, as seen with ADS Nb-FP fusions, which presumably causes approximation and complementation of caspase-9 homodimers. This tendency towards aggregation was also seen in many of the selectively stable nanobodies developed by Tang et al in their original investigations³³⁴, they do however report that some nanobodies did not display this issue. If such non-aggregatory binders could be isolated against the desired targets then the mechanistic pairing of selective stability and tandem binding could yet prove profitable.

Beyond altering the stability of the binder through structural modifications, it may also be possible to develop a selectively stable TRAPs in other ways. One possibility could leverage the protease function of caspase-9 upon activation to remove a fused domain which would otherwise reduce the half-life of the protein. This method could be somewhat conceptually similar to the SMASH tag³⁹⁹. Such a domain need not result in the aggregation of TRAP but may nonetheless reduce the protein's half-life. Preliminary work was undertaken to determine a small human protein fragment which could potentially perform this function and the ankyrin repeat fold 6 (AR6) of I κ B α ⁶³², an 11 amino acid region, was tested.

Experiments measuring its effect on the stability of a Nb-GFP were performed and showed an 8-fold reduction in the protein. Unfortunately when AR6 was fused to a TRAP via a LEHD (caspase-9 cleavage motif) containing linker no clear benefit with regards to potency or background killing was seen upon microscopic evaluation. The cause of this is unknown, it could potentially have been due to an inability to cleave the fusion away from the TRAP due to steric constraints or perhaps the level of complementation and subsequent cleavage was too insignificant to observe a real difference. Further work is needed to determine the legitimacy of this proposal.

In addition to decreasing unwanted background complementation it may be in some instances also desirable to increase the potency of the enzyme. In nature, caspase-9 is thought to function via forced homo-oligomerisation on the apoptosome but this mechanism is very significantly enhanced by interactions with APAF-1. This concept is supported by observations of very substantial increases in *in vitro* caspase-9 activity when supplemented with apoptosomal components in contrast to the dimer alone⁶²⁶. In this way caspase-9 likely functions both as a homodimer and as a holoenzyme with apaf-1. As such, the utilization of caspase-9 in the TRAP constructs likely does not reflect the full functional capacity of the enzyme and therefore higher concentrations of active complex would likely be required to kill the cell. Potentially this requirement for a heightened number of complexes could exclude effective TRAP responses against some lowly expressed antigens in addition requiring generally higher expression.

It may be possible to increase the activity of caspase-9 using high throughput mutagenesis and screening approaches, as has been done with numerous other enzymes^{201,633,634}. Conversely, potency could be increased by interfering with mechanisms of caspase-9 negative regulation. As mentioned previously, Malladi Et al⁶³⁵ propose that Caspase-9 may be prevented from undesirable over activity by a “molecular timer” function. They hypothesize that the cleavage occurring between the large and small subunits of caspase-9 during activation affects the affinity of the enzyme for itself leaving it vulnerable to dissociation. This dissociation could represent a mechanism for the control of aberrantly activated caspase-9 by ensuring that it remains active for a more finite period⁶²⁶. When non-cleavable mutants were produced that were incapable of the dissociating in this way, an increase in *in vitro* activity was observed. Potentially this mutation could be tested and included in the TRAP constructs to improve their potency. Clearly however this could also lead to dangerous levels of background activation and may be best combined with a Caspase-9 harbouring a modified dimer interface.

Resistance to apoptotic inhibition

As will be discussed this technique may also be applicable to some cancer types. Cancerous cells suppress apoptosis through a variety of modifications⁶¹⁷ affecting the cell death pathways. In some instances these modifications can alter sections of the apoptotic pathway related to or downstream of Caspase-9 which could potentially render the cell more resistant to any TRAP functioning inside that cell⁶³⁶.

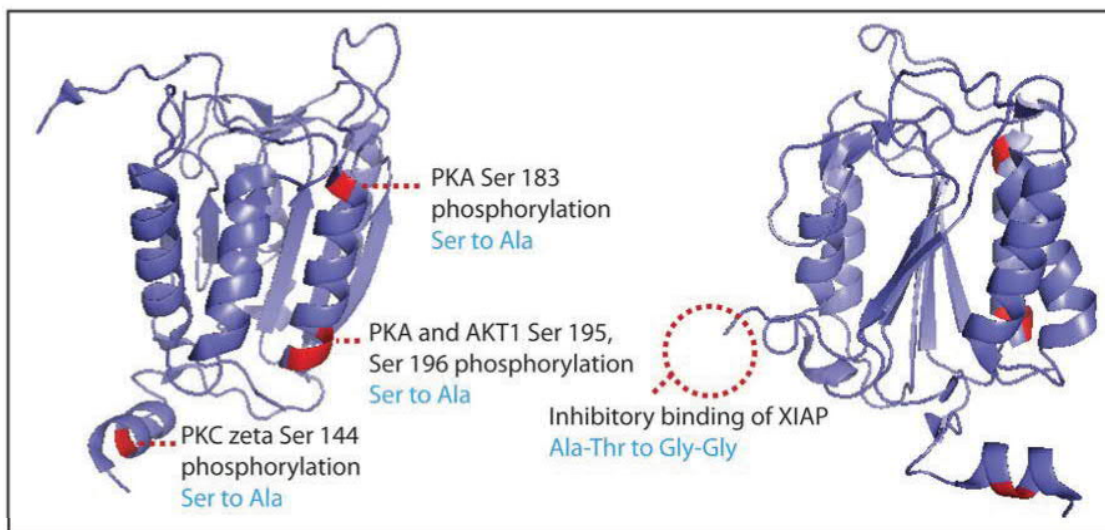


Figure 16. Generating a caspase-9 with improved resistance to inhibition. A cleaved and activated caspase-9 is shown (PDB 1JQX) with key residues for its inhibition coloured red. Mechanisms of inhibition and the associated proteins are seen in the annotations. Mutations generated to counteract inhibition are written in blue.

It should be possible to alleviate repression of a caspase-9 by modifying the protein such that its inhibitors cannot interact with it. The known mechanisms of caspase inhibition have been collated by Parrish et al⁶³⁷. Many of the proteins shown to inhibit Caspase-9 act on residues present in the CARD, since the Caspase-9 used in the TRAPs is a truncation which omits this domain, these inhibitors should be inert against TRAPs. We aimed to further improve the resistance of caspase-9 to inhibition by altering other residues which are sites of phosphorylation or direct binding. In preliminary work we mutated each of the serines at 144,183,195 and 196 to alanine and altered the dipeptide motif present in the small-large subunit linker⁶³⁸ to prevent inhibitory XIAP binding.

On simple visual inspection of transfections experiments all mutants seemed to retain comparable cell killing to the wild type with the exception of S183A and a caspase mutant containing all combined mutations excluding S183A, also appeared to be active. When transfected with XIAP and antigen the

caspase-9 mutant which was modified to resist XIAP mediated inhibition appeared to be markedly more cytotoxic than the wildtype. The effects of these transfections were not quantified but further investigation is merited.

Where mechanisms of resistance affect downstream of caspase-9 at the executioner caspases (3 and 7), TRAP function may also be impaired. To counteract this, it may be possible to supplement the TRAP with additional caspase-3 which could also be modified to be resistant to inhibition via phosphorylation of Serine 150 or XIAP binding⁶³⁷. Alternatively, it may be possible to include a modified caspase-9 activatable Gasdermin D. Gasdermin D is an executioner of the pyroptotic pathway, in its active form it is sufficient to execute cell death alone via pore formation⁶³⁹. Gasdermin is activated by caspase-1 but alteration of the caspase motif may permit cleavage by caspase-9 such that TRAP activation could potentially also lead to cell death via pyroptosis.

Potential targets

In the attached work we demonstrated apoptotic responses to viral proteins using our TRAP system. Whilst viral infections are clear potential candidates for this technology, we believe that this approach may also be applicable to other diseases, in particular cancer. TRAPs could perhaps be applied to proteins which are unique to or greatly upregulated in cancer cells. Furthermore, where TRAP expression can be controlled by a tissue specific promoter, or the TRAPs are delivered specifically enough, the protein need only be unique to that tissue⁶⁴⁰. It may be possible to target protein resulting from cancer specific splice variants⁶⁴¹, a single point mutation⁶⁴², or perhaps most interestingly oncofusion proteins could be targeted.

Oncofusion proteins are formed when genomic translocations stitch two genes together producing a sequence which encodes a chimeric protein consisting of N and C portions from separate origins. Oncofusion proteins are critical driver mutations in numerous cancers and are theoretically ideal targets for TRAPs since the proteins are unique to the target cells⁶⁴³. The AML1-ETO and PML-RAR α oncofusions, which are common drivers of leukemias, could be particularly interesting. These are each composed of DNA binding proteins in fusion with transcriptional repressors. The result of these chimeras is the aberrant silencing on multiple genes critical to the regulation of haematopoiesis and apoptosis.

TRAPs could be formed against each of these proteins in a number of ways. AML1-ETO consists of residues 1-177 of AML1 (RUNX1), a transcription factor which binds DNA as part of heterodimer with CBF β , and most of ETO, a transcriptional repressor which tetramerises via its NHR2 domain^{644,645}. TRAPs could potentially be paired on each AML1-ETO molecule using a binder against the AML1 portion and a second specific for the AML1-ETO junction, or a single binder could be directed to the AML1 protein and be dimerised by NHR2 driven tetramerisation. It's a similar story with PML-RAR α , in this instance RAR α functions in healthy cells as a heterodimer with RXR but can be forced into a homodimer when fused to PML⁶⁴⁶. As such, a single TRAP could be directed against RAR α in isolation and function upon homodimer establishment or a second could be targeted to the PML-RAR α junction area. It may also be possible to bypass the need for binders in favor of using the natural heterodimer partners of AML1 and RAR α , CBF β and RXR respectively. Fusing caspase-9 to the proteins should be inconsequential in a healthy cell since neither of these proteins oligomerises, whereas the homotetramers and dimers formed when the oncofusions are present could function to approximate caspase-9 dimers.

Targeted Protein Degradation

In the work entitled *'Tunable light and drug induced depletion of target proteins'* we demonstrate new tools for the modulation of proteostasis. As discussed in the introduction, direct protein level intervention can be highly appealing to researchers especially when investigating long half-life or essential proteins. Functional protein knockdowns can be performed by variant means, one approach is to introduce binders which occupy and inhibit functional regions on the protein such as active sites or protein interaction surfaces⁹². However, since many proteins are modular and/or exhibit numerous functions, achieving a complete functional knockdown using this approach can be difficult. Furthermore, eliciting antagonistic binding which is selective for only a particular PTM or splice variant would require that the active region and the unique region were one and the same, which frequently is not the case. A second approach is to relocalize the protein to a region within the cell where it cannot function^{368,370,647}. These 'Knock-sideways' type techniques are obviously limited to proteins that require a particular cellular compartment for the totality of their function. Both of these approaches assume significant prior understanding of protein function including knowledge of either the active regions or the environment. In addition, these methods require saturation of the target to function well and should therefore be expressed at a significantly higher level than the target.

In contrast to the above methods targeted degradation does not require constant saturation of the target and should be possible using much lower levels of the tools since a single E3 ligase can potentially ubiquitinate and degrade multiple targets. Targeted methods enable the degradation of pristine endogenous proteins and are also suitable for those desiring to target specific splice or PTM variants of the protein. Whilst the earliest SDB-E3 ligase formats could achieve impressive rates of knockdown^{69,424,425}, the lack of an inducible activation component meant that stable cell lines could not be generated for essential proteins. In addition, the production of cell lines incorporating these technologies will likely result in the stimulation of compensatory mechanisms in some instances³⁷⁵. The only way to avoid this is to transiently transfect the constructs, an approach which is then limited by the heterogeneity of transfection and the potential for transfection in a given cell line. The creation of transgenic organisms using such constructs is similarly limited. In response to this, subsequent works introduced induction via doxycycline to otherwise conceptually similar systems. This circumvents the problems of compensation and cell line production, although induction and knockdown times were somewhat protracted and reversibility is then determined by the half-life of the tool^{428,429}.

LiPD and DiPD Mediated Protein Degradation

More recently bipartite tools, including our own, have been introduced which utilize chemical or light induction to degrade proteins⁴³². Since these systems rely upon the dimerizing induction of stably expressed components rather than upon transcription, they are considerably more dynamic than earlier methods with degradations occurring in shorter timeframes and with a heightened capacity for reversibility. The LiPD system outlined in our work permits light based precision degradation of targets utilising the high temporal, spatial and dose control that has driven the broad uptake of optogenetic tools at large⁶⁴⁸. The DiPD tool is triggered instead by rapamycin, a workhorse molecule for chemogenetics which, whilst not inert, is typically well tolerated by biological systems. The DiPD tool displays good generality between proteins, highly efficient knockdown rates and multi-species functionality.

The tools are expressed from single cassettes featuring two highly similar promoters to assist in balancing stoichiometry which is important for the function of the method. Since, a great many biochemical assays are performed on batches of cells and population heterogeneity is therefore undesirable, we utilized the piggyBAC transposon technology⁶⁴⁹ to assist in cell line production. Aside from significantly increasing the rate of genomic integration relative to random integration, the

piggyBAC system also removes most bacterial elements from the integrated cassette which may reduce incidences of cassette silencing⁶⁵⁰. In addition, in comparison with viral integration methods, the piggyBAC system is simple to use and has low biological safety requirements meaning that it could be easily implemented in most molecular biology labs. The transposon has also been demonstrated to be appropriate for the creation of transgenic animals⁶⁵¹.

An interesting feature of these tools is their capacity to be used either in unison, to modulate two targets independently, or with multiple targeting subunits to simultaneously knockdown a selection of proteins. To our knowledge, the knockdown of multiple proteins on the protein level has not previously been reported in the literature, yet we anticipate that such approaches could be exceptionally useful for identifying cellular redundancy mechanisms, as well as understanding the branched nature of many cellular pathways. Of course they needn't be limited to use with one another but could also be implemented with other protein degradation systems such as doxycycline⁴²⁸ or auxin inducible methods⁴³². In this work we did not assess the function or auto-degradation of constructs using more than one binder but this prospect could be interesting for a few reasons. For example; bivalency could improve the function of tools by approximating multiple POIs to the E3 ligase simultaneously; biparatopic SDBs could be used to substantially increase the affinity of the complex with the POI and thereby reduce the effective concentration of the tool; and bispecific binder pairs could be used to achieve double knockdowns without the necessity to generate and maintain a stable cell line with multiple cassettes. Beyond purely protein level intervention the DiPD and LiPD tools could also be combined with RNAi methods which would not only to be another approach to multiple knockdowns but should also improve the quality of a single knockdown⁶⁵².

In this work we demonstrate that a DiPD tool of identical protein sequence to the original mammalian format, can be successfully applied for degradation in *C. elegans*. Whilst the LiPD tool is yet to be demonstrated in whole organisms the high spatial and dose control afforded make it a very interesting prospect. Using targeted activation with light, a subset of cells can be specifically manipulated and compared with unaltered cells of the organism which can act as excellent internal controls, an approach which is impossible with diffusive drugs. This promising cross-species breadth of application makes use of the high conservation of certain elements of the UPP pathway across eukaryotes and work from others has demonstrated the reach of SDB targeted degradation methods in model species such as *D. rerio*⁴²⁸, *D. melanogaster*⁴²⁴ and the plant *N. tabacum*⁴²⁷. Each of these targeted methods could perhaps be enhanced for use in model organisms through the implementation of tissue-specific promoters as has

been previously demonstrated in *C. elegans*⁶⁵³. However, driving tool expression directly with the tissue-specific promoter leaves the quality of tool function highly subject to the expression level of the promoter. In order to avoid this pitfall, cassettes could be produced which activate following recombinase mediated excision of a transcription inhibiting sequence. In this way a ubiquitous high expression promoter could be used in each case whilst the tissue specific promoter could be used to express the recombinase.

Failed or Incomplete Degradation

In some instances the tools were ineffective against their target proteins and in no instance did we achieve total removal of the protein. Whilst we did not investigate the causation when a target could not be degraded we propose the following considerations. As will be discussed, the orientation of the tool to the POI could have been significant. *In vivo* binder characteristics such as the accessibility of the epitope could also potentially affect function. Since many SDBs are generated and tested *in vitro*, the *in vivo* function of them is commonly unknown prior to application but may differ substantially³²⁷ and thus this should be considered. Lastly, properties of the POI including conformational stability could affect its capacity to be degraded by the UPP⁶⁵⁴.

After induction of the LiPD or DiPD tools an initial rapid decline in POI levels is followed by plateauing of protein levels. Our evidence shows that this plateau can last for several days suggesting that an equilibrium is reached between expression and degradation. Whilst tool adjustments cannot alter the parts of this equation which increase protein quantity, including rates of expression or deubiquitination, it should be possible to improve characteristics that aid degradation. For example as POI levels decrease the importance of affinity increases. Once the POI reaches a certain level, if the affinity of the SDB is insufficient, then it will no longer be bound and degraded at a rate greater than expression. Improvements to affinity should lower this point of equilibrium. Where possible, increasing the expression level of the tool should also serve to improve POI binding rates, as too could co-localising the tool and POI in the same cellular region to increase local concentration. The efficiency of ubiquitination should also strongly affect the degradation rate of the tool. This is perhaps what we witnessed when we trialed various DiPD linker lengths and determined that the looser constructs, which presumably approximated the E3 ligase less efficiently, were less effective. Imbalance between system components is another area in which efficiency could be lost. If the nanobody portion is not saturated with E3 ligase following tool induction then the tool cannot function fully. Therefore, the affinity between the two

portions of the tool could be important, although this relationship between affinity and efficiency is not entirely clear. It could, for example be useful to have off-rates that permit a decent degree of dissociation such that ligase subunits can more readily move between targeting subunits. In this scenario, even if the targeting subunits are never saturated then each individual subunit might be more likely to engage in an interaction at some point and therefore ubiquitination might improve. This could be particularly useful in cells where, due perhaps to uneven cassette expression, the binder subunit is expressed at a significantly higher level than the E3 ligase. Lastly, the E3 ligase used will affect the overall rate of ubiquitination. Each E3 associates with its own set of E2s which, beyond orientation differences, is likely to result in kinetic differences due to variant concentrations and affinities of the E2s as well as probable differences in the ubiquitination rates of the formed complexes.

Orientation Requirements and Improving Generality

In order for these protein degradation tools to function, the E3 ligase must be approximated to a surface lysine on the target protein. In addition, the E3 ligase must be sterically constrained so that it does not also ubiquitinate components of the tool. Clearly therefore, the tool's orientation to the POI is critical to its degradative function and numerous experimental observations made by us and others evidence this. For example, the specific binder used for targeting can be decisive in terms of function⁷² and proteins degraded by one tool are not necessarily also depleted by a second^{424,432}. We expect that orientation requirements contribute very significantly to the number of failed degradation incidences seen in our work and reported by others^{72,424}. Due to these structural considerations, it is highly challenging to generate robustly generalizable tools for protein degradation given the great diversity in protein morphology.

The challenge of E3 ligase orientation is also faced by the endogenous ubiquitination machinery of the cell. The natural solution has been to incorporate significant morphological diversity into the massive set of E3 ligases and accessory proteins tasked with organizing these spatial requirements^{406,655}. An analogous approach, one which implements significant structural diversity into the toolbox protein modulators, could be one solution to generating more robustly generalizable tools. This could be achieved both by using a selection of tool styles, including those already published, or via the exchange of modules within styles. Such module variations could include; the use of natural E3 ligase variance; the use of multiple dimerisation subunits; or the incorporation of flexible or rigid linkers or spacer protein subunits. A greater exploration of the efficacy of different module orientations, one which includes

more targets could be also undertaken. These variations may improve function in some instances as illustrated by the successful use of a module orientation different to our own for ubiquitination⁴³⁰. Since the target epitope utilized has been shown to significantly alter the efficacy of these tools⁷², the in context screening of candidate nanobodies panels should ideally be undertaken when determining a tool.

Work to assess a broader selection of tools, generated using the above considerations, against large panels of proteins which range in size, localisation and morphology could provide a clearer picture of the function of these technologies. In addition it could assist researchers in the selection of potential tools for their specific POIs. More complete investigations such as these could lead to wider uptake of these technologies which have to date been applied to only a sparse range of targets.

Off-target Considerations and Controls

Since each targeted E3 ligase method relies inherently upon the proximity dependent promiscuity of the ligase, off-target ubiquitination and degradation are ever present possibilities and have been reported in the literature^{429,430}. Off-target knockdowns can be very difficult to assess for, this is especially true if the interactors of a protein are not known, and could have the unfortunate effect of causing false phenotypes. For this reason further research is required to clarify the considerations most relevant to tool application.

Due to the many variables relating to ubiquitination, off-target knockdowns are impractical to predict accurately. However, some general considerations could be useful when contemplating the use of targeted protein depletion or the interpretation of its results. For example, the duration and frequency of the interaction between a target protein and its interactor are likely to play a role in the probability and extent of an off-target effect. An increase in either of these metrics is likely to correlate somewhat with increased off-target degradation. Generalizing from this assumption, one might be more cautious of off-targets with proteins such as those with permanent heterodimerisation partners and less concerned about those thought to engage in very transient interactions. A second possible consideration concerns the kinetic differences between off-target and targeted degradation. It is very likely the case that off-target degradations do not occur at the same rate as depletions of the true target since interactors only contact the E3 ligase secondarily through the POI, which is less efficient. Additionally, as the POI decreases, the likelihood of interactions with the POI also decrease following second order kinetics, therefore off-target degradations should also reduce. Depending upon factors

such as; the levels of the POI and its degraded interactor following induction; the nature of the POI-interactor interaction; and the rate of interactor expression, one may even find that the level of interactor recovers over time. If accurate, an important implication of this might be that more reliable phenotypes can generally be obtained at later time points following induction. At these times the level of POI should remain low, as demonstrated by our sustained induction DiPD experiment, but interactors which have been non-specifically degraded may have recovered. This effect could be experimentally explored by induced depletion time course experiments using pairs of interacting proteins fused to different fluorescent proteins.

The problem of off-targets when using these methods means that the quality of such research could benefit from further controls or additional experimental corroboration. If interactors are known, it may be possible to assess their levels to ensure that they remain unaffected by off-target knockdown. This could be roughly achieved with methods such as western blot or immunocytochemistry and potentially could also be performed using mass spectrometry, although at significant expense. Alternatively, in some instances it may be appropriate to confirm findings using methods that target the protein on the DNA or RNA level. Whilst RNAi methods also frequently suffer from off-target effects³⁸³, the mechanism by which these knockdowns occur is unrelated to the mechanism for protein level off-targets. As such, these techniques are highly appropriate to corroborate one another and the provision of additional lines of evidence for RNAi based work could be a major use for protein degradation techniques. It may in some instances also be possible to improve the quality of evidence using multiple SDB binding sites. For example, when degrading sufficiently large proteins it could be beneficial to run parallel depletion experiments using tools targeting epitopes which are distant from each other on the POI's surface. In this way, any off-target degradation is more likely to be against different interaction partners. Therefore if the same phenotype is seen in each successful knockdown, despite targeting different regions, it is likely that loss of the POI is causative.

Bipartite systems such as the LiPD and DiPD methods also require no binder or wt controls in addition to induced and uninduced modified samples. This is because, unlike dox inducible systems, the binder is always present in the cell line and may be affecting the function of the target protein. If these controls are not performed, and baseline readings are assumed from the uninduced control, then data regarding the function of the protein could be inaccurate.

Potential therapeutic Applications of Nb-E3 ligases.

The potentially therapeutic knockdown of intracellular disease proteins using SDB targeted depletion appears to have been only very minimally explored in the literature⁶⁵⁶ yet several aspects of the concept, some of which are similar to those of the TRAP system, suggest significant promise. For example, like the TRAP method, such a system could easily be composed entirely from human or human analogous proteins. As such, it should elicit minimal immune response following introduction and could perhaps be permanently integrated into tissues to generate sentinel cells. The high specificity of SDBs should mean that background degradation and related side effects could very minimal or absent. The degradation of pathogenic proteins could serve to stymie the disease process, perhaps even preventing the establishment of a replicative infection in the case of viruses, and may also increase the display of foreign antigens on MHC I molecules and thereby enhance the CD8⁺ T-cell mediated eradication of infected cells. This depletion mechanism could also be coupled with antagonistic binding through the careful selection of nanobodies, which would deliver an additional mechanism of interference.

Chronic viruses could potentially be great targets for such a system and have already been subject to considerable therapeutic intrabody research⁵¹¹. The hepatitis B virus could be of particular interest since it occupies cells which may be particularly conducive to *in vivo* genetic modification using adeno associated viruses (AAVs)⁶⁵⁷. Safeguarding high percentages of hepatocytes against the virus in such a way could have a dramatic effect on disease outcomes. Similarly, HIV, which is of significant interest for gene therapy through *ex vivo* bone marrow modification⁶²¹, might also be a good candidate for this type of approach. Such a method could also be of benefit in cancer if a means of reliable delivery could be formulated. A targeted E3 ligase could for example be used to degrade cancer driver proteins or membrane bound immune checkpoint molecules from the interior of the cell⁶⁵⁸.

Extended Outlook

Function Specific Intrabody Screening

The overwhelming majority of SDBs are selected by *in vitro* display methods and the applicability of these binders for intracellular use is therefore typically unknown. Potential differences between *in vivo* and *in vitro* discovery include; discrepancies in the target, which may include folding alterations, PTMs, or the occlusion of potential binding sites by other structures; and divergences in SDB function including of binding, specificity, stability and solubility, which could be due to differences in ion concentrations or pH, macromolecular crowding, folding and disulfide bond formation. Further to this, the intrabody technologies outlined in this work, amongst many others, are highly dependent upon the precise alignment of complexes for function and the SDB used must function well when fused with other protein subunits. With all this in mind, for the discovery of optimal intrabodies to pair with these technologies, it would be useful to develop high throughput screens which can identify highly functional binders in the context in which they will be ultimately used.

In the attached works we developed simplistic screens based upon single transfections to determine appropriate binders for each specific function. Unfortunately, due to the low throughput nature of these methods only minimal numbers of binders can be screened. Using such small candidate panels could be highly problematic where intrabodies are sought that fulfill highly specific roles such as pairing on a large antigen or binding to a particular surface. In addition, due to the variances inherent in transient transfection, the determination of a truly optimal binder or binder pair can be difficult. Importantly, each of these screens is dependent upon a panel which has been obtained via *in vitro* display. Clearly, large scale screens that can assist in the discovery of function specific intracellular binders could be extremely useful.

Aside from an amenability to high throughput screening, an ideal intrabody selection method should; replicate the desired function of the intrabody; be performed in an organism highly similar to that of the intended application; and deliver an output that is well correlated to the function of the intrabody. In addition, expense, biological safety requirements and tractability should be realistic. Unfortunately, to date intrabody selection methods have used a limited range of organisms^{48,242-244} and have delivered readouts based on two-hybrid expression, which do not necessarily correlate well with the quality of intracellular expression and affinity⁴⁹. We propose that a series of function specific fluorescence based

intrabody assays could be developed within mammalian cells that can be assessed via flow cytometry. These assays could deliver outputs which are tied to their function on the protein level and thus function should correlate well with normalized fluorescent signal. Such assays, which should improve the tractability, function and robustness of our tools, represent a major future avenue for this research and preliminary investigation and development has begun.

Cell lines for intrabody assays

Unlike bacterial transformations, which tend to result in the uptake of a single plasmid, mammalian transfections can introduce hundreds or thousands of plasmids to a cell⁶⁵⁹. If a library of plasmids is then simply transfected for assay, the signal-to-noise of any assay would likely be rendered unworkable and the extraction of functional binder sequences following selection would be greatly complicated both by the number of sequences and also by the likelihood that the desired plasmid would be lost from the cells. Therefore, methods which stably maintain a single copy of the assay components are required. We determined that the recombination of single or paired cassettes into promoters positioned in the genome would be good way to meet these criteria. Using this method, only correctly inserted binders would be expressed to a sufficient level and primers between the genomic region and the cassette could be used for sequence retrieval.

Using CRISPR technology, we constructed a cell line (HEK: 2xCAG-attP) which incorporates two copies of the highly active CAG promoter⁶⁶⁰ followed BXB1 attP sites into the AAVS1 genetic safe harbour⁶⁶¹ to drive expression of cassettes recombined into the locus (Figure 17). HEK cells, which are also used for cell surface display technology²³⁵, were selected for the use due to their high expression of transgenes, fast growth, high transfection rates and durability. Using HEK: 2xCAG-attP we constructed a second cell line (HEK: 1xCAG-attP) for the expression of single cassettes. This was created by inserting a blasticidin resistance cassette into one of the alleles to block further integrations. We propose that these two cell lines permitting integration of either one or two screening cassettes should be appropriate for a broad variety of screening techniques across a range of proteins beyond SDBs.

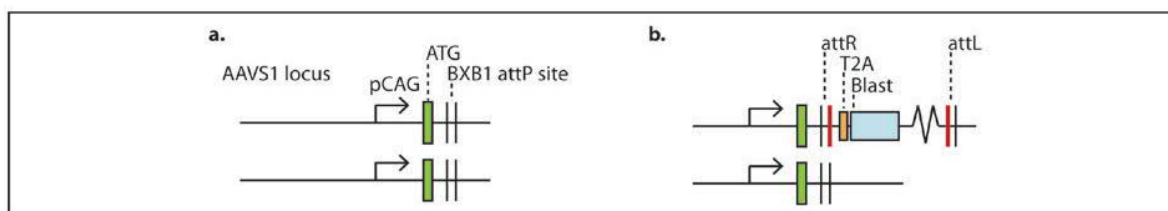


Figure 17. HEK293T Intrabody selection cell lines. (a) Two CAG promoters are integrated into the AAVS1 locus of HEK cells each followed by a start codon and BXB1 recombination site (HEK: 2xCAG-attp). Such a cell line could be suitable for various screens involving multiple components. **(b)** A single insertion site remains active following the incorporation of a blasticidin cassette into one allele (HEK: 1xCAG-attp). This cell line could be used to screen in cases where expression of only a single cassette is desirable for screening.

The clonal complexity which can be screened using these cell lines will be limited by the practicality of handling mammalian cells. Since the binder proteins are internal, MACs sorting cannot be applied prior to flow cytometry and therefore FACS is likely to be the limiting variable. The extent to which flow cytometry will limit this form of screening will be dependent upon the machine used, its capacity to sort at higher speeds and its accuracy at these speeds. Using our BD FACSAria™ II (BD biosciences) machine we could reasonably screen and sort confluent p100 plates in around 2hrs ($\sim 1 \times 10^7$ cells). Screening at such scales should be sufficient with libraries that have undergone a form of pre-selection, such as sdAb immune libraries or smaller affinity maturation libraries. For larger libraries, including synthetic libraries, it is likely best to pair the method with other display techniques to somewhat narrow the pool of potential binders before screening. We propose pairing the methods with phage display and accordingly we constructed a phage display vector with compatible restriction sites to our mammalian screening vectors.

A Fluorescent Intrabody Selection Assay (FISA)

We first constructed and performed preliminary testing on a simple assay to identify single active binders for a target *in vivo* (Figure 18). The assay employs the BiFC Venus method which we also used in earlier work. Generic cassettes were created to permit Venus fusions to the antigen N and C terminal and the binder C terminally. The cassettes contain long 6xGGGS linkers to reduce biases in complex formation due to alignment and spacing, although linker lengths could be varied to restrict selection to binders active in regions neighbouring the termini. The binder cassettes contain no promoter but rely instead upon integration into a single AAVS1 CAG promoter via BXB1 integrase mediated recombination.

The antigen is expressed from a rat EF1a promoter and a hygromycin resistance gene permits selection initially of the transfected cells and later those that stably maintain the plasmid.

Antigens are first cloned into the cassettes and thereafter pools of binders can be cloned into the specially designed BsaI sites directly from our phage display vector or from other sources following PCR with appropriate primers. These pooled clone cassettes are then co-transfected with BXB1 integrase and a single binder is expressed per cell after integration into the HEK: 1xCAG-attP cell line. An mRFP allows for the normalization of the Venus signal against the antigen expression. Since the mRFP is expressed from the antigen cassettes the normalized red vs yellow FACS readout is influenced both by the binding of antibody to antigen and by the expression and stability nanobody. As such, the screen optimizes for a combination of factors affecting complex formation. Cells with high Venus relative to mRFP can ultimately be singled and binder sequences are obtained via PCR using genomic DNA.

When we performed preliminary testing of this method using p24 and the CTD12nb with the HB2nb as a control we could easily separate the clustering of the control and the correct interactor. We also tested a dilution of 1/10000 correct binder cassette into incorrect binder for transfection and saw that we could sort out our correct cells over iterative rounds of flow cytometry with or without colony picking on a fluorescent microscope.

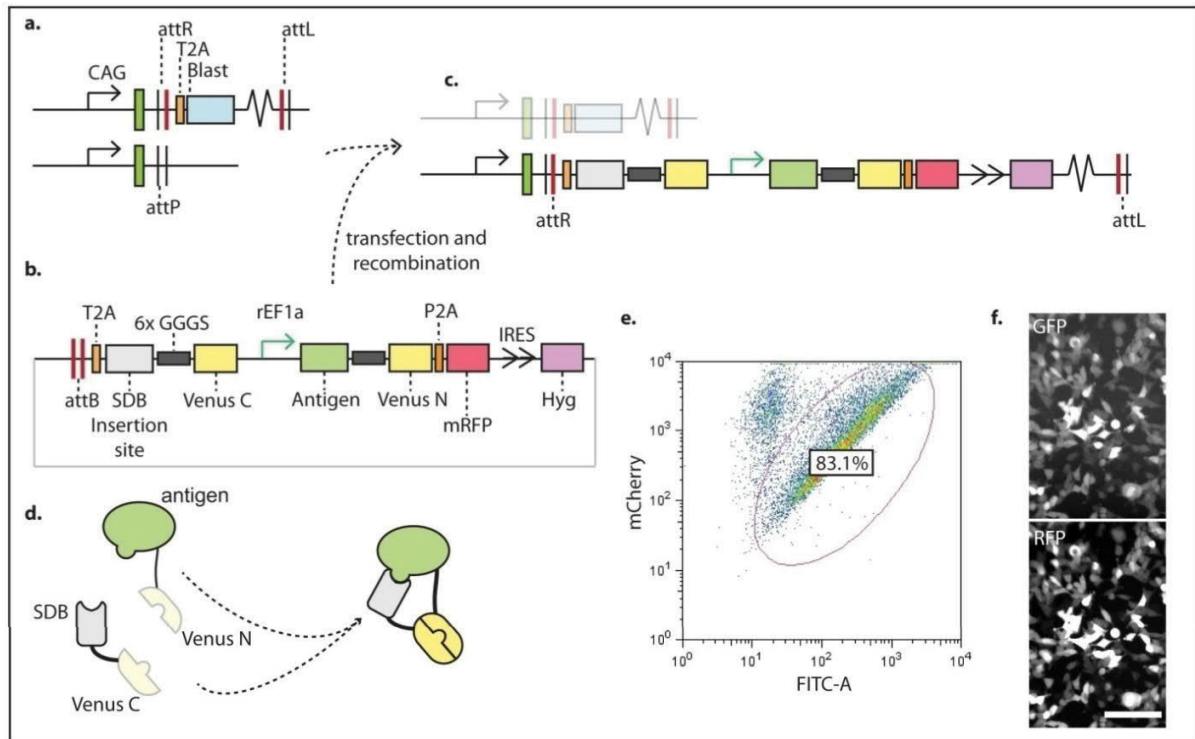


Figure 18. A Fluorescent Intrabody Selection Assay (FISA). A HEK cell line with a single AAVS1-CAG-attP BXB1 recombination site **(a)** is used for the transfection of cassettes containing a promoterless binder-Venus C fusion and the antigen in fusion with Venus N either C or N terminally **(b)**. The cassette recombines into the AAVS1 locus forming a stable cell line **(c)** and drives the expression of a single binder-Venus C fusion. **(d)** In the event of interaction between the binder and antigen, Venus halves pair to deliver a fluorescent output. **(e)** The FACS profile of FISA tested with p24 antigen and CTD12nb is shown. **(f)** p24 and CTD12nb FISA pairing seen under a fluorescent microscope.

Dual Fluorescent Intrabody Selection Assay (D-FISA)

The FISA approach outlined above can also be modified to permit screening for pairs of adjacent binders on an antigen. The dual-FISA (D-FISA) places both portions of the Venus protein C terminally on two separate binders transcribed from cassettes with different antibiotic resistances (Figure 14). These cassettes are then transfected with the BXB1 integrase and recombined into the HEK: 2xCAG-attP cell line. The antigen and mRFP are included on one of the plasmids and are also integrated into the genome. Both the selection of cells containing useful binder pairings and the extraction of sequences proceed in a similar way to the FISA method. Tests using p24 binders revealed that cells containing nanobodies known to pair on the antigen could be easily segregated from those with control nanobodies using flow cytometry.

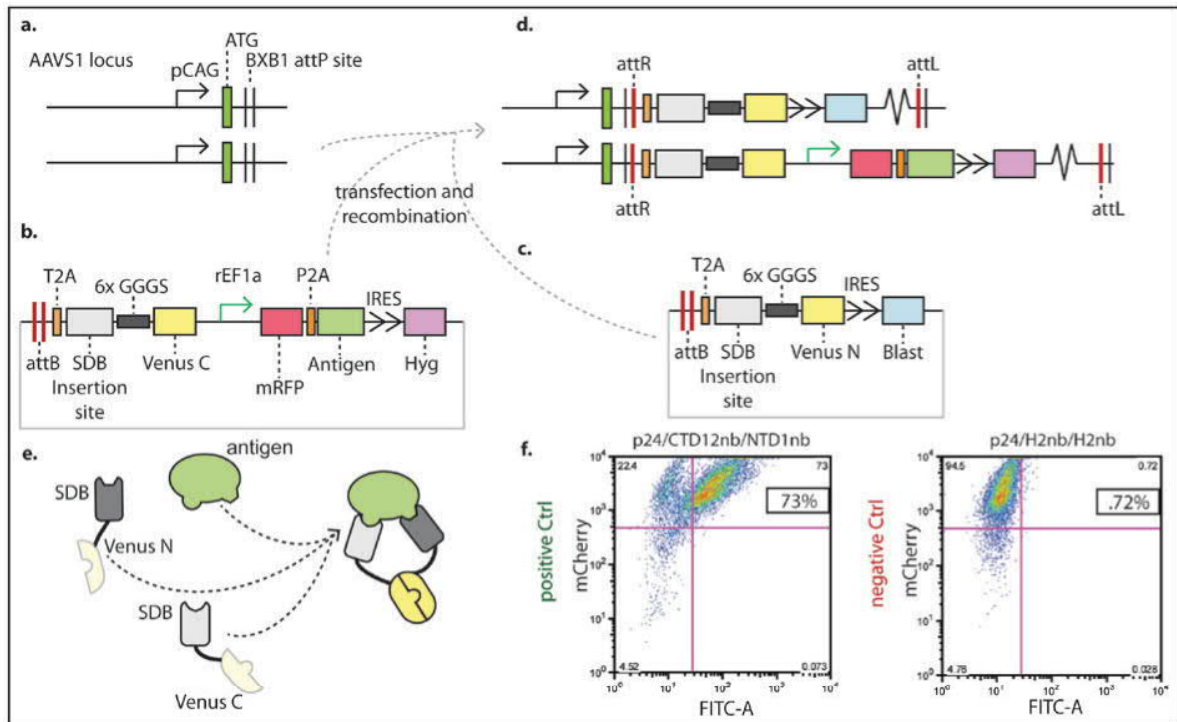


Figure 19. A Dual Fluorescent Intrabody Selection Assay (D-FISA). (b) Antigen is inserted into a cassette driven by a rat EF1a promoter and containing an mRFP for normalisation. (b,c) Pools of candidate binders are inserted into two cassettes with the two halves of split Venus and different resistance genes and the recombined into the HEK: 2xCAG-attP cell line (a) via triple transfection with BXB1 (d). In the event that both bind to the antigen with sufficient proximity, the Venus molecule complements and matures (e). (f) FACs profiles of functional and non-functional nb pairings on the p24 antigen are shown.

Fluorescent Intrabody Degradation Assay (FIDA)

As previously discussed, the successful degradation of target proteins is closely tied both to the alignment of the DiPD on the POI and to the binder's properties such as affinity, solubility and expression. In order to improve the function of future DiPD tools we began development of a screening system specific for this application called FIDA (fluorescent intrabody degradation assay) (Figure 15). A stable HEK cell line was generated which includes the E3 ligase-FRB portion of the DiPD on one AAVS1-CAG-attP allele, with the second allele remaining open for integration. The cassette for screening is designed such that binders can be inserted in fusion with FKBP to complete the DiPD tool. An mRFP is included for normalization and two different antibiotic resistances are used to ensure stable insertion of both halves. The antigen is placed initially in fusion with a GFP so that cells can be screened for high mRFP and low GFP following rapamycin induction. The GFP is designed to be inverted via recombinase sites on the cassette to disconnect it from the POI and replace it with an HA tag. This two step process

permits initial screening via flow cytometry to select cells in which the POI-GFP fusion is degraded, followed by recombinase transfection for inversion, and then immunocytochemistry on a reduced panel of candidates to ensure that the POI is targeted rather than the GFP.

Work on this system is incomplete and the method is untested. However, the technique has not only potential for large scale binder screening but should also make the assessment of single binders and small panels simpler and more robust. Checking individual binders for function in this way could be very useful since transient transfections can produce excessive levels of target antigen which can make the degradative effect of the DiPD difficult to see and evaluate. Using the FIDA tool one could easily stitch the antigen and binder into the cassette via Gibson assembly and then perform transfections to integrate them efficiently into the cell line. This would permit the assessment of lower levels of antigen in a well without the complexity of first producing an individual antigen expressing stable cell line.

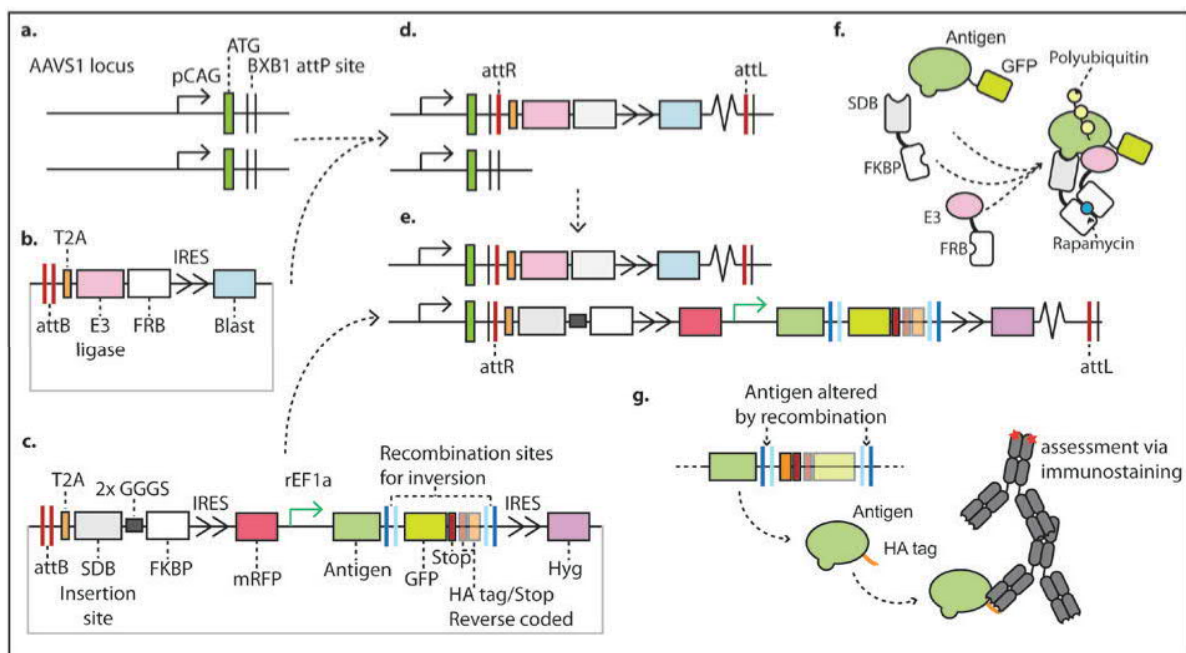


Figure 20. A Fluorescent Intrabody Degradation Assay (FIDA). A cassette featuring an E3 ligase and FRB fusion (**b**) is recombined into one allele of the HEK: 2xCAG-attp cell line (**a**) to form a stable cell line used for all FIDA studies (**d**). Antigens are inserted into a plasmid in fusion with a GFP in addition to candidate binders in fusion with FKBP (**c**). upon recombination of the cassette into the FIDA cell line the DiPD system and antigen are expressed and can be assessed for target degradation if induced (**f**). Once promising candidates are identified the GFP can be exchanged with an HA tag via inversion to assess for successful degradation of a more natural POI via immunocytochemistry (**g**).

Annex

References

- 1 Riera Romo, M., Perez-Martinez, D. & Castillo Ferrer, C. Innate immunity in vertebrates: an overview. *Immunology* **148**, 125-139, doi:10.1111/imm.12597 (2016).
- 2 Bonilla, F. A. & Oettgen, H. C. Adaptive immunity. *The Journal of allergy and clinical immunology* **125**, S33-40, doi:10.1016/j.jaci.2009.09.017 (2010).
- 3 Yam-Puc, J. C., Zhang, L., Zhang, Y. & Toellner, K. M. Role of B-cell receptors for B-cell development and antigen-induced differentiation. *F1000Res* **7**, 429, doi:10.12688/f1000research.13567.1 (2018).
- 4 Kumar, B. V., Connors, T. J. & Farber, D. L. Human T Cell Development, Localization, and Function throughout Life. *Immunity* **48**, 202-213, doi:10.1016/j.immuni.2018.01.007 (2018).
- 5 Hoffman, W., Lakkis, F. G. & Chalasani, G. B Cells, Antibodies, and More. *Clin J Am Soc Nephrol* **11**, 137-154, doi:10.2215/CJN.09430915 (2016).
- 6 Schroeder, H. W., Jr. & Cavacini, L. Structure and function of immunoglobulins. *The Journal of allergy and clinical immunology* **125**, S41-52, doi:10.1016/j.jaci.2009.09.046 (2010).
- 7 Padlan, E. A. Anatomy of the antibody molecule. *Mol Immunol* **31**, 169-217 (1994).
- 8 Hogarth, P. M. Fc Receptors: Introduction. *Immunological reviews* **268**, 1-5, doi:10.1111/imr.12372 (2015).
- 9 Wang, G. *et al.* Molecular Basis of Assembly and Activation of Complement Component C1 in Complex with Immunoglobulin G1 and Antigen. *Molecular cell* **63**, 135-145, doi:10.1016/j.molcel.2016.05.016 (2016).
- 10 Wang, Q., Chung, C. Y., Chough, S. & Betenbaugh, M. J. Antibody glycoengineering strategies in mammalian cells. *Biotechnol Bioeng* **115**, 1378-1393, doi:10.1002/bit.26567 (2018).
- 11 van de Bovenkamp, F. S., Hafkenscheid, L., Rispens, T. & Rombouts, Y. The Emerging Importance of IgG Fab Glycosylation in Immunity. *J Immunol* **196**, 1435-1441, doi:10.4049/jimmunol.1502136 (2016).
- 12 Jefferis, R. Glycosylation as a strategy to improve antibody-based therapeutics. *Nat Rev Drug Discov* **8**, 226-234, doi:10.1038/nrd2804 (2009).
- 13 Liu, H., Bulseco, G. G. & Sun, J. Effect of posttranslational modifications on the thermal stability of a recombinant monoclonal antibody. *Immunology letters* **106**, 144-153, doi:10.1016/j.imlet.2006.05.011 (2006).
- 14 Arnold, J. N., Wormald, M. R., Sim, R. B., Rudd, P. M. & Dwek, R. A. The impact of glycosylation on the biological function and structure of human immunoglobulins. *Annual review of immunology* **25**, 21-50, doi:10.1146/annurev.immunol.25.022106.141702 (2007).
- 15 Pento, J. T. Monoclonal Antibodies for the Treatment of Cancer. *Anticancer Res* **37**, 5935-5939, doi:10.21873/anticancer.12040 (2017).
- 16 Shepard, H. M., Phillips, G. L., C, D. T. & Feldmann, M. Developments in therapy with monoclonal antibodies and related proteins. *Clin Med (Lond)* **17**, 220-232, doi:10.7861/clinmedicine.17-3-220 (2017).
- 17 Navalkele, B. D. & Chopra, T. Bezlotoxumab: an emerging monoclonal antibody therapy for prevention of recurrent *Clostridium difficile* infection. *Biologics* **12**, 11-21, doi:10.2147/BTT.S127099 (2018).
- 18 Castle, D. & Robertson, N. P. Monoclonal antibodies for migraine: an update. *J Neurol* **265**, 1491-1492, doi:10.1007/s00415-018-8886-8 (2018).

- 19 Moek, K. L. *et al.* Theranostics Using Antibodies and Antibody-Related Therapeutics. *J Nucl Med* **58**, 83S-90S, doi:10.2967/jnumed.116.186940 (2017).
- 20 Lambert, J. M. & Berkenblit, A. Antibody-Drug Conjugates for Cancer Treatment. *Annu Rev Med* **69**, 191-207, doi:10.1146/annurev-med-061516-121357 (2018).
- 21 Ecker, D. M., Jones, S. D. & Levine, H. L. The therapeutic monoclonal antibody market. *MAbs* **7**, 9-14, doi:10.4161/19420862.2015.989042 (2015).
- 22 Kaplon, H. & Reichert, J. M. Antibodies to watch in 2018. *MAbs* **10**, 183-203, doi:10.1080/19420862.2018.1415671 (2018).
- 23 Sajid, M., Kawde, A.-N. & Daud, M. Designs, formats and applications of lateral flow assay: A literature review. *Journal of Saudi Chemical Society* **19**, 689-705 (2015).
- 24 Sharma, S., Byrne, H. & O'Kennedy, R. J. Antibodies and antibody-derived analytical biosensors. *Essays Biochem* **60**, 9-18, doi:10.1042/EBC20150002 (2016).
- 25 Byrne, B., Stack, E., Gilmartin, N. & O'Kennedy, R. Antibody-based sensors: principles, problems and potential for detection of pathogens and associated toxins. *Sensors (Basel)* **9**, 4407-4445, doi:10.3390/s90604407 (2009).
- 26 Bhatnagar, S., Deschenes, E., Liao, J., Cilliers, C. & Thurber, G. M. Multichannel imaging to quantify four classes of pharmacokinetic distribution in tumors. *Journal of pharmaceutical sciences* **103**, 3276-3286, doi:10.1002/jps.24086 (2014).
- 27 Baker, J. H. *et al.* Direct visualization of heterogeneous extravascular distribution of trastuzumab in human epidermal growth factor receptor type 2 overexpressing xenografts. *Clinical cancer research : an official journal of the American Association for Cancer Research* **14**, 2171-2179, doi:10.1158/1078-0432.CCR-07-4465 (2008).
- 28 Blumenthal, R. D. *et al.* The effect of antibody protein dose on the uniformity of tumor distribution of radioantibodies: an autoradiographic study. *Cancer Immunol Immunother* **33**, 351-358 (1991).
- 29 Lauwereys, M. *et al.* Potent enzyme inhibitors derived from dromedary heavy-chain antibodies. *The EMBO journal* **17**, 3512-3520, doi:10.1093/emboj/17.13.3512 (1998).
- 30 Kunert, R. & Reinhart, D. Advances in recombinant antibody manufacturing. *Applied microbiology and biotechnology* **100**, 3451-3461, doi:10.1007/s00253-016-7388-9 (2016).
- 31 Hernandez, I. *et al.* Pricing of monoclonal antibody therapies: higher if used for cancer? *The American journal of managed care* **24**, 109-112 (2018).
- 32 Voskuil, J. L. The challenges with the validation of research antibodies. *F1000Res* **6**, 161, doi:10.12688/f1000research.10851.1 (2017).
- 33 Bradbury, A. & Pluckthun, A. Reproducibility: Standardize antibodies used in research. *Nature* **518**, 27-29, doi:10.1038/518027a (2015).
- 34 Kontermann, R. E. & Brinkmann, U. Bispecific antibodies. *Drug discovery today* **20**, 838-847, doi:10.1016/j.drudis.2015.02.008 (2015).
- 35 Brinkmann, U. & Kontermann, R. E. The making of bispecific antibodies. *MAbs* **9**, 182-212, doi:10.1080/19420862.2016.1268307 (2017).
- 36 Thakur, A., Huang, M. & Lum, L. G. Bispecific antibody based therapeutics: Strengths and challenges. *Blood Rev* **32**, 339-347, doi:10.1016/j.blre.2018.02.004 (2018).
- 37 Bird, R. E. *et al.* Single-chain antigen-binding proteins. *Science* **242**, 423-426 (1988).
- 38 Ahmad, Z. A. *et al.* scFv antibody: principles and clinical application. *Clin Dev Immunol* **2012**, 980250, doi:10.1155/2012/980250 (2012).
- 39 Nelson, A. L. Antibody fragments: hope and hype. *MAbs* **2**, 77-83 (2010).
- 40 Davies, J. & Riechmann, L. 'Camelising' human antibody fragments: NMR studies on VH domains. *FEBS letters* **339**, 285-290 (1994).

- 41 Bayly, A. M., Kortt, A. A., Hudson, P. J. & Power, B. E. Large-scale bacterial fermentation and isolation of scFv multimers using a heat-inducible bacterial expression vector. *Journal of immunological methods* **262**, 217-227 (2002).
- 42 Power, B. E. & Hudson, P. J. Synthesis of high avidity antibody fragments (scFv multimers) for cancer imaging. *Journal of immunological methods* **242**, 193-204 (2000).
- 43 Kugler, J., Tomszak, F., Frenzel, A. & Hust, M. Construction of Human Immune and Naive scFv Libraries. *Methods Mol Biol* **1701**, 3-24, doi:10.1007/978-1-4939-7447-4_1 (2018).
- 44 Sidhu, S. S. & Fellouse, F. A. Synthetic therapeutic antibodies. *Nature chemical biology* **2**, 682-688, doi:10.1038/nchembio843 (2006).
- 45 Yang, H. Y., Kang, K. J., Chung, J. E. & Shim, H. Construction of a large synthetic human scFv library with six diversified CDRs and high functional diversity. *Mol Cells* **27**, 225-235, doi:10.1007/s10059-009-0028-9 (2009).
- 46 Huang, L., Su, X. & Federoff, H. J. Single-chain fragment variable passive immunotherapies for neurodegenerative diseases. *International journal of molecular sciences* **14**, 19109-19127, doi:10.3390/ijms140919109 (2013).
- 47 Xenaki, K. T., Oliveira, S. & van Bergen En Henegouwen, P. M. P. Antibody or Antibody Fragments: Implications for Molecular Imaging and Targeted Therapy of Solid Tumors. *Front Immunol* **8**, 1287, doi:10.3389/fimmu.2017.01287 (2017).
- 48 der Maur, A. A. *et al.* Direct in vivo screening of intrabody libraries constructed on a highly stable single-chain framework. *The Journal of biological chemistry* **277**, 45075-45085, doi:10.1074/jbc.M205264200 (2002).
- 49 Tanaka, T. & Rabbitts, T. H. Protocol for the selection of single-domain antibody fragments by third generation intracellular antibody capture. *Nature protocols* **5**, 67-92, doi:10.1038/nprot.2009.199 (2010).
- 50 Biocca, S., Ruberti, F., Tafani, M., Pierandrei-Amaldi, P. & Cattaneo, A. Redox state of single chain Fv fragments targeted to the endoplasmic reticulum, cytosol and mitochondria. *Biotechnology (N Y)* **13**, 1110-1115 (1995).
- 51 Stahl, S. *et al.* Affibody Molecules in Biotechnological and Medical Applications. *Trends in biotechnology* **35**, 691-712, doi:10.1016/j.tibtech.2017.04.007 (2017).
- 52 Pluckthun, A. Designed ankyrin repeat proteins (DARPs): binding proteins for research, diagnostics, and therapy. *Annu Rev Pharmacol Toxicol* **55**, 489-511, doi:10.1146/annurev-pharmtox-010611-134654 (2015).
- 53 Sha, F., Salzman, G., Gupta, A. & Koide, S. Monobodies and other synthetic binding proteins for expanding protein science. *Protein science : a publication of the Protein Society* **26**, 910-924, doi:10.1002/pro.3148 (2017).
- 54 Diem, M. D. *et al.* Selection of high-affinity Centyrin FN3 domains from a simple library diversified at a combination of strand and loop positions. *Protein Eng Des Sel* **27**, 419-429, doi:10.1093/protein/gzu016 (2014).
- 55 Richter, A., Eggenstein, E. & Skerra, A. Anticalins: exploiting a non-Ig scaffold with hypervariable loops for the engineering of binding proteins. *FEBS letters* **588**, 213-218, doi:10.1016/j.febslet.2013.11.006 (2014).
- 56 Steemson, J. D., Baake, M., Rakonjac, J., Arcus, V. L. & Liddament, M. T. Tracking molecular recognition at the atomic level with a new protein scaffold based on the OB-fold. *PloS one* **9**, e86050, doi:10.1371/journal.pone.0086050 (2014).
- 57 Kintzing, J. R. & Cochran, J. R. Engineered knottin peptides as diagnostics, therapeutics, and drug delivery vehicles. *Current opinion in chemical biology* **34**, 143-150, doi:10.1016/j.cbpa.2016.08.022 (2016).

- 58 Grabulovski, D., Kaspar, M. & Neri, D. A novel, non-immunogenic Fyn SH3-derived binding protein with tumor vascular targeting properties. *The Journal of biological chemistry* **282**, 3196-3204, doi:10.1074/jbc.M609211200 (2007).
- 59 Silverman, J. *et al.* Multivalent avimer proteins evolved by exon shuffling of a family of human receptor domains. *Nature biotechnology* **23**, 1556-1561, doi:10.1038/nbt1166 (2005).
- 60 Ebersbach, H. *et al.* Affilin-novel binding molecules based on human gamma-B-crystallin, an all beta-sheet protein. *Journal of molecular biology* **372**, 172-185, doi:10.1016/j.jmb.2007.06.045 (2007).
- 61 Leung, I., Jarvik, N. & Sidhu, S. S. A Highly Diverse and Functional Naive Ubiquitin Variant Library for Generation of Intracellular Affinity Reagents. *Journal of molecular biology* **429**, 115-127, doi:10.1016/j.jmb.2016.11.016 (2017).
- 62 Mitchell, A. C. *et al.* Engineering a potent inhibitor of matriptase from the natural hepatocyte growth factor activator inhibitor type-1 (HAI-1) protein. *The Journal of biological chemistry* **293**, 4969-4980, doi:10.1074/jbc.M117.815142 (2018).
- 63 Rhodes, C. A. & Pei, D. Bicyclic Peptides as Next-Generation Therapeutics. *Chemistry* **23**, 12690-12703, doi:10.1002/chem.201702117 (2017).
- 64 Suderman, R. J., Rice, D. A., Gibson, S. D., Strick, E. J. & Chao, D. M. Development of polyol-responsive antibody mimetics for single-step protein purification. *Protein Expr Purif* **134**, 114-124, doi:10.1016/j.pep.2017.04.008 (2017).
- 65 Tiede, C. *et al.* Adhiron: a stable and versatile peptide display scaffold for molecular recognition applications. *Protein Eng Des Sel* **27**, 145-155, doi:10.1093/protein/gzu007 (2014).
- 66 Stadler, L. K. *et al.* Structure-function studies of an engineered scaffold protein derived from Stefin A. II: Development and applications of the SQT variant. *Protein Eng Des Sel* **24**, 751-763, doi:10.1093/protein/gzr019 (2011).
- 67 Allen, J. E. *et al.* Targeting TRAIL death receptor 4 with trivalent DR4 Atrimer complexes. *Molecular cancer therapeutics* **11**, 2087-2095, doi:10.1158/1535-7163.MCT-12-0366 (2012).
- 68 Liao, H. I. *et al.* mRNA display design of fibronectin-based intrabodies that detect and inhibit severe acute respiratory syndrome coronavirus nucleocapsid protein. *The Journal of biological chemistry* **284**, 17512-17520, doi:10.1074/jbc.M901547200 (2009).
- 69 Brauchle, M. *et al.* Protein interference applications in cellular and developmental biology using DARPins that recognize GFP and mCherry. *Biol Open* **3**, 1252-1261, doi:10.1242/bio.201410041 (2014).
- 70 Miersch, S. & Sidhu, S. S. Intracellular targeting with engineered proteins. *F1000Res* **5**, doi:10.12688/f1000research.8915.1 (2016).
- 71 Simeon, R. & Chen, Z. In vitro-engineered non-antibody protein therapeutics. *Protein Cell* **9**, 3-14, doi:10.1007/s13238-017-0386-6 (2018).
- 72 Moutel, S. *et al.* NaLi-H1: A universal synthetic library of humanized nanobodies providing highly functional antibodies and intrabodies. *Elife* **5**, doi:10.7554/eLife.16228 (2016).
- 73 McMahon, C. *et al.* Yeast surface display platform for rapid discovery of conformationally selective nanobodies. *Nature structural & molecular biology* **25**, 289-296, doi:10.1038/s41594-018-0028-6 (2018).
- 74 Hamers-Casterman, C. *et al.* Naturally occurring antibodies devoid of light chains. *Nature* **363**, 446-448, doi:10.1038/363446a0 (1993).
- 75 Helma, J., Cardoso, M. C., Muyldermans, S. & Leonhardt, H. Nanobodies and recombinant binders in cell biology. *The Journal of cell biology* **209**, 633-644, doi:10.1083/jcb.201409074 (2015).
- 76 Greenberg, A. S. *et al.* A new antigen receptor gene family that undergoes rearrangement and extensive somatic diversification in sharks. *Nature* **374**, 168-173, doi:10.1038/374168a0 (1995).

- 77 Kovaleva, M., Ferguson, L., Steven, J., Porter, A. & Barelle, C. Shark variable new antigen receptor biologics - a novel technology platform for therapeutic drug development. *Expert opinion on biological therapy* **14**, 1527-1539, doi:10.1517/14712598.2014.937701 (2014).
- 78 Vincke, C. *et al.* General strategy to humanize a camelid single-domain antibody and identification of a universal humanized nanobody scaffold. *The Journal of biological chemistry* **284**, 3273-3284, doi:10.1074/jbc.M806889200 (2009).
- 79 Conrath, K. *et al.* Antigen binding and solubility effects upon the veneering of a camel VHH in framework-2 to mimic a VH. *Journal of molecular biology* **350**, 112-125, doi:10.1016/j.jmb.2005.04.050 (2005).
- 80 Muyldermans, S. Nanobodies: natural single-domain antibodies. *Annu Rev Biochem* **82**, 775-797, doi:10.1146/annurev-biochem-063011-092449 (2013).
- 81 Govaert, J. *et al.* Dual beneficial effect of interloop disulfide bond for single domain antibody fragments. *The Journal of biological chemistry* **287**, 1970-1979, doi:10.1074/jbc.M111.242818 (2012).
- 82 Kunz, P. *et al.* The structural basis of nanobody unfolding reversibility and thermoresistance. *Scientific reports* **8**, 7934, doi:10.1038/s41598-018-26338-z (2018).
- 83 Li, T. *et al.* Cell-penetrating anti-GFAP VHH and corresponding fluorescent fusion protein VHH-GFP spontaneously cross the blood-brain barrier and specifically recognize astrocytes: application to brain imaging. *FASEB journal : official publication of the Federation of American Societies for Experimental Biology* **26**, 3969-3979, doi:10.1096/fj.11-201384 (2012).
- 84 Muyldermans, S., Cambillau, C. & Wyns, L. Recognition of antigens by single-domain antibody fragments: the superfluous luxury of paired domains. *Trends Biochem Sci* **26**, 230-235 (2001).
- 85 Mitchell, L. S. & Colwell, L. J. Comparative analysis of nanobody sequence and structure data. *Proteins* **86**, 697-706, doi:10.1002/prot.25497 (2018).
- 86 Mitchell, L. S. & Colwell, L. J. Analysis of nanobody paratopes reveals greater diversity than classical antibodies. *Protein Eng Des Sel* **31**, 267-275, doi:10.1093/protein/gzy017 (2018).
- 87 Muyldermans, S. *et al.* Camelid immunoglobulins and nanobody technology. *Veterinary immunology and immunopathology* **128**, 178-183, doi:10.1016/j.vetimm.2008.10.299 (2009).
- 88 Sircar, A., Sanni, K. A., Shi, J. & Gray, J. J. Analysis and modeling of the variable region of camelid single-domain antibodies. *J Immunol* **186**, 6357-6367, doi:10.4049/jimmunol.1100116 (2011).
- 89 De Genst, E. *et al.* Molecular basis for the preferential cleft recognition by dromedary heavy-chain antibodies. *Proceedings of the National Academy of Sciences of the United States of America* **103**, 4586-4591, doi:10.1073/pnas.0505379103 (2006).
- 90 Zimmermann, I. *et al.* Synthetic single domain antibodies for the conformational trapping of membrane proteins. *Elife* **7**, doi:10.7554/eLife.34317 (2018).
- 91 Unger, M. *et al.* Selection of nanobodies that block the enzymatic and cytotoxic activities of the binary Clostridium difficile toxin CDT. *Scientific reports* **5**, 7850, doi:10.1038/srep07850 (2015).
- 92 Conrath, K. E. *et al.* Beta-lactamase inhibitors derived from single-domain antibody fragments elicited in the camelidae. *Antimicrob Agents Chemother* **45**, 2807-2812, doi:10.1128/AAC.45.10.2807-2812.2001 (2001).
- 93 Stijlemans, B. *et al.* Efficient targeting of conserved cryptic epitopes of infectious agents by single domain antibodies. African trypanosomes as paradigm. *The Journal of biological chemistry* **279**, 1256-1261, doi:10.1074/jbc.M307341200 (2004).
- 94 Dumoulin, M. *et al.* Single-domain antibody fragments with high conformational stability. *Protein science : a publication of the Protein Society* **11**, 500-515, doi:10.1110/ps.34602 (2002).
- 95 Kunz, P. *et al.* Exploiting sequence and stability information for directing nanobody stability engineering. *Biochimica et biophysica acta* **1861**, 2196-2205, doi:10.1016/j.bbagen.2017.06.014 (2017).

- 96 van der Linden, R. H. *et al.* Comparison of physical chemical properties of llama VHH antibody
fragments and mouse monoclonal antibodies. *Biochimica et biophysica acta* **1431**, 37-46 (1999).
- 97 Ladenson, R. C., Crimmins, D. L., Landt, Y. & Ladenson, J. H. Isolation and characterization of a
thermally stable recombinant anti-caffeine heavy-chain antibody fragment. *Analytical chemistry*
78, 4501-4508, doi:10.1021/ac058044j (2006).
- 98 Goldman, E. R., Liu, J. L., Zabetakis, D. & Anderson, G. P. Enhancing Stability of Camelid and
Shark Single Domain Antibodies: An Overview. *Front Immunol* **8**, 865,
doi:10.3389/fimmu.2017.00865 (2017).
- 99 Hussack, G., Hirama, T., Ding, W., Mackenzie, R. & Tanha, J. Engineered single-domain
antibodies with high protease resistance and thermal stability. *PloS one* **6**, e28218,
doi:10.1371/journal.pone.0028218 (2011).
- 100 Liu, J. L., Zabetakis, D., Brown, J. C., Anderson, G. P. & Goldman, E. R. Thermal stability and
refolding capability of shark derived single domain antibodies. *Mol Immunol* **59**, 194-199,
doi:10.1016/j.molimm.2014.02.014 (2014).
- 101 Perez, J. M. *et al.* Thermal unfolding of a llama antibody fragment: a two-state reversible
process. *Biochemistry* **40**, 74-83 (2001).
- 102 Harmsen, M. M., van Solt, C. B., van Zijderveld-van Bommel, A. M., Niewold, T. A. & van
Zijderveld, F. G. Selection and optimization of proteolytically stable llama single-domain
antibody fragments for oral immunotherapy. *Applied microbiology and biotechnology* **72**, 544-
551, doi:10.1007/s00253-005-0300-7 (2006).
- 103 Jaspers, L., Schon, O., Famm, K. & Winter, G. Aggregation-resistant domain antibodies selected
on phage by heat denaturation. *Nature biotechnology* **22**, 1161-1165, doi:10.1038/nbt1000
(2004).
- 104 Dolk, E. *et al.* Isolation of llama antibody fragments for prevention of dandruff by phage display
in shampoo. *Applied and environmental microbiology* **71**, 442-450, doi:10.1128/AEM.71.1.442-
450.2005 (2005).
- 105 van der Vaart, J. M. *et al.* Reduction in morbidity of rotavirus induced diarrhoea in mice by yeast
produced monovalent llama-derived antibody fragments. *Vaccine* **24**, 4130-4137,
doi:10.1016/j.vaccine.2006.02.045 (2006).
- 106 Wang, Y. *et al.* Nanobody-derived nanobiotechnology tool kits for diverse biomedical and
biotechnology applications. *Int J Nanomedicine* **11**, 3287-3303, doi:10.2147/IJN.S107194 (2016).
- 107 De Meyer, T., Muyltermans, S. & Depicker, A. Nanobody-based products as research and
diagnostic tools. *Trends in biotechnology* **32**, 263-270, doi:10.1016/j.tibtech.2014.03.001 (2014).
- 108 Ingram, J. R., Schmidt, F. I. & Ploegh, H. L. Exploiting Nanobodies' Singular Traits. *Annual review
of immunology* **36**, 695-715, doi:10.1146/annurev-immunol-042617-053327 (2018).
- 109 Els Conrath, K., Lauwereys, M., Wyns, L. & Muyltermans, S. Camel single-domain antibodies as
modular building units in bispecific and bivalent antibody constructs. *The Journal of biological
chemistry* **276**, 7346-7350, doi:10.1074/jbc.M007734200 (2001).
- 110 Fridy, P. C. *et al.* A robust pipeline for rapid production of versatile nanobody repertoires.
Nature methods **11**, 1253-1260, doi:10.1038/nmeth.3170 (2014).
- 111 He, L. *et al.* Enhanced Ability of Oligomeric Nanobodies Targeting MERS Coronavirus Receptor-
Binding Domain. *Viruses* **11**, doi:10.3390/v11020166 (2019).
- 112 Huet, H. A. *et al.* Multivalent nanobodies targeting death receptor 5 elicit superior tumor cell
killing through efficient caspase induction. *MAbs* **6**, 1560-1570,
doi:10.4161/19420862.2014.975099 (2014).
- 113 Peyvandi, F. *et al.* Caplacizumab reduces the frequency of major thromboembolic events,
exacerbations and death in patients with acquired thrombotic thrombocytopenic purpura. *J
Thromb Haemost* **15**, 1448-1452, doi:10.1111/jth.13716 (2017).

- 114 Bannas, P., Hambach, J. & Koch-Nolte, F. Nanobodies and Nanobody-Based Human Heavy Chain Antibodies As Antitumor Therapeutics. *Front Immunol* **8**, 1603, doi:10.3389/fimmu.2017.01603 (2017).
- 115 Detalle, L. *et al.* Generation and Characterization of ALX-0171, a Potent Novel Therapeutic Nanobody for the Treatment of Respiratory Syncytial Virus Infection. *Antimicrob Agents Chemother* **60**, 6-13, doi:10.1128/AAC.01802-15 (2016).
- 116 Witte, M. D. *et al.* Preparation of unnatural N-to-N and C-to-C protein fusions. *Proceedings of the National Academy of Sciences of the United States of America* **109**, 11993-11998, doi:10.1073/pnas.1205427109 (2012).
- 117 Stengl, A. *et al.* TuPPL: Tub-tag mediated C-terminal protein-protein-ligation using complementary click-chemistry handles. *Organic & biomolecular chemistry*, doi:10.1039/c9ob00508k (2019).
- 118 Zhao, H., Shen, A., Xiang, Y. K. & Corey, D. P. Three Recombinant Engineered Antibodies against Recombinant Tags with High Affinity and Specificity. *PLoS one* **11**, e0150125, doi:10.1371/journal.pone.0150125 (2016).
- 119 Tillib, S. V. *et al.* Formatted single-domain antibodies can protect mice against infection with influenza virus (H5N2). *Antiviral research* **97**, 245-254, doi:10.1016/j.antiviral.2012.12.014 (2013).
- 120 Zhang, J. *et al.* Pentamerization of single-domain antibodies from phage libraries: a novel strategy for the rapid generation of high-avidity antibody reagents. *Journal of molecular biology* **335**, 49-56 (2004).
- 121 Riazi, A. *et al.* Pentavalent single-domain antibodies reduce *Campylobacter jejuni* motility and colonization in chickens. *PLoS one* **8**, e83928, doi:10.1371/journal.pone.0083928 (2013).
- 122 Fan, K. *et al.* Fenobody: A Ferritin-Displayed Nanobody with High Apparent Affinity and Half-Life Extension. *Analytical chemistry* **90**, 5671-5677, doi:10.1021/acs.analchem.7b05217 (2018).
- 123 Boruah, B. M. *et al.* Single domain antibody multimers confer protection against rabies infection. *PLoS one* **8**, e71383, doi:10.1371/journal.pone.0071383 (2013).
- 124 Rozan, C. *et al.* Single-domain antibody-based and linker-free bispecific antibodies targeting FcγRIIIb induce potent antitumor activity without recruiting regulatory T cells. *Molecular cancer therapeutics* **12**, 1481-1491, doi:10.1158/1535-7163.MCT-12-1012 (2013).
- 125 Li, A. *et al.* A single-domain antibody-linked Fab bispecific antibody Her2-S-Fab has potent cytotoxicity against Her2-expressing tumor cells. *AMB Express* **6**, 32, doi:10.1186/s13568-016-0201-4 (2016).
- 126 Zhu, X. *et al.* COMBODY: one-domain antibody multimer with improved avidity. *Immunol Cell Biol* **88**, 667-675, doi:10.1038/icb.2010.21 (2010).
- 127 Arbabi Ghahroudi, M., Desmyter, A., Wyns, L., Hamers, R. & Muyldermans, S. Selection and identification of single domain antibody fragments from camel heavy-chain antibodies. *FEBS letters* **414**, 521-526 (1997).
- 128 Pardon, E. *et al.* A general protocol for the generation of Nanobodies for structural biology. *Nature protocols* **9**, 674-693, doi:10.1038/nprot.2014.039 (2014).
- 129 Deschaght, P. *et al.* Large Diversity of Functional Nanobodies from a Camelid Immune Library Revealed by an Alternative Analysis of Next-Generation Sequencing Data. *Front Immunol* **8**, 420, doi:10.3389/fimmu.2017.00420 (2017).
- 130 Kastelic, D. *et al.* A single-step procedure of recombinant library construction for the selection of efficiently produced llama VH binders directed against cancer markers. *Journal of immunological methods* **350**, 54-62, doi:10.1016/j.jim.2009.08.016 (2009).

- 131 Maass, D. R., Sepulveda, J., Pernthaler, A. & Shoemaker, C. B. Alpaca (Lama pacos) as a convenient source of recombinant camelid heavy chain antibodies (VHHs). *Journal of immunological methods* **324**, 13-25, doi:10.1016/j.jim.2007.04.008 (2007).
- 132 van der Linden, R. *et al.* Induction of immune responses and molecular cloning of the heavy chain antibody repertoire of Lama glama. *Journal of immunological methods* **240**, 185-195 (2000).
- 133 Sabir, J. S. *et al.* Construction of naive camelids VHH repertoire in phage display-based library. *C R Biol* **337**, 244-249, doi:10.1016/j.crvi.2014.02.004 (2014).
- 134 Yau, K. Y. *et al.* Selection of hapten-specific single-domain antibodies from a non-immunized llama ribosome display library. *Journal of immunological methods* **281**, 161-175 (2003).
- 135 Liu, J. L. *et al.* Selection of cholera toxin specific IgNAR single-domain antibodies from a naive shark library. *Mol Immunol* **44**, 1775-1783, doi:10.1016/j.molimm.2006.07.299 (2007).
- 136 Monegal, A. *et al.* Immunological applications of single-domain llama recombinant antibodies isolated from a naive library. *Protein Eng Des Sel* **22**, 273-280, doi:10.1093/protein/gzp002 (2009).
- 137 Vaughan, T. J. *et al.* Human antibodies with sub-nanomolar affinities isolated from a large non-immunized phage display library. *Nature biotechnology* **14**, 309-314, doi:10.1038/nbt0396-309 (1996).
- 138 Santagostino, A. *et al.* An Italian national multicenter study for the definition of reference ranges for normal values of peripheral blood lymphocyte subsets in healthy adults. *Haematologica* **84**, 499-504 (1999).
- 139 Ding, Y. *et al.* Reference values for peripheral blood lymphocyte subsets of healthy children in China. *The Journal of allergy and clinical immunology* **142**, 970-973 e978, doi:10.1016/j.jaci.2018.04.022 (2018).
- 140 Perez-Andres, M. *et al.* Human peripheral blood B-cell compartments: a crossroad in B-cell traffic. *Cytometry B Clin Cytom* **78 Suppl 1**, S47-60, doi:10.1002/cyto.b.20547 (2010).
- 141 Knappik, A. *et al.* Fully synthetic human combinatorial antibody libraries (HuCAL) based on modular consensus frameworks and CDRs randomized with trinucleotides. *Journal of molecular biology* **296**, 57-86, doi:10.1006/jmbi.1999.3444 (2000).
- 142 Yan, J., Li, G., Hu, Y., Ou, W. & Wan, Y. Construction of a synthetic phage-displayed Nanobody library with CDR3 regions randomized by trinucleotide cassettes for diagnostic applications. *Journal of translational medicine* **12**, 343, doi:10.1186/s12967-014-0343-6 (2014).
- 143 Tiller, T. *et al.* A fully synthetic human Fab antibody library based on fixed VH/VL framework pairings with favorable biophysical properties. *MAbs* **5**, 445-470, doi:10.4161/mabs.24218 (2013).
- 144 Seeger, M. A. *et al.* Design, construction, and characterization of a second-generation DARPin library with reduced hydrophobicity. *Protein science : a publication of the Protein Society* **22**, 1239-1257, doi:10.1002/pro.2312 (2013).
- 145 Gray, A. C., Sidhu, S. S., Chandrasekera, P. C., Hendriksen, C. F. M. & Borrebaeck, C. A. K. Animal-Friendly Affinity Reagents: Replacing the Needless in the Haystack. *Trends in biotechnology* **34**, 960-969, doi:10.1016/j.tibtech.2016.05.017 (2016).
- 146 Wagner, H. J., Wehrle, S., Weiss, E., Cavallari, M. & Weber, W. A Two-Step Approach for the Design and Generation of Nanobodies. *International journal of molecular sciences* **19**, doi:10.3390/ijms19113444 (2018).
- 147 Wingler, L. M., McMahan, C., Staus, D. P., Lefkowitz, R. J. & Kruse, A. C. Distinctive Activation Mechanism for Angiotensin Receptor Revealed by a Synthetic Nanobody. *Cell* **176**, 479-490 e412, doi:10.1016/j.cell.2018.12.006 (2019).

- 148 Manglik, A., Kobilka, B. K. & Steyaert, J. Nanobodies to Study G Protein-Coupled Receptor Structure and Function. *Annu Rev Pharmacol Toxicol* **57**, 19-37, doi:10.1146/annurev-pharmtox-010716-104710 (2017).
- 149 Koromyslova, A. D. & Hansman, G. S. Nanobodies targeting norovirus capsid reveal functional epitopes and potential mechanisms of neutralization. *PLoS pathogens* **13**, e1006636, doi:10.1371/journal.ppat.1006636 (2017).
- 150 Tang, J. C. *et al.* Cell type-specific manipulation with GFP-dependent Cre recombinase. *Nat Neurosci* **18**, 1334-1341, doi:10.1038/nn.4081 (2015).
- 151 Tang, J. C. *et al.* A nanobody-based system using fluorescent proteins as scaffolds for cell-specific gene manipulation. *Cell* **154**, 928-939, doi:10.1016/j.cell.2013.07.021 (2013).
- 152 Pinto Torres, J. E. *et al.* Development of a Nanobody-based lateral flow assay to detect active Trypanosoma congolense infections. *Scientific reports* **8**, 9019, doi:10.1038/s41598-018-26732-7 (2018).
- 153 Meksiriporn, B. *et al.* A survival selection strategy for engineering synthetic binding proteins that specifically recognize post-translationally phosphorylated proteins. *Nature communications* **10**, 1830, doi:10.1038/s41467-019-09854-y (2019).
- 154 Noel, F., Malpertuy, A. & de Brevern, A. G. Global analysis of VHHs framework regions with a structural alphabet. *Biochimie* **131**, 11-19, doi:10.1016/j.biochi.2016.09.005 (2016).
- 155 Ratanji, K. D., Derrick, J. P., Dearman, R. J. & Kimber, I. Immunogenicity of therapeutic proteins: influence of aggregation. *J Immunotoxicol* **11**, 99-109, doi:10.3109/1547691X.2013.821564 (2014).
- 156 Shim, H. Synthetic approach to the generation of antibody diversity. *BMB Rep* **48**, 489-494 (2015).
- 157 Zhai, W. *et al.* Synthetic antibodies designed on natural sequence landscapes. *Journal of molecular biology* **412**, 55-71, doi:10.1016/j.jmb.2011.07.018 (2011).
- 158 Prassler, J. *et al.* HuCAL PLATINUM, a synthetic Fab library optimized for sequence diversity and superior performance in mammalian expression systems. *Journal of molecular biology* **413**, 261-278, doi:10.1016/j.jmb.2011.08.012 (2011).
- 159 Goldman, E. R. *et al.* Facile generation of heat-stable antiviral and antitoxin single domain antibodies from a semisynthetic llama library. *Analytical chemistry* **78**, 8245-8255, doi:10.1021/ac0610053 (2006).
- 160 Yan, C., Wu, F., Jernigan, R. L., Dobbs, D. & Honavar, V. Characterization of protein-protein interfaces. *Protein J* **27**, 59-70, doi:10.1007/s10930-007-9108-x (2008).
- 161 Kabat, E. A., Wu, T. T. & Bilofsky, H. Unusual distributions of amino acids in complementarity-determining (hypervariable) segments of heavy and light chains of immunoglobulins and their possible roles in specificity of antibody-combining sites. *The Journal of biological chemistry* **252**, 6609-6616 (1977).
- 162 Gonzalez-Munoz, A. *et al.* Tailored amino acid diversity for the evolution of antibody affinity. *MAbs* **4**, 664-672, doi:10.4161/mabs.21728 (2012).
- 163 Collis, A. V., Brouwer, A. P. & Martin, A. C. Analysis of the antigen combining site: correlations between length and sequence composition of the hypervariable loops and the nature of the antigen. *Journal of molecular biology* **325**, 337-354 (2003).
- 164 Roberts, R. W. & Szostak, J. W. RNA-peptide fusions for the in vitro selection of peptides and proteins. *Proceedings of the National Academy of Sciences of the United States of America* **94**, 12297-12302 (1997).
- 165 Jenkins, N., Murphy, L. & Tyther, R. Post-translational modifications of recombinant proteins: significance for biopharmaceuticals. *Mol Biotechnol* **39**, 113-118, doi:10.1007/s12033-008-9049-4 (2008).

- 166 Muyldermans, S., Atarhouch, T., Saldanha, J., Barbosa, J. A. & Hamers, R. Sequence and structure of VH domain from naturally occurring camel heavy chain immunoglobulins lacking light chains. *Protein Eng* **7**, 1129-1135 (1994).
- 167 Li, X. *et al.* Comparative Analysis of Immune Repertoires between Bactrian Camel's Conventional and Heavy-Chain Antibodies. *PLoS one* **11**, e0161801, doi:10.1371/journal.pone.0161801 (2016).
- 168 Silacci, M. *et al.* Design, construction, and characterization of a large synthetic human antibody phage display library. *Proteomics* **5**, 2340-2350, doi:10.1002/pmic.200401273 (2005).
- 169 Nissim, A. *et al.* Antibody fragments from a 'single pot' phage display library as immunochemical reagents. *The EMBO journal* **13**, 692-698 (1994).
- 170 Virnekas, B. *et al.* Trinucleotide phosphoramidites: ideal reagents for the synthesis of mixed oligonucleotides for random mutagenesis. *Nucleic acids research* **22**, 5600-5607 (1994).
- 171 Schilling, J., Schoppe, J. & Pluckthun, A. From DARPin to LoopDARPin: novel LoopDARPin design allows the selection of low picomolar binders in a single round of ribosome display. *Journal of molecular biology* **426**, 691-721, doi:10.1016/j.jmb.2013.10.026 (2014).
- 172 Winter, G. & Milstein, C. Man-made antibodies. *Nature* **349**, 293-299, doi:10.1038/349293a0 (1991).
- 173 Baran, D. *et al.* Principles for computational design of binding antibodies. *Proceedings of the National Academy of Sciences of the United States of America* **114**, 10900-10905, doi:10.1073/pnas.1707171114 (2017).
- 174 Petsko, G. A. The grail problem. *Genome Biol* **1**, COMMENT002, doi:10.1186/gb-2000-1-1-comment002 (2000).
- 175 Butterfield, G. L. *et al.* Evolution of a designed protein assembly encapsulating its own RNA genome. *Nature* **552**, 415-420, doi:10.1038/nature25157 (2017).
- 176 Huang, P. S., Boyken, S. E. & Baker, D. The coming of age of de novo protein design. *Nature* **537**, 320-327, doi:10.1038/nature19946 (2016).
- 177 Dou, J. *et al.* De novo design of a fluorescence-activating beta-barrel. *Nature* **561**, 485-491, doi:10.1038/s41586-018-0509-0 (2018).
- 178 Fischman, S. & Ofran, Y. Computational design of antibodies. *Curr Opin Struct Biol* **51**, 156-162, doi:10.1016/j.sbi.2018.04.007 (2018).
- 179 Adolf-Bryfogle, J. *et al.* RosettaAntibodyDesign (RABD): A general framework for computational antibody design. *PLoS Comput Biol* **14**, e1006112, doi:10.1371/journal.pcbi.1006112 (2018).
- 180 Chevalier, A. *et al.* Massively parallel de novo protein design for targeted therapeutics. *Nature* **550**, 74-79, doi:10.1038/nature23912 (2017).
- 181 Nimrod, G. *et al.* Computational Design of Epitope-Specific Functional Antibodies. *Cell reports* **25**, 2121-2131 e2125, doi:10.1016/j.celrep.2018.10.081 (2018).
- 182 Entzminger, K. C. *et al.* De novo design of antibody complementarity determining regions binding a FLAG tetra-peptide. *Scientific reports* **7**, 10295, doi:10.1038/s41598-017-10737-9 (2017).
- 183 McCafferty, J., Griffiths, A. D., Winter, G. & Chiswell, D. J. Phage antibodies: filamentous phage displaying antibody variable domains. *Nature* **348**, 552-554, doi:10.1038/348552a0 (1990).
- 184 Smith, G. P. Filamentous fusion phage: novel expression vectors that display cloned antigens on the virion surface. *Science* **228**, 1315-1317 (1985).
- 185 Ledsgaard, L., Kilstrup, M., Karatt-Vellatt, A., McCafferty, J. & Laustsen, A. H. Basics of Antibody Phage Display Technology. *Toxins (Basel)* **10**, doi:10.3390/toxins10060236 (2018).
- 186 Bazan, J., Calkosinski, I. & Gamian, A. Phage display--a powerful technique for immunotherapy: 1. Introduction and potential of therapeutic applications. *Human vaccines & immunotherapeutics* **8**, 1817-1828, doi:10.4161/hv.21703 (2012).

- 187 Koide, A. *et al.* Accelerating phage-display library selection by reversible and site-specific
biotinylation. *Protein Eng Des Sel* **22**, 685-690, doi:10.1093/protein/gzp053 (2009).
- 188 Schofield, D. J. *et al.* Application of phage display to high throughput antibody generation and
characterization. *Genome Biol* **8**, R254, doi:10.1186/gb-2007-8-11-r254 (2007).
- 189 Rauth, S. *et al.* High-affinity Anticalins with aggregation-blocking activity directed against the
Alzheimer beta-amyloid peptide. *The Biochemical journal* **473**, 1563-1578,
doi:10.1042/BCJ20160114 (2016).
- 190 Lorey, S. *et al.* Novel ubiquitin-derived high affinity binding proteins with tumor targeting
properties. *The Journal of biological chemistry* **289**, 8493-8507, doi:10.1074/jbc.M113.519884
(2014).
- 191 Parmley, S. F. & Smith, G. P. Antibody-selectable filamentous fd phage vectors: affinity
purification of target genes. *Gene* **73**, 305-318 (1988).
- 192 Smith, G. P. & Scott, J. K. Libraries of peptides and proteins displayed on filamentous phage.
Methods in enzymology **217**, 228-257 (1993).
- 193 Clackson, T. *Phage display : a practical approach.* (Oxford Univ. Press, 2009).
- 194 Frei, J. C. & Lai, J. R. Protein and Antibody Engineering by Phage Display. *Methods in enzymology*
580, 45-87, doi:10.1016/bs.mie.2016.05.005 (2016).
- 195 Jones, M. L. *et al.* Targeting membrane proteins for antibody discovery using phage display.
Scientific reports **6**, 26240, doi:10.1038/srep26240 (2016).
- 196 Lloyd, C. *et al.* Modelling the human immune response: performance of a 1011 human antibody
repertoire against a broad panel of therapeutically relevant antigens. *Protein Eng Des Sel* **22**,
159-168, doi:10.1093/protein/gzn058 (2009).
- 197 Pepper, L. R., Cho, Y. K., Boder, E. T. & Shusta, E. V. A decade of yeast surface display technology:
where are we now? *Comb Chem High Throughput Screen* **11**, 127-134 (2008).
- 198 Boder, E. T. & Wittrup, K. D. Yeast surface display for screening combinatorial polypeptide
libraries. *Nature biotechnology* **15**, 553-557, doi:10.1038/nbt0697-553 (1997).
- 199 Uchanski, T. *et al.* An improved yeast surface display platform for the screening of nanobody
immune libraries. *Scientific reports* **9**, 382, doi:10.1038/s41598-018-37212-3 (2019).
- 200 Kondo, A. & Ueda, M. Yeast cell-surface display--applications of molecular display. *Applied
microbiology and biotechnology* **64**, 28-40, doi:10.1007/s00253-003-1492-3 (2004).
- 201 Chen, I., Dorr, B. M. & Liu, D. R. A general strategy for the evolution of bond-forming enzymes
using yeast display. *Proceedings of the National Academy of Sciences of the United States of
America* **108**, 11399-11404, doi:10.1073/pnas.1101046108 (2011).
- 202 Lipovsek, D. *et al.* Selection of horseradish peroxidase variants with enhanced enantioselectivity
by yeast surface display. *Chemistry & biology* **14**, 1176-1185,
doi:10.1016/j.chembiol.2007.09.008 (2007).
- 203 Sivelse, C. *et al.* Fab is the most efficient format to express functional antibodies by yeast surface
display. *MAbs* **10**, 720-729, doi:10.1080/19420862.2018.1468952 (2018).
- 204 Tillotson, B. J., de Larrinoa, I. F., Skinner, C. A., Klavas, D. M. & Shusta, E. V. Antibody affinity
maturation using yeast display with detergent-solubilized membrane proteins as antigen
sources. *Protein Eng Des Sel* **26**, 101-112, doi:10.1093/protein/gzs077 (2013).
- 205 Chao, G. *et al.* Isolating and engineering human antibodies using yeast surface display. *Nature
protocols* **1**, 755-768, doi:10.1038/nprot.2006.94 (2006).
- 206 Cherf, G. M. & Cochran, J. R. Applications of Yeast Surface Display for Protein Engineering.
Methods Mol Biol **1319**, 155-175, doi:10.1007/978-1-4939-2748-7_8 (2015).
- 207 VanAntwerp, J. J. & Wittrup, K. D. Fine affinity discrimination by yeast surface display and flow
cytometry. *Biotechnol Prog* **16**, 31-37, doi:10.1021/bp990133s (2000).

- 208 Boder, E. T., Midelfort, K. S. & Wittrup, K. D. Directed evolution of antibody fragments with
monovalent femtomolar antigen-binding affinity. *Proceedings of the National Academy of
Sciences of the United States of America* **97**, 10701-10705, doi:10.1073/pnas.170297297 (2000).
- 209 Gai, S. A. & Wittrup, K. D. Yeast surface display for protein engineering and characterization.
Curr Opin Struct Biol **17**, 467-473, doi:10.1016/j.sbi.2007.08.012 (2007).
- 210 Ulrich, H. D., Patten, P. A., Yang, P. L., Romesberg, F. E. & Schultz, P. G. Expression studies of
catalytic antibodies. *Proceedings of the National Academy of Sciences of the United States of
America* **92**, 11907-11911 (1995).
- 211 Bowley, D. R., Labrijn, A. F., Zwick, M. B. & Burton, D. R. Antigen selection from an HIV-1
immune antibody library displayed on yeast yields many novel antibodies compared to selection
from the same library displayed on phage. *Protein Eng Des Sel* **20**, 81-90,
doi:10.1093/protein/gzl057 (2007).
- 212 Feldhaus, M. J. *et al.* Flow-cytometric isolation of human antibodies from a nonimmune
Saccharomyces cerevisiae surface display library. *Nature biotechnology* **21**, 163-170,
doi:10.1038/nbt785 (2003).
- 213 Becker, D. M. & Guarente, L. High-efficiency transformation of yeast by electroporation.
Methods in enzymology **194**, 182-187 (1991).
- 214 Kim, C. C., Wilson, E. B. & DeRisi, J. L. Improved methods for magnetic purification of malaria
parasites and haemozoin. *Malar J* **9**, 17, doi:10.1186/1475-2875-9-17 (2010).
- 215 Kruse, A. C. *et al.* Activation and allosteric modulation of a muscarinic acetylcholine receptor.
Nature **504**, 101-106, doi:10.1038/nature12735 (2013).
- 216 Konning, D. *et al.* Semi-synthetic vNAR libraries screened against therapeutic antibodies
primarily deliver anti-idiotypic binders. *Scientific reports* **7**, 9676, doi:10.1038/s41598-017-
10513-9 (2017).
- 217 Packer, M. S. & Liu, D. R. Methods for the directed evolution of proteins. *Nat Rev Genet* **16**, 379-
394, doi:10.1038/nrg3927 (2015).
- 218 Salema, V. & Fernandez, L. A. *Escherichia coli* surface display for the selection of nanobodies.
Microb Biotechnol **10**, 1468-1484, doi:10.1111/1751-7915.12819 (2017).
- 219 Daugherty, P. S. Protein engineering with bacterial display. *Curr Opin Struct Biol* **17**, 474-480,
doi:10.1016/j.sbi.2007.07.004 (2007).
- 220 Fleetwood, F. *et al.* Surface display of a single-domain antibody library on Gram-positive
bacteria. *Cellular and molecular life sciences : CMLS* **70**, 1081-1093, doi:10.1007/s00018-012-
1179-y (2013).
- 221 Kronqvist, N., Lofblom, J., Jonsson, A., Wernerus, H. & Stahl, S. A novel affinity protein selection
system based on staphylococcal cell surface display and flow cytometry. *Protein Eng Des Sel* **21**,
247-255, doi:10.1093/protein/gzm090 (2008).
- 222 Fleetwood, F., Andersson, K. G., Stahl, S. & Lofblom, J. An engineered autotransporter-based
surface expression vector enables efficient display of Affibody molecules on OmpT-negative *E.*
coli as well as protease-mediated secretion in OmpT-positive strains. *Microb Cell Fact* **13**, 179,
doi:10.1186/s12934-014-0179-z (2014).
- 223 Moghaddam-Taaheri, P., Ikonomova, S. P., Gong, Z., Wisniewski, J. Q. & Karlsson, A. J. Bacterial
Inner-membrane Display for Screening a Library of Antibody Fragments. *J Vis Exp*,
doi:10.3791/54583 (2016).
- 224 Harvey, B. R. *et al.* Anchored periplasmic expression, a versatile technology for the isolation of
high-affinity antibodies from *Escherichia coli*-expressed libraries. *Proceedings of the National
Academy of Sciences of the United States of America* **101**, 9193-9198,
doi:10.1073/pnas.0400187101 (2004).

- 225 Harvey, B. R. *et al.* Engineering of recombinant antibody fragments to methamphetamine by anchored periplasmic expression. *Journal of immunological methods* **308**, 43-52, doi:10.1016/j.jim.2005.09.017 (2006).
- 226 Salema, V. *et al.* Selection of single domain antibodies from immune libraries displayed on the surface of E. coli cells with two beta-domains of opposite topologies. *PLoS one* **8**, e75126, doi:10.1371/journal.pone.0075126 (2013).
- 227 Salema, V. & Fernandez, L. A. High yield purification of nanobodies from the periplasm of E. coli as fusions with the maltose binding protein. *Protein Expr Purif* **91**, 42-48, doi:10.1016/j.pep.2013.07.001 (2013).
- 228 Salema, V. *et al.* High affinity nanobodies against human epidermal growth factor receptor selected on cells by E. coli display. *MAbs* **8**, 1286-1301, doi:10.1080/19420862.2016.1216742 (2016).
- 229 Karlsson, A. J. *et al.* Engineering antibody fitness and function using membrane-anchored display of correctly folded proteins. *Journal of molecular biology* **416**, 94-107, doi:10.1016/j.jmb.2011.12.021 (2012).
- 230 Higuchi, K. *et al.* Cell display library for gene cloning of variable regions of human antibodies to hepatitis B surface antigen. *Journal of immunological methods* **202**, 193-204 (1997).
- 231 Ho, M., Nagata, S. & Pastan, I. Isolation of anti-CD22 Fv with high affinity by Fv display on human cells. *Proceedings of the National Academy of Sciences of the United States of America* **103**, 9637-9642, doi:10.1073/pnas.0603653103 (2006).
- 232 Akamatsu, Y., Pakabunto, K., Xu, Z., Zhang, Y. & Tsurushita, N. Whole IgG surface display on mammalian cells: Application to isolation of neutralizing chicken monoclonal anti-IL-12 antibodies. *Journal of immunological methods* **327**, 40-52, doi:10.1016/j.jim.2007.07.007 (2007).
- 233 Beerli, R. R. *et al.* Isolation of human monoclonal antibodies by mammalian cell display. *Proceedings of the National Academy of Sciences of the United States of America* **105**, 14336-14341, doi:10.1073/pnas.0805942105 (2008).
- 234 Zhou, C., Jacobsen, F. W., Cai, L., Chen, Q. & Shen, W. D. Development of a novel mammalian cell surface antibody display platform. *MAbs* **2**, 508-518, doi:10.4161/mabs.2.5.12970 (2010).
- 235 Zhang, J. *et al.* Mammalian cell display for rapid screening scFv antibody therapy. *Acta biochimica et biophysica Sinica* **46**, 859-866, doi:10.1093/abbs/gmu079 (2014).
- 236 McConnell, A. D. *et al.* High affinity humanized antibodies without making hybridomas; immunization paired with mammalian cell display and in vitro somatic hypermutation. *PLoS one* **7**, e49458, doi:10.1371/journal.pone.0049458 (2012).
- 237 Bowers, P. M. *et al.* Mammalian cell display for the discovery and optimization of antibody therapeutics. *Methods* **65**, 44-56, doi:10.1016/j.ymeth.2013.06.010 (2014).
- 238 Qin, C. F. & Li, G. C. Mammalian cell display technology coupling with AID induced SHM in vitro: an ideal approach to the production of therapeutic antibodies. *International immunopharmacology* **23**, 380-386, doi:10.1016/j.intimp.2014.09.017 (2014).
- 239 Bowers, P. M. *et al.* Coupling mammalian cell surface display with somatic hypermutation for the discovery and maturation of human antibodies. *Proceedings of the National Academy of Sciences of the United States of America* **108**, 20455-20460, doi:10.1073/pnas.1114010108 (2011).
- 240 King, D. J., Bowers, P. M., Kehry, M. R. & Horlick, R. A. Mammalian cell display and somatic hypermutation in vitro for human antibody discovery. *Curr Drug Discov Technol* **11**, 56-64 (2014).
- 241 Kuscu, C. & Adli, M. CRISPR-Cas9-AID base editor is a powerful gain-of-function screening tool. *Nature methods* **13**, 983-984, doi:10.1038/nmeth.4076 (2016).

- 242 Matz, J. *et al.* Selection of intracellular single-domain antibodies targeting the HIV-1 Vpr protein by cytoplasmic yeast two-hybrid system. *PLoS one* **9**, e113729, doi:10.1371/journal.pone.0113729 (2014).
- 243 Fu, X. *et al.* Design and selection of a camelid single-chain antibody yeast two-hybrid library produced de novo for the cap protein of porcine circovirus type 2 (PCV2). *PLoS one* **8**, e56222, doi:10.1371/journal.pone.0056222 (2013).
- 244 Pellis, M. *et al.* A bacterial-two-hybrid selection system for one-step isolation of intracellularly functional Nanobodies. *Archives of biochemistry and biophysics* **526**, 114-123, doi:10.1016/j.abb.2012.04.023 (2012).
- 245 Wada, A. Development of Next-Generation Peptide Binders Using In vitro Display Technologies and Their Potential Applications. *Front Immunol* **4**, 224, doi:10.3389/fimmu.2013.00224 (2013).
- 246 Mattheakis, L. C., Bhatt, R. R. & Dower, W. J. An in vitro polysome display system for identifying ligands from very large peptide libraries. *Proceedings of the National Academy of Sciences of the United States of America* **91**, 9022-9026 (1994).
- 247 Li, R., Kang, G., Hu, M. & Huang, H. Ribosome Display: A Potent Display Technology used for Selecting and Evolving Specific Binders with Desired Properties. *Mol Biotechnol* **61**, 60-71, doi:10.1007/s12033-018-0133-0 (2019).
- 248 Bencurova, E., Pulzova, L., Flachbartova, Z. & Bhide, M. A rapid and simple pipeline for synthesis of mRNA-ribosome-V(H)H complexes used in single-domain antibody ribosome display. *Molecular bioSystems* **11**, 1515-1524, doi:10.1039/c5mb00026b (2015).
- 249 Seelig, B. mRNA display for the selection and evolution of enzymes from in vitro-translated protein libraries. *Nature protocols* **6**, 540-552, doi:10.1038/nprot.2011.312 (2011).
- 250 Mochizuki, Y. *et al.* One-pot preparation of mRNA/cDNA display by a novel and versatile puromycin-linker DNA. *ACS Comb Sci* **13**, 478-485, doi:10.1021/co2000295 (2011).
- 251 Yamaguchi, J. *et al.* cDNA display: a novel screening method for functional disulfide-rich peptides by solid-phase synthesis and stabilization of mRNA-protein fusions. *Nucleic acids research* **37**, e108, doi:10.1093/nar/gkp514 (2009).
- 252 Ishizawa, T., Kawakami, T., Reid, P. C. & Murakami, H. TRAP display: a high-speed selection method for the generation of functional polypeptides. *Journal of the American Chemical Society* **135**, 5433-5440, doi:10.1021/ja312579u (2013).
- 253 Doshi, R. *et al.* In vitro nanobody discovery for integral membrane protein targets. *Scientific reports* **4**, 6760, doi:10.1038/srep06760 (2014).
- 254 Cho, G., Keefe, A. D., Liu, R., Wilson, D. S. & Szostak, J. W. Constructing high complexity synthetic libraries of long ORFs using in vitro selection. *Journal of molecular biology* **297**, 309-319, doi:10.1006/jmbi.2000.3571 (2000).
- 255 Galan, A. *et al.* Library-based display technologies: where do we stand? *Molecular bioSystems* **12**, 2342-2358, doi:10.1039/c6mb00219f (2016).
- 256 Hoogenboom, H. R. Selecting and screening recombinant antibody libraries. *Nature biotechnology* **23**, 1105-1116, doi:10.1038/nbt1126 (2005).
- 257 Baker, M. Protein engineering: navigating between chance and reason. *Nature methods* **8**, 623-626, doi:10.1038/nmeth.1654 (2011).
- 258 Odegrip, R. *et al.* CIS display: In vitro selection of peptides from libraries of protein-DNA complexes. *Proceedings of the National Academy of Sciences of the United States of America* **101**, 2806-2810, doi:10.1073/pnas.0400219101 (2004).
- 259 Reiersen, H. *et al.* Covalent antibody display--an in vitro antibody-DNA library selection system. *Nucleic acids research* **33**, e10, doi:10.1093/nar/gni010 (2005).

- 260 Masai, H., Kaziro, Y. & Arai, K. Definition of oriR, the minimum DNA segment essential for
initiation of R1 plasmid replication in vitro. *Proceedings of the National Academy of Sciences of
the United States of America* **80**, 6814-6818 (1983).
- 261 Eldridge, B. *et al.* An in vitro selection strategy for conferring protease resistance to ligand
binding peptides. *Protein Eng Des Sel* **22**, 691-698, doi:10.1093/protein/gzp052 (2009).
- 262 Patel, S., Mathonet, P., Jaulent, A. M. & Ullman, C. G. Selection of a high-affinity WW domain
against the extracellular region of VEGF receptor isoform-2 from a combinatorial library using
CIS display. *Protein Eng Des Sel* **26**, 307-315, doi:10.1093/protein/gzt003 (2013).
- 263 Tawfik, D. S. & Griffiths, A. D. Man-made cell-like compartments for molecular evolution. *Nature
biotechnology* **16**, 652-656, doi:10.1038/nbt0798-652 (1998).
- 264 Sepp, A., Tawfik, D. S. & Griffiths, A. D. Microbead display by in vitro compartmentalisation:
selection for binding using flow cytometry. *FEBS letters* **532**, 455-458 (2002).
- 265 Doi, N. & Yanagawa, H. STABLE: protein-DNA fusion system for screening of combinatorial
protein libraries in vitro. *FEBS letters* **457**, 227-230 (1999).
- 266 Yonezawa, M., Doi, N., Higashinakagawa, T. & Yanagawa, H. DNA display of biologically active
proteins for in vitro protein selection. *Journal of biochemistry* **135**, 285-288 (2004).
- 267 Bertschinger, J. & Neri, D. Covalent DNA display as a novel tool for directed evolution of proteins
in vitro. *Protein Eng Des Sel* **17**, 699-707, doi:10.1093/protein/gzh082 (2004).
- 268 Stein, V., Sielaff, I., Johnsson, K. & Hollfelder, F. A covalent chemical genotype-phenotype
linkage for in vitro protein evolution. *ChemBiochem* **8**, 2191-2194, doi:10.1002/cbic.200700459
(2007).
- 269 Houlihan, G., Lowe, D. & Hollfelder, F. SNAP display - an in vitro method for the selection of
protein binders. *Curr Pharm Des* **19**, 5421-5428 (2013).
- 270 Yonezawa, M., Doi, N., Kawahashi, Y., Higashinakagawa, T. & Yanagawa, H. DNA display for in
vitro selection of diverse peptide libraries. *Nucleic acids research* **31**, e118 (2003).
- 271 Frenken, L. G. *et al.* Isolation of antigen specific llama VHH antibody fragments and their high
level secretion by *Saccharomyces cerevisiae*. *Journal of biotechnology* **78**, 11-21 (2000).
- 272 Rajabi-Memari, H. *et al.* Expression and characterization of a recombinant single-domain
monoclonal antibody against MUC1 mucin in tobacco plants. *Hybridoma* **25**, 209-215,
doi:10.1089/hyb.2006.25.209 (2006).
- 273 Gomez-Sebastian, S. *et al.* Rotavirus A-specific single-domain antibodies produced in
baculovirus-infected insect larvae are protective in vivo. *BMC biotechnology* **12**, 59,
doi:10.1186/1472-6750-12-59 (2012).
- 274 Liu, Y. & Huang, H. Expression of single-domain antibody in different systems. *Applied
microbiology and biotechnology* **102**, 539-551, doi:10.1007/s00253-017-8644-3 (2018).
- 275 Agrawal, V. *et al.* Stable expression of chimeric heavy chain antibodies in CHO cells. *Methods
Mol Biol* **911**, 287-303, doi:10.1007/978-1-61779-968-6_18 (2012).
- 276 Harmsen, M. M. & De Haard, H. J. Properties, production, and applications of camelid single-
domain antibody fragments. *Applied microbiology and biotechnology* **77**, 13-22,
doi:10.1007/s00253-007-1142-2 (2007).
- 277 Arbabi-Ghahroudi, M., Tanha, J. & MacKenzie, R. Prokaryotic expression of antibodies. *Cancer
Metastasis Rev* **24**, 501-519, doi:10.1007/s10555-005-6193-1 (2005).
- 278 Pugsley, A. P. The complete general secretory pathway in gram-negative bacteria. *Microbiol Rev*
57, 50-108 (1993).
- 279 Kooijmans, S. A. A. *et al.* PEGylated and targeted extracellular vesicles display enhanced cell
specificity and circulation time. *Journal of controlled release : official journal of the Controlled
Release Society* **224**, 77-85, doi:10.1016/j.jconrel.2016.01.009 (2016).

- 280 Tripathi, N. K. Production and Purification of Recombinant Proteins from Escherichia coli. *ChemBioEng Reviews* **3**, 116-133, doi:doi:10.1002/cben.201600002 (2016).
- 281 Shriver-Lake, L. C., Goldman, E. R., Zabetakis, D. & Anderson, G. P. Improved production of single domain antibodies with two disulfide bonds by co-expression of chaperone proteins in the Escherichia coli periplasm. *Journal of immunological methods* **443**, 64-67, doi:10.1016/j.jim.2017.01.007 (2017).
- 282 Schlapschy, M., Grimm, S. & Skerra, A. A system for concomitant overexpression of four periplasmic folding catalysts to improve secretory protein production in Escherichia coli. *Protein Eng Des Sel* **19**, 385-390, doi:10.1093/protein/gzl018 (2006).
- 283 Maggi, M. & Scotti, C. Enhanced expression and purification of camelid single domain VHH antibodies from classical inclusion bodies. *Protein Expr Purif* **136**, 39-44, doi:10.1016/j.pep.2017.02.007 (2017).
- 284 Bessette, P. H., Aslund, F., Beckwith, J. & Georgiou, G. Efficient folding of proteins with multiple disulfide bonds in the Escherichia coli cytoplasm. *Proceedings of the National Academy of Sciences of the United States of America* **96**, 13703-13708 (1999).
- 285 Zarschler, K., Witcey, S., Kapplusch, F., Foerster, C. & Stephan, H. High-yield production of functional soluble single-domain antibodies in the cytoplasm of Escherichia coli. *Microb Cell Fact* **12**, 97, doi:10.1186/1475-2859-12-97 (2013).
- 286 Rahbarizadeh, F., Rasaee, M. J., Forouzandeh, M. & Allameh, A. A. Over expression of anti-MUC1 single-domain antibody fragments in the yeast Pichia pastoris. *Mol Immunol* **43**, 426-435, doi:10.1016/j.molimm.2005.03.003 (2006).
- 287 Joosten, V., Gouka, R. J., van den Hondel, C. A., Verrips, C. T. & Lokman, B. C. Expression and production of llama variable heavy-chain antibody fragments (V(HH)s) by Aspergillus awamori. *Applied microbiology and biotechnology* **66**, 384-392, doi:10.1007/s00253-004-1689-0 (2005).
- 288 Okazaki, F. *et al.* Efficient heterologous expression and secretion in Aspergillus oryzae of a llama variable heavy-chain antibody fragment V(HH) against EGFR. *Applied microbiology and biotechnology* **96**, 81-88, doi:10.1007/s00253-012-4158-1 (2012).
- 289 Matthews, C. B. *et al.* Reexamining opportunities for therapeutic protein production in eukaryotic microorganisms. *Biotechnol Bioeng* **114**, 2432-2444, doi:10.1002/bit.26378 (2017).
- 290 Gerngross, T. U. Advances in the production of human therapeutic proteins in yeasts and filamentous fungi. *Nature biotechnology* **22**, 1409-1414, doi:10.1038/nbt1028 (2004).
- 291 Nielsen, J. Production of biopharmaceutical proteins by yeast: advances through metabolic engineering. *Bioengineered* **4**, 207-211, doi:10.4161/bioe.22856 (2013).
- 292 Werten, M. W., van den Bosch, T. J., Wind, R. D., Mooibroek, H. & de Wolf, F. A. High-yield secretion of recombinant gelatins by Pichia pastoris. *Yeast* **15**, 1087-1096, doi:10.1002/(SICI)1097-0061(199908)15:11<1087::AID-YEA436>3.0.CO;2-F (1999).
- 293 Thomassen, Y. E., Meijer, W., Sierkstra, L. & Verrips, C. T. Large-scale production of VHH antibody fragments by Saccharomyces cerevisiae. *Enzyme and microbial technology* **30**, 273-278 (2002).
- 294 van de Laar, T. *et al.* Increased heterologous protein production by Saccharomyces cerevisiae growing on ethanol as sole carbon source. *Biotechnol Bioeng* **96**, 483-494, doi:10.1002/bit.21150 (2007).
- 295 Schotte, P. *et al.* Pichia pastoris Mut(S) strains are prone to misincorporation of O-methyl-L-homoserine at methionine residues when methanol is used as the sole carbon source. *Microb Cell Fact* **15**, 98, doi:10.1186/s12934-016-0499-2 (2016).
- 296 Priestersbach, A., Kubicek, J., Schafer, F., Block, H. & Maertens, B. Purification of His-Tagged Proteins. *Methods in enzymology* **559**, 1-15, doi:10.1016/bs.mie.2014.11.003 (2015).

- 297 Olichon, A., Schweizer, D., Muyldermans, S. & de Marco, A. Heating as a rapid purification method for recovering correctly-folded thermotolerant VH and VHH domains. *BMC biotechnology* **7**, 7, doi:10.1186/1472-6750-7-7 (2007).
- 298 Pardee, K. *et al.* Portable, On-Demand Biomolecular Manufacturing. *Cell* **167**, 248-259 e212, doi:10.1016/j.cell.2016.09.013 (2016).
- 299 Stech, M. *et al.* Cell-free synthesis of functional antibodies using a coupled in vitro transcription-translation system based on CHO cell lysates. *Scientific reports* **7**, 12030, doi:10.1038/s41598-017-12364-w (2017).
- 300 Matsuda, T. *et al.* Cell-free synthesis of functional antibody fragments to provide a structural basis for antibody-antigen interaction. *PLoS one* **13**, e0193158, doi:10.1371/journal.pone.0193158 (2018).
- 301 Boles, K. S. *et al.* Digital-to-biological converter for on-demand production of biologics. *Nature biotechnology* **35**, 672-675, doi:10.1038/nbt.3859 (2017).
- 302 Chalfie, M., Tu, Y., Euskirchen, G., Ward, W. W. & Prasher, D. C. Green fluorescent protein as a marker for gene expression. *Science* **263**, 802-805 (1994).
- 303 Chudakov, D. M., Matz, M. V., Lukyanov, S. & Lukyanov, K. A. Fluorescent proteins and their applications in imaging living cells and tissues. *Physiol Rev* **90**, 1103-1163, doi:10.1152/physrev.00038.2009 (2010).
- 304 Li, C., Tebo, A. G. & Gautier, A. Fluorogenic Labeling Strategies for Biological Imaging. *International journal of molecular sciences* **18**, doi:10.3390/ijms18071473 (2017).
- 305 Traenkle, B. & Rothbauer, U. Under the Microscope: Single-Domain Antibodies for Live-Cell Imaging and Super-Resolution Microscopy. *Front Immunol* **8**, 1030, doi:10.3389/fimmu.2017.01030 (2017).
- 306 Gilbreth, R. N. *et al.* Isoform-specific monobody inhibitors of small ubiquitin-related modifiers engineered using structure-guided library design. *Proceedings of the National Academy of Sciences of the United States of America* **108**, 7751-7756, doi:10.1073/pnas.1102294108 (2011).
- 307 Sato, Y. *et al.* Genetically encoded system to track histone modification in vivo. *Scientific reports* **3**, 2436, doi:10.1038/srep02436 (2013).
- 308 Kimura, H., Hayashi-Takanaka, Y., Stasevich, T. J. & Sato, Y. Visualizing posttranslational and epigenetic modifications of endogenous proteins in vivo. *Histochem Cell Biol* **144**, 101-109, doi:10.1007/s00418-015-1344-0 (2015).
- 309 Koo, M. Y. *et al.* Selective inhibition of the function of tyrosine-phosphorylated STAT3 with a phosphorylation site-specific intrabody. *Proceedings of the National Academy of Sciences* **111**, 6269-6274, doi:10.1073/pnas.1316815111 (2014).
- 310 Beghein, E. & Gettemans, J. Nanobody Technology: A Versatile Toolkit for Microscopic Imaging, Protein-Protein Interaction Analysis, and Protein Function Exploration. *Front Immunol* **8**, 771, doi:10.3389/fimmu.2017.00771 (2017).
- 311 Dmitriev, O. Y., Lutsenko, S. & Muyldermans, S. Nanobodies as Probes for Protein Dynamics in Vitro and in Cells. *The Journal of biological chemistry* **291**, 3767-3775, doi:10.1074/jbc.R115.679811 (2016).
- 312 Jullien, D. *et al.* Chromatibody, a novel non-invasive molecular tool to explore and manipulate chromatin in living cells. *Journal of cell science* **129**, 2673-2683, doi:10.1242/jcs.183103 (2016).
- 313 Traenkle, B. *et al.* Monitoring interactions and dynamics of endogenous beta-catenin with intracellular nanobodies in living cells. *Molecular & cellular proteomics : MCP* **14**, 707-723, doi:10.1074/mcp.M114.044016 (2015).
- 314 Virant, D. *et al.* A peptide tag-specific nanobody enables high-quality labeling for dSTORM imaging. *Nature communications* **9**, 930, doi:10.1038/s41467-018-03191-2 (2018).

- 315 Beghein, E. *et al.* A new survivin tracer tracks, delocalizes and captures endogenous survivin at
different subcellular locations and in distinct organelles. *Scientific reports* **6**, 31177,
doi:10.1038/srep31177 (2016).
- 316 Rothbauer, U. *et al.* Targeting and tracing antigens in live cells with fluorescent nanobodies.
Nature methods **3**, 887-889, doi:10.1038/nmeth953 (2006).
- 317 Chiu, H. Y. *et al.* Intracellular chromobody delivery by mesoporous silica nanoparticles for
antigen targeting and visualization in real time. *Scientific reports* **6**, 25019,
doi:10.1038/srep25019 (2016).
- 318 Herce, H. D. *et al.* Cell-permeable nanobodies for targeted immunolabelling and antigen
manipulation in living cells. *Nat Chem* **9**, 762-771, doi:10.1038/nchem.2811 (2017).
- 319 Klein, A. *et al.* Live-cell labeling of endogenous proteins with nanometer precision by transduced
nanobodies. *Chem Sci* **9**, 7835-7842, doi:10.1039/c8sc02910e (2018).
- 320 Buser, D. P., Schleicher, K. D., Prescianotto-Baschong, C. & Spiess, M. A versatile nanobody-
based toolkit to analyze retrograde transport from the cell surface. *Proceedings of the National
Academy of Sciences of the United States of America* **115**, E6227-E6236,
doi:10.1073/pnas.1801865115 (2018).
- 321 Modi, S., Higgs, N. F., Sheehan, D., Griffin, L. D. & Kittler, J. T. Quantum dot conjugated
nanobodies for multiplex imaging of protein dynamics at synapses. *Nanoscale* **10**, 10241-10249,
doi:10.1039/c7nr09130c (2018).
- 322 Panza, P., Maier, J., Schmees, C., Rothbauer, U. & Sollner, C. Live imaging of endogenous protein
dynamics in zebrafish using chromobodies. *Development* **142**, 1879-1884,
doi:10.1242/dev.118943 (2015).
- 323 Bothma, J. P., Norstad, M. R., Alamos, S. & Garcia, H. G. LlamaTags: A Versatile Tool to Image
Transcription Factor Dynamics in Live Embryos. *Cell* **173**, 1810-1822 e1816,
doi:10.1016/j.cell.2018.03.069 (2018).
- 324 Harmansa, S., Alborelli, I., Bieli, D., Caussin, E. & Affolter, M. A nanobody-based toolset to
investigate the role of protein localization and dispersal in *Drosophila*. *Elife* **6**,
doi:10.7554/eLife.22549 (2017).
- 325 Gomes, J. R. *et al.* Delivery of an anti-transthyretin Nanobody to the brain through intranasal
administration reveals transthyretin expression and secretion by motor neurons. *J Neurochem*
145, 393-408, doi:10.1111/jnc.14332 (2018).
- 326 Gorshkova, E. N. *et al.* Properties of Fluorescent Far-Red Anti-TNF Nanobodies. *Antibodies* **7**, 43
(2018).
- 327 Rajan, M. *et al.* Generation of an alpaca-derived nanobody recognizing gamma-H2AX. *FEBS Open
Bio* **5**, 779-788, doi:10.1016/j.fob.2015.09.005 (2015).
- 328 Nalbant, P., Hodgson, L., Kraynov, V., Touthkine, A. & Hahn, K. M. Activation of endogenous
Cdc42 visualized in living cells. *Science* **305**, 1615-1619, doi:10.1126/science.1100367 (2004).
- 329 Renard, M., Belkadi, L. & Bedouelle, H. Deriving topological constraints from functional data for
the design of reagentless fluorescent immunosensors. *Journal of molecular biology* **326**, 167-175
(2003).
- 330 Ueda, H. & Dong, J. From fluorescence polarization to Quenchbody: Recent progress in
fluorescent reagentless biosensors based on antibody and other binding proteins. *Biochimica et
biophysica acta* **1844**, 1951-1959, doi:10.1016/j.bbapap.2014.06.005 (2014).
- 331 Kummer, L. *et al.* Knowledge-based design of a biosensor to quantify localized ERK activation in
living cells. *Chemistry & biology* **20**, 847-856, doi:10.1016/j.chembiol.2013.04.016 (2013).
- 332 Gulyani, A. *et al.* A biosensor generated via high-throughput screening quantifies cell edge Src
dynamics. *Nature chemical biology* **7**, 437-444, doi:10.1038/nchembio.585 (2011).

- 333 Brient-Litzler, E., Pluckthun, A. & Bedouelle, H. Knowledge-based design of reagentless fluorescent biosensors from a designed ankyrin repeat protein. *Protein Eng Des Sel* **23**, 229-241, doi:10.1093/protein/gzp074 (2010).
- 334 Tang, J. C. *et al.* Detection and manipulation of live antigen-expressing cells using conditionally stable nanobodies. *Elife* **5**, doi:10.7554/eLife.15312 (2016).
- 335 Keller, B. M. *et al.* Chromobodies to Quantify Changes of Endogenous Protein Concentration in Living Cells. *Molecular & cellular proteomics : MCP* **17**, 2518-2533, doi:10.1074/mcp.TIR118.000914 (2018).
- 336 de Bruin, R. C. G. *et al.* Highly specific and potently activating Vgamma9Vdelta2-T cell specific nanobodies for diagnostic and therapeutic applications. *Clin Immunol* **169**, 128-138, doi:10.1016/j.clim.2016.06.012 (2016).
- 337 Peyrassol, X. *et al.* Development by Genetic Immunization of Monovalent Antibodies (Nanobodies) Behaving as Antagonists of the Human ChemR23 Receptor. *J Immunol* **196**, 2893-2901, doi:10.4049/jimmunol.1500888 (2016).
- 338 Peyrassol, X. *et al.* Development by Genetic Immunization of Monovalent Antibodies Against Human Vasoactive Intestinal Peptide Receptor 1 (VPAC1), New Innovative, and Versatile Tools to Study VPAC1 Receptor Function. *Front Endocrinol (Lausanne)* **9**, 153, doi:10.3389/fendo.2018.00153 (2018).
- 339 Fang, T. *et al.* Nanobody immunostaining for correlated light and electron microscopy with preservation of ultrastructure. *Nature methods* **15**, 1029-1032, doi:10.1038/s41592-018-0177-x (2018).
- 340 Pleiner, T., Bates, M. & Gorlich, D. A toolbox of anti-mouse and anti-rabbit IgG secondary nanobodies. *The Journal of cell biology* **217**, 1143-1154, doi:10.1083/jcb.201709115 (2018).
- 341 Schumacher, D., Helma, J., Schneider, A. F. L., Leonhardt, H. & Hackenberger, C. P. R. Nanobodies: Chemical Functionalization Strategies and Intracellular Applications. *Angewandte Chemie* **57**, 2314-2333, doi:10.1002/anie.201708459 (2018).
- 342 Pleiner, T. *et al.* Nanobodies: site-specific labeling for super-resolution imaging, rapid epitope-mapping and native protein complex isolation. *Elife* **4**, e11349, doi:10.7554/eLife.11349 (2015).
- 343 Ries, J., Kaplan, C., Platonova, E., Eghlidi, H. & Ewers, H. A simple, versatile method for GFP-based super-resolution microscopy via nanobodies. *Nature methods* **9**, 582-584, doi:10.1038/nmeth.1991 (2012).
- 344 Moore, R. P. & Legant, W. R. Improving probes for super-resolution. *Nature methods* **15**, 659-660, doi:10.1038/s41592-018-0120-1 (2018).
- 345 Jungmann, R. *et al.* Single-molecule kinetics and super-resolution microscopy by fluorescence imaging of transient binding on DNA origami. *Nano Lett* **10**, 4756-4761, doi:10.1021/nl103427w (2010).
- 346 Schlichthaerle, T. *et al.* Site-Specific Labeling of Affimers for DNA-PAINT Microscopy. *Angewandte Chemie* **57**, 11060-11063, doi:10.1002/anie.201804020 (2018).
- 347 Nieves, D. J., Gaus, K. & Baker, M. A. B. DNA-Based Super-Resolution Microscopy: DNA-PAINT. *Genes (Basel)* **9**, doi:10.3390/genes9120621 (2018).
- 348 Agasti, S. S. *et al.* DNA-barcoded labeling probes for highly multiplexed Exchange-PAINT imaging. *Chem Sci* **8**, 3080-3091, doi:10.1039/c6sc05420j (2017).
- 349 Schueder, F. *et al.* Universal Super-Resolution Multiplexing by DNA Exchange. *Angewandte Chemie* **56**, 4052-4055, doi:10.1002/anie.201611729 (2017).
- 350 Kijanka, M. *et al.* A novel immuno-gold labeling protocol for nanobody-based detection of HER2 in breast cancer cells using immuno-electron microscopy. *J Struct Biol* **199**, 1-11, doi:10.1016/j.jsb.2017.05.008 (2017).

- 351 Ariotti, N. *et al.* Modular Detection of GFP-Labeled Proteins for Rapid Screening by Electron
Microscopy in Cells and Organisms. *Dev Cell* **35**, 513-525, doi:10.1016/j.devcel.2015.10.016
(2015).
- 352 Ariotti, N. *et al.* Ultrastructural localisation of protein interactions using conditionally stable
nanobodies. *PLoS Biol* **16**, e2005473, doi:10.1371/journal.pbio.2005473 (2018).
- 353 Herce, H. D., Deng, W., Helma, J., Leonhardt, H. & Cardoso, M. C. Visualization and targeted
disruption of protein interactions in living cells. *Nature communications* **4**, 2660,
doi:10.1038/ncomms3660 (2013).
- 354 Kirchofer, A. *et al.* Modulation of protein properties in living cells using nanobodies. *Nature
structural & molecular biology* **17**, 133-138, doi:10.1038/nsmb.1727 (2010).
- 355 Kunzl, F., Fruholz, S., Fassler, F., Li, B. & Pimpl, P. Receptor-mediated sorting of soluble vacuolar
proteins ends at the trans-Golgi network/early endosome. *Nat Plants* **2**, 16017,
doi:10.1038/nplants.2016.17 (2016).
- 356 Drees, C. *et al.* Engineered Upconversion Nanoparticles for Resolving Protein Interactions inside
Living Cells. *Angewandte Chemie* **55**, 11668-11672, doi:10.1002/anie.201603028 (2016).
- 357 Li, J. W. *et al.* Molecular imprint of enzyme active site by camel nanobodies: rapid and efficient
approach to produce abzymes with alliinase activity. *The Journal of biological chemistry* **287**,
13713-13721, doi:10.1074/jbc.M111.336370 (2012).
- 358 Kromann-Hansen, T. *et al.* A Camelid-derived Antibody Fragment Targeting the Active Site of a
Serine Protease Balances between Inhibitor and Substrate Behavior. *The Journal of biological
chemistry* **291**, 15156-15168, doi:10.1074/jbc.M116.732503 (2016).
- 359 Vercruyse, T., Pardon, E., Vanstreels, E., Steyaert, J. & Daelemans, D. An intrabody based on a
llama single-domain antibody targeting the N-terminal alpha-helical multimerization domain of
HIV-1 rev prevents viral production. *The Journal of biological chemistry* **285**, 21768-21780,
doi:10.1074/jbc.M110.112490 (2010).
- 360 Schoonaert, L. *et al.* Identification and characterization of Nanobodies targeting the EphA4
receptor. *The Journal of biological chemistry* **292**, 11452-11465, doi:10.1074/jbc.M116.774141
(2017).
- 361 Bradley, M. E. *et al.* Potent and efficacious inhibition of CXCR2 signaling by biparatopic
nanobodies combining two distinct modes of action. *Molecular pharmacology* **87**, 251-262,
doi:10.1124/mol.114.094821 (2015).
- 362 Van den Abbeele, A. *et al.* A llama-derived gelsolin single-domain antibody blocks gelsolin-G-
actin interaction. *Cellular and molecular life sciences : CMLS* **67**, 1519-1535, doi:10.1007/s00018-
010-0266-1 (2010).
- 363 Danquah, W. *et al.* Nanobodies that block gating of the P2X7 ion channel ameliorate
inflammation. *Sci Transl Med* **8**, 366ra162, doi:10.1126/scitranslmed.aaf8463 (2016).
- 364 Scholler, P. *et al.* Allosteric nanobodies uncover a role of hippocampal mGlu2 receptor
homodimers in contextual fear consolidation. *Nature communications* **8**, 1967,
doi:10.1038/s41467-017-01489-1 (2017).
- 365 Truttmann, M. C. *et al.* HypE-specific nanobodies as tools to modulate HypE-mediated target
AMPylation. *The Journal of biological chemistry* **290**, 9087-9100, doi:10.1074/jbc.M114.634287
(2015).
- 366 Mishra, N. *et al.* Increased zymogen activity of thrombin-activatable fibrinolysis inhibitor
prolongs clot lysis. *J Thromb Haemost* **10**, 1091-1099, doi:10.1111/j.1538-7836.2012.04738.x
(2012).
- 367 Li, J. *et al.* Single domain antibody-based bispecific antibody induces potent specific anti-tumor
activity. *Cancer biology & therapy* **17**, 1231-1239, doi:10.1080/15384047.2016.1235659 (2016).

- 368 Van Audenhove, I. *et al.* Stratifying fascin and cortactin function in invadopodium formation using inhibitory nanobodies and targeted subcellular delocalization. *FASEB journal : official publication of the Federation of American Societies for Experimental Biology* **28**, 1805-1818, doi:10.1096/fj.13-242537 (2014).
- 369 Vigano, M. A. *et al.* DARPin recognizing mTFP1 as novel reagents for in vitro and in vivo protein manipulations. *Biol Open* **7**, doi:10.1242/bio.036749 (2018).
- 370 Rothbauer, U. *et al.* A versatile nanotrap for biochemical and functional studies with fluorescent fusion proteins. *Molecular & cellular proteomics : MCP* **7**, 282-289, doi:10.1074/mcp.M700342-MCP200 (2008).
- 371 Schornack, S. *et al.* Protein mislocalization in plant cells using a GFP-binding chromobody. *The Plant journal : for cell and molecular biology* **60**, 744-754, doi:10.1111/j.1365-313X.2009.03982.x (2009).
- 372 Haruki, H., Nishikawa, J. & Laemmli, U. K. The anchor-away technique: rapid, conditional establishment of yeast mutant phenotypes. *Molecular cell* **31**, 925-932, doi:10.1016/j.molcel.2008.07.020 (2008).
- 373 Robinson, M. S. & Hirst, J. Rapid inactivation of proteins by knocksideways. *Curr Protoc Cell Biol* **61**, 15 20 11-17, doi:10.1002/0471143030.cb1520s61 (2013).
- 374 Adli, M. The CRISPR tool kit for genome editing and beyond. *Nature communications* **9**, 1911, doi:10.1038/s41467-018-04252-2 (2018).
- 375 El-Brolosy, M. A. & Stainier, D. Y. R. Genetic compensation: A phenomenon in search of mechanisms. *PLoS genetics* **13**, e1006780, doi:10.1371/journal.pgen.1006780 (2017).
- 376 Kim, D. & Rossi, J. RNAi mechanisms and applications. *BioTechniques* **44**, 613-616, doi:10.2144/000112792 (2008).
- 377 Fire, A. *et al.* Potent and specific genetic interference by double-stranded RNA in *Caenorhabditis elegans*. *Nature* **391**, 806-811, doi:10.1038/35888 (1998).
- 378 Heasman, J., Kofron, M. & Wylie, C. Beta-catenin signaling activity dissected in the early *Xenopus* embryo: a novel antisense approach. *Dev Biol* **222**, 124-134, doi:10.1006/dbio.2000.9720 (2000).
- 379 Summerton, J. & Weller, D. Morpholino antisense oligomers: design, preparation, and properties. *Antisense Nucleic Acid Drug Dev* **7**, 187-195, doi:10.1089/oli.1.1997.7.187 (1997).
- 380 Blum, M., De Robertis, E. M., Wallingford, J. B. & Niehrs, C. Morpholinos: Antisense and Sensibility. *Dev Cell* **35**, 145-149, doi:10.1016/j.devcel.2015.09.017 (2015).
- 381 Moore, C. B., Guthrie, E. H., Huang, M. T. & Taxman, D. J. Short hairpin RNA (shRNA): design, delivery, and assessment of gene knockdown. *Methods Mol Biol* **629**, 141-158, doi:10.1007/978-1-60761-657-3_10 (2010).
- 382 Kisielow, M., Kleiner, S., Nagasawa, M., Faisal, A. & Nagamine, Y. Isoform-specific knockdown and expression of adaptor protein ShcA using small interfering RNA. *The Biochemical journal* **363**, 1-5 (2002).
- 383 Deng, Y. *et al.* Therapeutic potentials of gene silencing by RNA interference: principles, challenges, and new strategies. *Gene* **538**, 217-227, doi:10.1016/j.gene.2013.12.019 (2014).
- 384 Huntzinger, E. & Izaurralde, E. Gene silencing by microRNAs: contributions of translational repression and mRNA decay. *Nat Rev Genet* **12**, 99-110, doi:10.1038/nrg2936 (2011).
- 385 Hannus, M. *et al.* siPools: highly complex but accurately defined siRNA pools eliminate off-target effects. *Nucleic acids research* **42**, 8049-8061, doi:10.1093/nar/gku480 (2014).
- 386 Kok, F. O. *et al.* Reverse genetic screening reveals poor correlation between morpholino-induced and mutant phenotypes in zebrafish. *Dev Cell* **32**, 97-108, doi:10.1016/j.devcel.2014.11.018 (2015).

- 387 Gentsch, G. E. *et al.* Innate Immune Response and Off-Target Mis-splicing Are Common Morpholino-Induced Side Effects in *Xenopus*. *Dev Cell* **44**, 597-610 e510, doi:10.1016/j.devcel.2018.01.022 (2018).
- 388 Stainier, D. Y., Kontarakis, Z. & Rossi, A. Making sense of anti-sense data. *Dev Cell* **32**, 7-8, doi:10.1016/j.devcel.2014.12.012 (2015).
- 389 Kurreck, J. siRNA efficiency: structure or sequence-that is the question. *J Biomed Biotechnol* **2006**, 83757, doi:10.1155/JBB/2006/83757 (2006).
- 390 Pan, W. J., Chen, C. W. & Chu, Y. W. siPRED: predicting siRNA efficacy using various characteristic methods. *PLoS one* **6**, e27602, doi:10.1371/journal.pone.0027602 (2011).
- 391 He, F. *et al.* Predicting siRNA efficacy based on multiple selective siRNA representations and their combination at score level. *Scientific reports* **7**, 44836, doi:10.1038/srep44836 (2017).
- 392 Campbell, A. E. & Bennett, D. Targeting protein function: the expanding toolkit for conditional disruption. *The Biochemical journal* **473**, 2573-2589, doi:10.1042/BCJ20160240 (2016).
- 393 Bachmair, A., Finley, D. & Varshavsky, A. In vivo half-life of a protein is a function of its amino-terminal residue. *Science* **234**, 179-186 (1986).
- 394 Varshavsky, A. The N-end rule pathway and regulation by proteolysis. *Protein science : a publication of the Protein Society* **20**, 1298-1345, doi:10.1002/pro.666 (2011).
- 395 Dohmen, R. J., Wu, P. & Varshavsky, A. Heat-inducible degron: a method for constructing temperature-sensitive mutants. *Science* **263**, 1273-1276 (1994).
- 396 Johnston, J. A., Johnson, E. S., Waller, P. R. & Varshavsky, A. Methotrexate inhibits proteolysis of dihydrofolate reductase by the N-end rule pathway. *The Journal of biological chemistry* **270**, 8172-8178 (1995).
- 397 Banaszynski, L. A., Chen, L. C., Maynard-Smith, L. A., Ooi, A. G. & Wandless, T. J. A rapid, reversible, and tunable method to regulate protein function in living cells using synthetic small molecules. *Cell* **126**, 995-1004, doi:10.1016/j.cell.2006.07.025 (2006).
- 398 Taxis, C., Stier, G., Spadaccini, R. & Knop, M. Efficient protein depletion by genetically controlled deprotection of a dormant N-degron. *Mol Syst Biol* **5**, 267, doi:10.1038/msb.2009.25 (2009).
- 399 Chung, H. K. *et al.* Tunable and reversible drug control of protein production via a self-excising degron. *Nature chemical biology* **11**, 713-720, doi:10.1038/nchembio.1869 (2015).
- 400 Nishimura, K., Fukagawa, T., Takisawa, H., Kakimoto, T. & Kanemaki, M. An auxin-based degron system for the rapid depletion of proteins in nonplant cells. *Nature methods* **6**, 917-922, doi:10.1038/nmeth.1401 (2009).
- 401 Iwamoto, M., Bjorklund, T., Lundberg, C., Kirik, D. & Wandless, T. J. A general chemical method to regulate protein stability in the mammalian central nervous system. *Chemistry & biology* **17**, 981-988, doi:10.1016/j.chembiol.2010.07.009 (2010).
- 402 Bongor, K. M., Rakhit, R., Payumo, A. Y., Chen, J. K. & Wandless, T. J. General method for regulating protein stability with light. *ACS chemical biology* **9**, 111-115, doi:10.1021/cb400755b (2014).
- 403 Renicke, C., Schuster, D., Usherenko, S., Essen, L. O. & Taxis, C. A LOV2 domain-based optogenetic tool to control protein degradation and cellular function. *Chemistry & biology* **20**, 619-626, doi:10.1016/j.chembiol.2013.03.005 (2013).
- 404 Pratt, M. R., Schwartz, E. C. & Muir, T. W. Small-molecule-mediated rescue of protein function by an inducible proteolytic shunt. *Proceedings of the National Academy of Sciences of the United States of America* **104**, 11209-11214, doi:10.1073/pnas.0700816104 (2007).
- 405 Janse, D. M., Crosas, B., Finley, D. & Church, G. M. Localization to the proteasome is sufficient for degradation. *The Journal of biological chemistry* **279**, 21415-21420, doi:10.1074/jbc.M402954200 (2004).

- 406 Morreale, F. E. & Walden, H. Types of Ubiquitin Ligases. *Cell* **165**, 248-248 e241, doi:10.1016/j.cell.2016.03.003 (2016).
- 407 McDowell, G. S. & Philpott, A. Non-canonical ubiquitylation: mechanisms and consequences. *The international journal of biochemistry & cell biology* **45**, 1833-1842, doi:10.1016/j.biocel.2013.05.026 (2013).
- 408 Yau, R. & Rape, M. The increasing complexity of the ubiquitin code. *Nature cell biology* **18**, 579-586, doi:10.1038/ncb3358 (2016).
- 409 Shah, S. A., Potter, M. W. & Callery, M. P. Ubiquitin proteasome pathway: implications and advances in cancer therapy. *Surg Oncol* **10**, 43-52 (2001).
- 410 Sakamoto, K. M. *et al.* Protacs: chimeric molecules that target proteins to the Skp1-Cullin-F box complex for ubiquitination and degradation. *Proceedings of the National Academy of Sciences of the United States of America* **98**, 8554-8559, doi:10.1073/pnas.141230798 (2001).
- 411 Neklesa, T. K., Winkler, J. D. & Crews, C. M. Targeted protein degradation by PROTACs. *Pharmacol Ther* **174**, 138-144, doi:10.1016/j.pharmthera.2017.02.027 (2017).
- 412 Gu, S., Cui, D., Chen, X., Xiong, X. & Zhao, Y. PROTACs: An Emerging Targeting Technique for Protein Degradation in Drug Discovery. *Bioessays* **40**, e1700247, doi:10.1002/bies.201700247 (2018).
- 413 Zhou, P., Bogacki, R., McReynolds, L. & Howley, P. M. Harnessing the ubiquitination machinery to target the degradation of specific cellular proteins. *Molecular cell* **6**, 751-756 (2000).
- 414 Cong, F., Zhang, J., Pao, W., Zhou, P. & Varmus, H. A protein knockdown strategy to study the function of beta-catenin in tumorigenesis. *BMC Mol Biol* **4**, 10, doi:10.1186/1471-2199-4-10 (2003).
- 415 Su, Y., Ishikawa, S., Kojima, M. & Liu, B. Eradication of pathogenic beta-catenin by Skp1/Cullin/F box ubiquitination machinery. *Proceedings of the National Academy of Sciences of the United States of America* **100**, 12729-12734, doi:10.1073/pnas.2133261100 (2003).
- 416 Zhang, J., Zheng, N. & Zhou, P. Exploring the functional complexity of cellular proteins by protein knockout. *Proceedings of the National Academy of Sciences of the United States of America* **100**, 14127-14132, doi:10.1073/pnas.2233012100 (2003).
- 417 Cohen, J. C. *et al.* Transient in utero knockout (TIUKO) of C-MYC affects late lung and intestinal development in the mouse. *BMC Dev Biol* **4**, 4, doi:10.1186/1471-213X-4-4 (2004).
- 418 Hatakeyama, S., Watanabe, M., Fujii, Y. & Nakayama, K. I. Targeted destruction of c-Myc by an engineered ubiquitin ligase suppresses cell transformation and tumor formation. *Cancer research* **65**, 7874-7879, doi:10.1158/0008-5472.CAN-05-1581 (2005).
- 419 Ma, Y. *et al.* Targeted degradation of KRAS by an engineered ubiquitin ligase suppresses pancreatic cancer cell growth in vitro and in vivo. *Molecular cancer therapeutics* **12**, 286-294, doi:10.1158/1535-7163.MCT-12-0650 (2013).
- 420 Kong, F. *et al.* Engineering a single ubiquitin ligase for the selective degradation of all activated ErbB receptor tyrosine kinases. *Oncogene* **33**, 986-995, doi:10.1038/onc.2013.33 (2014).
- 421 Liu, J., Stevens, J., Matsunami, N. & White, R. L. Targeted degradation of beta-catenin by chimeric F-box fusion proteins. *Biochemical and biophysical research communications* **313**, 1023-1029 (2004).
- 422 Chen, W., Lee, J., Cho, S. Y. & Fine, H. A. Proteasome-mediated destruction of the cyclin a/cyclin-dependent kinase 2 complex suppresses tumor cell growth in vitro and in vivo. *Cancer research* **64**, 3949-3957, doi:10.1158/0008-5472.CAN-03-3906 (2004).
- 423 Colas, P., Cohen, B., Ko Ferrigno, P., Silver, P. A. & Brent, R. Targeted modification and transportation of cellular proteins. *Proceedings of the National Academy of Sciences of the United States of America* **97**, 13720-13725, doi:10.1073/pnas.97.25.13720 (2000).

- 424 Caussinus, E., Kanca, O. & Affolter, M. Fluorescent fusion protein knockout mediated by anti-GFP nanobody. *Nature structural & molecular biology* **19**, 117-121, doi:10.1038/nsmb.2180 (2012).
- 425 Portnoff, A. D., Stephens, E. A., Varner, J. D. & DeLisa, M. P. Ubiquibodies, synthetic E3 ubiquitin ligases endowed with unnatural substrate specificity for targeted protein silencing. *The Journal of biological chemistry* **289**, 7844-7855, doi:10.1074/jbc.M113.544825 (2014).
- 426 Zuin, A., Isasa, M. & Crosas, B. Ubiquitin signaling: extreme conservation as a source of diversity. *Cells* **3**, 690-701, doi:10.3390/cells3030690 (2014).
- 427 Baudisch, B., Pfort, I., Sorge, E. & Conrad, U. Nanobody-Directed Specific Degradation of Proteins by the 26S-Proteasome in Plants. *Frontiers in plant science* **9**, 130, doi:10.3389/fpls.2018.00130 (2018).
- 428 Shin, Y. J. *et al.* Nanobody-targeted E3-ubiquitin ligase complex degrades nuclear proteins. *Scientific reports* **5**, 14269, doi:10.1038/srep14269 (2015).
- 429 Fulcher, L. J. *et al.* An affinity-directed protein missile system for targeted proteolysis. *Open Biol* **6**, doi:10.1098/rsob.160255 (2016).
- 430 Kanner, S. A., Morgenstern, T. & Colecraft, H. M. Sculpting ion channel functional expression with engineered ubiquitin ligases. *Elife* **6**, doi:10.7554/eLife.29744 (2017).
- 431 Komander, D. The emerging complexity of protein ubiquitination. *Biochem Soc Trans* **37**, 937-953, doi:10.1042/BST0370937 (2009).
- 432 Daniel, K. *et al.* Conditional control of fluorescent protein degradation by an auxin-dependent nanobody. *Nature communications* **9**, 3297, doi:10.1038/s41467-018-05855-5 (2018).
- 433 Kubota, T., Nishimura, K., Kanemaki, M. T. & Donaldson, A. D. The Elg1 replication factor C-like complex functions in PCNA unloading during DNA replication. *Molecular cell* **50**, 273-280, doi:10.1016/j.molcel.2013.02.012 (2013).
- 434 Clift, D. *et al.* A Method for the Acute and Rapid Degradation of Endogenous Proteins. *Cell* **171**, 1692-1706 e1618, doi:10.1016/j.cell.2017.10.033 (2017).
- 435 Clift, D., So, C., McEwan, W. A., James, L. C. & Schuh, M. Acute and rapid degradation of endogenous proteins by Trim-Away. *Nature protocols* **13**, 2149-2175, doi:10.1038/s41596-018-0028-3 (2018).
- 436 Foss, S., Watkinson, R., Sandlie, I., James, L. C. & Andersen, J. T. TRIM21: a cytosolic Fc receptor with broad antibody isotype specificity. *Immunological reviews* **268**, 328-339, doi:10.1111/imr.12363 (2015).
- 437 Keeble, A. H., Khan, Z., Forster, A. & James, L. C. TRIM21 is an IgG receptor that is structurally, thermodynamically, and kinetically conserved. *Proceedings of the National Academy of Sciences of the United States of America* **105**, 6045-6050, doi:10.1073/pnas.0800159105 (2008).
- 438 Harwood, N. E. & Batista, F. D. Early events in B cell activation. *Annual review of immunology* **28**, 185-210, doi:10.1146/annurev-immunol-030409-101216 (2010).
- 439 Schafer, Z. T. & Kornbluth, S. The apoptosome: physiological, developmental, and pathological modes of regulation. *Dev Cell* **10**, 549-561, doi:10.1016/j.devcel.2006.04.008 (2006).
- 440 Broz, P. & Dixit, V. M. Inflammasomes: mechanism of assembly, regulation and signalling. *Nature reviews. Immunology* **16**, 407-420, doi:10.1038/nri.2016.58 (2016).
- 441 Wehr, M. C. & Rossner, M. J. Split protein biosensor assays in molecular pharmacological studies. *Drug discovery today* **21**, 415-429, doi:10.1016/j.drudis.2015.11.004 (2016).
- 442 Shekhawat, S. S. & Ghosh, I. Split-protein systems: beyond binary protein-protein interactions. *Current opinion in chemical biology* **15**, 789-797, doi:10.1016/j.cbpa.2011.10.014 (2011).
- 443 Johnsson, N. & Varshavsky, A. Split ubiquitin as a sensor of protein interactions in vivo. *Proceedings of the National Academy of Sciences of the United States of America* **91**, 10340-10344 (1994).

- 444 Ghosh, I., Hamilton, A. D. & Regan, L. Antiparallel Leucine Zipper-Directed Protein Reassembly: Application to the Green Fluorescent Protein. *Journal of the American Chemical Society* **122**, 5658-5659, doi:10.1021/ja994421w (2000).
- 445 Chiu, H. Y. *et al.* Nanoparticle mediated delivery and small molecule triggered activation of proteins in the nucleus. *Nucleus* **9**, 530-542, doi:10.1080/19491034.2018.1523665 (2018).
- 446 Straathof, K. C. *et al.* An inducible caspase 9 safety switch for T-cell therapy. *Blood* **105**, 4247-4254, doi:10.1182/blood-2004-11-4564 (2005).
- 447 Fields, S. & Song, O. A novel genetic system to detect protein-protein interactions. *Nature* **340**, 245-246, doi:10.1038/340245a0 (1989).
- 448 Scheller, L., Strittmatter, T., Fuchs, D., Bojar, D. & Fussenegger, M. Generalized extracellular molecule sensor platform for programming cellular behavior. *Nature chemical biology* **14**, 723-729, doi:10.1038/s41589-018-0046-z (2018).
- 449 Bojar, D., Scheller, L., Hamri, G. C., Xie, M. & Fussenegger, M. Caffeine-inducible gene switches controlling experimental diabetes. *Nature communications* **9**, 2318, doi:10.1038/s41467-018-04744-1 (2018).
- 450 Cartwright, A. N., Griggs, J. & Davis, D. M. The immune synapse clears and excludes molecules above a size threshold. *Nature communications* **5**, 5479, doi:10.1038/ncomms6479 (2014).
- 451 Keyaerts, M. *et al.* Phase I Study of 68Ga-HER2-Nanobody for PET/CT Assessment of HER2 Expression in Breast Carcinoma. *J Nucl Med* **57**, 27-33, doi:10.2967/jnumed.115.162024 (2016).
- 452 Oliveira, S. *et al.* Rapid visualization of human tumor xenografts through optical imaging with a near-infrared fluorescent anti-epidermal growth factor receptor nanobody. *Molecular imaging* **11**, 33-46 (2012).
- 453 Van Heeke, G. *et al.* Nanobodies(R) as inhaled biotherapeutics for lung diseases. *Pharmacol Ther* **169**, 47-56, doi:10.1016/j.pharmthera.2016.06.012 (2017).
- 454 Pant, N. *et al.* Lactobacilli expressing variable domain of llama heavy-chain antibody fragments (lactobodies) confer protection against rotavirus-induced diarrhea. *The Journal of infectious diseases* **194**, 1580-1588, doi:10.1086/508747 (2006).
- 455 Gurbatri, C. *et al.* Engineered probiotics for local tumor delivery of checkpoint blockade nanobodies. *bioRxiv*, 562785, doi:10.1101/562785 (2019).
- 456 Kontermann, R. E. Strategies to extend plasma half-lives of recombinant antibodies. *BioDrugs* **23**, 93-109, doi:10.2165/00063030-200923020-00003 (2009).
- 457 Tijink, B. M. *et al.* Improved tumor targeting of anti-epidermal growth factor receptor Nanobodies through albumin binding: taking advantage of modular Nanobody technology. *Molecular cancer therapeutics* **7**, 2288-2297, doi:10.1158/1535-7163.MCT-07-2384 (2008).
- 458 Lo, A. W. *et al.* The molecular mechanism of Shiga toxin Stx2e neutralization by a single-domain antibody targeting the cell receptor-binding domain. *The Journal of biological chemistry* **289**, 25374-25381, doi:10.1074/jbc.M114.566257 (2014).
- 459 Ardekani, L. S. *et al.* A novel nanobody against urease activity of Helicobacter pylori. *Int J Infect Dis* **17**, e723-728, doi:10.1016/j.ijid.2013.02.015 (2013).
- 460 Sun, X. *et al.* PD-L1 Nanobody Competitively Inhibits the Formation of the PD-1/PD-L1 Complex: Comparative Molecular Dynamics Simulations. *International journal of molecular sciences* **19**, doi:10.3390/ijms19071984 (2018).
- 461 Schepens, B. *et al.* Nanobodies(R) specific for respiratory syncytial virus fusion protein protect against infection by inhibition of fusion. *The Journal of infectious diseases* **204**, 1692-1701, doi:10.1093/infdis/jir622 (2011).
- 462 Finan, C. *et al.* The druggable genome and support for target identification and validation in drug development. *Sci Transl Med* **9**, doi:10.1126/scitranslmed.aag1166 (2017).

- 463 Dang, C. V., Reddy, E. P., Shokat, K. M. & Soucek, L. Drugging the 'undruggable' cancer targets. *Nat Rev Cancer* **17**, 502-508, doi:10.1038/nrc.2017.36 (2017).
- 464 Singh, S. *et al.* Monoclonal Antibodies: A Review. *Curr Clin Pharmacol* **13**, 85-99, doi:10.2174/1574884712666170809124728 (2018).
- 465 de Bruin, R. C. G. *et al.* A bispecific nanobody approach to leverage the potent and widely applicable tumor cytolytic capacity of Vgamma9Vdelta2-T cells. *Oncoimmunology* **7**, e1375641, doi:10.1080/2162402X.2017.1375641 (2017).
- 466 Xing, J. *et al.* BiHC, a T-Cell-Engaging Bispecific Recombinant Antibody, Has Potent Cytotoxic Activity Against Her2 Tumor Cells. *Transl Oncol* **10**, 780-785, doi:10.1016/j.tranon.2017.07.003 (2017).
- 467 Lin, L. *et al.* A HER2 bispecific antibody can be efficiently expressed in Escherichia coli with potent cytotoxicity. *Oncol Lett* **16**, 1259-1266, doi:10.3892/ol.2018.8698 (2018).
- 468 Molgaard, K. *et al.* Bispecific light T-cell engagers for gene-based immunotherapy of epidermal growth factor receptor (EGFR)-positive malignancies. *Cancer Immunol Immunother* **67**, 1251-1260, doi:10.1007/s00262-018-2181-5 (2018).
- 469 Chanier, T. & Chames, P. Nanobody Engineering: Toward Next Generation Immunotherapies and Immunoimaging of Cancer. *Antibodies* **8**, 13 (2019).
- 470 Van de Broek, B. *et al.* Specific cell targeting with nanobody conjugated branched gold nanoparticles for photothermal therapy. *ACS nano* **5**, 4319-4328, doi:10.1021/nn1023363 (2011).
- 471 Wu, T. *et al.* Transglutaminase mediated PEGylation of nanobodies for targeted nano-drug delivery. *Journal of Materials Chemistry B* **6**, 1011-1017, doi:10.1039/C7TB03132G (2018).
- 472 Hu, Y., Liu, C. & Muyldermans, S. Nanobody-Based Delivery Systems for Diagnosis and Targeted Tumor Therapy. *Front Immunol* **8**, 1442, doi:10.3389/fimmu.2017.01442 (2017).
- 473 Altintas, I. *et al.* Nanobody-albumin nanoparticles (NANAPs) for the delivery of a multikinase inhibitor 17864 to EGFR overexpressing tumor cells. *Journal of controlled release : official journal of the Controlled Release Society* **165**, 110-118, doi:10.1016/j.jconrel.2012.11.007 (2013).
- 474 Poulin, K. L. *et al.* Retargeting of adenovirus vectors through genetic fusion of a single-chain or single-domain antibody to capsid protein IX. *Journal of virology* **84**, 10074-10086, doi:10.1128/JVI.02665-09 (2010).
- 475 Kaliberov, S. A. *et al.* Adenoviral targeting using genetically incorporated camelid single variable domains. *Laboratory Investigation* **94**, 893, doi:10.1038/labinvest.2014.82 (2014).
- 476 Oliveira, S. *et al.* Downregulation of EGFR by a novel multivalent nanobody-liposome platform. *Journal of controlled release : official journal of the Controlled Release Society* **145**, 165-175, doi:10.1016/j.jconrel.2010.03.020 (2010).
- 477 Li, N. *et al.* Surfactant protein-A nanobody-conjugated liposomes loaded with methylprednisolone increase lung-targeting specificity and therapeutic effect for acute lung injury. *Drug Deliv* **24**, 1770-1781, doi:10.1080/10717544.2017.1402217 (2017).
- 478 Cortez-Retamozo, V. *et al.* Efficient cancer therapy with a nanobody-based conjugate. *Cancer research* **64**, 2853-2857 (2004).
- 479 Behdani, M. *et al.* Development of VEGFR2-specific Nanobody Pseudomonas exotoxin A conjugated to provide efficient inhibition of tumor cell growth. *N Biotechnol* **30**, 205-209, doi:10.1016/j.nbt.2012.09.002 (2013).
- 480 Fang, T. *et al.* Structurally Defined alphaMHC-II Nanobody-Drug Conjugates: A Therapeutic and Imaging System for B-Cell Lymphoma. *Angewandte Chemie* **55**, 2416-2420, doi:10.1002/anie.201509432 (2016).
- 481 D'Huyvetter, M. *et al.* Targeted radionuclide therapy with A 177Lu-labeled anti-HER2 nanobody. *Theranostics* **4**, 708-720, doi:10.7150/thno.8156 (2014).

- 482 Debie, P., Devoogdt, N. & Hernot, S. Targeted Nanobody-Based Molecular Tracers for Nuclear
Imaging and Image-Guided Surgery. *Antibodies* **8**, 12 (2019).
- 483 Kijanka, M. *et al.* Rapid optical imaging of human breast tumour xenografts using anti-HER2
VHHs site-directly conjugated to IRDye 800CW for image-guided surgery. *Eur J Nucl Med Mol
Imaging* **40**, 1718-1729, doi:10.1007/s00259-013-2471-2 (2013).
- 484 Debie, P. *et al.* Improved Debulking of Peritoneal Tumor Implants by Near-Infrared Fluorescent
Nanobody Image Guidance in an Experimental Mouse Model. *Mol Imaging Biol* **20**, 361-367,
doi:10.1007/s11307-017-1134-2 (2018).
- 485 van Driel, P. *et al.* EGFR targeted nanobody-photosensitizer conjugates for photodynamic
therapy in a pre-clinical model of head and neck cancer. *Journal of controlled release : official
journal of the Controlled Release Society* **229**, 93-105, doi:10.1016/j.jconrel.2016.03.014 (2016).
- 486 Iri-Sofla, F. J., Rahbarizadeh, F., Ahmadvand, D. & Rasaei, M. J. Nanobody-based chimeric
receptor gene integration in Jurkat cells mediated by phiC31 integrase. *Exp Cell Res* **317**, 2630-
2641, doi:10.1016/j.yexcr.2011.08.015 (2011).
- 487 Hassani, M. *et al.* Construction of a chimeric antigen receptor bearing a nanobody against
prostate a specific membrane antigen in prostate cancer. *Journal of cellular biochemistry* **120**,
10787-10795, doi:10.1002/jcb.28370 (2019).
- 488 Xie, Y. J. *et al.* Nanobody-based CAR T cells that target the tumor microenvironment inhibit the
growth of solid tumors in immunocompetent mice. *Proceedings of the National Academy of
Sciences* **116**, 7624-7631, doi:10.1073/pnas.1817147116 (2019).
- 489 Pettitt, D. *et al.* CAR-T Cells: A Systematic Review and Mixed Methods Analysis of the Clinical
Trial Landscape. *Molecular therapy : the journal of the American Society of Gene Therapy* **26**,
342-353, doi:10.1016/j.ymthe.2017.10.019 (2018).
- 490 De Munter, S. *et al.* Nanobody Based Dual Specific CARs. *International journal of molecular
sciences* **19**, doi:10.3390/ijms19020403 (2018).
- 491 Jamnani, F. R. *et al.* T cells expressing VHH-directed oligoclonal chimeric HER2 antigen receptors:
towards tumor-directed oligoclonal T cell therapy. *Biochimica et biophysica acta* **1840**, 378-386,
doi:10.1016/j.bbagen.2013.09.029 (2014).
- 492 Sharifzadeh, Z. *et al.* Genetically engineered T cells bearing chimeric nanoconstructed receptors
harboring TAG-72-specific camelid single domain antibodies as targeting agents. *Cancer letters*
334, 237-244, doi:10.1016/j.canlet.2012.08.010 (2013).
- 493 Redman, J. M., Hill, E. M., AlDeghaither, D. & Weiner, L. M. Mechanisms of action of therapeutic
antibodies for cancer. *Mol Immunol* **67**, 28-45, doi:10.1016/j.molimm.2015.04.002 (2015).
- 494 van de Water, J. A. *et al.* Therapeutic stem cells expressing variants of EGFR-specific nanobodies
have antitumor effects. *Proceedings of the National Academy of Sciences of the United States of
America* **109**, 16642-16647, doi:10.1073/pnas.1202832109 (2012).
- 495 del Rio, B. *et al.* Lactic Acid Bacteria as a Live Delivery System for the in situ Production of
Nanobodies in the Human Gastrointestinal Tract. *Frontiers in Microbiology* **9**,
doi:10.3389/fmicb.2018.03179 (2019).
- 496 Venkatachalam, M. A. & Rennke, H. G. The structural and molecular basis of glomerular
filtration. *Circulation research* **43**, 337-347 (1978).
- 497 Lin, J. H. Pharmacokinetics of biotech drugs: peptides, proteins and monoclonal antibodies. *Curr
Drug Metab* **10**, 661-691 (2009).
- 498 Kontermann, R. E. Strategies for extended serum half-life of protein therapeutics. *Current
opinion in biotechnology* **22**, 868-876, doi:10.1016/j.copbio.2011.06.012 (2011).
- 499 Zhao, G. *et al.* A Novel Nanobody Targeting Middle East Respiratory Syndrome Coronavirus
(MERS-CoV) Receptor-Binding Domain Has Potent Cross-Neutralizing Activity and Protective
Efficacy against MERS-CoV. *Journal of virology* **92**, doi:10.1128/JVI.00837-18 (2018).

- 500 Cantante, C. *et al.* Albumin-binding domain from *Streptococcus zooepidemicus* protein Zag as a novel strategy to improve the half-life of therapeutic proteins. *Journal of biotechnology* **253**, 23-33, doi:10.1016/j.jbiotec.2017.05.017 (2017).
- 501 Harmsen, M. M., Van Solt, C. B., Fijten, H. P. & Van Setten, M. C. Prolonged in vivo residence times of llama single-domain antibody fragments in pigs by binding to porcine immunoglobulins. *Vaccine* **23**, 4926-4934, doi:10.1016/j.vaccine.2005.05.017 (2005).
- 502 Van Roy, M. *et al.* The preclinical pharmacology of the high affinity anti-IL-6R Nanobody(R) ALX-0061 supports its clinical development in rheumatoid arthritis. *Arthritis research & therapy* **17**, 135, doi:10.1186/s13075-015-0651-0 (2015).
- 503 Strohl, W. R. Fusion Proteins for Half-Life Extension of Biologics as a Strategy to Make Biobetters. *BioDrugs* **29**, 215-239, doi:10.1007/s40259-015-0133-6 (2015).
- 504 Hoefman, S., Ottevaere, I., Baumeister, J. & Sargentini-Maier, M. L. Pre-Clinical Intravenous Serum Pharmacokinetics of Albumin Binding and Non-Half-Life Extended Nanobodies®. *Antibodies* **4**, 141-156 (2015).
- 505 Torres, T., Romanelli, M. & Chiricozzi, A. A revolutionary therapeutic approach for psoriasis: bispecific biological agents. *Expert Opin Investig Drugs* **25**, 751-754, doi:10.1080/13543784.2016.1187130 (2016).
- 506 Duncan, R. The dawning era of polymer therapeutics. *Nat Rev Drug Discov* **2**, 347-360, doi:10.1038/nrd1088 (2003).
- 507 Vugmeyster, Y. *et al.* Pharmacokinetic, biodistribution, and biophysical profiles of TNF nanobodies conjugated to linear or branched poly(ethylene glycol). *Bioconjugate chemistry* **23**, 1452-1462, doi:10.1021/bc300066a (2012).
- 508 Wesolowski, J. *et al.* Single domain antibodies: promising experimental and therapeutic tools in infection and immunity. *Med Microbiol Immunol* **198**, 157-174, doi:10.1007/s00430-009-0116-7 (2009).
- 509 Vanmarsenille, C. *et al.* Nanobodies targeting conserved epitopes on the major outer membrane protein of *Campylobacter* as potential tools for control of *Campylobacter* colonization. *Vet Res* **48**, 86, doi:10.1186/s13567-017-0491-9 (2017).
- 510 Wu, Y., Jiang, S. & Ying, T. Single-Domain Antibodies As Therapeutics against Human Viral Diseases. *Front Immunol* **8**, 1802, doi:10.3389/fimmu.2017.01802 (2017).
- 511 De Vlieger, D., Ballegeer, M., Rossey, I., Schepens, B. & Saelens, X. Single-Domain Antibodies and Their Formatting to Combat Viral Infections. *Antibodies* **8**, 1 (2018).
- 512 Stijlemans, B. *et al.* Nanobodies As Tools to Understand, Diagnose, and Treat African Trypanosomiasis. *Frontiers in immunology* **8**, 724-724, doi:10.3389/fimmu.2017.00724 (2017).
- 513 Fernandes, C. F. C. *et al.* Camelid Single-Domain Antibodies As an Alternative to Overcome Challenges Related to the Prevention, Detection, and Control of Neglected Tropical Diseases. *Front Immunol* **8**, 653, doi:10.3389/fimmu.2017.00653 (2017).
- 514 Abskharon, R. N. *et al.* Probing the N-terminal beta-sheet conversion in the crystal structure of the human prion protein bound to a nanobody. *Journal of the American Chemical Society* **136**, 937-944, doi:10.1021/ja407527p (2014).
- 515 Herrera, C., Tremblay, J. M., Shoemaker, C. B. & Mantis, N. J. Mechanisms of Ricin Toxin Neutralization Revealed through Engineered Homodimeric and Heterodimeric Camelid Antibodies. *The Journal of biological chemistry* **290**, 27880-27889, doi:10.1074/jbc.M115.658070 (2015).
- 516 Moayeri, M. *et al.* A heterodimer of a VHH (variable domains of camelid heavy chain-only) antibody that inhibits anthrax toxin cell binding linked to a VHH antibody that blocks oligomer formation is highly protective in an anthrax spore challenge model. *The Journal of biological chemistry* **290**, 6584-6595, doi:10.1074/jbc.M114.627943 (2015).

- 517 Laustsen, A. H. *et al.* Pros and cons of different therapeutic antibody formats for recombinant
antivenom development. *Toxicon* **146**, 151-175, doi:10.1016/j.toxicon.2018.03.004 (2018).
- 518 Laustsen, A. H., Johansen, K. H., Engmark, M. & Andersen, M. R. Recombinant snakebite
antivenoms: A cost-competitive solution to a neglected tropical disease? *PLoS Negl Trop Dis* **11**,
e0005361, doi:10.1371/journal.pntd.0005361 (2017).
- 519 Sadeghian-Rizi, T., Behdani, M., Khanahmad, H., Sadeghi, H. M. & Jahanian-Najafabadi, A.
Generation and Characterization of a Functional Nanobody Against Inflammatory Chemokine
CXCL10, as a Novel Strategy for the Treatment of Multiple Sclerosis. *CNS Neurol Disord Drug
Targets* **18**, 141-148, doi:10.2174/1871527317666181114134518 (2019).
- 520 Caljon, G. *et al.* Using microdialysis to analyse the passage of monovalent nanobodies through
the blood–brain barrier. *British Journal of Pharmacology* **165**, 2341-2353, doi:10.1111/j.1476-
5381.2011.01723.x (2012).
- 521 Bélanger, K. *et al.* Single-Domain Antibodies as Therapeutic and Imaging Agents for the
Treatment of CNS Diseases. *Antibodies* **8**, 27 (2019).
- 522 Scully, M. *et al.* Caplacizumab Treatment for Acquired Thrombotic Thrombocytopenic Purpura.
The New England journal of medicine **380**, 335-346, doi:10.1056/NEJMoa1806311 (2019).
- 523 Lipinski, C. A., Lombardo, F., Dominy, B. W. & Feeney, P. J. Experimental and computational
approaches to estimate solubility and permeability in drug discovery and development settings.
Adv Drug Deliv Rev **46**, 3-26 (2001).
- 524 Yang, N. J. & Hinner, M. J. Getting across the cell membrane: an overview for small molecules,
peptides, and proteins. *Methods Mol Biol* **1266**, 29-53, doi:10.1007/978-1-4939-2272-7_3
(2015).
- 525 Stewart, M. P., Langer, R. & Jensen, K. F. Intracellular Delivery by Membrane Disruption:
Mechanisms, Strategies, and Concepts. *Chemical reviews* **118**, 7409-7531,
doi:10.1021/acs.chemrev.7b00678 (2018).
- 526 Komarova, Y., Peloquin, J. & Borisy, G. Microinjection of protein samples. *CSH Protoc* **2007**, pdb
prot4657, doi:10.1101/pdb.prot4657 (2007).
- 527 Choi, S. O. *et al.* Intracellular protein delivery and gene transfection by electroporation using a
microneedle electrode array. *Small* **8**, 1081-1091, doi:10.1002/smll.201101747 (2012).
- 528 D'Astolfo, D. S. *et al.* Efficient intracellular delivery of native proteins. *Cell* **161**, 674-690,
doi:10.1016/j.cell.2015.03.028 (2015).
- 529 Morris, M. C., Depollier, J., Mery, J., Heitz, F. & Divita, G. A peptide carrier for the delivery of
biologically active proteins into mammalian cells. *Nature biotechnology* **19**, 1173-1176,
doi:10.1038/nbt1201-1173 (2001).
- 530 Fu, A., Tang, R., Hardie, J., Farkas, M. E. & Rotello, V. M. Promises and pitfalls of intracellular
delivery of proteins. *Bioconjugate chemistry* **25**, 1602-1608, doi:10.1021/bc500320j (2014).
- 531 Zhang, Y., Roise, J. J., Lee, K., Li, J. & Murthy, N. Recent developments in intracellular protein
delivery. *Current opinion in biotechnology* **52**, 25-31, doi:10.1016/j.copbio.2018.02.009 (2018).
- 532 Barua, S. & Mitragotri, S. Challenges associated with Penetration of Nanoparticles across Cell
and Tissue Barriers: A Review of Current Status and Future Prospects. *Nano Today* **9**, 223-243,
doi:10.1016/j.nantod.2014.04.008 (2014).
- 533 Alexis, F., Pridgen, E., Molnar, L. K. & Farokhzad, O. C. Factors affecting the clearance and
biodistribution of polymeric nanoparticles. *Mol Pharm* **5**, 505-515, doi:10.1021/mp800051m
(2008).
- 534 Stohrer, M., Boucher, Y., Stangassinger, M. & Jain, R. K. Oncotic pressure in solid tumors is
elevated. *Cancer research* **60**, 4251-4255 (2000).
- 535 Ferrari, M. Frontiers in cancer nanomedicine: directing mass transport through biological
barriers. *Trends in biotechnology* **28**, 181-188, doi:10.1016/j.tibtech.2009.12.007 (2010).

- 536 Blanco, E., Shen, H. & Ferrari, M. Principles of nanoparticle design for overcoming biological
barriers to drug delivery. *Nature biotechnology* **33**, 941-951, doi:10.1038/nbt.3330 (2015).
- 537 Bottger, R., Hoffmann, R. & Knappe, D. Differential stability of therapeutic peptides with
different proteolytic cleavage sites in blood, plasma and serum. *PloS one* **12**, e0178943,
doi:10.1371/journal.pone.0178943 (2017).
- 538 Owens, D. E., 3rd & Peppas, N. A. Opsonization, biodistribution, and pharmacokinetics of
polymeric nanoparticles. *Int J Pharm* **307**, 93-102, doi:10.1016/j.ijpharm.2005.10.010 (2006).
- 539 Moghimi, S. M. & Davis, S. S. Innovations in avoiding particle clearance from blood by Kupffer
cells: cause for reflection. *Crit Rev Ther Drug Carrier Syst* **11**, 31-59 (1994).
- 540 He, X. *et al.* In vivo study of biodistribution and urinary excretion of surface-modified silica
nanoparticles. *Analytical chemistry* **80**, 9597-9603, doi:10.1021/ac801882g (2008).
- 541 Patel, H. M. & Moghimi, S. M. Serum-mediated recognition of liposomes by phagocytic cells of
the reticuloendothelial system - The concept of tissue specificity. *Adv Drug Deliv Rev* **32**, 45-60
(1998).
- 542 Zolnik, B. S., Gonzalez-Fernandez, A., Sadrieh, N. & Dobrovolskaia, M. A. Nanoparticles and the
immune system. *Endocrinology* **151**, 458-465, doi:10.1210/en.2009-1082 (2010).
- 543 Villaverde, G. & Baeza, A. Targeting strategies for improving the efficacy of nanomedicine in
oncology. *Beilstein J Nanotechnol* **10**, 168-181, doi:10.3762/bjnano.10.16 (2019).
- 544 Behzadi, S. *et al.* Cellular uptake of nanoparticles: journey inside the cell. *Chemical Society
reviews* **46**, 4218-4244, doi:10.1039/c6cs00636a (2017).
- 545 Smith, S. A., Selby, L. I., Johnston, A. P. R. & Such, G. K. The Endosomal Escape of Nanoparticles:
Toward More Efficient Cellular Delivery. *Bioconjugate chemistry* **30**, 263-272,
doi:10.1021/acs.bioconjchem.8b00732 (2019).
- 546 Herce, H. D., Rajan, M., Lattig-Tunnemann, G., Fillies, M. & Cardoso, M. C. A novel cell
permeable DNA replication and repair marker. *Nucleus* **5**, 590-600, doi:10.4161/nucl.36290
(2014).
- 547 Slastnikova, T. A., Ulasov, A. V., Rosenkranz, A. A. & Sobolev, A. S. Targeted Intracellular Delivery
of Antibodies: The State of the Art. *Frontiers in pharmacology* **9**, 1208,
doi:10.3389/fphar.2018.01208 (2018).
- 548 Guidotti, G., Brambilla, L. & Rossi, D. Cell-Penetrating Peptides: From Basic Research to Clinics.
Trends Pharmacol Sci **38**, 406-424, doi:10.1016/j.tips.2017.01.003 (2017).
- 549 Kristensen, M., Birch, D. & Morck Nielsen, H. Applications and Challenges for Use of Cell-
Penetrating Peptides as Delivery Vectors for Peptide and Protein Cargos. *International journal of
molecular sciences* **17**, doi:10.3390/ijms17020185 (2016).
- 550 McNaughton, B. R., Cronican, J. J., Thompson, D. B. & Liu, D. R. Mammalian cell penetration,
siRNA transfection, and DNA transfection by supercharged proteins. *Proceedings of the National
Academy of Sciences of the United States of America* **106**, 6111-6116,
doi:10.1073/pnas.0807883106 (2009).
- 551 Fuchs, S. M. & Raines, R. T. Arginine grafting to endow cell permeability. *ACS chemical biology* **2**,
167-170, doi:10.1021/cb600429k (2007).
- 552 Thompson, D. B., Cronican, J. J. & Liu, D. R. Engineering and identifying supercharged proteins
for macromolecule delivery into mammalian cells. *Methods in enzymology* **503**, 293-319,
doi:10.1016/B978-0-12-396962-0.00012-4 (2012).
- 553 Rabideau, A. E. & Pentelute, B. L. Delivery of Non-Native Cargo into Mammalian Cells Using
Anthrax Lethal Toxin. *ACS chemical biology* **11**, 1490-1501, doi:10.1021/acschembio.6b00169
(2016).
- 554 Verdurmen, W. P., Luginbuhl, M., Honegger, A. & Pluckthun, A. Efficient cell-specific uptake of
binding proteins into the cytoplasm through engineered modular transport systems. *Journal of*

- controlled release : official journal of the Controlled Release Society* **200**, 13-22, doi:10.1016/j.jconrel.2014.12.019 (2015).
- 555 Aguilera, T. A., Olson, E. S., Timmers, M. M., Jiang, T. & Tsien, R. Y. Systemic in vivo distribution of activatable cell penetrating peptides is superior to that of cell penetrating peptides. *Integrative biology : quantitative biosciences from nano to macro* **1**, 371-381, doi:10.1039/b904878b (2009).
- 556 Shi, N. Q. & Qi, X. R. Taming the Wildness of "Trojan-Horse" Peptides by Charge-Guided Masking and Protease-Triggered Demasking for the Controlled Delivery of Antitumor Agents. *ACS Appl Mater Interfaces* **9**, 10519-10529, doi:10.1021/acsami.7b01056 (2017).
- 557 Verdurmen, W. P. R., Mazlami, M. & Pluckthun, A. A quantitative comparison of cytosolic delivery via different protein uptake systems. *Scientific reports* **7**, 13194, doi:10.1038/s41598-017-13469-y (2017).
- 558 Patel, S. G. *et al.* Cell-penetrating peptide sequence and modification dependent uptake and subcellular distribution of green florescent protein in different cell lines. *Scientific reports* **9**, 6298, doi:10.1038/s41598-019-42456-8 (2019).
- 559 Solaro, R., Chiellini, F. & Battisti, A. Targeted Delivery of Protein Drugs by Nanocarriers. *Materials* **3**, 1928-1980, doi:10.3390/ma3031928 (2010).
- 560 Uthaman, S., Huh, K. M. & Park, I.-K. Tumor microenvironment-responsive nanoparticles for cancer thernagnostic applications. *Biomater Res* **22**, 22-22, doi:10.1186/s40824-018-0132-z (2018).
- 561 Galliani, M., Tremolanti, C. & Signore, G. Nanocarriers for Protein Delivery to the Cytosol: Assessing the Endosomal Escape of Poly(Lactide-co-Glycolide)-Poly(Ethylene Imine) Nanoparticles. *Nanomaterials (Basel)* **9**, doi:10.3390/nano9040652 (2019).
- 562 Chou, M. J. *et al.* Highly Efficient Intracellular Protein Delivery by Cationic Polyethyleneimine-Modified Gelatin Nanoparticles. *Materials (Basel)* **11**, doi:10.3390/ma11020301 (2018).
- 563 Rohovie, M. J., Nagasawa, M. & Swartz, J. R. Virus-like particles: Next-generation nanoparticles for targeted therapeutic delivery. *Bioeng Transl Med* **2**, 43-57, doi:10.1002/btm2.10049 (2017).
- 564 Zhao, H. *et al.* Polymer-based nanoparticles for protein delivery: design, strategies and applications. *Journal of Materials Chemistry B* **4**, 4060-4071, doi:10.1039/C6TB00308G (2016).
- 565 Ray, M., Lee, Y. W., Scaletti, F., Yu, R. & Rotello, V. M. Intracellular delivery of proteins by nanocarriers. *Nanomedicine (Lond)* **12**, 941-952, doi:10.2217/nnm-2016-0393 (2017).
- 566 Ghosh, P. *et al.* Intracellular delivery of a membrane-impermeable enzyme in active form using functionalized gold nanoparticles. *Journal of the American Chemical Society* **132**, 2642-2645, doi:10.1021/ja907887z (2010).
- 567 Xu, C., Lei, C. & Yu, C. Mesoporous Silica Nanoparticles for Protein Protection and Delivery. *Front Chem* **7**, 290, doi:10.3389/fchem.2019.00290 (2019).
- 568 Slowing, I. I., Vivero-Escoto, J. L., Trewyn, B. G. & Lin, V. S. Y. Mesoporous silica nanoparticles: structural design and applications. *Journal of Materials Chemistry* **20**, 7924-7937, doi:10.1039/C0JM00554A (2010).
- 569 Sun, Y. *et al.* Formation pathways of mesoporous silica nanoparticles with dodecagonal tiling. *Nature communications* **8**, 252, doi:10.1038/s41467-017-00351-8 (2017).
- 570 Alvarez-Berr *et al.* Hybrid Nanomaterials Based on Iron Oxide Nanoparticles and Mesoporous Silica Nanoparticles: Overcoming Challenges in Current Cancer Treatments. *Journal of Chemistry* **2016**, 15, doi:10.1155/2016/2672740 (2016).
- 571 Watermann, A. & Brieger, J. Mesoporous Silica Nanoparticles as Drug Delivery Vehides in Cancer. *Nanomaterials (Basel)* **7**, doi:10.3390/nano7070189 (2017).

- 572 Ashley, C. E. *et al.* The targeted delivery of multicomponent cargos to cancer cells by nanoporous particle-supported lipid bilayers. *Nat Mater* **10**, 389-397, doi:10.1038/nmat2992 (2011).
- 573 Chauhan, S., Manivasagam, G., Kumar, P. & Ambasta, R. K. Cellular Toxicity of Mesoporous Silica Nanoparticle in SHSY5Y and BMMNCs Cell. *Pharm Nanotechnol* **6**, 245-252, doi:10.2174/2211738506666181031160108 (2018).
- 574 Omar, H. *et al.* Biodegradable Magnetic Silica@Iron Oxide Nanovectors with Ultra-Large Mesopores for High Protein Loading, Magnetothermal Release, and Delivery. *Journal of controlled release : official journal of the Controlled Release Society* **259**, 187-194, doi:10.1016/j.jconrel.2016.11.032 (2017).
- 575 Kong, M. *et al.* Biodegradable Hollow Mesoporous Silica Nanoparticles for Regulating Tumor Microenvironment and Enhancing Antitumor Efficiency. *Theranostics* **7**, 3276-3292, doi:10.7150/thno.19987 (2017).
- 576 Wu, S. H., Mou, C. Y. & Lin, H. P. Synthesis of mesoporous silica nanoparticles. *Chemical Society reviews* **42**, 3862-3875, doi:10.1039/c3cs35405a (2013).
- 577 Chiu, H.-Y., Leonhardt, H. & Bein, T. Synthesis and Functionalization of Ordered Large-Pore Mesoporous Silica Nanoparticles for Biomedical Applications. *Chemie Ingenieur Technik* **89**, 876-886, doi:doi:10.1002/cite.201700021 (2017).
- 578 Xuan, M., Shao, J., Dai, L., He, Q. & Li, J. Macrophage Cell Membrane Camouflaged Mesoporous Silica Nanocapsules for In Vivo Cancer Therapy. *Adv Healthc Mater* **4**, 1645-1652, doi:10.1002/adhm.201500129 (2015).
- 579 Liu, X. *et al.* A dual responsive targeted drug delivery system based on smart polymer coated mesoporous silica for laryngeal carcinoma treatment. *New Journal of Chemistry* **38**, 4830-4836, doi:10.1039/C4NJ00579A (2014).
- 580 Shi, J. *et al.* An MSN-PEG-IP drug delivery system and IL13Ralpha2 as targeted therapy for glioma. *Nanoscale* **9**, 8970-8981, doi:10.1039/c6nr08786h (2017).
- 581 Qu, H. *et al.* A redox responsive controlled release system using mesoporous silica nanoparticles capped with Au nanoparticles. *RSC Advances* **7**, 35704-35710, doi:10.1039/C7RA04444E (2017).
- 582 Kesse, S. *et al.* Mesoporous Silica Nanomaterials: Versatile Nanocarriers for Cancer Theranostics and Drug and Gene Delivery. *Pharmaceutics* **11**, doi:10.3390/pharmaceutics11020077 (2019).
- 583 Keasberry, N. A., Yapp, C. W. & Idris, A. Mesoporous Silica Nanoparticles as a Carrier Platform for Intracellular Delivery of Nucleic Acids. *Biochemistry (Mosc)* **82**, 655-662, doi:10.1134/S0006297917060025 (2017).
- 584 Liu, H. J. & Xu, P. Smart Mesoporous Silica Nanoparticles for Protein Delivery. *Nanomaterials (Basel)* **9**, doi:10.3390/nano9040511 (2019).
- 585 Lin, Y. H. *et al.* Approach To Deliver Two Antioxidant Enzymes with Mesoporous Silica Nanoparticles into Cells. *ACS Appl Mater Interfaces* **8**, 17944-17954, doi:10.1021/acsami.6b05834 (2016).
- 586 Mody, K. T. *et al.* Mesoporous silica nanoparticles as antigen carriers and adjuvants for vaccine delivery. *Nanoscale* **5**, 5167-5179, doi:10.1039/c3nr00357d (2013).
- 587 Cha, B. G., Jeong, J. H. & Kim, J. Extra-Large Pore Mesoporous Silica Nanoparticles Enabling Co-Delivery of High Amounts of Protein Antigen and Toll-like Receptor 9 Agonist for Enhanced Cancer Vaccine Efficacy. *ACS Cent Sci* **4**, 484-492, doi:10.1021/acscentsci.8b00035 (2018).
- 588 Narayan, R., Nayak, U. Y., Raichur, A. M. & Garg, S. Mesoporous Silica Nanoparticles: A Comprehensive Review on Synthesis and Recent Advances. *Pharmaceutics* **10**, doi:10.3390/pharmaceutics10030118 (2018).

- 589 Xie, X., Liao, J., Shao, X., Li, Q. & Lin, Y. The Effect of shape on Cellular Uptake of Gold Nanoparticles in the forms of Stars, Rods, and Triangles. *Scientific reports* **7**, 3827, doi:10.1038/s41598-017-04229-z (2017).
- 590 Lu, F., Wu, S. H., Hung, Y. & Mou, C. Y. Size effect on cell uptake in well-suspended, uniform mesoporous silica nanoparticles. *Small* **5**, 1408-1413, doi:10.1002/smll.200900005 (2009).
- 591 Albanese, A., Tang, P. S. & Chan, W. C. The effect of nanoparticle size, shape, and surface chemistry on biological systems. *Annu Rev Biomed Eng* **14**, 1-16, doi:10.1146/annurev-bioeng-071811-150124 (2012).
- 592 Gratton, S. E. *et al.* The effect of particle design on cellular internalization pathways. *Proceedings of the National Academy of Sciences of the United States of America* **105**, 11613-11618, doi:10.1073/pnas.0801763105 (2008).
- 593 Toy, R., Peiris, P. M., Ghaghada, K. B. & Karathanasis, E. Shaping cancer nanomedicine: the effect of particle shape on the in vivo journey of nanoparticles. *Nanomedicine (Lond)* **9**, 121-134, doi:10.2217/nnm.13.191 (2014).
- 594 Hoshyar, N., Gray, S., Han, H. & Bao, G. The effect of nanoparticle size on in vivo pharmacokinetics and cellular interaction. *Nanomedicine (Lond)* **11**, 673-692, doi:10.2217/nnm.16.5 (2016).
- 595 Peiris, P. M. *et al.* Enhanced delivery of chemotherapy to tumors using a multicomponent nanochain with radio-frequency-tunable drug release. *ACS nano* **6**, 4157-4168, doi:10.1021/nn300652p (2012).
- 596 Wang, Y. *et al.* The investigation of MCM-48-type and MCM-41-type mesoporous silica as oral solid dispersion carriers for water insoluble cilostazol. *Drug Dev Ind Pharm* **40**, 819-828, doi:10.3109/03639045.2013.788013 (2014).
- 597 Jia, L. *et al.* Successfully tailoring the pore size of mesoporous silica nanoparticles: exploitation of delivery systems for poorly water-soluble drugs. *Int J Pharm* **439**, 81-91, doi:10.1016/j.ijpharm.2012.10.011 (2012).
- 598 Yildirim, A., Ozgur, E. & Bayindir, M. Impact of mesoporous silica nanoparticle surface functionality on hemolytic activity, thrombogenicity and non-specific protein adsorption. *Journal of Materials Chemistry B* **1**, 1909-1920, doi:10.1039/C3TB20139B (2013).
- 599 Chen, Y.-P. *et al.* Surface charge effect in intracellular localization of mesoporous silica nanoparticles as probed by fluorescent ratiometric pH imaging. *RSC Advances* **2**, 968-973, doi:10.1039/C1RA00586C (2012).
- 600 Slowing, II, Trewyn, B. G. & Lin, V. S. Mesoporous silica nanoparticles for intracellular delivery of membrane-impermeable proteins. *Journal of the American Chemical Society* **129**, 8845-8849, doi:10.1021/ja0719780 (2007).
- 601 Sudo, K. *et al.* Human-derived fusogenic peptides for the intracellular delivery of proteins. *Journal of controlled release : official journal of the Controlled Release Society* **255**, 1-11, doi:10.1016/j.jconrel.2017.03.398 (2017).
- 602 Yezhelyev, M. V., Qi, L., O'Regan, R. M., Nie, S. & Gao, X. Proton-sponge coated quantum dots for siRNA delivery and intracellular imaging. *Journal of the American Chemical Society* **130**, 9006-9012, doi:10.1021/ja800086u (2008).
- 603 He, Q. *et al.* The effect of PEGylation of mesoporous silica nanoparticles on nonspecific binding of serum proteins and cellular responses. *Biomaterials* **31**, 1085-1092, doi:10.1016/j.biomaterials.2009.10.046 (2010).
- 604 Shi, H. *et al.* Charge-Selective Delivery of Proteins Using Mesoporous Silica Nanoparticles Fused with Lipid Bilayers. *ACS Appl Mater Interfaces* **11**, 3645-3653, doi:10.1021/acsami.8b15390 (2019).

- 605 Tietjen, G. T., Bracaglia, L. G., Saltzman, W. M. & Pober, J. S. Focus on Fundamentals: Achieving Effective Nanoparticle Targeting. *Trends Mol Med* **24**, 598-606, doi:10.1016/j.molmed.2018.05.003 (2018).
- 606 He, Q., Zhang, Z., Gao, Y., Shi, J. & Li, Y. Intracellular localization and cytotoxicity of spherical mesoporous silica nano- and microparticles. *Small* **5**, 2722-2729, doi:10.1002/smll.200900923 (2009).
- 607 Lee, Y. W. *et al.* Protein Delivery into the Cell Cytosol using Non-Viral Nanocarriers. *Theranostics* **9**, 3280-3292, doi:10.7150/thno.34412 (2019).
- 608 Nel, A. E. *et al.* Understanding biophysicochemical interactions at the nano-bio interface. *Nat Mater* **8**, 543-557, doi:10.1038/nmat2442 (2009).
- 609 Larsson, S. *et al.* Cell line-based xenograft mouse model of paediatric glioma stem cells mirrors the clinical course of the patient. *Carcinogenesis* **39**, 1304-1309, doi:10.1093/carcin/bgy091 (2018).
- 610 Li, Z., Zhang, Y. & Feng, N. Mesoporous silica nanoparticles: synthesis, classification, drug loading, pharmacokinetics, biocompatibility, and application in drug delivery. *Expert Opin Drug Deliv* **16**, 219-237, doi:10.1080/17425247.2019.1575806 (2019).
- 611 Rincon-Restrepo, M. *et al.* Vaccine nanocarriers: Coupling intracellular pathways and cellular biodistribution to control CD4 vs CD8 T cell responses. *Biomaterials* **132**, 48-58, doi:10.1016/j.biomaterials.2017.03.047 (2017).
- 612 Gustafson, H. H., Holt-Casper, D., Grainger, D. W. & Ghandehari, H. Nanoparticle Uptake: The Phagocyte Problem. *Nano Today* **10**, 487-510, doi:10.1016/j.nantod.2015.06.006 (2015).
- 613 Clem, A. S. Fundamentals of vaccine immunology. *J Glob Infect Dis* **3**, 73-78, doi:10.4103/0974-777X.77299 (2011).
- 614 Pati, R., Shevtsov, M. & Sonawane, A. Nanoparticle Vaccines Against Infectious Diseases. *Front Immunol* **9**, 2224, doi:10.3389/fimmu.2018.02224 (2018).
- 615 Gasteiger, G. *et al.* Cellular Innate Immunity: An Old Game with New Players. *J Innate Immun* **9**, 111-125, doi:10.1159/000453397 (2017).
- 616 Wieczorek, M. *et al.* Major Histocompatibility Complex (MHC) Class I and MHC Class II Proteins: Conformational Plasticity in Antigen Presentation. *Front Immunol* **8**, 292, doi:10.3389/fimmu.2017.00292 (2017).
- 617 Letai, A. Apoptosis and Cancer. *Annual Review of Cancer Biology* **1**, 275-294, doi:10.1146/annurev-cancerbio-050216-121933 (2017).
- 618 Shahryari, A. *et al.* Development and Clinical Translation of Approved Gene Therapy Products for Genetic Disorders. *Front Genet* **10**, 868, doi:10.3389/fgene.2019.00868 (2019).
- 619 Salmon, F., Grosios, K. & Petry, H. Safety profile of recombinant adeno-associated viral vectors: focus on alipogene tiparvovec (Glybera(R)). *Expert Rev Clin Pharmacol* **7**, 53-65, doi:10.1586/17512433.2014.852065 (2014).
- 620 Chan, K. Y. *et al.* Engineered AAVs for efficient noninvasive gene delivery to the central and peripheral nervous systems. *Nat Neurosci* **20**, 1172-1179, doi:10.1038/nn.4593 (2017).
- 621 Herrera-Carrillo, E. & Berkhout, B. Bone Marrow Gene Therapy for HIV/AIDS. *Viruses* **7**, 3910-3936, doi:10.3390/v7072804 (2015).
- 622 Zheng, C. & Baum, B. J. in *Gene Therapy Protocols: Design and Characterization of Gene Transfer Vectors* (ed Joseph M. Le Doux) 205-219 (Humana Press, 2008).
- 623 Brown, B. D., Venneri, M. A., Zingale, A., Sergi, L. & Naldini, L. Endogenous microRNA regulation suppresses transgene expression in hematopoietic lineages and enables stable gene transfer. *Nature medicine* **12**, 585-591, doi:10.1038/nm1398 (2006).
- 624 Freund, I., Eigenbrod, T., Helm, M. & Dalpke, A. H. RNA Modifications Modulate Activation of Innate Toll-Like Receptors. *Genes (Basel)* **10**, doi:10.3390/genes10020092 (2019).

- 625 Renatus, M., Stennicke, H. R., Scott, F. L., Liddington, R. C. & Salvesen, G. S. Dimer formation drives the activation of the cell death protease caspase 9. *Proceedings of the National Academy of Sciences of the United States of America* **98**, 14250-14255, doi:10.1073/pnas.231465798 (2001).
- 626 Wu, C. C. *et al.* The Apaf-1 apoptosome induces formation of caspase-9 homo- and heterodimers with distinct activities. *Nature communications* **7**, 13565, doi:10.1038/ncomms13565 (2016).
- 627 Wang, D. *et al.* Engineering nanoparticles to locally activate T cells in the tumor microenvironment. *Sci Immunol* **4**, doi:10.1126/sciimmunol.aau6584 (2019).
- 628 Park, B. *et al.* Proteolytic cleavage in an endolysosomal compartment is required for activation of Toll-like receptor 9. *Nature immunology* **9**, 1407-1414, doi:10.1038/ni.1669 (2008).
- 629 Nakagawa, C., Inahata, K., Nishimura, S. & Sugimoto, K. Improvement of a Venus-based bimolecular fluorescence complementation assay to visualize bFos-bJun interaction in living cells. *Bioscience, biotechnology, and biochemistry* **75**, 1399-1401 (2011).
- 630 Boatright, K. M. *et al.* A unified model for apical caspase activation. *Molecular cell* **11**, 529-541, doi:10.1016/s1097-2765(03)00051-0 (2003).
- 631 Monera, O. D., Sereda, T. J., Zhou, N. E., Kay, C. M. & Hodges, R. S. Relationship of sidechain hydrophobicity and alpha-helical propensity on the stability of the single-stranded amphipathic alpha-helix. *J Pept Sci* **1**, 319-329, doi:10.1002/psc.310010507 (1995).
- 632 Fortmann, K. T., Lewis, R. D., Ngo, K. A., Fagerlund, R. & Hoffmann, A. A Regulated, Ubiquitin-Independent Degron in I κ B α . *Journal of molecular biology* **427**, 2748-2756, doi:10.1016/j.jmb.2015.07.008 (2015).
- 633 Chen, T. & Romesberg, F. E. Directed polymerase evolution. *FEBS letters* **588**, 219-229, doi:10.1016/j.febslet.2013.10.040 (2014).
- 634 Sanchez, M. I. & Ting, A. Y. Directed evolution improves the catalytic efficiency of TEV protease. *Nature methods*, doi:10.1038/s41592-019-0665-7 (2019).
- 635 Malladi, S., Challa-Malladi, M., Fearnhead, H. O. & Bratton, S. B. The Apaf-1*procaspase-9 apoptosome complex functions as a proteolytic-based molecular timer. *The EMBO journal* **28**, 1916-1925, doi:10.1038/emboj.2009.152 (2009).
- 636 Ghavami, S. *et al.* Apoptosis and cancer: mutations within caspase genes. *Journal of Medical Genetics* **46**, 497-510, doi:10.1136/jmg.2009.066944 (2009).
- 637 Parrish, A. B., Freel, C. D. & Kornbluth, S. Cellular mechanisms controlling caspase activation and function. *Cold Spring Harb Perspect Biol* **5**, doi:10.1101/cshperspect.a008672 (2013).
- 638 Srinivasula, S. M. *et al.* A conserved XIAP-interaction motif in caspase-9 and Smac/DIABLO regulates caspase activity and apoptosis. *Nature* **410**, 112-116, doi:10.1038/35065125 (2001).
- 639 Lieberman, J., Wu, H. & Kagan, J. C. Gasdermin D activity in inflammation and host defense. *Sci Immunol* **4**, doi:10.1126/sciimmunol.aav1447 (2019).
- 640 Fukazawa, T., Maeda, Y., Sladek, F. M. & Owen-Schaub, L. B. Development of a cancer-targeted tissue-specific promoter system. *Cancer research* **64**, 363-369, doi:10.1158/0008-5472.can-03-2507 (2004).
- 641 El Marabti, E. & Younis, I. The Cancer Spliceome: Reprogramming of Alternative Splicing in Cancer. *Front Mol Biosci* **5**, 80, doi:10.3389/fmolb.2018.00080 (2018).
- 642 Chambers, J. S., Brend, T. & Rabbitts, T. H. Cancer cell killing by target antigen engagement with engineered complementary intracellular antibody single domains fused to pro-caspase3. *Scientific reports* **9**, 8553-8553, doi:10.1038/s41598-019-44908-7 (2019).
- 643 Martens, J. H. & Stunnenberg, H. G. The molecular signature of oncofusion proteins in acute myeloid leukemia. *FEBS letters* **584**, 2662-2669, doi:10.1016/j.febslet.2010.04.002 (2010).

- 644 Liu, Y. *et al.* The tetramer structure of the Nervy homology two domain, NHR2, is critical for AML1/ETO's activity. *Cancer cell* **9**, 249-260, doi:10.1016/j.ccr.2006.03.012 (2006).
- 645 Sun, X. J. *et al.* A stable transcription factor complex nucleated by oligomeric AML1-ETO controls leukaemogenesis. *Nature* **500**, 93-97, doi:10.1038/nature12287 (2013).
- 646 Zhu, J. *et al.* RXR Is an Essential Component of the Oncogenic PML/RARA Complex In Vivo. *Cancer cell* **12**, 23-35, doi:<https://doi.org/10.1016/j.ccr.2007.06.004> (2007).
- 647 Robinson, M. S., Sahlender, D. A. & Foster, S. D. Rapid inactivation of proteins by rapamycin-induced rerouting to mitochondria. *Dev Cell* **18**, 324-331, doi:10.1016/j.devcel.2009.12.015 (2010).
- 648 Repina, N. A., Rosenbloom, A., Mukherjee, A., Schaffer, D. V. & Kane, R. S. At Light Speed: Advances in Optogenetic Systems for Regulating Cell Signaling and Behavior. *Annu Rev Chem Biomol Eng* **8**, 13-39, doi:10.1146/annurev-chembioeng-060816-101254 (2017).
- 649 Wilson, M. H., Coates, C. J. & George, A. L., Jr. PiggyBac transposon-mediated gene transfer in human cells. *Molecular therapy : the journal of the American Society of Gene Therapy* **15**, 139-145, doi:10.1038/sj.mt.6300028 (2007).
- 650 Matzke, M. A., Mette, M. F. & Matzke, A. J. Transgene silencing by the host genome defense: implications for the evolution of epigenetic control mechanisms in plants and vertebrates. *Plant molecular biology* **43**, 401-415 (2000).
- 651 Ding, S. *et al.* Efficient transposition of the piggyBac (PB) transposon in mammalian cells and mice. *Cell* **122**, 473-483, doi:10.1016/j.cell.2005.07.013 (2005).
- 652 Hannah, J. & Zhou, P. Maximizing target protein ablation by integration of RNAi and protein knockout. *Cell Res* **21**, 1152-1154, doi:10.1038/cr.2011.89 (2011).
- 653 Wang, S. *et al.* A toolkit for GFP-mediated tissue-specific protein degradation in *C. elegans*. *Development* **144**, 2694-2701, doi:10.1242/dev.150094 (2017).
- 654 Peth, A., Uchiki, T. & Goldberg, A. L. ATP-dependent steps in the binding of ubiquitin conjugates to the 26S proteasome that commit to degradation. *Molecular cell* **40**, 671-681, doi:10.1016/j.molcel.2010.11.002 (2010).
- 655 Zheng, N. & Shabek, N. Ubiquitin Ligases: Structure, Function, and Regulation. *Annu Rev Biochem* **86**, 129-157, doi:10.1146/annurev-biochem-060815-014922 (2017).
- 656 Fulcher, L. J., Hutchinson, L. D., Macartney, T. J., Turnbull, C. & Sapkota, G. P. Targeting endogenous proteins for degradation through the affinity-directed protein missile system. *Open Biol* **7**, doi:10.1098/rsob.170066 (2017).
- 657 Paulk, N. K. *et al.* Bioengineered AAV Capsids with Combined High Human Liver Transduction In Vivo and Unique Humoral Seroreactivity. *Molecular therapy : the journal of the American Society of Gene Therapy* **26**, 289-303, doi:10.1016/j.ymthe.2017.09.021 (2018).
- 658 Park, Y. J., Kuen, D. S. & Chung, Y. Future prospects of immune checkpoint blockade in cancer: from response prediction to overcoming resistance. *Exp Mol Med* **50**, 109, doi:10.1038/s12276-018-0130-1 (2018).
- 659 Cohen, R. N., van der Aa, M. A., Macaraeg, N., Lee, A. P. & Szoka, F. C., Jr. Quantification of plasmid DNA copies in the nucleus after lipoplex and polyplex transfection. *Journal of controlled release : official journal of the Controlled Release Society* **135**, 166-174, doi:10.1016/j.jconrel.2008.12.016 (2009).
- 660 Qin, J. Y. *et al.* Systematic comparison of constitutive promoters and the doxycycline-inducible promoter. *PloS one* **5**, e10611, doi:10.1371/journal.pone.0010611 (2010).
- 661 Sadelain, M., Papapetrou, E. P. & Bushman, F. D. Safe harbours for the integration of new DNA in the human genome. *Nat Rev Cancer* **12**, 51-58, doi:10.1038/nrc3179 (2011).

Abbreviations

AAV:	Adeno Associated Virus
Ab:	Antibody
ADC:	Antibody Drug Conjugate
ADCC:	Antibody Dependent Cellular Cytotoxicity
ADPh:	Antibody Dependent Phagocytosis
ADS:	Antigen Dependent Stability
Ag:	Antigen
AID:	Auxin inducible degron
APCs:	Antigen Presenting Cells
AR6:	Ankyrin repeat fold 6 (of I κ B α)
BiFC:	Bimolecular Fluorescence Complementation
C9:	Caspase-9
CAR:	Chimeric Antigen Receptors
CDC:	Complement Dependent Cytotoxicity
CDR:	Complementarity Determining Region
CPP:	Cell Penetrating Peptide
CTD:	C-terminal domain (of p24)
DARPin:	Designed Ankyrin Repeat Protein
D-FISA:	Dual Fluorescent Intrabody Selection Assay
DiPD:	Drug Inducible Protein Degradation
Dox:	Doxycyclin
EM:	Electron Microscopy
ER:	Endoplasmic Reticulum
F3H:	Fluorescent-3-Hybrid assay
FACS:	Fluorescent Activated Cell Sorting
FC:	Fluorescent complementation component
Fc:	Fragment Crystallizable
FcR:	Fragment Crystallizable Receptor
FIDA:	Fluorescent Intrabody Degradation Assay
FISA:	Fluorescent Intrabody Selection Assay
FKBP:	FK506 binding protein
FR:	Framework region
FRB:	FBKP Rapamycin Binding Protein
FRET:	Förster Resonance Energy transfer
Fv:	Fragment variable
GFP:	Green Fluorescent Protein
GPCR:	G protein-coupled receptors
HBV:	Hepatitis B Virus
HcAb:	Heavy chain only antibody
HIV:	Human Immunodeficiency Virus
IgNAR:	Immunoglobulin New Antigen Receptor
IVC:	In Vitro Compartmentalisation
IVT:	In vitro transcribed

LiPD:	Light Inducible Protein Degradar
LRET:	Lanthanide-based resonance energy transfer
MAB:	Monoclonal Antibody
MACS:	Magnetic Activated Cell Sorting
mAID:	Mini Auxin inducible degraon
MHC:	Major Histocompatibility Complex
MO:	Morpholino
MPS:	Mononuclear Phagocytic system
mRFP:	Monomeric Red Fluorescent Protein
mRNA:	Messenger RNA
MSN:	Mesoporous Silica Nanoparticle
Nb:	Nanobody
NTD:	N-terminal domain (of p24)
PDT:	Photodynamic Therapy
PEG:	Polyethylene Glycol
PET:	Positron emission tomography
POI:	Protein of Interest
PROTACs:	Proteolysis Targeting Chimeras
PTM:	Post Translational Modification
scFv:	Single chain fragment variable
sdAb:	Single Domain Antibody
SDB:	Single Domain binder
SHM:	Somatic Hypermutation
shRNA:	Short Hairpin RNA
siRNA:	Silencing RNA
SPECT:	Single-Photon Emission Computed Tomography
ssRNA:	Single Stranded RNA
TCR:	T-Cell Receptor
TRAP:	Target Responsive Apoptotic Protein
TRIM:	Trinucleotide Mutagenesis
TRNT:	Targeted Radionuclide therapeutics
UCNP:	Upconversion Nanoparticle
UPP:	Ubiquitin Proteosomal Pathway
VC:	Venus C-terminal fragment
VH:	Variable Fragment of the Heavy Chain
VHH:	Variable Fragment of the Heavy Chain of a Heavy chain only antibody
VL:	Variable Fragment of the Light Chain
VLP:	Virus-Like Particles
VN:	Venus N-terminal fragment
vNAR:	Variable New Antigen Receptor

List of Publications

1. Balaji, R.; Bielmeier, C.; Harz, H.; Bates, J.; Stadler, C.; Hildebrand, A.; Classen, A. K., Calcium spikes, waves and oscillations in a large, patterned epithelial tissue. *Scientific reports* 2017, 7, 42786.
2. Chiu, H. Y.; Bates, J. A.; Helma, J.; Engelke, H.; Harz, H.; Bein, T.; Leonhardt, H., Nanoparticle mediated delivery and small molecule triggered activation of proteins in the nucleus. *Nucleus* 2018, 9 (1), 530-542.
3. Deng, W.; Bates, J. A.; Wei, H.; Bartoschek, M. D.; Conradt, B.; Leonhardt, H., Tunable light and drug induced depletion of target proteins. *Nature communications* **2020**, 11 (1), 304.
4. Bates, J. A.; Qin, W.; Leonhardt, H.; Helma, J., Engineering binder-guided apoptotic proteins responsive to intracellular antigens. *Manuscript in Preparation*

Contributions

Declaration of Contributions to ***“Nanoparticle mediated delivery and small molecule triggered activation of proteins in the nucleus”***: The project was conceived by Heinrich Leonhardt. Hsin-Yi Chiu and Thomas Bein developed the large pore MSNs with Ni-NTA technology. Heinrich Leonhardt and I designed the Venus sensor. I constructed the sensor and accompanying cell line. Hsin-Yi Chiu and I performed all experimentation. Hartmann Harz assisted with Microscopy. Jonas Helma assisted with protein purification. Heinrich Leonhardt, Hsin-Yi Chiu and myself co-wrote the manuscript.

Declaration of Contributions to ***“Engineering binder-guided apoptotic proteins responsive to intracellular antigens”***: Jonas Helma and Heinrich Leonhardt conceived of the project. Jonas Helma performed preliminary experiments. I performed all experiments present in the paper. Heinrich Leonhardt, Jonas Helma and I designed the experiments. Weihua Qin produced the IVT mRNAs. I wrote the manuscript.

Declaration of Contributions to ***“Tunable light and drug induced depletion of target proteins”***: Wen Deng and Heinrich Leonhardt conceived of the project. Wen Deng, Hai Wei and I performed the experiments. Wen Deng, Heinrich Leonhardt, Barbara Conradt, Hai Wei and I designed the experiments. Heinrich Leonhardt and Wen Deng wrote the manuscript, I contributed significantly to the manuscript with text and discussion.

Declaration of Contributions to ***“Function Specific Intrabody Screens”***: Heinrich Leonhardt conceived of the project. Heinrich Leonhardt and I designed the assays. Heinrich Leonhardt and I designed the experiments. I developed and tested the assays.

Declaration

Eidesstattliche Erklärung

Ich versichere hiermit an Eides statt, dass die vorgelegte Dissertation von mir selbständig und ohne unerlaubte Hilfe angefertigt ist.

München, den 23.01.2020 Jack Anthony Bates

(Unterschrift)

Erklärung

Hiermit erkläre ich, *

- dass die Dissertation nicht ganz oder in wesentlichen Teilen einer anderen Prüfungskommission vorgelegt worden ist.
- dass ich mich anderweitig einer Doktorprüfung ohne Erfolg **nicht** unterzogen habe.
- dass ich mich mit Erfolg der Doktorprüfung im Hauptfach
und in den Nebenfächern
bei der Fakultät für der
(Hochschule/Universität)
unterzogen habe.
- dass ich ohne Erfolg versucht habe, eine Dissertation einzureichen oder mich der Doktorprüfung zu unterziehen.

München, den 23.01.2020 Jack Anthony Bates

(Unterschrift)

*) Nichtzutreffendes streichen